REMOTE SENSING OF SPATIOTEMPORAL PHYTOPLANKTON DYNAMICS OF THE OPTICALLY COMPLEX LAKE BALATON

Thesis submitted for the degree of
Doctor of Philosophy
at the University of Leicester

by

Stephanie C. J. Palmer MSc

Department of Geography
University of Leicester

2015

Abstract

Remote sensing of spatiotemporal phytoplankton dynamics of the optically complex Lake Balaton

Stephanie C. J. Palmer

This thesis explores the use of remote sensing to measure the phytoplankton biomass of Lake Balaton, Hungary via the proxy pigment, chlorophyll-*a* (chl-*a*). Several scales of spatial and temporal variability are considered, using a ten year time series of Medium Resolution Imaging Spectrometer (MERIS) satellite imagery, ship-mounted Light Detection and Ranging (LiDAR), and water sampling and laboratory measurements from punctual and ongoing campaigns. Existing remote sensing methods are adapted to Lake Balaton for the first time, and novel directions are demonstrated which may be applied to other lakes in the future. Several chl-*a* retrieval algorithms applied to archive MERIS data are calibrated and validated using an extensive dataset of coinciding *in situ* measurements and results from each are compared. The application of two atmospheric correction algorithms is also validated and their influence on chl-*a* retrieval is considered in comparison with the use of un- atmospherically corrected, top-of-Atmosphere (TOA) data. The fluorescence line height (FLH) algorithm applied to TOA MERIS data is found to accurately and robustly retrieve Lake Balaton chl-*a* ($R^2 = 0.87$; RMSE = 4.19 mg m^{-3}), particularly during high biomass bloom events (chl-*a* $\geq$ 10 mg m^{-3}). This algorithm is then applied to the full MERIS archive (2002-2012), resulting chl-*a* time series are smoothed at the pixel level, and phytoplankton phenology metrics are extracted and mapped. Phenology metric mapping in lakes using MERIS remote sensing is demonstrated and significant spatiotemporal variability in bloom metrics is apparent. Laboratory tank and *in situ* ship-mounted Ultraviolet Fluorescence LiDAR (UFL) measurements indicate another novel direction for lake remote sensing. Chl-*a*, as well as total suspended matter (TSM) and coloured dissolved organic matter (CDOM), were measured and cyanobacteria was distinguished from chlorophyta via fluorescence emission spectra. The feasibility of retrieving accurate and quantitative information on Lake Balaton phytoplankton biomass dynamics through the use of remote sensing techniques is confirmed, and the resulting added value for both science and management is highlighted.

Acknowledgements

I would like to thank my thesis supervisors, Professor Heiko Balzter and Dr. Virginia Nicolás-Perea for the guidance, encouragement and wisdom that they have provided throughout, as well as for their leadership of the GIONET Initial Training Network more broadly.

Huge thanks to Dr. Viktor Tóth, of the Balaton Limnological Institute (BLI), for all of his mentorship, support, good humour and many efforts in helping me to navigate through so many aspects of science, administration and life in Hungary. Thanks to Dr. András Zlinszky for the opportunity to carry out my PhD research as part of GIONET at the BLI, and for his enthusiasm and creativity in science and his clear love of ecology, Lake Balaton and remote sensing. Thanks also to Dr. Mátyás Présing, for his kind guidance as well as for providing archive *in situ* datasets used in the thesis work, to Dr. Présing, Hajnalka Horváth and Teréz Horváth for their patience and cheer throughout the extensive lab analyses that went along with the fieldwork, as well as to Dr. Attila Kovács for providing phytoplankton cultures used in Chapter 7 experiments and for sharing part of his extensive knowledge of algae. I am grateful to many members of BLI and U. of Leicester administrative and technical staff for help with various things along the way. Thanks to Dr. Stephen Thackeray for his thoughtful and encouraging review of my thesis and for a very enjoyable discussion.

Thanks to Dr. Vadim V. Pelevin and Dr. Igor Goncharenko for making the long train trip from Moscow for the collaborative fieldwork described in Chapter 7, and for the sense of adventure, exploration and fun that they brought to the work. I would like to express my sincere appreciation to Dr. Peter D. Hunter, Professor Andrew N. Tyler and Dr. Vagelis Spyrakos for hosting me and including me in their team during my visit to the University of Stirling and their continuing, invaluable support and collaboration. I am grateful for the guidance of and discussions with Dr. Alistair Lamb, and to Dr. Thomas Lankester and Dr. Steven Hubbard of Airbus Defence and Space (Farnborough, UK) for adapting their PHAVEOS processing chain and providing the MERIS products used in Chapter 4 as well as for their patience and enthusiasm throughout this process. Thanks also to Dr. Jose Antonio Dominguez Gomez for having processed and provided the SCAPE-M_B2 products used in Chapter 5 and to Dr. Carsten Brockmann and Dr. Daniel Odermatt for making data available and for the CALVALUS processing of MERIS imagery used in Chapter 6. I am grateful for these collaborations and have really enjoyed and learned a lot from each. The time, knowledge, expertise and friendship that have been shared with me are greatly appreciated.

Funding for this research, as well as the possibility to attend several conferences and training workshops which have been crucial to my learning of the broader field of research, was provided by GIONET, funded by the European Commission, Marie Curie Programme Initial

Training Network, Grant Agreement PITN-GA-2010-264509. A doctoral scholarship from the Fonds de recherche du Québec – Nature et technologies, and is also gratefully acknowledged.

Personally, I am grateful to the friends I have had the opportunity to meet during the course of my PhD, especially the Pinter family, László, Emőke, Kamilla, Margareta and Marci, for so generously and readily including us in your family and offering much inspiration, advice and support. Also, Geri, Izabella, Zoltán T., Nóra, Péter T., Péter S., Diána, Attila, Zoltán V. and others for the good times at Pedro and cooking together which will remain nice memories of our time in Hungary. Kinga, Imre and the big Horváth family, for the countless times you have extended your welcome and generosity to us through many family meals, offerings of fruit and cakes, cups of tea (and pálinka), and more. Anci, for her patient and good-humoured introduction to the Hungarian language. The warm and welcoming community of PhD and post doc researchers, and my wonderful officemates from Biological and Environmental Sciences at the University of Stirling. Fellow GIONET ESRs, Dimitris, Linda, Christoff, Martyna, Max, Sybrand, Bernard, Pedro, James, Shailesh, Matthew, Jessica and Penelope, with whom I have shared much of this experience of the past three years and from whom I have learned much. Thanks to various members of the inland and coastal waters remote sensing community for welcoming a new researcher and for helpful discussions at different stages, as well as to the many fellow PhD students whom I have encountered during different training courses and conferences for their friendship, encouragement and interesting scientific discussion along the way.

The support of my friends and family far away, from PEI, Montréal, France and elsewhere, has meant so much to me and has provided comfort and motivation in so many moments. There is no way I could thank each of you enough. The all too rare times together during these past three years are cherished and I look forward to many more shared moments in the future.

My endless gratitude and love goes to Thibaut, who has shared this entire adventure with me, moving from Canada to Hungary and supporting me throughout the good as well as the many challenging times, always with positivity and encouragement. I learn so much from you and could not have done it without you!

This thesis is dedicated to my parents, Beryl and Allen, who never waver in their love and support of myself, their family and each other. You are, and always have been, great friends and inspirations to me.

Table of contents

List of figures

List of tables

List of acronyms and abbreviations

(A)ATSR	(Advanced) Along Track Scanning Radiometer
a	absorption
a_pig(443)	Pigment absorbance at 443 nm, retrieved by C2R, EUL, BL
$a_{pl}(440)$	Pigment absorbance at 440 nm, retrieved by FUB/WeW
$a_{CDOM}(440)$	CDOM absorbance at 440 nm
ALI	Advanced Land Imager
AMORGOS	Accurate MERIS Ortho-Rectified Geo-location Operational Software
ANOVA	Analysis of Variance
AOP	Apparent Optical Properties
AOT	Aerosol Optical Thickness
ARC-Lake	ATSR Reprocessing for Climate: Lake Surface Water Temperature & Ice Cover project
AVHRR	Advanced Very High Resolution Radiometer
β	Volume scattering function
b	total scattering coefficient
b_b	backscattering
BEAM	Basic ERS & ENVISAT (A)ASTER MERIS
BL	Boreal Lake processor
BLI	Balaton Limnological Institute
c	coefficient of beam attenuation
C2R	Case 2 Regional processor
Calvalus	Cal/Val and User Services

CDOM	Coloured Dissolved Organic Matter
Chl-*a*	Chlorophyll-*a* pigment
CWV	Columnar Water Vapour
CZCS	Coastal Zone Color Scanner
DOM	Dissolved organic matter
E_d	Downwelling radiance
EO	Earth Observation
ESA	European Space Agency
EUL	Eutrophic Lake processor
FLH	Fluorescence Line Height
FR	Full Resolution
FSG	full swath, georeferenced
FUB/WeW	Free University of Berlin Water processor
GMES	Global monitoring for environment and security (now "Copernicus")
GIONET	Copernicus (formerly GMES) Initial Operations Network for Earth Observation Research Training
HAB	Harmful Algal Bloom
ICOL	Improved Contrast between Ocean and Land
IOCCG	International Ocean Colour Coordinating Group
IOP	Inherent Optical Properties
KBWPS	Kis Balaton Water Protection System
L1b, L2	Level 1b, Level 2, etc. satellite imagery
KdKVI	Közép-dunántúli Környezetvédelmi, Természetvedelmiés Vízügyi Felügyeloség (*Central Transdanubian (Regional) Inspectorate for Environmental Protection, Nature Conservation and Water Management*)
LiDAR	Light Detection and Ranging

LST	Land Surface Temperature
LSWT	Lake Surface Water Temperature
L_u	Upwelling radiance
masl	metres above sea level
MCI	Maximum Chlorophyll Index
MERIS	Medium Resolution Imaging Spectrometer
MISR	Multi-angle Remote Sensing
MODIS	Moderate Resolution Imaging Spectrometer
MSI	Multispectral Imager
NASA	National Aeronautics and Space Administration
NIR	Near-infrared
NN	Neural network
OECD	Organization for Economic Cooperation and Development
OLCI	Ocean and Land Colour Imager
PAR	Photosynthetically Available Radiation
PHAVEOS	PHenology And Vegetation Earth Observation Service
PSI, PSII	Photosystem I, II
ROI	Region of interest
RR	Reduced Resolution
RMSE	Root Mean Square Error
R_{rs}	Remote sensing reflectance
SCAPE-M	Self-Contained Atmospheric Parameters Estimation for MERIS data
SD	Standard deviation
SeaWiFS	Sea-Viewing Wide Field-of-View Sensor
SIOP	(Mass) Specific IOP

SPOT	Satellite Pour l'Observation de la Terre (*Satellite for Earth observation*)
SST	Sea Surface Temperature
SWIR	Shortwave-infrared
TOA	Top-of-Atmosphere
TSM	Total suspended matter
UFL	Ultraviolet fluorescence LiDAR
UV	Ultraviolet
VI	Vegetation Index
WFD	Water Framework Directive
β	Volume scattering function

Chapter 1

Introduction and thesis overview

1.1 Research context

Freshwater resources provide a myriad of habitats, resources and ecosystem services, both extractable and non-extractable. Lakes in particular have been found to be sensitive sentinels to changes in the adjacent landscape and in climate conditions (Adrian et al. 2009; Williamson et al. 2009), and to face a broad range of threats to their ecological functioning and biodiversity (Beeton 2002; Brönmark and Hansson 2002; Duker and Borre 2001). Symptoms of eutrophication, such as intensified algal blooms and altered phytoplankton species composition, have been observed to increase under warming scenarios which are predicted with climate change (Moss 2012). As such, lake phytoplankton monitoring has increasingly been recognized by both science and policy realms as vital. Satellite remote sensing has been proposed as a powerful tool to monitor a number of water quality parameters, notably phytoplankton biomass via the remotely sensed optical signal of the pigment chlorophyll-*a* (chl-*a*) (IOCCG 2000). Robust chl-*a* concentration and other biogeochemical parameter retrievals have been demonstrated to be possible, although not consistently so, in a broad range of lake settings using satellite imagery (Matthews 2011; Odermatt et al. 2012).

Numerous challenges continue to impose upon the remote sensing of lake water constituents, due in large part to the high optical complexity and variability associated with inland waters. The study site of this thesis, Lake Balaton in western Hungary, itself presents a broad range of optical conditions and water constituent concentrations which vary over space and time, and thus presents particular challenge and opportunity from a remote sensing perspective. Likewise, historical eutrophication and the regular recurrence of algal blooms affect water quality, tourism and lake ecology more broadly. Phytoplankton monitoring is of great interest for the management and research of Lake Balaton, and a vast *in situ* chl-*a* dataset is available from conventional monitoring programs for the development and validation of remote sensing products. This thesis intends to build upon achievements and progress made by the lake remote sensing research community over the past decades and to contribute via quantitative evaluation, application and adaptation of existing approaches to the Lake Balaton context as well as through the development, testing and demonstration of novel directions linking remote sensing and limnology.

Given increasingly robust chl-*a* retrievals for many inland waters for example, it is now timely to consider ways to go beyond mapping concentrations to quantitative spatiotemporal analyses that make use of the regular periodicity of satellite remote sensing. Phytoplankton phenology metrics are proposed here as a suite of parameters that have the potential to serve as important ecological indicators, as has been demonstrated via *in situ*, mesocosm and modeling data from other lake sites. Analogous parameters have a long history of retrieval via remote sensing for terrestrial vegetation (Boyd et al. 2011; Dash et al. 2013; Justice et al. 1985; Malingreau 1986), and increasingly in open ocean settings (Platt et al. 2010; Platt et al. 2009; Racault et al. 2012; Sasaoka et al. 2011; Siegel et al. 2002), as well as to a certain extent for a limited number of lakes (Binding et al. 2011; Duan et al. 2014; Hu et al. 2010; Matthews 2014; Stumpf et al. 2012) which suggest the potential for further development in this area.

Following the validation and comparison of several chl-*a* retrieval algorithms applied to Medium Resolution Imaging Spectrometer (MERIS) imagery of Lake Balaton (Palmer et al. 2015a), as well as deliberation on the underlying causes of the relative success and failure of the different algorithms, the measurement and mapping of phytoplankton phenology metrics in the lake is undertaken using MERIS imagery (Palmer et al. 2015b). Another remote sensing approach common in oceanic settings but not yet applied extensively to inland freshwaters, making use of active, laser-induced fluorescence of phytoplankton pigments (Babichenko 2008) is also investigated. The performance of ship-mounted fluorescence light detection and ranging (LiDAR) measurements of chl-*a* and other water constituents is tested under a range of possible freshwater conditions through a series of laboratory tank experiments and field measurements carried out on Lake Balaton (Palmer et al. 2013).

For a great many lakes worldwide, remote sensing offers enormous potential for new insights, particularly where *in situ* monitoring may be absent or sparse due to the given geographic, political or economic context. However, remote sensing methods must be developed and tested through comparison with trusted conventional data before their reliable application in such data-limited settings. As such, Lake Balaton provides an ideal case study, with a long history of active research and available monitoring data spanning the MERIS archive considered in this thesis. Not only do measurements encompass multiple years, but all seasons as well, and are distributed across the spatial extent of the lake. Furthermore, even in lakes where conventional monitoring is underway, remote

sensing data offer an additional view with regards to its cohesive spatial and temporal resolutions and coverage, and should be considered a complementary data source. Certain limitations of conventional data have the potential to be more fully addressed through the use of satellite products, and *vice versa*. This thesis aims to test and develop such satellite, as well as ship-mounted remote sensing products toward adding to the knowledge of Lake Balaton phytoplankton dynamics on the one hand, and demonstrating novel remote sensing approaches that might be applied to other lake systems on the other.

1.2 Thesis structure, objectives and questions

The thesis chapters are largely grouped into three sections (Figure 1.1). First, chapters one through three together present the general context and background information; introducing the thesis itself, the broader field of study, and the study site and related previous works undertaken there. Chapters four through seven present the analyses carried out in order to answer the research questions described below and the results thereof, with validation results from chapters four and five informing the phenological analyses carried out in chapter six. Chapter seven presents the exploratory field and laboratory measurements of a novel, fluorescence LiDAR approach to lake remote sensing. Chapter eight provides a synopsis of the thesis work, highlighting the main achievements and conclusions as well as identifying future research priorities revealed by the thesis findings.

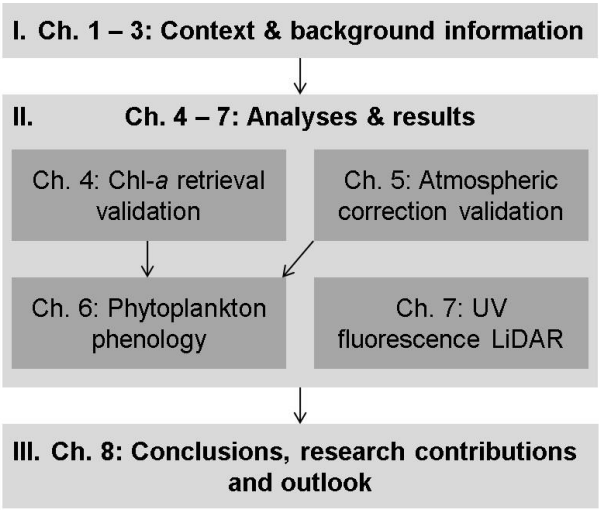

Figure 1.1. Sections and subsections comprising the thesis structure.

In light of the general research context described in Chapter 1.1, the following questions are sought to be addressed through this thesis. Chapters four and five report the validation exercises applied to satellite image chl-*a* retrieval and atmospheric correction algorithms, and resulting implications. In chapter four, the comparison of calibration and validation results of six chl-*a* algorithms is carried out using extensive archive *in situ* data from the study site, Lake Balaton. The performance of two atmospheric correction models are considered in chapter five along with the influence of atmospheric correction on chl-*a* retrievals from MERIS imagery. The overall performances of the tested chl-*a* retrieval and atmospheric correction algorithms, as well as spatial and temporal patterns uncovered, are discussed and validation is considered in mapping and through application to multi-year time series. In particular, the following questions are addressed:

How do the chl-a retrievals of different algorithms compare for Lake Balaton?

What is the influence of atmospheric correction on chl-a retrieval performance?

Which algorithms are best suited for the mapping and monitoring of Lake Balaton phytoplankton blooms from MERIS satellite data?

In chapter six, the application of the selected chl-*a* retrieval algorithm, informed by the results of chapters four and five, to the full MERIS image archive from 2002 to 2012 is undertaken so as to examine satellite-derived phytoplankton biomass time series, and phenology metrics in particular. Although commonly retrieved from remote sensing in analyses of terrestrial vegetation, and increasingly for oceanic phytoplankton, freshwater phytoplankton phenology has not yet been fully considered through a remote sensing approach. This is examined here, and ecological indicators related to phenology are extracted, mapped and evaluated in application to Lake Balaton. The following questions are addressed:

Can phytoplankton phenology metrics be derived from and mapped using MERIS satellite imagery and TIMESAT software in a lake setting?

How does phytoplankton phenology vary inter-annually in Lake Balaton?

How do phenology features vary spatially across Lake Balaton?

Although not uncommon in oceanographic research, the use of ship-mounted ultraviolet fluorescence LiDAR (UFL) has not yet been tested or applied in an inland water setting. A series of experimental laboratory tank and field measurements on Lake Balaton was carried out to investigate potential challenges posed by the more optically complex nature of inland waters compared with pelagic oceanic settings, as well as to identify insights that UFL can contribute through measurements of chl-*a*, as well as other important optically significant water quality parameters, coloured dissolved organic matter (CDOM) and total suspended matter (TSM). The following questions are addressed in Chapter seven:

Can UFL present a reliable means to measure chl-a, as well as TSM and CDOM in optically complex lake settings?

Do UFL measurements remain robust at high chl-a and TSM concentrations, achieved through laboratory tank measurements?

Can UFL retrieved signals of different phytoplankton taxa be distinguished?

Chapter 2

Remote sensing of lake water quality

This chapter begins by highlighting some of the challenges facing water resources and aquatic ecosystems that have been observed throughout the world. Although remote sensing may provide a tool to assist managers and researchers concerned with such issues, its use and interpretation are not straightforward. The biophysical principles behind the remote sensing of water constituents are introduced, as are some of the difficulties associated with this task, including those that distinguish the remote sensing of so-called optically complex coastal and inland waters from that in open ocean settings. The general methodology behind the retrieval of water constituents, including chl-*a*, are presented, and several key features and achievements associated with MERIS, used in this thesis, are highlighted.

2.1 Remote sensing for lake water quality monitoring

Lakes are important components and regulators of global carbon, nitrogen and phosphorous cycling, are vital within the hydrologic cycle, in addition to providing diverse habitat for rich biodiversity (Bastviken et al. 2011; Brönmark and Hansson 2002; Duker and Borre 2001). Human populations also rely on lake systems for the provision of food and of water for drinking, other household uses, industry, irrigation, as well as for energy, recreational and cultural uses (Johnson et al. 2001; Postel 2000). As freshwater resources are limited, their various uses are in direct competition with one another where they co-occur. Furthermore, inland aquatic ecosystems are sensitive to environmental changes, and face increasing, synergistic threats. These are related to climate change, the introduction, establishment and spread of exotic (alien or invasive) species, contamination (organic and inorganic), eutrophication, acidification, loss of biodiversity and the diversion of upstream source waters. Such stresses lead to changes in the physiochemical and biological structures of lakes and impacts cascade throughout associated ecosystems, including to humans (Brönmark and Hansson 2002; Khan and Ansari 2005; Ricciardi and Rasmussen 1999; Sala et al. 2000; Suski and Cooke 2007).

Due to their sensitivity to environmental change, and particularly to their capacity to integrate changes in the adjacent landscape (catchments) and atmosphere, lakes have widely been considered potential sentinels of climate change, with several measureable signals identified (Adrian et al. 2009; Williamson et al. 2009). Planktonic species are

affected by temperature and nutrient changes, are characterized by short generation times, and are thus considered especially sensitive indicators of climate and other environmental change (Adrian et al. 2009; Carvalho et al. 2013; Hays et al. 2005; Richardson 2008; Taylor et al. 2002). Results generally concur that warming trends will result in increased and intensified effects of eutrophication (Moss 2012), and ongoing monitoring has an important role to play in attributing and quantifying changes (Carvalho et al. 2013; Lovett et al. 2007).

The current and anticipated degradation of freshwaters and associated ecosystems have become increasingly apparent and pressing over recent decades, and policy actions have been called upon as means to measure, mitigate and remediate such degradation (Bates et al. 2008; Dudgeon et al. 2006). In the United States, the Environmental Protection Agency's Clean Water Act, dating back to 1972 and updated through amendments as recently as 2002, regulates pollution discharge to water bodies and water quality monitoring (US Congress, 1977). The Water Framework Directive (WFD) of the European Commission (EC Guidance Document No 10, 2003) aims to protect and enhance the quality of European waters and aquatic ecosystems (Chen et al. 2007; Dworak et al. 2005a; Dworak et al. 2005b; Hering et al. 2013). The importance of assessment across multiple spatial scales is emphasized within the WFD, with a focus on the catchment scale and on on-going monitoring so as to quantify trends in the degradation or the rehabilitation of systems to a desired status. In the case of the WFD, all European surface waters (lakes, rivers, coastal and transitional waters) are required to achieve a status of "good" by the year 2015 (Hering et al. 2013).

Given the high level of diversity in biological, chemical, physical, hydrological and morphological characteristics from lake to lake, and typically even within a given lake, a precise definition of "good" can be difficult to achieve. A number of indices and indicators, both physiochemical- and biologically-based, have been proposed, as have various classification schemes that make use of different combinations of such indicators. Changes in some of these parameters may be useful in indicating overall changes in water quality. The widely-used biological classification scheme of the Organization for Economic Cooperation and Development (OECD) is based on the trophic state index of the lake, an absolute measure of biomass, nutrient status and transparency of a lake system at a given time. Lakes, or parts of lakes, are classified as either hypertrophic, eutrophic, mesotrophic, oligotrophic, or ultra-oligotrophic (OECD 1982). The classification system

promoted by the WFD makes use of biological indicators, known as biological quality elements (BQEs), which are divided into phytoplankton, aquatic flora, fish and benthic invertebrates (Hering et al. 2013). The WFD aims to incorporate numerous hydromorphological, biological and physiochemical parameters, as well as the notion of ecoregions, which are generally identified as "areas within which there is spatial coincidence in characteristics of geographical phenomena associated with differences in the quality, health, and integrity of ecosystems" (Omernik 2004, page S33) and other geographical and abiotic features in an attempt to standardize the classification of inland water bodies while taking into account the diverse landscapes and climates of Europe (Dworak et al. 2005a). Carvalho et al. (2013) report the assessment of a variety of metrics for monitoring phytoplankton as part of the WFD across a range of European Union Member States, and have identified chlorophyll-*a* (chl-*a*), cyanobacteria biovolume and Phytoplankton Trophic Index (PTI), a measure of taxonomic composition, as most suitable. The use of the proposed metrics was further supported by results of Thackeray et al. (2013), that more than 85 % of the variance in the metric scores was among the sampled lakes, rather than due to differences related to sample processing, and was well predicted by total phosphorous concentration which is a main indicator of eutrophication. It should be noted that monitoring, in terms of identifying anthropogenic impacts for example, based on any system or set of parameters first requires knowledge of some baseline condition with which to compare (Lovett et al. 2007), and this notion is also embedded within the WFD classification guidelines (EC Guidance Document No 10, 2003).

The natural variability of lakes over time, seasonal or otherwise, is potentially difficult to untangle from anthropogenic-induced changes and poses a significant challenge to monitoring strategies, in addition to the inter- and intra- lake spatial variability. Such natural variability is also often crucial to the health and functioning of lake ecosystems, as is the case for most ecosystem types, and may itself be desirable to preserve or recover (Erlandsson et al. 2008; Landres et al. 1999). Accounting for the natural variability of systems while attempting to identify and minimize anthropogenic change augments the demand placed on both baseline and monitoring information in terms of temporal and spatial coverage. Likewise, causes and effects of environmental change on lake systems, as well as signs of recovery and restoration, occur at diverse spatial and temporal scales, which is an important consideration in the interpretation of

monitoring data (Hering et al. 2013). A minimum sampling frequency has therefore been calculated and proposed for the phytoplankton metrics associated with the WFD, mentioned above (Thackeray et al. (Appendix 2) in Mischke et al. 2012).

Traditional monitoring through point samples or measurements can be limited and resource-intensive, however, and in many instances globally is simply impossible. The latter case occurs particularly when lakes are remote or when resources necessary to undertake monitoring are insufficient. Remote sensing has been identified as an alternative, or more realistically as a complementary source of data, having the potential to play an important role in the spatially and temporally cohesive monitoring of lake water quality, providing regular measurements of entire lake surfaces on the order of daily, weekly or monthly, depending on the satellite sensor and lake geographic context in question (Bresciani et al. 2011; Chen et al. 2007; Glasgow et al. 2004). Although many parameters required to be monitored by the WFD cannot be measured using remote sensing technologies, some proxies can be derived, including remotely sensed chl-*a* concentration as a proxy for phytoplankton biomass, as will be discussed further in Chapter 2.2.

Space-based, satellite remote sensing of lake water quality is a promising complement to traditional point sampling strategies, though its development and implementation for lake waters is complex and on-going (Matthews 2011; Odermatt et al. 2012). Airborne and ship-mounted remote sensing solutions may further complement the satellite data able to be acquired, providing data at small to intermediate spatial scales (< 1 – 100 m). Although such approaches are limited in terms of providing regular, continuous datasets through time, their punctual campaigns have the advantage of being quite flexible in terms of targeting a specific period or geographic location, for example so as to capture an event or process of interest (algal bloom, terrestrial runoff, etc.), and their often high spatial and spectral resolutions are also advantageous (Matthews 2011). Furthermore, *in situ* point measurements remain crucial within the larger framework of remote sensing, as sufficient reference data are required to develop and test the accuracies of models relating satellite remote sensing data to *in situ* water quality parameters so as to reliably apply them to mapping more broadly (Sriwongsitanon et al. 2011). A combination of datasets covering a range of temporal and spatial resolutions, including both remote sensing and *in situ* sampling, would thus be ideal.

2.2 Remote sensing of optically significant water quality parameters

2.2.1 Optically significant substances

The study of water quality parameters through remote sensing can largely be understood through their influence on water colour, given that some parameters of interest (optically significant substances) reflect or absorb solar radiation at different wavelengths across the visible and near-infrared electromagnetic spectrum. Water containing very little dissolved or suspended matter tends to appear dark blue, absorbing the least amount of light in the wavelengths associated with that colour (400-500 nm) (Braun and Smirnov 1993). In the context of the optical properties of a water column, three main groups of optically significant substances affect water-leaving radiance through the scattering and absorption of light, in addition to the effect of pure water, which is a hypothetical medium consisting of only water molecules and dissolved inorganic matter. These are (1) phytoplankton, (2) total suspended matter (TSM), also known as suspended particulate material and occasionally broken down into living and non-living, or organic and inorganic components which can be distinguished optically, and (3) coloured dissolved organic matter (CDOM), also known as gelbstoff, yellow substance, or gilvin (IOCCG 2000). It should be noted that substances that do not substantially alter the optical signal of the water, such as bacteria or viruses, are very important for overall water quality but cannot be directly measured through remote sensing.

Phytoplankton are microscopic, free-floating, autotrophic organisms that are found in the upper, sunlit layer of water bodies (oceanic as well as freshwater). Through carbon fixation and photosynthesis, they form the base of aquatic and oceanic food chains and play a major role in the global carbon cycle (Reynolds 2006). Phytoplankton in very high concentrations, known as algal blooms, can be detrimental to aquatic ecosystems, however. Under eutrophic and hyper-eutrophic systems, large quantities of algal biomass block sunlight and lead to depleted oxygen conditions as dead plant matter decomposes (Istvánovics 2010). The presence and amount of phytoplankton biomass is commonly determined through measurements of biovolume or of chl-*a*, the main pigment common to phytoplankton species. Chl-*a* is characterized optically by strong absorption at blue

and red wavelengths (Hunter et al. 2008a; Sváb et al. 2005), as well as a strong and narrow fluorescence signal at 685 nm (Barbini et al. 1998), and a peak at around 705 nm is also typical under high biomass conditions due to phytoplankton backscattering.

Thousands of phytoplankton species have been identified, however, and many taxa are associated with distinguishing auxiliary pigments in addition to chl-*a*, such as chlorophyll-*b*, phycocyanin, carotenes and xanthophylls, which each have their own characteristic absorption, reflectance and fluorescence signals. Individual phytoplankton groups thus display variation in their spectral response profiles due to characteristic reflectance and absorbance of visible light at distinct wavelengths (Aguirre-Gómez et al. 2001a; Aguirre-Gómez et al. 2001b; Vaillancourt et al. 2004). In addition to measuring phytoplankton biomass in general, it can therefore be possible to measure that of certain individual, targeted taxa given adequate spectral coverage and resolution (Hunter et al. 2010; Hunter et al. 2008a). Taxonomic composition within a given water body can vary over time and space, and some taxa may be considered more important to identify and monitor than others. For example cyanobacteria, commonly known as blue-green algae, may produce cyanotoxins and form potentially harmful algal blooms (HABs) (Hunter et al. 2008b; Paerl and Huisman 2008, 2009).

TSM encompasses the broad range of organic and inorganic, living and non-living material found suspended in the water column. The inorganic component is generally dominated by sediment introduced by rivers or resuspended from the bottom through wave action and currents, and thus occurs predominantly in relatively shallow coastal zones or inland waters rather than in deep open-ocean water where surface energy is unlikely to reach the bottom (IOCCG 2000; Miller and McKee 2004). Concentrations of suspended material are closely linked to the clarity or turbidity of the water, and consequently the light availability for photosynthesizing aquatic organisms (Havens et al. 2011; James et al. 2009). Nutrient dynamics and pollutant transport have also been found to be influenced by suspended sediment concentrations (Martin and Windom 1990; Mayer et al. 1998; Miller and McKee 2004). The characteristic response spectrum of suspended matter in the visible range tends to be quite broad as a result of its general reflectance, lacking specific absorption or fluorescence features such as described above for phytoplankton. It can, however, be somewhat variable in its specific effect on water colour depending on sediment type (e.g., red, iron-rich clays versus white, calcareous silts or sands) (IOCCG 2000).

The CDOM component consists of the light-absorbing fraction of dissolved organic material (DOM) (Kutser et al. 2005), mainly humic and fulvic acids produced by the degradation of organic particles such as phytoplankton cells and wetland vegetation (IOCCG 2000). High concentrations can also be transported by rivers and thus do not necessarily reflect local processes originating within the lake. Imported terrestrial CDOM is important to lake ecosystems due to the external source of carbon provided and its influence on light availability for aquatic biota, including protection from potentially-harmful UV-B radiation (Kutser et al. 2005). CDOM is rapidly photodegraded (broken down through exposure to UV radiation from the sun) (V.-Balogh et al. 2003). Although the water-leaving spectral response related to CDOM tends to be variable, absorbance between 420 and 440 nm is a commonly used proxy, and a broad fluorescence peak centred at 440 nm is also known to exist (Brezonik et al. 2005; Hu et al. 2004; Kutser et al. 2005; Lee et al. 1994).

2.2.2 Inherent and Apparent Optical Properties

Inherent Optical Properties (IOPs) describe the wavelength-dependent absorption (a) and the Volume Scattering Function (β), from which the total scattering coefficient (b) is determined, and their cumulative effect on the coefficient of beam attenuation (c) (eq. 2.1) (IOCCG 2006). Backscattering (b_b) integrates the volume scattering function (β) over the angles 90-180°. The total absorption ($a_{total}(\lambda)$) and backscattering ($b_{b\ total}(\lambda)$) can be further broken down into the contributions from each of the three optically significant constituent types described above (phytoplankton - $a_{ph}(\lambda)$, $b_{b\ ph}(\lambda)$; tripton (non-living suspended matter) $a_t(\lambda)$, $b_{b\ t}(\lambda)$; CDOM - $a_{CDOM}(\lambda)$) and from the water itself (a_w, $b_{b,w}$) (eq. 2.2 and 2.3). The IOPs are characteristic of the media, without influence from ambient light conditions (Kirk 1994).

$$c(\lambda) = a_{total}(\lambda) + b_{b\ total}(\lambda) \qquad \text{Equation 2.1}$$

$$a_{total}(\lambda) = a_w(\lambda) + a_{ph}(\lambda) + a_t(\lambda) + a_{CDOM}(\lambda) \qquad \text{Equation 2.2}$$

$$b_{b\ total}(\lambda) = b_{b\ w}(\lambda) + b_{b\ ph}(\lambda) + b_{b\ t}(\lambda) \qquad \text{Equation 2.3}$$

Measurements via remote sensing, however, also include the influence of the light field at the time of measurement, as well as sensor and measurement geometry. Measurements are therefore of Apparent Optical Properties (AOPs), such as remote sensing reflectance (R_{rs}) which is the ratio of radiance upwelling from the surface of the water (L_u) to that downwelling from the sun (E_d) (eq. 2.4). AOPs can be related quantitatively to IOPs via the use of a constant, *f*, dependant on the measurement light field and β (eq. 2.5) (Gordon et al. 1975; Preisendorfer 1961), and IOPs to concentrations of optically significant substances through applying tuned coefficients, known as specific inherent optical properties (SIOPs).

$$R_{rs}(\lambda) = L_u(\lambda)/E_d(\lambda) \qquad \text{Equation 2.4}$$

$$R_{rs}(\lambda) = f\,(b_{b\ total}(\lambda) / a_{\ total}(\lambda) + b_{b\ total}(\lambda)) \qquad \text{Equation 2.5}$$

2.2.3 Optical water types

A general optical classification of natural surface waters (both freshwater and oceanic) into Case 1 and Case 2 types was introduced (Morel and Prieur 1977) and later updated (Gordon and Morel 1983; Morel 1988). The main distinction between the two classes is the much greater optical complexity inherent to Case 2 waters. Case 1 waters are those whose optical properties are dominated by phytoplankton. Though other components (CDOM, TSM) may be present, their influence on the overall optical properties of the host water is insignificant given their generally low concentrations and the fact that they co-vary linearly with, and are typically by-products of, phytoplankton (IOCCG 2000). The optical properties of Case 2 waters on the other hand are influenced independently and to varying degrees by all three components described above, which may each be present in a broad range of concentrations. Furthermore, the influence of each component on the water-leaving spectral response of a water body overlaps with the others and unique signatures are thus difficult to distinguish. Rather, at any given wavelength studied, a linear, one-to-one relationship with any of the components cannot be assumed (IOCCG 2000).

Although not universally the case, Case 1 waters are generally open-ocean waters, which tend to be relatively transparent due to the lack of or low inorganic suspended matter or externally-sourced CDOM influence, whereas coastal zone and inland waters are often of Case 2 type due to the potential for bottom sediment resuspension or suspended matter and CDOM input from adjacent terrestrial environments (river inflow or surface runoff), and generally higher phytoplankton biomass. The majority (> 90%) of the world's surface waters are of the Case 1 type; however the possible optical variety presented by Case 2 waters is much greater. In fact, whereas Case 1 waters are strictly defined as being optically dominated by phytoplankton, Case 2 can be understood as everything that is not Case 1 (IOCCG 2000). These include waters dominated by one component other than phytoplankton (either TSM or CDOM), those dominated by a combination of two components with the third playing a minor role, and those where all three components are important (IOCCG 2000). The diversity of the so-called Case 2 waters poses an enormous challenge to their remote sensing, requiring either site-specific or extremely broad retrieval algorithm calibration so as to encompass the full range of conditions possible to encounter.

The relative difficulty of remotely sensing Case 2 waters compared with the remote sensing of Case 1 waters stems from this optical complexity and variability. This is both in terms of potential sensors, which require much greater spectral resolution and coverage and radiometric accuracy and precision (high signal-to-noise ratio), as well as more complex algorithms to successfully derive different components from their overlapping spectral responses (IOCCG 2000). It should also be noted that although this traditional classification system is still commonly used and referred to, its discontinuation has been proposed due to the continuum that the two cases comprise in reality both in terms of concentrations of parameters (there is no real, quantitative divide distinguishing so-called Case 1 from so-called Case 2 waters) and because of the temporal variability (i.e., a location may be classified as Case 1 at some times (e.g., high tide) but Case 2 at other times (e.g., low tide)) (Mobley et al. 2004).

2.2.4 Additional challenges in lake remote sensing

In addition to the high optical complexity characterising the water itself, several other features specific to lakes add to the challenge of measuring their water quality components using remote sensing techniques.

Atmospheric correction

The atmosphere contributes as much as 90 % of the top-of-atmosphere (TOA) signal measured by a satellite sensor over water (Siegel et al. 2000; Vidot and Santer 2005). Accounting for and removing this contribution, particularly scattering by aerosols, can therefore be important in the retrieval of water constituents such as phytoplankton biomass, but is challenging due to the optical complexity and high degree of spatial and temporal variability in both atmospheric and in-water conditions. Atmospheric correction methods successfully used for remote sensing of open ocean water quality rarely work when applied to coastal zones or lake waters. Bands considered to only reflect atmospheric conditions (specifically bands in the near-infrared part of the spectrum between 765 and 865 nm), known as the "black" or "dark" pixel assumption, may contain a signal from the higher concentrations and additional components of optically complex, so-called Case 2 waters, particularly suspended particulate matter (IOCCG 2000; Moore et al. 1999; Ruddick et al. 2000; Siegel et al. 2000). The use of longer, shortwave-infrared (SWIR) bands (wavelength > 800 nm) has been proposed as an alternative (Wang 2007), but a non-negligible water-leaving signal in this spectral range has since been demonstrated for very turbid waters (Knaeps et al. 2012; Shi and Wang 2009).

A variety of approaches have also been presented that invert of top-of-atmosphere (TOA) radiances through radiative transfer modelling, such as Second Simulation of the Satellite Signal in the Solar Spectrum (6S) atmospheric correction (Vermote et al. 1997), or using artificial neural network techniques, including neural networks designed specifically for use over optically complex waters (Schroeder et al. 2007a). Depending on the size and geographic context of a given lake, atmospheric correction models used over land and extrapolated or interpolated over the water surface may suffice, as in the case of the coastal Waters and Ocean MODTRAN-4 Based ATmospheric correction (c-Wombat-c) model (Brando 2008) and the Self-Contained Atmospheric Parameters Estimation for MERIS data (SCAPE-M) model (Guanter et al. 2007; Guanter et al. 2008;

Guanter et al. 2010). Though each of these approaches and specific models has been proven to perform well in some instances, none is universally successful. Rather a case-by-case approach is generally followed, though a more broadly robust approach is currently a priority of the coastal and inland water remote sensing community. Although temporal variability in atmospheric conditions unaccounted for in uncorrected, TOA data or in only partially corrected, bottom-of-Raleigh data introduces a source of error, this has nonetheless been found to result in robust water constituent retrievals (Matthews et al. 2010; Matthews et al. 2012; Palmer et al. 2015a).

Adjacency effect

The adjacency effect, also referred to as the background or environmental effect, is related to the reflectance of much brighter land next to the generally darker water, leading to the contamination of the optical signal of water pixels. Light reflected from land is in some instances forward scattered into the adjacent water pixels causing a blurring between land and water pixels. This may skew water quality parameter measurements and/or result in the breakdown of atmospheric correction (Sterckx et al. 2011). The adjacency effect was first reported in association with Landsat imagery in the 1980s in both coastal and inland water settings (Kaufman and Joseph 1982), and has been identified in airborne and satellite-based hyper- and multispectral imagery since (Reinersman and Carder 1995; Van Mol and Ruddick 2004). This effect can largely be removed through some atmospheric correction codes such as 6S, Scape-M and Moderate Resolution Transmission (MODTRAN) or through dedicated modelling. The Improved Contrast between Ocean and Land (ICOL) algorithm (Santer and Zagolski 2008) has provided major improvements to or had a neutral effect on atmospheric correction and constituent retrieval in some cases (Sterckx et al. 2011; Sterckx et al. 2012; Vermote et al. 1997). However, overcompensating for such effects through over-modelling has been observed elsewhere, and can be equally damaging to the reliability of derived data (Sterckx et al. 2011; Sterckx et al. 2012; Vermote et al. 1997).

Size and geometry

Due to their inland location, relatively small size and often irregular geometry, a large number of lake water pixels tend to also contain land components (these are commonly referred to as mixed pixels, imaging both land and water in various proportions) (Kay et al. 2005; Sentlinger et al. 2008). As the remote sensing reflectance

determined for a given pixel will be influenced by all surfaces contained within that pixel, information pertaining to the water body alone cannot (or is very difficult to) be attained. The relative importance of mixed pixels for a given lake also depends on the spatial resolution of the sensor. For example, the spatial resolution of sensors designed primarily for use in ocean colour remote sensing such as the Coastal Zone Colour Scanner (CZCS), the Sea-Viewing Wide Field-of-View Sensor (SeaWiFS) and the ocean colour bands of the Moderate Resolution Imaging Spectroradiometer (MODIS) is approximately one kilometre. Although this is perfectly suitable for open-ocean measurement and monitoring applications, most lakes would contain too few, if any, pure, unmixed water pixels at this spatial resolution for remote sensing to be directly applied (Sentlinger et al. 2008). As the spatial resolution of imagery improves, the total area lost to mixed pixels is reduced. Some multispectral sensors designed and tested as suitable for remote sensing of Case 2 water quality parameters improve upon such spatial resolutions, offering 300 m resolution in the case of ENVISAT's MERIS, or 250 – 500 m resolution in the case of some MODIS bands. However, in the cases of many lakes these too prove inadequate.

Bottom effect

Depending on the combination of water depth and transparency, lakes can be considered either "optically shallow", whereby incoming solar radiation can penetrate the full water column and reflect back off the bottom to be detected by a sensor, or "optically deep", whereby incoming radiation is attenuated more rapidly, does not reach and is not reflected by the bottom because of the highly turbid and/or very deep water. Where waters are optically shallow, the bottom effect must be accounted for, adding yet another component to consider in modelling water-leaving radiance (Giardino et al. 2011; IOCCG 2000; Ma et al. 2011; Voss et al. 2003). Whether a lake can be expected to be optically deep or shallow depends upon optical properties and depth of the water and the optical properties of the bottom (Lodhi and Rundquist 2001). The bottom effect has been calculated to be negligible when secchi depth (a measure of transparency whereby the water depth after which a black and white disk is no longer visible is estimated) is 2.5 – 3 times less than total water depth (Mueller and Austin 1995). In cases where the bottom effect cannot be assumed to be negligible, its albedo can be measured, included in bio-optical modelling and removed from total water-leaving radiance (Albert and Mobley 2003; Giardino et al. 2011; Lee et al. 1994; Lee et al. 1999).

2.2.5 Constituent retrieval algorithms

Given the wavelength specificity of different optically significant substances on the optical properties of the water column, different models have been proposed to quantitatively relate remotely sensed AOPs to constituent concentrations, either directly or via quantification of IOPs. Band arithmetic type models directly fit statistical relationships between reflectance measured at one or more different wavelengths (different bands of a given sensor) and the constituent concentrations (Matthews 2011). Such algorithms deriving chl-*a* concentrations in lakes typically make use of chl-*a* absorption, backscattering or fluorescence features in the red and near-infrared range which are less affected by other optically significant substances, compared with the blue and green range typically used in open ocean (so-called Case 1) settings (Dall'Olmo et al. 2005; Gower et al. 1999). Relationships are determined for one constituent at a time, and coefficients and even band combinations found to successfully retrieve concentrations at one site are likely to completely fail at another, where site-specific calibration and coefficient tuning is required. The same has been found to be true at the same lake, from season to season or year to year or from different parts of the same lake; the algorithm is dependent on the calibration dataset for which it was trained. On the other hand, many band arithmetic type algorithms have been found to very robustly retrieve constituent concentrations for the site and conditions for which they were trained, and several band combinations have proven transferable between sites given the local calibration of model coefficients (Matthews 2011; Odermatt et al. 2012)

Another algorithm type makes use of radiative transfer-based bio-optical modelling (Lee et al. 2002; Maritorena et al. 2002; Mobley 1994; Preisendorfer 1961). A forward model relating IOPs to AOPs is inverted to acquire IOPs from remotely sensed AOPs. Despite their strong, physical basis, these algorithms are also limited in that they require large datasets of difficult to obtain optical properties and extensive parameterization, not feasible for many sites and often acquired only during punctual campaigns. Furthermore, the retrieval of chl-*a* and other constituent concentrations from the retrieved IOPs depends on the specific inherent optical property coefficients (SIOPs) relating IOPs to constituent concentrations for a given site, and is therefore also site specific. The high *in situ* data requirement is also the case for training neural network type algorithms, which typically use remotely sensed AOP data as the input layer, and

IOPs and constituent concentrations as the output (Doerffer and Schiller 2007; Doerffer and Schiller 2008; Schroeder et al. 2007a).

2.2.6 MEdium Resolution Imaging Spectrometer (MERIS)

The remote sensing of lakes and coastal zones has evolved in part from adaptations and advances to the sensor and algorithm design used in open ocean waters (IOCCG 2000). It should be noted that although these are not generally suitable themselves for the remote sensing of coastal and inland waters due to their low spatial resolutions and spectral characteristics, ocean colour satellite sensors are extremely useful and well-suited for exactly the purpose for which they were designed – the monitoring of chl-*a* and the broad estimation of phytoplankton biomass over large open-ocean areas – and are now used in operational monitoring (Gordon 2010; IOCCG 2000). Furthermore, coarse resolution ocean colour satellite sensors have been applied in the case of very large lakes, such as the American/Canadian Laurentian Great Lakes (Binding et al. 2007; Pozdnyakov et al. 2005; Shuchman et al. 2006), Lake Lagoda (Pozdnyakov et al. 2013) and Lake Baikal (Heim et al. 2005).

Higher spatial resolution sensors intended primarily for terrestrial purposes, ALI, Landsat and SPOT have also been used in lake water quality measurements (e.g., Dekker and Peters 1993; Dekker et al. 2002; Kutser et al. 2005; Tebbs et al. 2013; Torbick et al. 2013; Trescott and Park 2013; Tyler et al. 2006), though spectral resolution and coverage, and therefore applications and results, tend to be limited (Matthews 2011). Commonly employed are the medium resolution multispectral sensors. The Moderate Resolution Imaging Spectroradiometer (MODIS), aboard Aqua and Terra satellites of the NASA EOS-1 mission, launched in 1999 and 2002, has been especially useful in the retrieval of TSM and related parameters (turbidity, Secchi depth) using the two 250-m resolution bands in the red/near-infrared spectral range (e.g., Doxaran et al. 2009; Miller and McKee 2004; Petus et al. 2010; Wu et al. 2008; Wu et al. 2009). Although chl-*a* retrievals in lakes have been reported using MODIS (e.g.,Chavula et al. 2009), a limitation in many cases is the spectral band placement in the red/near infrared spectral range.

Although oceanographic imaging was the primary intention, with the goal of adding to the understanding of ocean processes and productivity within the climate

system context (ESA 2013a), MEdium Resolution Imaging Spectrometer (MERIS) has proven to be revolutionary in the remote sensing of inland waters, providing a combination of radiometric, spectral, spatial and temporal resolutions suitable for retrieving meaningful signals from medium to large size optically complex waters. MERIS has thus been applied to a large number of wide-ranging lake studies from phytoplankton and cyanobacteria biomass mapping (e.g., Binding et al. 2013; Binding et al. 2010; Binding et al. 2011; Binding et al. 2012; Bresciani et al. 2013; Chawira et al. 2013; Giardino et al. 2005; Gons et al. 2008; Gower et al. 2005; Matthews 2014; Matthews et al. 2010; Matthews et al. 2012; Matthews and Odermatt 2015; Moses et al. 2009a, b; Odermatt et al. 2010; Odermatt et al. 2008; Wynne et al. 2013a; Wynne et al. 2013b) to TSM (e.g., Eleveld 2012; Tarrant et al. 2010) and CDOM mapping (e.g., Kutser et al. 2014), as well as various combinations of these and other parameters (e.g., Alikas and Reinart 2008; Campbell et al. 2011; Candiani et al. 2005; Giardino et al. 2010; Giardino et al. 2011; Koponen et al. 2008), and is used in this thesis work.

MERIS, aboard the polar-orbiting Envisat satellite platform of the European Space Agency (ESA), is a push broom, multispectral imaging sensor, measuring in fifteen spectral bands ranging from the visible (band one; centred at 412.5 nm) to the near-infrared range (band fifteen; centred at 900 nm) (Table 2.1; ESA 2013a). Its spectral band placement was intended to allow the various optically significant substances suspended or dissolved in the water column to be distinguished spectrally. In the context of oceanic and inland waters measurements, a number of band placement decisions were made in association with the spectral signatures of chl-*a* and other pigments, CDOM and TSM (Table 2.2; ESA 2013a). In particular, the presence of MERIS band 8, centred at 681.25 to capture the chlorophyll fluorescence peak, and band 9, centred at 709 nm and which captures a peak related to phytoplankton blooms at high biomass (Gower et al. 2004; Gower et al. 1999; Gower et al. 2005) have contributed to its unique value in the remote sensing of lakes. Given its ability to focus on the red-near infrared spectral region for chl-*a* retrievals, the interference by CDOM and TSM, most prominent in the blue-green range, is largely avoided.

Given its intended use over water, which tends to be very dark (approximately 90% of the signal received by the sensor is from atmospheric scattering, and less than about 10% from the water itself, due to the high absorbance of water (Brivio et al. 2001; Maul 1985)), the radiometric sensitivity was of high priority in the sensor design. A

radiometric resolution of less than 0.03 Wm^{-2} sr^{-1} mm^{-1} was identified as necessary to discriminate chl-*a* concentrations at the level of 1 mg m^{-3} (ESA 2013a). MERIS has a swath width of 1150 km, measured by five overlapping cameras, and operates on two spatial resolutions; full resolution (FR), with a pixel size of 300 m intended for land and coastal zone applications, and reduced resolution (RR), with a pixel size of 1200 m at nadir intended for global ocean applications. Two to three day overpass frequency allows for sufficient temporal resolution of data to closely follow phytoplankton bloom dynamics. A ten year archive of MERIS imagery data from June, 2002 to April, 2012 remains, although Envisat is no longer active.

Table 2.1. Spectral positioning and resolution of the 15 MERIS bands, and potential aquatic, vegetation and atmospheric applications. Adapted from ©ESA Earthnet Online 2000 – 2013 (ESA 2013a).

Band number	**Band centre (nm)**	**Bandwidth (nm)**	**Potential application**
1	412.5	10	Yellow substance, pigments
2	442.5	10	Chl-*a* absorption maximum
3	490	10	Chl-*a*, other pigments
4	510	10	Suspended sediment, red tides
5	560	10	Chl-*a* absorption minimum
6	620	10	Suspended sediment
7	665	10	Chl-*a* absorption, fluorescence reference
8	681.25	7.5	Chl-*a* fluorescence peak
9	708.75	10	Fluorescence reference, atmospheric correction
10	753.75	7.5	Vegetation, cloud
11	760.625	3.75	Oxygen absorption
12	778.75	15	Atmospheric correction
13	865	20	Vegetation, water vapour reference
14	885	10	Atmospheric correction
15	900	10	Water vapour, land

Chapter 3

Study site

This chapter presents the study site of the thesis, Lake Balaton, Hungary, which is not only the largest lake in central Europe by surface area, but is also an extremely important resource, at the centre of the region's tourism and recreation economy. The general biogeographical context as well as features of specific relevance to the thesis – such as previous knowledge of the spatiotemporal phytoplankton dynamics – are presented. Due to its historic and current influence on Lake Balaton water quality, features of the Kis-Balaton Water Protection System are also described. Several past and ongoing remote sensing works on various facets of Lake Balaton water quality and on vegetation mapping are also presented to provide context for the current thesis work.

3.1 Lake Balaton

Lake Balaton, located in the western Transdanubian region of Hungary (105.1 m above Adriatic sea level), is by surface area (597 km^2) the largest lake in Hungary (Figure 3.1) and in Central Europe (Herodek et al. 1988; Szabó et al. 2011). The lake is elongated along a predominantly northeast-southwest axis, is 78 km in length and on average 7.6 km wide, pinched to 1.5 km wide at the location of the Tihany peninsula (Figure 3.2). There are four main, consecutive basins (from west to east: Keszthely (1), Szigliget (2), Szemes (3), and Siófok (4); Figure 3.2). Water depth decreases gradually from northeast to southwest. Sediment deposition and carbonate precipitation occur predominantly at the southwestern end at the location of inflow from the Zala River (average monthly discharge ranging from 5 to 10 $m^3 s^{-1}$), the main inflow of surface water to the lake (Figure 3.2; Korponai et al. 2010). Likewise, the lake is characterized by a biological or trophic gradient from typically oligo- to mesotrophic in the northeast (Basin 4; Figure 3.2) to eu- to hypertrophic in the southwest (Basin 1; Figure 3.2), as a result of the nutrient-rich inflow from the Zala River and predominant water circulation patterns (Mózes et al. 2006; Présing et al. 2008). However, periodic and seasonal variability superimposed upon this gradient is also observed.

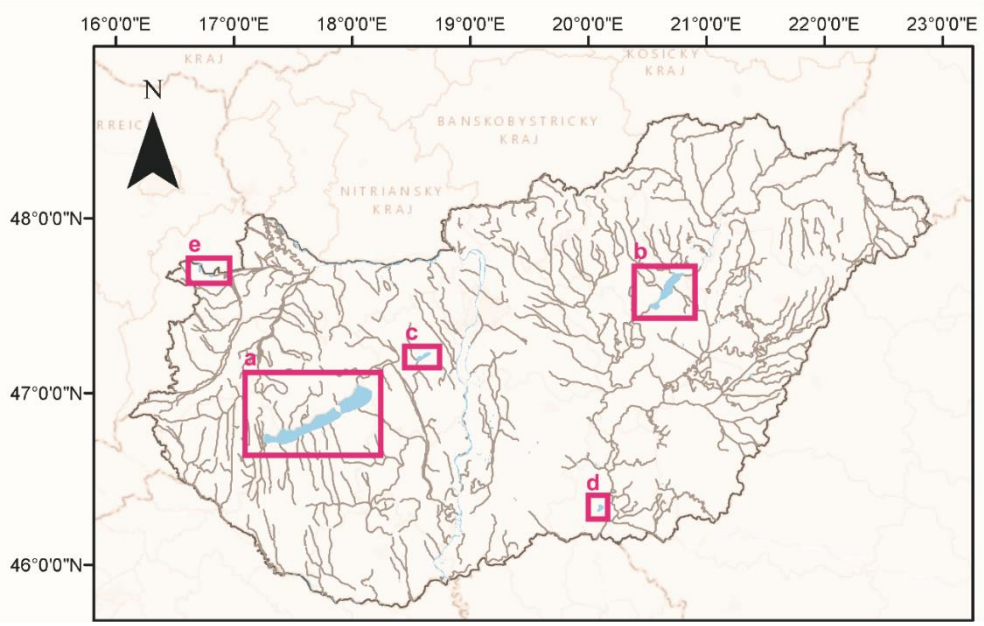

Figure 3.1. Locations of the principle inland water bodies and rivers of Hungary; the study site, Lake Balaton (a), Lake Tisza (b), Lake Velence (c), Lake Fehér (d) and Lake Fertő (e), also known as Neusiedler See on the Austrian side.

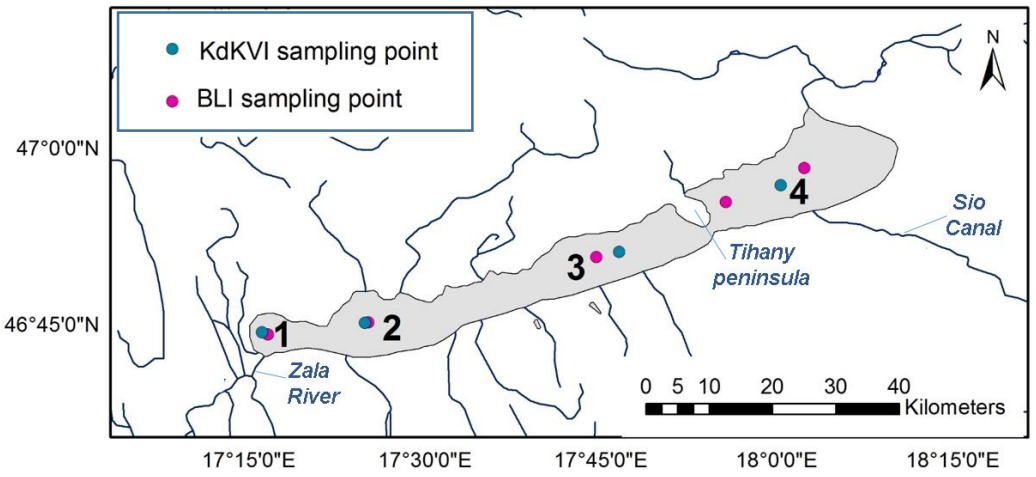

Figure 3.2. The four main basins of Lake Balaton (1: Keszthely, 2: Szigliget, 3: Szemes, 4: Siófok), as well as the principle water inlet (the Zala River) and outlet (the Sio Canal), and sampling locations of the Balaton Limnological Institute (BLI) and of the Central Transdanubian (Regional) Inspectorate for Environmental Protection, Nature Conservation and Water Management (Közép-dunántúli Környezetvédelmi, Természetvedelmiés Vízügyi Felügyeloség (KdKVI)).

Balaton is a shallow lake, with a mean depth of 3.3 m at current service levels (max. depth 10.2 m) (Zlinszky and Molnár 2008), and an average residence time of 4.17 years (V.-Balogh et al. 2003). Water flow out of Lake Balaton is controlled by an outflow gate constructed in 1863 on the only outflow from the lake, the Sio Canal which connects to the Danube River (Figure 3.2) (Herodek et al. 1988; Korponai et al. 2010; Tátrai et al. 2008). Turbidity is generally high, with typical secchi depth ranging from between less than 20 cm and approximately one meter depending largely on wind and other meteorological conditions (Herodek et al. 1988). As a result, the lake can be classified as "optically deep" for the purposes of remote sensing, whereby light reflected off the bottom does not contribute to total water-leaving reflectance (IOCCG 2000; Mueller and Austin 1995). The total catchment area drained by Lake Balaton is 5775 km^2, of which 2622 km^2 is drained by the Zala River, and 1175 and 820 km^2 are drained by sub-catchments of the northern and southern shores respectively (Herodek et al. 1988).

Approximately 250,000 full-time residents inhabit the Lake Balaton region year-round. Though agriculture is the predominant land use activity, with forest cover also important (Figure 3.3), tourism has been estimated at approximately twelve times more important economically (LBDCA 2005). The tourism industry associated with Lake Balaton is long lived, with tourism development already well underway in the 1840s (Puczkó and Rátz 2000). The development of the transportation network to and within the region allowed easier access and thus accelerated the growth of tourism as of the 1860s and continuing into the 20th and 21st centuries with road and highway improvements and expansion. Shifting political and economic conditions in Hungary and in neighbouring countries over time resulted in fluctuations in tourism, and currently more than a million tourists visit the region per year, mainly concentrated in the six to eight week "high" period in July and August (LBDCA 2005; Puczkó and Rátz 2000). Such an intensive tourism industry results in consequent pressure on the Lake Balaton system as a result of increased resource use and waste production. Likewise, the nationally and regionally important Lake Balaton tourism industry is heavily dependent on the lake as a natural resource and as such is very sensitive to lake water quality and ecosystem features and processes.

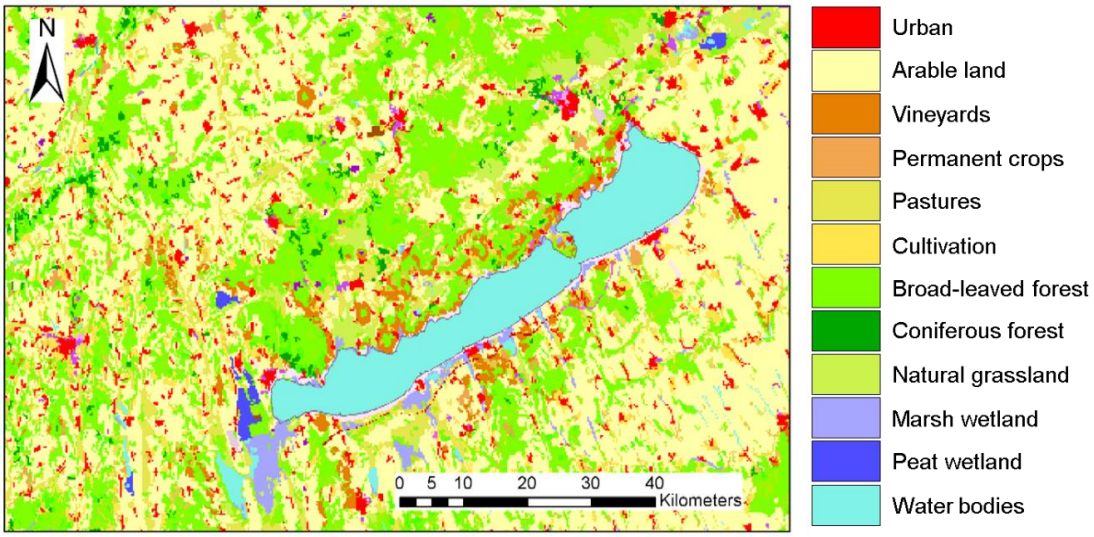

Figure 3.3. CORINE land cover map (2006) for the Lake Balaton region, highlighting principally forestry and agricultural land covers. © European Environment Agency Corine Land Cover 2006 raster data (published 2010).

In recent decades, several events have been cause for alarm regarding lake water quality and sustainability. These include periodic droughts and consequent drastic drops in water level (notably occurring over the period 2000-2004 (Martinez et al. 2011; Padisak et al. 2006)), and a massive eel die-off in 1992 (Puczkó and Rátz 2000). Fluctuations in, and degradation of water quality, especially eutrophication and the presence of potentially harmful algal blooms (HABs) are of on-going concern. Of particular importance was the severe eutrophication that took place in the 1970s and 1980s. Several major remediation and mitigation measures were implemented, including the development of a new sewage diversion system and treatment facility, and the construction of the Kis-Balaton Water Protection System, which have largely been found to be successful in remediating water quality to pre-1970s conditions (Herodek et al. 1988; Istvánovics et al. 2007). Two annual phytoplankton blooms still typically occur in Lake Balaton, however; a smaller spring bloom (~ April) and a larger late summer bloom (~ August/September) (Mózes et al. 2006; Présing et al. 2008). Water quality monitoring takes the form of sampling two to five points at the centre of the different basins of the lake once to twice monthly (Figure 3.2). Samples are analysed for chl-*a* and TSM, and water temperature, secchi depth and euphotic depth are also recorded. This has been carried out by both the Balaton Limnoligical Institute (BLI) and the Central Transdanubian (Regional) Inspectorate for Environmental Protection, Nature

Conservation and Water Management (KdKVI; *"Közép-dunántúli Környezetvédelmi, Természetvedelmi és Vízügyi Felügyeloség"*) (Section 4.1.1).

3.2 Kis-Balaton Water Protection System

The Kis-Balaton wetland was originally the fifth basin of Lake Balaton and became separated early in the nineteenth century as a result of water drainage, dredging and land cover conversion for agricultural uses (Zlinszky and Timár 2013). As such activities continued and intensified throughout the nineteenth and twentieth centuries, the wetland became severely degraded in quality and area (Dömötörfy et al. 2003; Korponai et al. 2010). As a result, nutrient-rich water transported by the Zala River which had previously been filtered by the wetland flowed directly into the Keszthely basin (basin 1; Figure 3.2) of Lake Balaton. Furthermore, the nutrient load of the Zala River increased as population and agricultural pressures increased, and by the early 1970s signs of the severe eutrophication of Lake Balaton were already obvious as a result (Herodek et al. 1988).

The Kis-Balaton Water Protection System (KBWPS) was designed for nutrient retention in response to the increasingly eutrophic conditions of Lake Balaton (Pomogyi 1993). The KBWPS was constructed at the site of the former Kis-Balaton wetland in two phases. Construction began in 1981 and the first phase was operational in 1985. It is essentially a eutrophic pond (surface area 21.5 km^2) with a water residence time of approximately 30 days. The second phase became partially operational in 1992 as a constructed wetland with a residence time of approximately 60 days (surface area 54 km^2 with macrophyte coverage (primarily reed) over approximately 95%) (Hatvani et al. 2011; Korponai et al. 2010; Tátrai et al. 2000). This second phase is an important habitat for birds (particularly water fowl) and aquatic species, and is a protected nature conservation area under the 1971 Ramsar Convention (Ramsar Convention, 1971). Water level is artificially modified throughout the system by a series of dykes to remain constant in both pond and wetland sections (Hatvani et al. 2011). The KBWPS, in combination with sewage diversion and treatment, was found to be successful overall in reducing the nutrient load from the Zala River to Lake Balaton (Pomogyi 1993; Tátrai et al. 2011; Tátrai et al. 2000). Currently, speculation surrounds the reversal of KBWPS performance,

with sediment saturating in terms of nutrient uptake capacity and nutrient release consequently occurring (unpublished KdKVI data, 2011; Horváth et al. 2013). This is yet to be confirmed, but will be important to consider in ongoing monitoring.

3.3 Remote sensing of Lake Balaton to date

Several remote sensing studies of the Lake Balaton system have been undertaken in recent years, and Landsat 1 imagery was used qualitatively as early as 1970 to visually inform hydraulic studies of lake currents and sedimentation patterns (Dr. László Rákoczi, personal communication in June 2012). Simultaneous spectral and water constituent (e.g., chl-*a*, TSM, dissolved organic matter) concentration measurements were made across the lake in 1985, 1986 and 1988 toward developing optical retrieval models, and included spectral simulation of Landsat MSS bands (Gitelson et al. 1993). More recently, algorithms were developed through the use of cascading Principle Component Analysis to differentiate spectrally unique end-members that can be unmixed to quantify chl-*a* and total suspended sediment. This was first approached through simulating Landsat ETM+ data in controlled tank and field spectrophotometer measurements (Sváb et al. 2005), followed by the application of resulting algorithms to a series of Landsat ETM+ images (Tyler et al. 2006). These studies resulted in high accuracies of derived chl-*a* and TSM measurements, suggesting the potential application to lake monitoring, but were not continued in application to further time series data.

A United Kingdom Natural Environment Research Council (NERC) and European Facility for Airborne Research (EUFAR) funded campaign resulted in AISA hyperspectral and laser scanning (LiDAR) altimetry point-cloud data of Lake Balaton open water and shoreline. These data are being used to develop methods to distinguish phytoplankton species groups of Lake Balaton, particularly cyanobacteria, and in bio-optical (HydroLight) modelling (C. Riddick PhD research (University of Stirling), in progress). In the context of aquatic vegetation, data collected during this campaign are also being used in the monitoring of shoreline wetland vegetation, for mapping (Zlinszky et al. 2012a; Zlinszky et al. 2012b) and for the identification of wetland vegetation species and vegetation health (Stratoulias et al. 2015; D. Stratoulias PhD research (University of Leicester), in progress). Measurements of Lake Balaton bio-optical properties and

laboratory analyses of chl-*a*, TSM and CDOM were carried out in Basin 4 (Figure 3.2) as part of the EULAKES project (Ref. Nr. 2CE243P3) led by the CNR (National Research Council) IREA (Institute for Electromagnetic Sensing of the Environment) (Bresciani and Giardini 2011). Parameter (chl-*a*, CDOM, TSM) retrieval was then extended to MERIS imagery, and applied to 39 images from 2004 through 2010, though the image retrieval performance was not validated.

Lake Balaton was one of 258 large lakes included in the University of Edinburgh ARC-Lake project aiming to retrieve and reconstruct (filling gaps where necessary) lake surface water temperature (LSWT) and lake ice cover products from 2002 to 2010 (MacCallum and Merchant 2012). Lake Balaton is also included in the ongoing UK (NERC) funded GloboLakes project (globolakes.stir.ac.uk), coordinated by the University of Stirling, the ESA funded Diversity-2 project (diversity2.info), coordinated by Brockmann Consults GmBH, and the EU FP7 project Improved monitoring and forecasting of ecological status of European INland waters by combining Future earth ObseRvation data and Models (INFORM; http://www.copernicus-inform.eu/) coordinated by the Flemish Institute for Technological Research (VITO). These projects are of international scope, intended to develop, test and apply common remote sensing, modelling and interpretation approaches and methodology to a broad range of lakes from around Europe (INFORM) and the world (GloboLakes, Diversity-2).

Chapter 4

MEdium Resolution Imaging Spectrometer (MERIS) chlorophyll retrieval, mapping and time series validation

Parts of the work presented in this chapter have published as:

Palmer, S. C. J. *et al.* (2015a). Validation of Envisat MERIS algorithms for chlorophyll retrieval in a large, turbid and optically-complex shallow lake. *Remote Sensing of Environment*, *157*, 158-169.

4.1 Introduction & rationale

In Chapter 2, "Remote sensing of lake water quality", the importance of measuring and monitoring phytoplankton was introduced with regards to its influence on both water quality and aquatic ecosystem productivity. The potential additional insight afforded by the use of satellite imagery in this respect was also discussed, not only in terms of regular and frequent satellite overpass and cohesive spatial mapping of phytoplankton biomass, but also in terms of access to remote and under- or un-sampled sites. The quantification of phytoplankton biomass via remote sensing techniques using the proxy pigment chl-*a* was presented. Likewise, algorithms of varying architectures that have been developed to retrieve chl-*a* concentrations in optically complex conditions were introduced.

Several neural network and band difference algorithms have been automated and made available as part of the Basic ERS & ENVISAT (A)ASTER MERIS (BEAM) toolbox developed by Brockmann Consult, Hamburg (Fomferra and Brockmann 2005). The free availability and automation of these tools and image processing software, as well as the ever increasing availability of satellite image data, means that remote sensing can be applied more widely than ever before for use in research, monitoring and management activities. However, prior to the reliable use of satellite-derived chl-*a* concentration maps for use in scientific activities or management applications, such as regular phytoplankton biomass measurement toward meeting the WFD goals of the European Commission, validation of retrieval algorithm performance is essential.

A large number of validation exercises have been carried out for lakes around the world, particularly in application to MEdium Resolution Imaging Spectrometer (MERIS) imagery which has been found to be especially suitable for medium to large lakes given its unprecedented combination of spectral, temporal, spatial and radiometric resolutions (Koponen et al. 2008; Matthews 2011; Odermatt et al. 2012). A validation of the Case 2

Regional (C2R), Boreal Lake (BL) and Eutrophic Lake (EUL) neural network processors, contained within BEAM, retrieving atmospherically-corrected reflectance, and a range of IOPs and constituent concentrations (including chl-*a*), was undertaken for several European and African lakes (Koponen et al. 2008; Ruiz-Verdú et al. 2008a). Chl-*a* concentration retrievals were validated during an algal bloom in the Canadian/American border lake, Lake of the Woods, using C2R, the standard MERIS algal_2 product, and the band difference Fluorescence Line Height (FLH) and Maximum Chlorophyll Index (MCI) algorithms (Binding et al. 2010). C2R, EUL and several semi-empirical algorithms were compared in application to the high phytoplankton biomass Lake Zeekoevlei in South Africa (Matthews et al. 2010). C2R, with and without the use of ICOL, was validated for perialpine lakes (Odermatt et al. 2010), for Lake Constance, Germany (Odermatt et al. 2008) and for Lake Trasimeno, Italy (Giardino et al. 2010). Chl-*a* concentration retrievals from the standard MERIS Case 1 and Case 2 algal products were validated for Lakes Vattern and Vanern, Sweden, and Lake Peipus, Estonia/Russia (Alikas and Reinart 2008).

It is important to note that results from these and other validation exercises are highly variable when the same algorithm is applied to different sites. This is largely a result of the optical complexity and range of conditions that are encompassed by lake waters and under the conventional Case 2 classification (IOCCG 2000), as detailed in Chapter 2.2.3. It can thus be expected that algorithms that perform well for some sites perform poorly for others and vice versa, rendering site-specific validation crucial (Kallio et al. 2001; Matthews 2011; Odermatt et al. 2012). Furthermore, most previous validation exercises cover only a limited time span and may not be fully representative of the systems for which they are undertaken. Even within Lake Balaton a broad range of water constituent concentrations and thus optical properties are present, particularly due to the trophic gradient along the southwest-northeast axis, the seasonality of phytoplankton dynamics and the high spatial- and temporal variability of suspended matter. It could be expected therefore that certain algorithms perform best in certain seasons or parts of the lake as a result and vice versa. As such it is important that the validation of MERIS chl-*a* concentration retrievals for Lake Balaton encompass as broadly as possible all conditions, through *in situ* measurements coinciding with satellite overpass across seasons and years, as well as across the full spatial extent of the lake. A number of punctual validation exercises have previously been carried out for Lake Balaton

(Bresciani and Giardini 2011; Gitelson et al. 1993; Tyler et al. 2006), as discussed in Chapter 3.3. However these all comprise limited timeframes (generally one to two weeks at most, and with none or only few coinciding satellite images acquired) or spatial extents (e.g., *in situ* measurements only from Basin 4 (Bresciani and Giardini 2011)). Although data are no longer being acquired by MERIS as of April 2012, preventing the extension of the current analyses to the present despite the ongoing collection of *in situ* data, more than ten years of archive data remain to be more fully exploited once adequate validation has been carried out. The future ESA Sentinel-3 Ocean and Land Colour Instrument (OLCI) will provide continuity to MERIS, and the development and testing of methodology in application to MERIS will also serve to inform strategies for the use of OLCI data.

4.2 Objectives

Given the availability of archive MERIS image data coinciding with a large archive *in situ* dataset spanning all four basins of Lake Balaton, over several years and all seasons, the current chapter intends primarily to present the results of the first extensive chl-*a* retrieval algorithm validation for Lake Balaton. Several neural network and band difference algorithms reported to have robustly retrieved chl-*a* concentrations under optically complex conditions elsewhere, and available through BEAM, are tested and results are compared. The main objectives of this chapter are thus:

(1) To validate a range of MERIS chl-*a* concentration retrieval algorithms of varying architecture types across all conditions encountered at Lake Balaton;

(2) To compare the algorithm performances and select from among them the best for application in the full time series processing;

(3) To apply and evaluate algorithms and how the results vary spatially; and

(4) To demonstrate the utility of satellite-derived chl-*a* concentration mapping for Lake Balaton monitoring and scientific purposes.

4.3 Methods

4.3.1 Selected chl-*a* retrieval algorithms

Neural network algorithms

The neural network algorithms chosen for the evaluation of chl-*a* concentration retrieval for Lake Balaton have been trained using *in situ* data from elsewhere, and bio-optical modeling and radiative transfer simulations to extend the quantity of training data available. These have been developed in an attempt to cover a broad range of conditions, and automated for use within the BEAM toolbox. Since extensive data are required to train neural networks, the availability of such pre-trained algorithms is an advantage for sites such as Lake Balaton where optical *in situ* data are limited or unavailable. For Balaton, measurements of IOPs, AOPs and mass-specific IOP (SIOP) coefficients which relate the IOPs to constituent concentrations, used in the development of these neural networks, are not available. Given that the training of these algorithms did not specifically include data from Lake Balaton, their validation prior to use is, however, of particular importance. The chosen neural network algorithms are the following:

The Water processor, developed at the Free University of Berlin (FUB/WeW) uses four separate neural networks trained using the results of radiative transfer modeling and covering broad variations of atmospheric and Case 2 in-water conditions. Level 1b top-of-atmosphere (TOA) radiance data are used as input, and log concentrations of chl-*a* and TSM and log absorbance of CDOM are output along with parameters resulting from the simultaneous atmospheric correction – aerosol optical thickness (AOT) at four wavelengths (440, 550, 670 and 870 nm) and water-leaving remote sensing reflectance (R_{rs} (sr^{-1})) at eight wavelengths corresponding to MERIS bands one to seven and nine (412, 442, 490, 510, 560, 620, 665 and 708 nm). The training ranges of water constituents are 0.05 to 50 mg m^{-3} chl-*a* concentration, 0.05 to 50 g m^{-3} TSM concentration and 0.005 to 1 m^{-1} CDOM absorbance (Table 4.1) (Schroeder et al. 2007b).

The Case 2 Regional (C2R) processor was also selected for validation. The C2R algorithms were developed to achieve accurate and efficient mass image processing by

the MERIS ground segment in response to the failure of the neural network algorithm designed for use over the so-called Case 1 waters in optically-complex waters (Doerffer and Schiller 2007; Morel and Antoine 2000)). Unlike the FUB/WeW processor, IOPs are retrieved in a separate step after atmospheric correction by the processor is complete, which takes place in a distinct neural network module. The C2R atmospheric correction module is described in further detail in the Chapter 5. Atmospherically-corrected MERIS reflectance in eight channels, as well as image viewing and solar geometry are input into the in-water module. IOPs at MERIS band two (443 nm) are output, and are also converted to constituent concentrations via simple equations that make use of specific inherent optical property (SIOP) coefficients. These coefficients can be adjusted by the user, as IOPs are provided by the processor (Doerffer and Schiller 2007). The bio-optical model underlying the C2R in-water module was established using *in situ* data from the North Sea, the North Atlantic, the Baltic Sea and the Mediterranean Sea. This was followed by the production of a large, simulated reflectance dataset through HydroLight (Sequoia Scientific, Inc.) radiative transfer modeling to train the NN. The C2R training ranges of the water constituents are 0.016 to 43.18 mg m^{-3} chl-*a* concentration, 0.0086 to 51.6 g m^{-3} TSM concentration and 0.005 to 5 m^{-1} CDOM absorbance (Table 4.1) (Doerffer and Schiller 2007).

Both the Eutrophic Lake (EUL) and Boreal Lake (BL) algorithms make use of same neural network architecture and atmospheric correction module as the C2R processor, and the same input data (MERIS L1b data at eight spectral channels and image geometry) and output parameters (IOPs and constituent concentrations) are used (Doerffer and Schiller 2008). However, the datasets used to train the underlying bio-optical models are distinct, making use of *in situ* data obtained from eutrophic Spanish lakes and boreal Finnish lakes respectively. The training ranges of the water constituents for the EUL algorithm are 1 to 120 mg m^{-3} chl-*a* concentration, 0.42 to 50.9 g m^{-3} TSM concentration and 0.1 to 3 m^{-1} CDOM absorbance. Those for the BL algorithm are 0.5 to 50 mg m^{-3} chl-*a* concentration, 0.1 to 20 g m^{-3} TSM concentration and 0.25 to 10 m^{-1} CDOM absorbance (Table 4.1; Doerffer and Schiller 2008).

Table 4.1. Water constituent concentration limits of neural network algorithms. From Palmer et al. (2015a).

Algorithm	**Chl-*a*** ($mg\ m^{-3}$)	**TSM** ($g\ m^{-3}$)	**CDOM** ($a440\ m^{-1}$)
C2R[a]	0.016 – 43.18	0.0086 – 51.6	0.005 – 5
EUL[b]	1 – 120	0.42 – 50.9	0.1 – 3
BL[b]	0.5 – 50	0.1 – 20	0.25 – 10
FUB WeW[c]	0.05 – 50	0.05 – 50	0.005 – 1

[a]Doerffer and Schiller (2007)

[b]Doerffer and Schiller (2008)

[c]Schroeder et al. (2007)

Band difference algorithms

Two band difference algorithms were also validated for Lake Balaton. These make use of different combinations of spectral bands in the red and near-infrared spectral range, which is less affected by water constituents other than phytoplankton biomass than the blue and green range used to retrieve chl-*a* concentrations in pelagic open ocean settings and can thus be expected to relate more directly to chl-*a* in optically complex waters (Gower et al. 1999). An index is derived according to equation 4.1 and converted to chl-*a* concentration through tuning of coefficients with coinciding *in situ* data. These band difference algorithms, the Fluorescence Line Height (FLH) (Gower et al. 2004; Gower et al. 1999) and Maximum Chlorophyll Index (MCI) (Gower et al. 2005) have also been implemented as automated image processing tools within the BEAM toolbox. Both of these make use of a height-above-baseline approach, with the FLH drawing a baseline between radiance or reflectance measured at 664 (band 7) and 708 nm (band 9) and measuring the height above this baseline at 681 nm (band 8), typically related to the chl-*a* fluorescence maximum near this wavelength. The MCI draws a baseline between radiance or reflectance measured at 681 (band 8) and 753 nm (band 10) and measures the height above this baseline at 708 nm (band 9), related to the backscattering of phytoplankton particles at high concentrations captured by this wavelength (Figure 4.1). Both MCI and FLH algorithms take the form presented in Equation 4.1, where L2/ λ2 are

the radiance or reflectance and wavelength of the peak above the baseline created between L1/ λ1 and L3/ λ3. The constant, *k*, is set to 1.005 as a default in BEAM.

$$FLH/MCI = L2 - k \times [L1 + (L3 - L1)\ ((\lambda 2 - \lambda 1)/(\lambda 3 - \lambda 1))] \qquad \text{Equation 4.1}$$

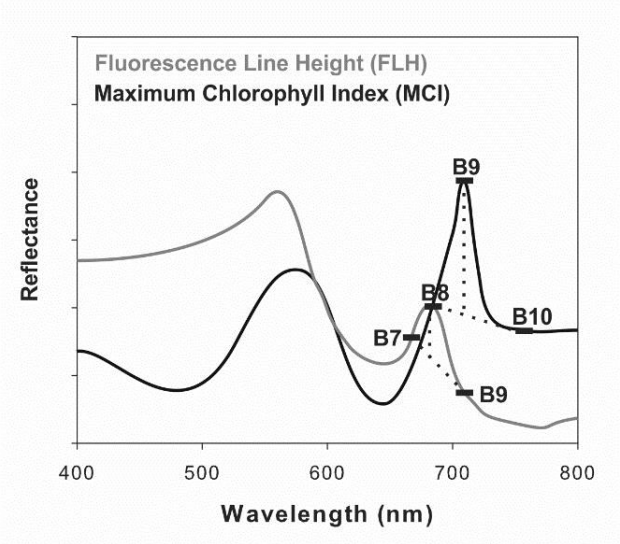

Figure 4.1. Schematic drawing of the biophysical underpinnings of the FLH and MCI algorithms. B7, B8, B9 and B10 refer to the corresponding MERIS bands, used in the FLH and MCI algorithms, of 664, 681, 708 and 753 nm center wavelength respectively.

4.3.2 MERIS image processing

Processing of the C2R, BL, EUL, FLH and MCI algorithms for all MERIS images fully or partially overpassing Lake Balaton during the full 2007 through 2012 period was carried out using the the PHenology And Vegetation Earth Observation Service (PHAVEOS) at Airbus, UK (formerly known as the Astrium GeoInformation Division). Image output from each of the algorithms, as well as the L1b MERIS 300 m full resolution, full swath, georeferenced (FSG) data used as input were provided as part of a collaboration undertaken during a GIONET industrial secondment during PhD research. The development of PHAVEOS was undertaken as part of the ESA Earth Observation Market Development programme Value Adding Element (Lankester et al. 2010). The original concept underlying the PHAVEOS processing chain was the mass extraction of terrestrial vegetation indices and biophysical parameters such as Normalized Differential

Vegetation Index, Leaf Area Index and fraction of Absorbed Photosynthetically Active Radiation from very large volumes of data. However, biophysical parameters related to water quality, such as the concentrations or indices from the algorithms listed in the preceding section, are analogous to the terrestrial examples listed above. Therefore PHAVEOS is equally applicable in aquatic settings upon substituting the relevant algorithms.

PHAVEOS first uses a vector-based region of interest (ROI) mask to extract MERIS image tiles that include Lake Balaton from the archive. Accurate MERIS Ortho-Rectified Geo-location Operational Software (AMORGOS; Bicheron et al. 2008) is then used for geolocation of the extracted images, and small variations in central spectral wavelength in pixels across the MERIS field of view due to optical characteristics and slight misalignments in sub-systems of the sensor, known as the SMILE effect (Bourg et al. 2008), are corrected. Images are then processed using the code for C2R, EUL and BL, both atmospheric correction and in-water modules, as well as MCI and FLH which was adapted for use within PHAVEOS. For chl-*a* concentration retrieval validation, both chl-*a* concentration and the related IOP, pigment absorption at 443 nm (a_pig(443)) were produced by the C2R, EUL and BL processors and MCI and FLH indices by the respective algorithms. Output data are resampled to a spatial resolution of 250 m pixels (Figure 4.2). A 3 x 3 kernel pixel, covering a total surface area of approximately 800 m^2, was averaged and extracted for each coinciding date (± approximately three hours) and sampling location (Figure 3.2). For each clear-sky matchup identified from the PHAVEOS processing chain, the corresponding L1b MERIS FGS image was processed separately in BEAM using the FUB/WeW processor, and a 3 x 3 pixel kernel centred on the coinciding *in situ* matchup extracted from the log chl-*a* concentration (*algal_2*) layer.

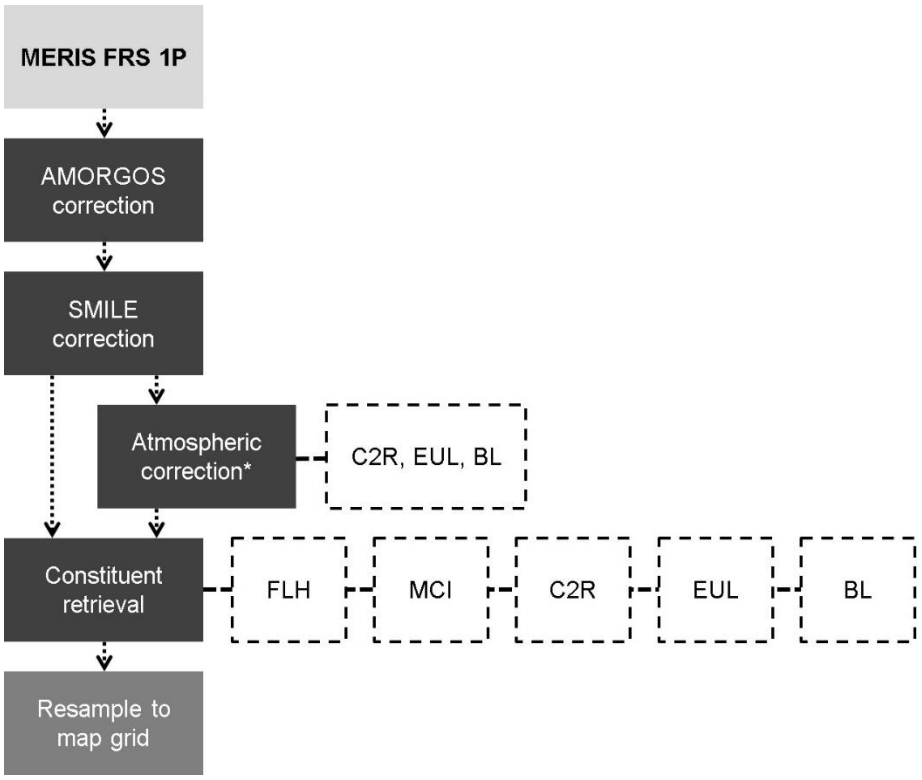

Figure 4.2. PHAVEOS processing chain used in the current work. From Palmer et al. (2015a).

4.3.3 Validation analysis

In situ validation data

Regular, on-going water sampling at fixed locations across Lake Balaton (Figure 3.2), for the purpose of water quality monitoring, is conducted by researchers of the BLI as well as by the regional water authority, KdKVI, and was used as *in situ* reference data in the current study. One litre samples collected from each site by the BLI are average concentrations throughout the water column (integrated, bulk water column sampling method), whereas KdKVI samples are taken from the surface water layer (depth < 50 cm). Chl-*a* concentrations (mg m^{-3}) measured at the Nutrient Cycling Laboratory of the BLI are determined through spectrophotometric analysis using a Shimadzu spectrophotometer, model UV 160A following extraction by hot methanol from known volumes (Iwamura et al. 1970). The chl-*a* analysis carried out by the KdKVI differ in that hot ethanol is used in the place of hot methanol.

Given the intended use of archive chl-*a* data from both BLI and KdKVI sampling campaigns for comparison with remotely sensed measurements of the water surface, potential systematic differences between the two data sets that might arise from the aforementioned discrepancies in sampling and laboratory methodologies were investigated. Coinciding surface water layer and bulk water column samples were taken during biweekly BLI measurements at four sampling sites across the lake over the full, ice-free 2012 sampling season, from April to November (n = 80 pairs). Samples span diverse seasonal and meteorological conditions, notably wind speeds and temperatures. Likewise, several coinciding (same date and sampled basin) BLI and KdKVI samples were identified during this study and compared (n = 7 pairs), allowing limited additional insight into potential differences resulting from varying sampling methodologies as well as chl-*a* extraction specifics. Regression analyses were performed to assess the comparability of the two archive *in situ* datasets.

Chl-a retrieval algorithm performance evaluation

Matchups flagged at either the Level 1, indicating invalid, coastline or land, bright, suspect or at risk of glint pixels, or at the Level 2 in the case of the NN processors, indicating out of input or output training ranges were removed from further analysis. Data were then randomly divided 70:30 for separate calibration and validation of each of the algorithms to ensure robust algorithm performance (Matthews, 2011). Due to the differing Level 2 flagging of each, largely resulting from different algorithm training ranges, this corresponds with different final numbers of matchups for each algorithm. Using the calibration datasets (70 % of the valid matchups for the given algorithm), coefficients relating the retrieved FLH and MCI indices to *in situ* measured chl-*a* concentrations were obtained through ordinary least squares regression. Neural networks were partially locally tuned in a similar way, using regression to calibrate SIOP coefficients between NN-retrieved pigment absorption (a_pig(443) of C2R, BL and EUL processors) and *in situ* measured chl-*a*. Although pigment absorption is not produced by the FUB/WeW NN processor, this was calculated from the retrieved log chl-*a* concentration by using the relationships and coefficients used in the processor to retrieve it from pigment absorption ($a_{pl}(440)$) (Bricaud et al. 1998; Schroeder 2005) (Table 4.3). Linear, power and exponential calibration relationships were tested for all six algorithms, and that resulting in the highest R^2 was selected.

Following calibration, the remaining 30% of the datasets were then used to validate the locally-tuned chl-*a* concentration retrievals. The retrieval performance of all algorithms was then evaluated by the resulting coefficient of determination (R^2) (equation 4.2), bias (equation 4.3), and absolute and relative root mean standard error (RMSE) (equations 4.4 and 4.5 respectively) relative to the *in situ* matchup dataset.

$$R^2 = 1 - \frac{\sum_{i=1}^{N}\left(X_i - \bar{\hat{X}}\right)^2}{\sum_{i=1}^{N}(X_i - \bar{X})^2} \qquad \text{Equation 4.2}$$

$$\text{Bias} = \frac{\sum_{i=1}^{N}(X_i - \hat{X})}{N} \qquad \text{Equation 4.3}$$

$$\text{RMSE} = \sqrt{\frac{\sum_{i=1}^{N}(X_i - \hat{X})^2}{N}} \qquad \text{Equation 4.4}$$

$$\text{Relative RMSE} = \left(\frac{\sqrt{\frac{\sum_{i=1}^{N}\left(X_i - \bar{\hat{X}}\right)^2}{N}}}{\bar{X}_i} \right) * 100\% \qquad \text{Equation 4.5}$$

4.4 Results

4.4.1 Comparability of *in situ* datasets

Results of regression analysis suggest no significant difference resulting from the two sampling methodologies; surface sampling, as carried out by the KdKVI in their regular monitoring, versus water column integrated sampling, as carried out in the regular monitoring by the BLI (Figure 4.3a; $R^2 = 0.95$ ($P < 0.001$); RMSE = 0.94 mg m^{-3}; slope = 0.95; intercept = 0.82). Similarly, results of regression analyses also indicate no significant difference resulting from samples collected on the same date and from the centre of the same basin from the two institutes and analysed in their respective laboratories, for both BLI water column (Figure 4.3b; $R^2 = 0.90$ ($P = 0.001$); RMSE = 2.46 mg m^{-3}; slope = 1.00; intercept = -0.44) and surface samples (Figure 4.3b; $R^2 = 0.86$ ($P = 0.002$); RMSE = 2.88 mg m^{-3}; slope = 0.96; intercept = 0.37) compared with KdKVI

surface samples respectively. These results support the combination of the two datasets for common use in the validation of chl-*a* algorithms applied to archive satellite imagery.

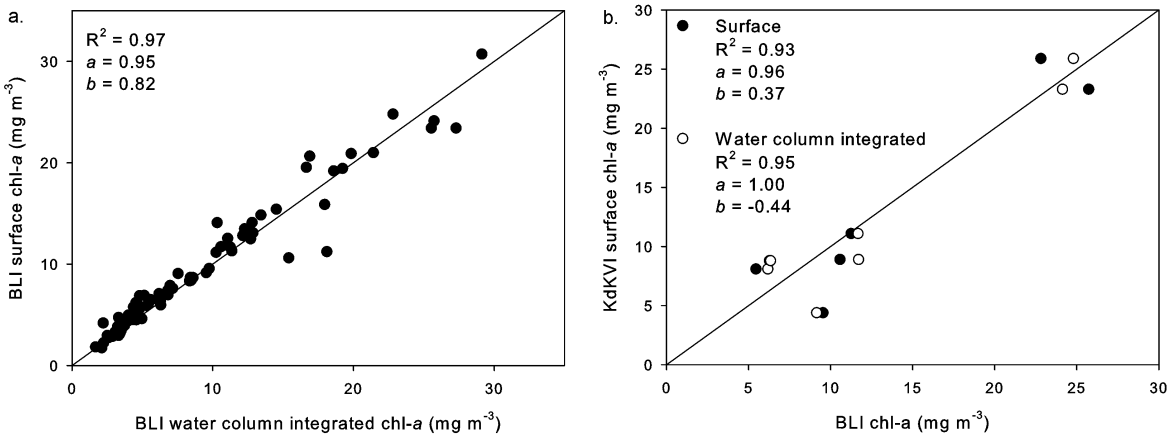

Figure 4.3. Comparison of chl-*a* concentrations of simultaneous water column-integrated and surface samples collected and analyzed at the BLI during the full 2012 sampling season (April through December) (a) and same day chl-*a* concentration measurements by the KdKVI (surface sampling) and the BLI (surface and water column-integrated sampling) in 2012. From Palmer et al. (2015a).

4.4.2 Matchup data and chl-*a* retrieval

Of the 1409 MERIS images that included all or part of Lake Balaton acquired between January 2007 and April 2012, extracted by the PHAVEOS processing chain, 68 both exhibited clear-sky conditions and were acquired on the same day as *in situ* sampling by the BLI and/or the KdKVI. From these 68 images, a total of 289 matchup data points resulted. 201 remained after removing the matchups flagged at the Level 1 as invalid, coastline or land, bright, suspect or at risk of glint pixels. The final number of matchup points varied for the different processors, as flagging at the Level 2 associated with exceeding algorithm training ranges is different for each of the NN processors, and no Level 2 flagging is carried out by either MCI or FLH (n = 201 for each of these after Level 1 flagged matchups were removed). The C2R and EUL processors raised flags similarly (remaining n = 166 and 168 respectively), the BL raised flags in addition to those raised by C2R and EUL because of water-leaving reflectance out of range

("wlr_oor"), and the FUB/WeW processor was found to exclude more matchups than the other three neural network-based algorithms (remaining n = 108). Notably, all matchups where *in situ* chl-*a* exceeded 30 mg m^{-3} were excluded by FUB/WeW flagging (Figure 6.4d and 6.6d). Also removed prior to performance evaluation were several unflagged matchups for which *in situ* measurements exceeded the training ranges of the NNs (Table 4.1).

The full, *in situ* matchup dataset after removing Level 1 flags common to all algorithms ranged from 1.50 to 57.0 mg m^{-3}, with higher concentrations measured in the west and lower concentrations measured in the east consistent with the strong productivity gradient described in Chapter 3.1. Further descriptive statistics of the *in situ* dataset for the full lake and per basin are presented in Table 4.2. The conversion of MCI and FLH indices to chl-*a* concentration and local tuning of the NN chl-*a* retrievals, as described in Section 4.3.3, is presented in Figure 4.4 and Table 4.3. Power functions were found to best fit neural network a_pig(443) and a_{pl}(440) to coinciding *in situ* chl-*a* measurements in all cases (R^2 = 0.46 for C2R, R^2 = 0.42 for EUL, R^2 = 0.48 for BL, and R^2 = 0.36 for FUB/WeW), and linear relationships for both FLH and MCI indices (R^2 = 0.78 and 0.62 respectively). A comparison of the default SIOP coefficients of each of the NN processors, and those locally tuned here is found in Table 4.3.

Table 4.2. *In situ* chl-*a* concentration (mg m^{-3}) matchup dataset descriptive statistics. From Palmer et al. (2015a). Basin locations are provided in Figure 3.2 and in the schema below.

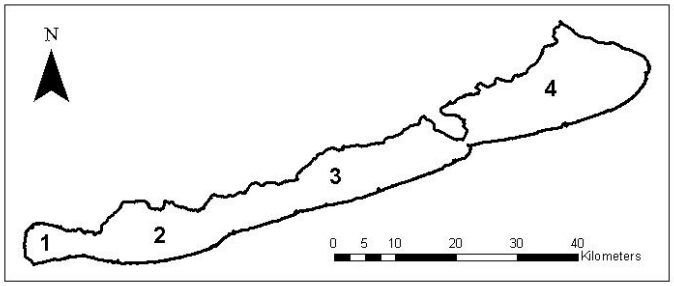

Basin	n*	Min.	Max.	Mean	Median	SD
Full lake	201	1.50	57.00	12.75	8.90	11.14
1	59	3.03	57.00	17.37	12.69	12.65
2	47	4.04	46.48	16.09	11.92	11.34
3	38	2.20	41.45	12.87	9.21	10.57
4	57	1.50	13.62	5.14	4.30	2.72

*Remaining matchup points after removing those flagged at the Level 1 by the given processor.

Table 4.3. Algorithm calibration, using 70 % of the matchup dataset between *in situ* Lake Balaton chl-*a* measurements and a_pig(443), apl(440) or MCI/FLH indices. From Palmer et al. (2015a).

Processor	n	R^2	Locally tuned equation	Original equation
C2R	116	0.46	Chl-*a* = $33.42*a\_pig(443)^{0.91}$	[a]Chl-*a* = $21*a\_pig(443)^{1.04}$
EUL	118	0.42	Chl-*a* = $61.84*a\_pig(443)^{1.01}$	[b]Chl-*a* = 31.45* a_pig(443)
BL	91	0.48	Chl-*a* = $35.06*a\_pig(443)^{0.85}$	[b]Chl-*a* = $62.61*a\_pig(443)^{1.29}$
FUB/WeW	76	0.36	Chl-*a* = $20.41*a_{pl}(440)^{0.58}$	[c]Chl-*a* = $105.21*a_{pl}(440)^{1.58}$
L1b FLH	141	0.78	Chl-*a* = -8.08*FLH + 10.33	n.a.
L1b MCI	141	0.62	Chl-*a* = 3.91*MCI + 11.31	n.a.

[a] Doerffer and Schiller (2007).

[b] Doerffer and Schiller (2008).

[c] Schröder (2005); Bricaud et al. (1998).

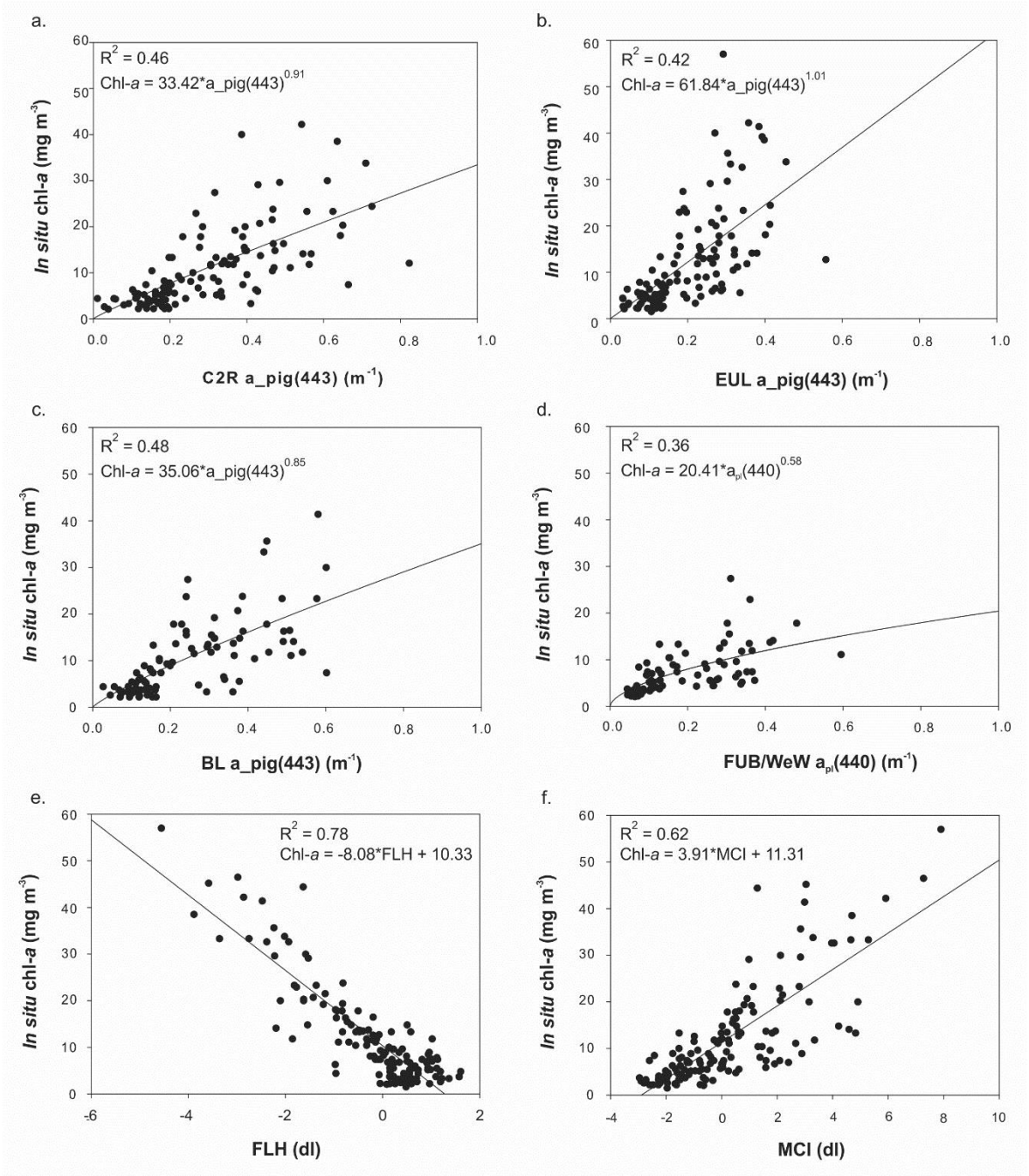

Figure 4.4. Calibration of algorithms using 70 % of the matchup dataset, to establish the equations between the indices or pigment absorption to apply for locally-tuned validation. From Palmer et al. (2015a).

The chl-*a* retrieval validation of the six algorithms evaluated here, using the 30 % of the matchup data remaining after calibration, is found in Figure 4.5, with points colour-coded by basin. Table 4.4 contains additional performance indicators; R^2, bias, RMSE and relative RMSE, as well as coefficients from the linear relationships between each MERIS-derived chl-*a* concentration and the corresponding *in situ* matchup. Overall, performance indicators revealed that FLH performed highest of all tested algorithms (R^2 = 0.87; RMSE = 4.19 mg m^{-3} (30.75 %)). However, this is found to be highly variable from basin to basin, with basins 1 through 3 performing very highly ($0.91 < R^2 < 0.92$; 23.25 % < relative RMSE < 27.76 %) and basin 4 performing poorly (R^2 = 0.11; relative RMSE = 68.86 %). In fact, FLH is found to perform least well of all evaluated algorithms for Basin 4. Most matchups from Basin 4 are characterized by oligotrophic conditions (chl-*a* ≤ 8 to 10 mg m^{-3}), and similarly, most oligotrophic matchups from the full dataset are from Basin 4. It can therefore be concluded that FLH is not suitable under oligotrophic conditions at Lake Balaton, but is highly suited to the measurement of eutrophic and hypertrophic (chl-*a* ≥ 8 to 10 mg m^{-3}) conditions at this site. Although the neural network processors tend to show the inverse trend, with higher retrieval performances at lower chl-*a* concentration levels, none performs particularly well for Basin 4 retrievals. FUB/WeW obtained the best results, with relative RMSE = 32.17 %. Neural network retrievals are very poor for the higher chl-*a* concentrations characteristic of Basins 1 through 3, with relative RMSE as high as 82.12 % for the EUL processor in Basin 1. All neural network-based algorithms, as well as the MCI algorithm, resulted in underestimations of coinciding *in situ* measured chl-*a* concentrations at concentrations exceeding approximately 10 mg m^{-3} (Figure 4.5).

Table 4.4. Algorithm performance, using the 30 %, validation dataset. From Palmer et al. (2015a).

Basin	Processor	n	Slope	Intercept	R^2	Bias ($mg\ m^{-3}$)	RMSE ($mg\ m^{-3}$)	Rel. RMSE (%)
Full lake	C2R	50	0.38	7.02	0.43	-0.10	9.98	65.98
	EUL	50	0.50	6.49	0.33	1.46	8.33	68.31
	BL	39	0.39	7.02	0.48	-2.22	9.97	60.61
	FUB/WeW	32	0.43	4.09	0.65	-0.76	5.53	45.43
	L1b FLH	60	0.85	1.52	0.87	-0.49	4.19	30.75
	L1b MCI	60	0.65	3.83	0.69	-0.91	6.62	48.63
1	C2R	13	0.22	13.80	0.21	1.71	15.70	66.23
	EUL	12	0.20	13.92	0.01	5.01	13.02	82.12
	BL	12	0.22	14.94	0.18	-1.60	12.35	55.62
	FUB/WeW	6	0.08	9.39	0.16	-0.17	6.71	46.63
	L1b FLH	16	0.93	-1.51	0.92	-2.91	4.77	23.25
	L1b MCI	16	0.48	6.79	0.58	-3.80	9.69	47.18
2	C2R	12	0.24	8.75	0.40	-2.11	9.12	58.67
	EUL	15	0.25	10.86	0.27	-0.53	9.26	58.32
	BL	8	0.21	10.15	0.59	-6.70	13.33	56.36
	FUB/WeW	6	0.26	6.29	0.56	-3.47	5.59	42.75
	L1b FLH	14	1.19	-2.48	0.91	0.05	3.64	26.58
	L1b MCI	14	1.06	1.67	0.77	2.54	5.65	41.29
3	C2R	8	0.31	6.97	0.53	-3.05	9.13	54.11
	EUL	8	0.93	0.72	0.72	0.09	3.55	30.20
	BL	8	0.37	7.20	0.56	-2.81	6.71	39.78
	FUB/WeW	8	0.47	3.53	0.74	-1.02	7.53	42.61
	L1b FLH	12	0.79	1.41	0.91	-2.10	4.65	27.76
	L1b MCI	12	0.68	1.31	0.86	-4.06	6.82	40.73
4	C2R	17	0.23	5.04	0.23	1.32	2.81	58.53
	EUL	15	0.22	4.61	0.04	1.33	2.58	61.62
	BL	11	0.09	5.09	0.02	0.80	2.90	61.47
	FUB/WeW	12	0.63	2.34	0.81	0.48	1.61	32.17
	L1b FLH	18	0.48	5.08	0.11	2.30	3.67	68.86
	L1b MCI	18	0.62	3.11	0.23	1.08	2.62	49.18

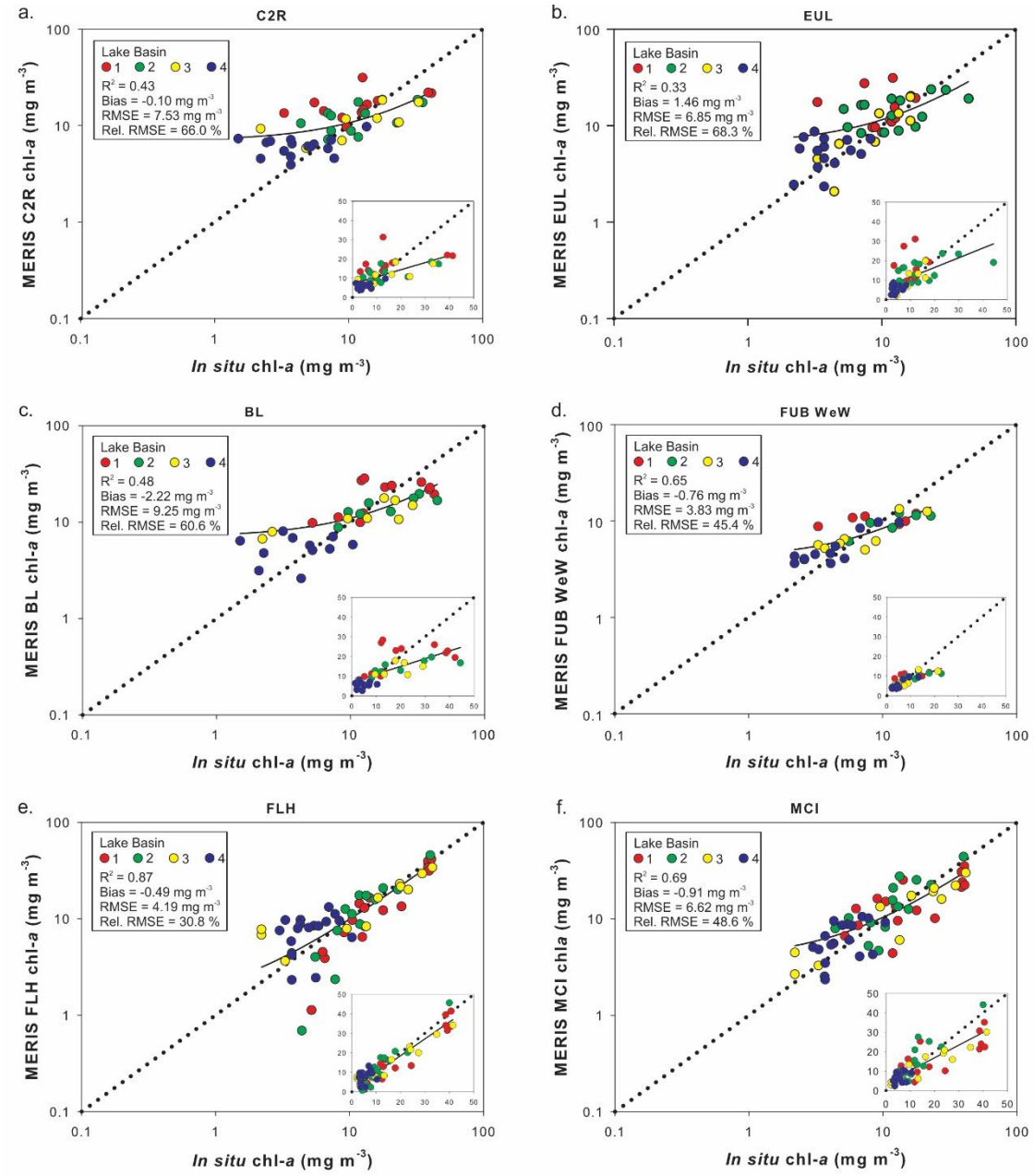

Figure 4.5. Chl-*a* concentration retrieval performance of the six selected algorithms, colour-coded by basin. Insets are plotted in normal and main graphs in log space. From Palmer et al. (2015a).

When applied to mapping (Figure 4.6a), the implications of the variable algorithm chl-*a* retrieval performance for phytoplankton bloom monitoring are clear. Chl-*a* concentration maps produced during a bloom event in August 2010 using each of the algorithms compared here show that the bloom event is accurately captured and detailed spatially by the FLH algorithm, although the low concentrations measured *in situ* in Basin 4 are overestimated, and are more accurately retrieved by the NNs. *In situ* chl-*a* concentration in Basin 1 measured on the same date as image acquisition is 38.5 mg m^{-3}, and that measured in Basin 4 is 7.0 mg m^{-3} (Figure 4.6b). Although the other five algorithms reveal a spatial gradient from high to low concentrations from Basin 1 to 4, the bloom concentrations are not accurately retrieved. MCI only slightly underestimates bloom concentrations, but all neural network processors, and especially FUB/WeW greatly underestimate concentrations. Considered over the full five-year study period assessed here, FLH is found to accurately and consistently retrieve bloom events, compared with *in situ* chl-*a* measurements. (Figure 4.7).

Figures 4.8 and 4.9 present the FLH-derived chl-*a* concentration time series spanning pre- to post-bloom conditions in summer 2010, using select fully or partially cloud-free MERIS imagery from across this period to highlight the spatiotemporal patterns. Of the total 34 MERIS overpasses between July 17 and September 13, 17 images included full or partial cloud-free coverage of the lake. The development and progression of the bloom is clear through the FLH maps (Figure 4.8), including expansion over the surface area of the southwestern portion of the lake, from the confluence of the Zala River in the southwest, extending northeastward. Nuance and shifting in the spatial patterns of phytoplankton biomass can also be observed and may be related to wind and related water circulation superimposed upon the general southwest-northeast gradient. In addition to this spatial nuance, the FLH chl-*a* maps capture the onset and intensification of the bloom, as well as dynamics of post-peak concentrations in late August/early September. Translation of the maps from Figure 4.8 to the classification used by the KdKVI for EU WFD chl-*a* reporting (Table 4.5) is presented in Figure 4.9.

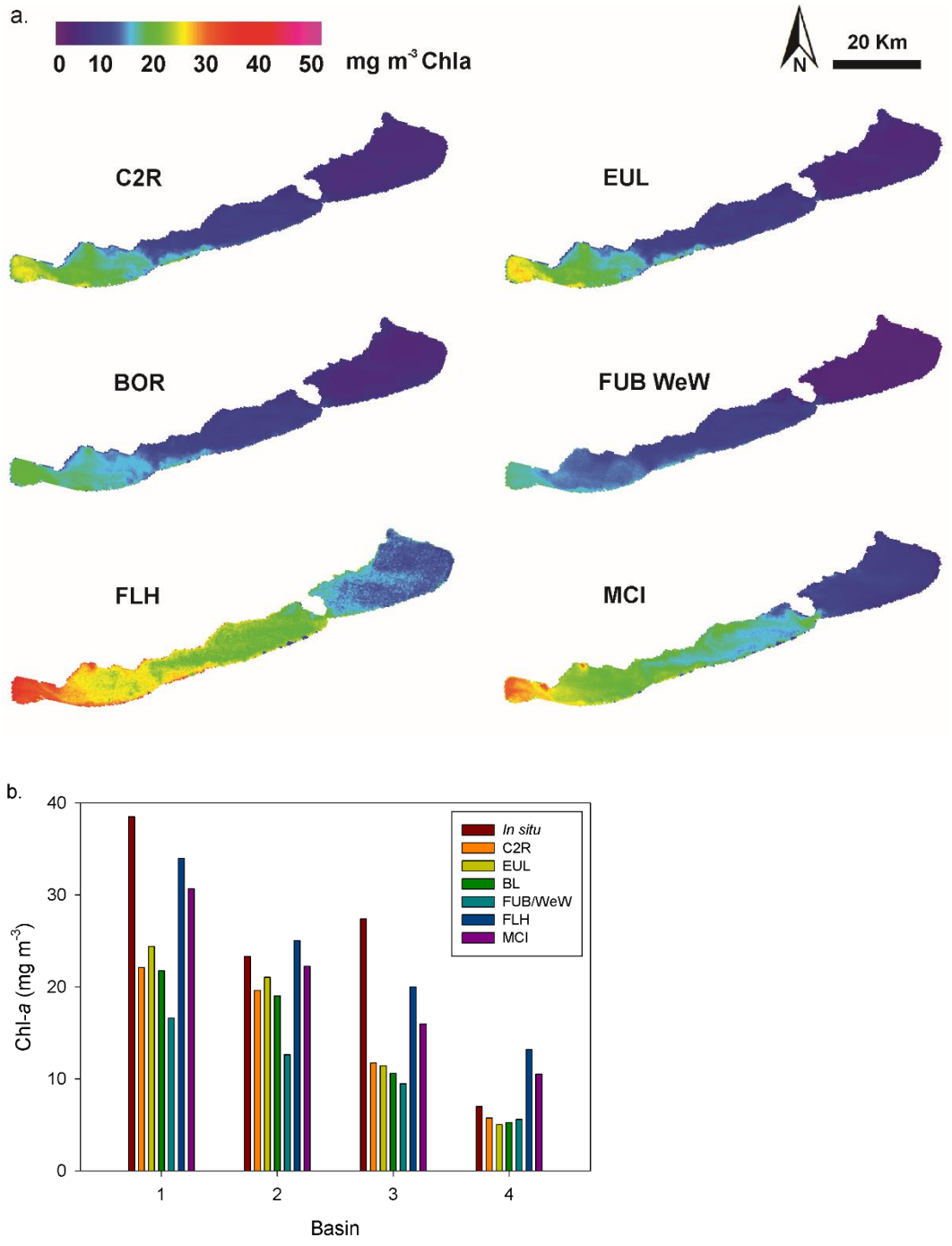

Figure 4.6. Comparison of selected algorithms' chl-*a* mapping during a phytoplankton bloom in Basins 1 and 2 through mapping (a) and in comparison with *in situ* concentrations (b). From Palmer et al. (2015a).

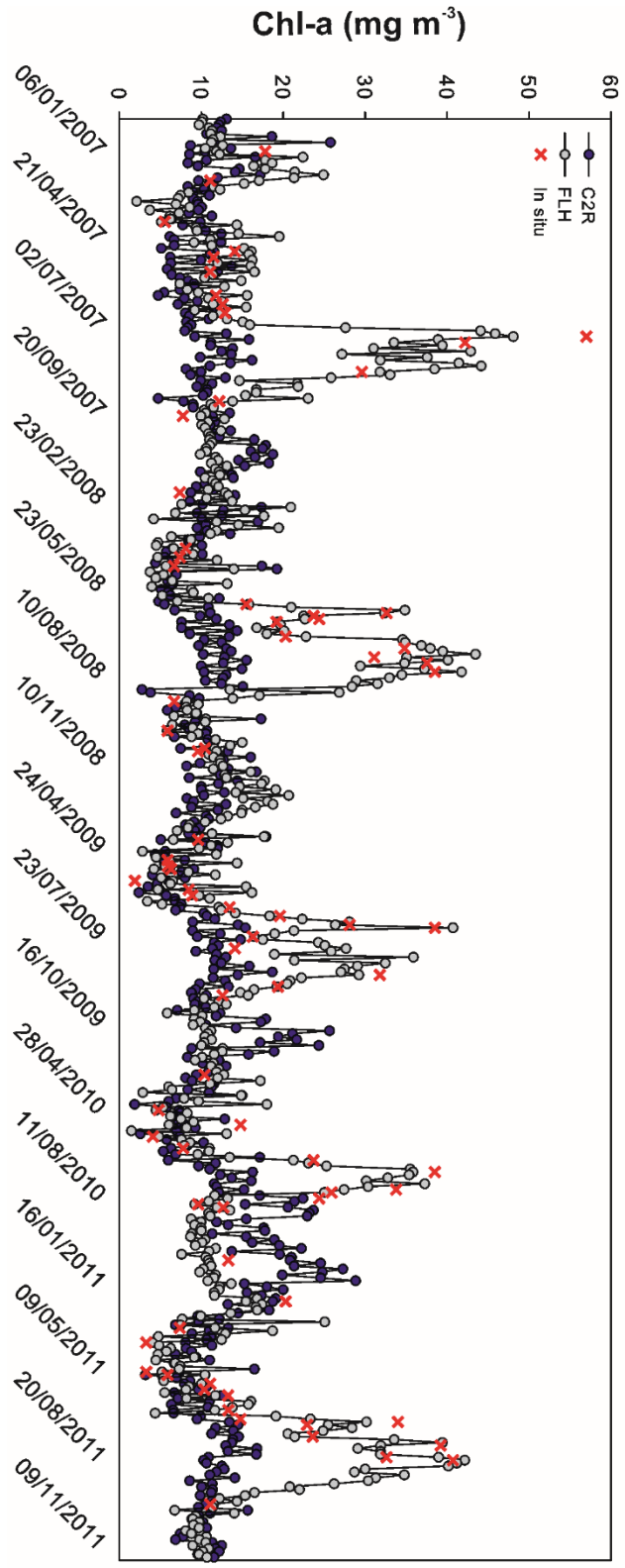

Figure 4.7. Five year time series comparing FLH, C2R and *in situ* measurements. From Palmer et al. (2015a).

Table 4.5. Chl-*a* concentration classification used by the KdKVI in Lake Balaton WFD reporting (personal communication with KdKVI, 2014).

Chl-*a* (mg m^{-3})	**OECD classification**	**WFD classification**
< 8	Oligotrophic	High
8 – 25	Mesotrophic	Good
25 – 75	Eutrophic	Average
> 75	Hypertrophic	Poor

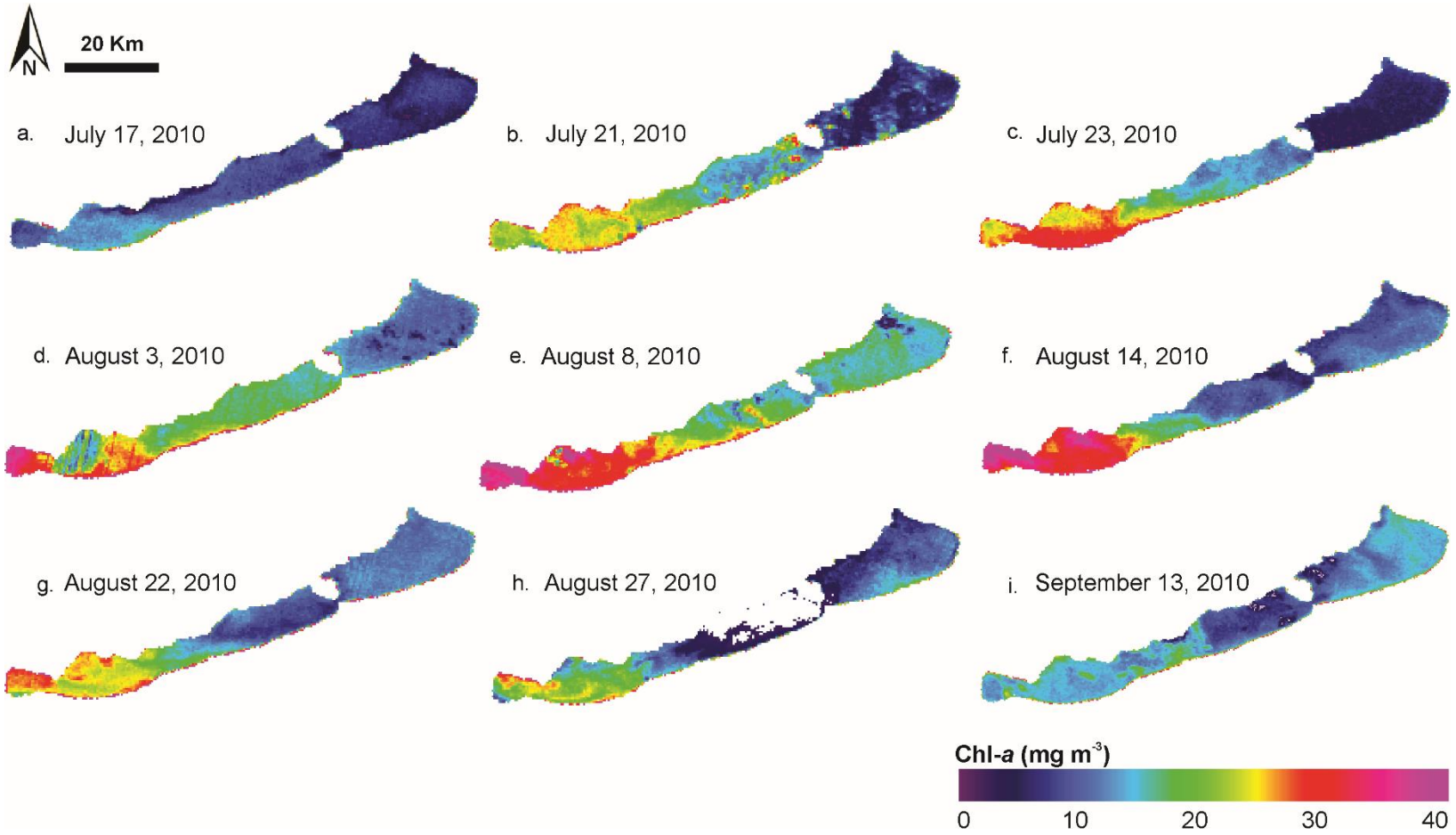

Figure 4.8. FLH retrieved chl-*a* concentration maps during the July-August 2010 bloom event.

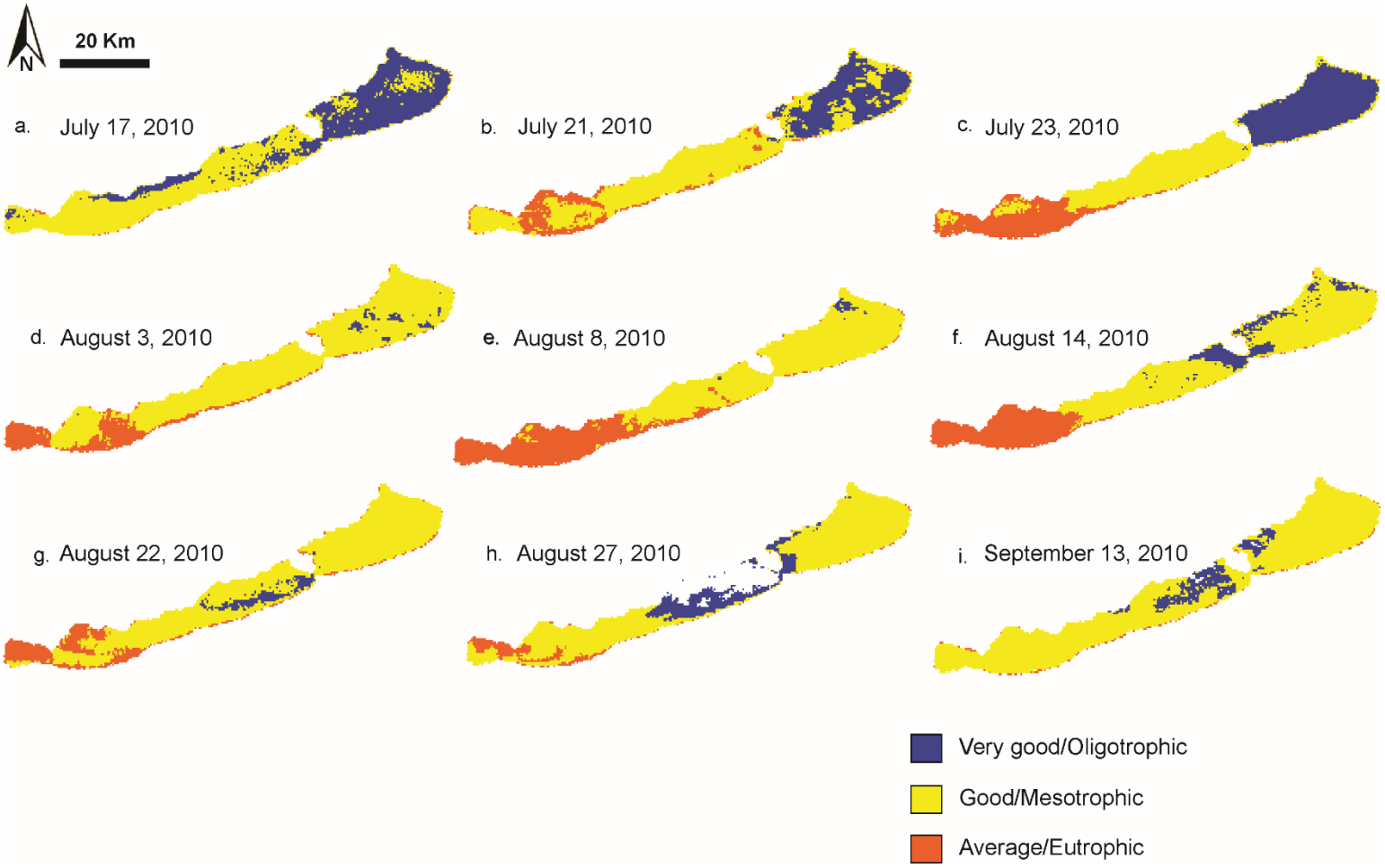

Figure 4.9. FLH retrieved chl-*a* concentration maps, according to WFD classification, during the July-August 2010 bloom event.

4.5 Discussion

The semi-empirical, band difference algorithms evaluated here, and particularly FLH, performed much better than the evaluated neural network algorithms. Coefficients specific to Lake Balaton were determined and used to convert the FLH index to chl-*a* concentrations, as was done for the MCI algorithm and to relate pigment absorption (a_pig(443) or $a_{pl}(440)$) of the neural networks to *in situ* chl-*a* concentrations. These coefficients would not be expected to result in the retrieval of accurate chl-*a* concentrations when applied to another site. Rather, site-specific local tuning would be required. MCI chl-*a* retrievals were also validated using Level 1b data during an extreme bloom event in Lake of the Woods spanning the Canada/US border (Binding et al. 2010). If the slope and intercept coefficients used to tune chl-*a* retrievals there (6.166 and 6.347 respectively) were applied to the retrieved MCI for Lake Balaton, chl-*a* concentrations would be greatly underestimated (bias = -5.61 mg m^{-3}, relative RMSE = 74.67 %, compared with bias = -0.91 and RMSE = 48.63 % found through local tuning here) for example. Similarly, SIOP coefficients locally tuned to retrieve Lake Balaton chl-*a* from NN processors' pigment absorption would not be transferrable to another site, as apparent in differences between the original and tuned coefficients (Table 4.3), and recalibration would again be necessary. Despite the improvement to neural network retrievals through local calibration, overall performance for all four algorithms remained low relative to FLH and MCI chl-*a* retrievals, and it can be concluded that the a_pig(443) and $a_{pl}(440)$ are themselves poorly retrieved by the processors for Lake Balaton, precluding robust chl-*a* concentration retrievals from them.

It should also be noted that the FLH and MCI algorithms made use of TOA L1b radiance in the current work whereas each of the neural network algorithms carries out a neural network -based atmospheric correction, either simultaneous to the chl-*a* retrieval or prior to it in a separate module (Doerffer and Schiller 2007; Doerffer and Schiller 2008; Schroeder et al. 2007a). The influence of atmospheric correction on the poor chl-*a* of the neural networks relative to the contribution of IOP or constituent retrieval failure itself is unknown, but may indeed be substantial. For example, *in situ* spectrometer-measured reflectance from high phytoplankton biomass Spanish lakes were input directly into the in-water module of the EUL processor, bypassing the

atmospheric correction (Koponen et al. 2008). Although the spatial scale may also have had an influence (i.e., the *in situ* spectrum is from exactly the same point as the matchup chl-*a*, rather than aggregated values from a 300 × 300 m pixel as is the case when MERIS imagery is input. The subpixel spatial variability is expected to also be a source of error), a significant improvement in retrievals was reported compared with when the atmospheric correction module was also employed.

Whereas the FLH originally has its physical underpinnings in the chl-*a* fluorescence maximum near 681.5 nm (MERIS band 8), above a baseline between lower adjacent values (Gower et al. 1999), as described above, and should therefore correlate positively with increasing phytoplankton biomass, a negative relationship was revealed here for chl-*a* concentrations greater than approximately 10 mg m^{-3}. Similar findings have been reported elsewhere under meso-, eu- and hypertophic conditions (Binding et al. 2010; Gons et al. 2008; Matthews et al. 2012), and may be explained by the dominance of phytoplankton backscattering captured by MERIS band 9 (709 nm) over the fluorescence signal captured by band 8 (681 nm). Nonetheless, the trough at band 8 under the baseline between bands 7 (619 nm) and 9 more robustly retrieves *in situ* chl-*a* concentrations than does the band 9 peak above the band 8 to 10 (753 nm) baseline (i.e., the MCI algorithm). The lack of a strong fluorescence signal might be explained by cyanobacteria dominance (Binding et al. 2010; Matthews et al. 2012; Wynne et al. 2008), as chl-*a* is located for the most part in the non-fluorescence Photosystem I (PSI) of cyanobacteria (Johnsen and Sakshaug 1996; Matthews et al. 2012; Mimuro and Fujita 1977), whereas most chl-*a* is stored in the fluorescing Photosystem II (PSII) in most other phytoplankton divisions (e.g., chlorophyta). Wynne et al. (2008) and several subsequent studies (Lunetta et al. 2015; Stumpf et al. 2012; Wynne et al. 2013a) make use of the same formulation as FLH in their Cyanobacteria Index (CI), whereby negative FLH values indicate cyanobacteria blooms and correlate with cyanobacteria bloom magnitude, since cyanobacteria do not produce a chl-*a* fluorescence signal near 685 nm and do produce a fluorescence signal near 664 nm. Positive FLH values therefore indicate the absence of a cyanobacteria bloom. A similar configuration is also adopted in the cyanobacteria flag of the MPH algorithm (Matthews et al. 2012), where cyanobacteria dominance is distinguished by a negative peak at MERIS band 8 above a baseline between bands 7 and 9 (i.e, FLH) coinciding

with a positive peak at band 7 (664 nm) above a baseline between bands 6 and 8. As such, it considered likely that the negative FLH values retrieved for Lake Balaton chl-*a* concentrations > 10 mg m^{-3} are indicative of cyanobacteria dominance. Previous works on Lake Balaton phytoplankton community composition and eutrophication (e.g., Hajnal and Padisák 2008; Istvánovics et al. 2002; Padisák and Reynolds 1998) have also indicated cyanobacteria dominance of the large summer blooms, and particularly that of the subtropical invader Cylindrospermopsis raciborskii. However, *in situ* data on species composition or phycocyanin concentrations are lacking in the current work, precluding definitive confirmation. Therefore, phytoplankton blooms more generally are referred to here.

FLH is found to perform better at higher chl-*a* concentrations, within the concentration range assessed here. In the oligotrophic Basin 4, FLH performance is poorest of all tested algorithms, and FUB/WeW chl-*a* retrievals are found to be better. The failure of red-NIR band math algorithms such as FLH at concentrations lower than between 8 and 20 mg m^{-3} has also been observed elsewhere (Domínguez Gómez et al. 2011; Matthews et al. 2012). Although overall neural network performance was found to generally be poor for C2R, EUL, CL and FUB/WeW alike, these tended to perform slightly better at lower concentration levels, such as found in Basin 4 (Table 4.4). An ensemble approach, whereby FLH was applied and concentrations retrieved as < 10 mg m^{-3} were subsequently excluded and processed with the FUB/WeW processor, was explored and found to slightly improve low concentration results (4.28 % improvement overall and 10.61 % improvement for concentrations < 10 mg m^{-3}). Despite this slight improvement, the use of FLH alone is found to be sufficient for monitoring the onset and development of high biomass bloom events, and as such will be applied and considered more fully in Chapter 6.

The inaccurate chl-*a* concentration retrievals resulting from neural network application were apparent in mapped products (Figure 4.7), calibration (Figure 4.4) as well as validation matchup statistics (Figure 4.6; Table 4.2) alike. Within the context of monitoring and mapping Lake Balaton algal blooms, this underscores that the use of these algorithms would not result in reliable products. Similar to results found here, the analysis of a Lake of the Woods bloom (1.9 – 70.5 mg m^{-3}), revealed significant bloom underestimation by the C2R processor (Binding et al. 2010), and the Validation Report of the ESA Development of MERIS lake water algorithms project

including Spanish, Finnish, German and African lakes found that Spanish lake chl-*a* concentrations (1.2 – 53.2 mg m^{-3}) were greatly underestimated by the EUL processor (Koponen et al. 2008). Although matchups with chl-*a* concentrations that exceeded the various neural network training ranges were excluded here via Case 2 flagging (out of training range flags) and manually removed where they remained after flagging, information lacking for other constituents (TSM, CDOM) as well as IOPs and water-leaving reflectance made it impossible to do the same for all parameters. It could therefore be the case that although the chl-*a* concentration training range was not exceeded, other parameters were out of range despite adhering to neural network flagging. This is an important consideration in the current case, and also for other sites where *in situ* data may be fully or partially lacking. Although remote sensing is often over-sold as a replacement for *in situ* sampling and analysis, in reality validation with *in situ* measurements is an important component of remote sensing. The fuller and more robust a validation that is possible, the more reliable will be the produced satellite image-derived maps and interpretations. It is recommended that validation of water constituents, IOPs and AOPs be carried out whenever possible, however it must also be understood that in many cases, such as Balaton, archive datasets able to be acquired will be incomplete and that a compromise must be struck.

The use of FLH in a classification exercise carried out in accordance with WFD reporting requirements demonstrated the added spatial information possible using satellite products relative to the use of conventional monitoring measurements (Figure 4.9). For example, point measurement-based classification might indicate that two of four basins are eutrophic (or "average"), but this could correspond to anywhere from 20 to 40 % of the total lake surface area. Although satellite image products, such as chl-*a* maps, have the potential to provide an informative tool to water resource managers, the volume of the associated data is often overwhelming (for example in the case of daily, or even dekad-binned, spatially cohesive maps of one or possibly several parameters (TSM, CDOM, secchi depth, temperature, etc.)). The classification proposed here in association with WFD reporting requirements offers a compromise between added spatial information possible through satellite imagery, and a partially digested data product which can more easily be integrated into management activities.

4.6 Conclusions

The use of MERIS satellite imagery has been demonstrated in application to Lake Balaton chl-*a* concentration mapping, however the accuracy of chl-*a* maps is strongly dependant on the retrieval algorithm employed. This highlights the importance of algorithm validation covering as broad a range as possible of optical conditions and constituent concentrations expected to be encountered for a given site or region. Caution is advised when applying un- or under-validated algorithms, despite the availability of automated algorithms. FLH was found to perform best after local tuning of all band arithmetic and neural network algorithms, and to successfully retrieve *in situ* chl-*a* concentrations and bloom dynamics over the full five years of the study period. The negative relationship between FLH and *in situ* chl-*a* concentrations suggests cyanobacteria dominance and absorption and backscattering rather than fluorescence as a physical underpinning of the algorithm for Lake Balaton. Its performance varies with the chl-*a* concentrations encountered, performing less well in low phytoplankton biomass (oligotrophic) waters than those characterized by high biomass conditions (eutrophic). This was not found to interfere with detection or monitoring of large blooms, however, and the application of FLH in full time series processing to improve spatiotemporal analysis of phytoplankton over ten years is concluded to be warranted. The ability of FLH to accurately delineate the temporal and spatial dynamics of Lake Balaton phytoplankton biomass has been demonstrated inter-annually as well as for a case study bloom event. Corresponding WFD reporting classifications also demonstrate the potential of remote sensing in informing and complementing required management reporting.

Chapter 5

MERIS atmospheric correction validation and influence on chlorophyll-*a* retrieval

5.1 Introduction & rationale

Atmospheric correction is an important processing step in the interpretation of optical satellite imagery, but is known to be a particular challenge over optically complex inland and coastal waters (Gordon and Wang 1994), as was introduced in the "Additional Challenges in lake remote sensing" section of Chapter 2. This is due to the synergistic effect of several factors. Firstly, water-leaving reflectance tends to be very low, comprising only a small percentage (ca. < 10 %) of the bulk signal measured by the satellite sensor; the remaining ca. > 90 % is related to atmospheric scattering (Siegel et al. 2000; Vidot and Santer 2005). As a result, small amounts of error in atmospheric correction will have a proportionately large impact over water bodies, which themselves have a very low signal, relative to typically much brighter terrestrial surfaces. Secondly, both atmospheric and water-leaving contributions of the signal received by the sensor comprise multiple variable scattering and absorbing components which overlap in optical signal. A related difficulty in optically complex waters results from the break-down of the conventional "black-pixel assumption" commonly employed in oceanic settings (Gordon 1997; Gordon and Clark 1981). In the so-called Case 1 waters of the pelagic ocean, an insignificant fraction of the signal measured by satellite sensors in the near-infrared range (between ca. 765 and 865 nm) is assumed to be from the water and water constituents. Rather, zero water-leaving reflectance in this spectral range can be assumed, and any radiance that is detected can be assumed to be of atmospheric origin. The atmospheric signal measured in the NIR range can then be proportionately removed from the visible spectral range (Gordon and Clark 1981; Siegel et al. 2000). However, in optically complex waters where water constituents occur in higher proportions and more variably, this does not hold true. Notably, NIR reflectance has been demonstrated to be non-negligible under conditions of high suspended particulate matter or phytoplankton biomass (IOCCG 2000, 2006; Moore et al. 1999; Ruddick et al. 2000; Siegel et al. 2000).

An alternative approach proposed to avoid this issue in optically complex waters is to defer to the longer, shortwave infrared (SWIR) spectral range, instead employing the black-pixel assumption at wavelengths greater than 900 nm (Wang and Shi 2007). However, it has more recently been demonstrated that in very productive or highly turbid waters, the water-leaving reflectance even at SWIR wavelengths cannot be considered non-negligible (Knaeps et al. 2012;

Shi and Wang 2009). Furthermore, contributions to the total measured signal from the water and the atmosphere at any given wavelength are both highly variable over time, reflecting changes and variability in atmospheric conditions, as well as in-water constituents. Radiative transfer modeling to invert the TOA measured radiance has been demonstrated to be robust over lakes, although it requires extensive, highly specialized and site-specific *in situ* measurements (Brando and Dekker 2003; Chavula et al. 2009; Doxaran et al. 2009; Petus et al. 2010; Vermote et al. 2011). Neural network algorithms have been found to perform well, but also require large volumes of training data, and are not expected to perform well outside their training ranges such that they also tend to be somewhat site specific. A number of NN approaches to atmospheric correction have trained using a broad range of atmospheric conditions from above coastal and inland waters in an attempt to be more broadly applicable (Doerffer and Schiller 2007; Moore et al. 1999; Schroeder et al. 2007a). Several of these can easily be applied within the BEAM image processing toolbox to MERIS imagery. However, as was demonstrated for the neural network chl-*a* retrievals in Chapter 4, validation is imperative so as to understand the associated reliability and uncertainty levels.

Other atmospheric correction approaches proven to perform well for inland waters in several instances make use of the relative straightforwardness of estimating and removing atmospheric contributions to the sensor measured signal over land surfaces. These characterize atmospheric conditions for a given scene over an adjacent land mass, and extrapolate or interpolate these conditions over the inland or coastal waters within a predefined radius prior to their removal (Guanter et al. 2010; Vidot and Santer 2005). As such, there is no reliance on the complex and difficult to characterize optical conditions of the water body itself within the atmospheric procedure. A similar approach was developed for use over coastal waters, however instead of determining and extrapolating atmospheric conditions from adjacent land masses, Case 1 pixels are identified and atmospheric conditions constrained above these (Hu et al. 2000; Ruddick et al. 2000). The determined atmospheric conditions are then extrapolated to pixels identified as Case 2 within a 50 to 100 km radius and removed. The major limitation of applying this stepwise Case1/Case 2 approach in inland waters is that most inland water bodies, such as Lake Balaton, consist only of so-called Case 2 pixels and are not located near enough to oceanic Case 1 pixels for the atmospheric homogeneity assumption to hold. Furthermore, atmospheric correction in marine settings applies the condition of atmospheric pressure at sea level, which is not necessarily

true for lakes which may be situated at any elevation (Vidot and Santer 2005), e.g., ~105 m. a. s. l. in the case of Lake Balaton).

As is true for the chl-*a* concentration retrieval algorithms evaluated in the preceding chapter, each atmospheric correction architecture type and specific model has its own associated advantages and disadvantages over lake waters. None can be assumed *a priori* to perform well or poorly based on results obtained elsewhere, as conditions between optically complex water sites are highly variable. Furthermore, the use of uncorrected TOA Level 1b radiance, or partially corrected bottom-of-Raleigh data has been proven to retrieve chl-*a* concentration and other parameters of interest with high accuracy in a number of cases (Binding et al. 2010; Matthews et al. 2010; Matthews et al. 2012), including the results presented in Chapter 4. A reasonable criticism of using only partially corrected or uncorrected data is the inherent inconsistency due to the inability to account for variable atmospheric conditions over time using such data (Binding et al. 2010). However, the error imposed by atmospheric variability on time series chl-*a* retrievals relative to the contribution of different atmospheric correction models' error to subsequent chl-*a* retrieval performance is largely unquantified. The coinciding and extensive archive image and *in situ* datasets for Lake Balaton permit the exploration of this question.

5.2 Objectives

In light of the sensitivity and importance of atmospheric correction selection over inland waters prior to retrieving water constituents, as well as the range of models and model types developed and tested in the literature for other water bodies, the overarching objective of this chapter is the atmospheric correction and validation thereof of MERIS imagery overpassing Lake Balaton. Additionally, the impact of atmospheric correction performance on subsequent chl-*a* concentration retrieval from the same image set is determined. Specific objectives are as follows:

(1) To atmospherically correct a subset of Lake Balaton MERIS imagery spanning several years and all seasons using selected approaches;

(2) To compare the performance of the selected atmospheric correction models quantitatively through a validation of retrieved water-leaving reflectance with *in situ* measured spectra;

(3) To investigate the influence of matchup sampling timeframe interval (time between *in situ* measurement and satellite image acquisition) on water-leaving reflectance retrieval accuracy;

(4) To consider the underlying mechanisms governing atmospheric correction performance, including intermediate processing steps and spatial resolutions of the algorithms; and

(5) To assess the influence of atmospheric correction performance, and use of uncorrected data on subsequent chl-*a* concentration retrieval.

5.3 Methods

5.3.1 Atmospheric correction algorithms

C2R atmospheric correction module

As introduced in the preceding chapter, the C2R, EUL and BL neural network processors consist of separate modules to first carry out atmospheric correction, and subsequently retrieve IOPs and water constituents (Doerffer and Schiller 2007; Doerffer and Schiller 2008). Whereas the constituent retrieval modules of the three processors are distinct, with *in situ* data from different sites and vastly different conditions used to train their respective bio-optical models, the atmospheric correction module is common to all three processors (Doerffer and Schiller 2008). The atmospheric correction neural network uses image geometry (solar and viewing zenith and azimuth angles) and TOA radiance measured in 12 visible-NIR MERIS bands (1-10, 12-13) as input to produce water-leaving reflectance in the same bands. In addition to water-leaving reflectance, path radiance reflectance, transmittance, and aerosol optical thickness (AOT) at four wavelengths (443, 550, 778, 865 nm) are also output from the neural network, and the aerosol

angstrom coefficient is calculated from the AOT at 443 and 865 nm. A number of flags are assessed as part of the algorithm, indicating input or output pixels that are out of the training range, pixels possibly contaminated by sun glint and invalid pixels (Doerffer and Schiller 2008). The C2R/Lake processors' neural networks are applied on a per pixel basis, resulting in products at the 300 m spatial scale when using MERIS full resolution imagery.

SCAPE-M_B2

The Self-Contained Atmospheric Parameters Estimation for MERIS data (SCAPE-M) model performs sequential cloud masking, atmospheric characterization and retrieval of surface reflectance through the analytical inversion of the radiative transfer equation (Guanter et al. 2007; Guanter et al. 2008). SCAPE-M functions on the assumption of homogeneous atmospheric conditions over areas of a given size, by default a 30 by 30 km cell, into which the input TOA Level 1b MERIS radiance image is divided. Water pixels are masked, and reference land pixels within each cell are selected so as to maximize the spectral contrast between them, spanning a range from highly vegetated to bare soil pixels in an ideal case. Assuming constant atmospheric conditions throughout each cell, the contrast in the surface reference pixels are used to discriminate the contribution of the surface from that of the atmosphere to the top of atmosphere (TOA) signal (Guanter et al. 2008).

Reference pixels are modelled as a function of vegetated and bare soil end members for three vegetation type options and Aerosol Optical Thickness (AOT) associated with the best fitting end member combinations is chosen (Guanter et al. 2008). Visibility is calculated as a function of AOT and elevation and applied to the cell. Visibility is thusly derived for each of the 30 by 30 km cells of the image, the cell mosaic is smoothed to the pixel scale and blank cells (for example, over a water body; cloud cover remains masked) are filled via interpolation. AOT at 550 nm of the image is mapped as a function of visibility and elevation at the pixel scale (Guanter et al. 2008).

Columnar Water Vapour (CWV) is then determined using view and sun angles, derived AOT, surface elevation and surface slope. Reflectance of bands 14 and 15 are also required, and are determined iteratively by solving reflectance in bands 13 and 14 with a default CWV of 2 g cm^{-2}, and linearly extrapolating this to band 15 (Guanter et al. 2008). The resulting CWV is then applied again to improve the reflectance retrieval for bands 13 and 14, since band 14 may also be

slightly affected by water vapour. CWV, AOT, surface elevation and topography and angular information are then used in inversion of the TOA signal to retrieve surface reflectance for bands 1-10, 12-14. Reflectance of 11 and 15 are determined through extrapolation or interpolation of neighbouring bands, because they are affected by oxygen and water vapour absorption. SCAPE-M also interpolates to determine reflectance for band 2, as the gain coefficient is optimized for the higher reflectance of water bodies in the blue spectral range and it is typically applied over land surfaces (Guanter et al. 2008). SCAPE-M_B2 makes use of the known relationship between the originally retrieved reflectance value and the interpolated value to optimize band 2 reflectance retrievals for over inland waters (Domínguez Gómez et al. 2011), and otherwise follows the same processing chain as SCAPE-M. An adjacency effect correction is carried out for full resolution data, and subsequent geometric correction is optional (Guanter et al. 2008).

Although not specifically designed for optically complex waters, SCAPE-M, and more optimally the SCAPE-M_B2 adaptation, can be applied over inland and coastal waters that are within the maximum distance of the cell size from land (Guanter et al. 2010). The default setting for SCAPE-M processing over inland water pixels, outside of which pixels are masked, is water pixels within less than 20 km of a land mass, or of an area less than 1600 km^2, surrounded by a land mass. Since the atmospheric correction over land is extended (interpolated or extrapolated) over the water body, the need for extensive, difficult to obtain information regarding the optical conditions of the water itself is avoided. The performance of SCAPE-M over several lakes in Europe has been tested (Guanter et al. 2010). Generally, SCAPE-M was found to perform well over turbid and productive waters and to perform poorly in relatively clear, oligotrophic lakes where reflectance was overestimated. SCAPE-M_B2 was also validated over a number of highly productive Spanish lakes, reservoirs and lagoons, demonstrating accurate reflectance retrievals compared with several other atmospheric correction models (Domínguez Gómez et al. 2011). Good, but variable results using SCAPE-M in comparison with several other models were also reported in application to Lake Kasumigaura, Japan (Jaelani et al. 2013).

5.3.2 Chl-*a* concentration retrieval

In addition to FLH and MCI, considered in the Chapter 4 analysis of BEAM-implemented chl-*a* retrieval algorithms, several other band math algorithms also make use of varying combinations of MERIS red and NIR channels. The band combinations evaluated here, along with reference studies and reported chl-*a* concentration and correlation coefficient ranges therein, are listed in Table 5.1.

Table 5.1. Selected bandmath algorithms, previously reported to successfully retrieve chl-*a* over the approximate concentration range typically encountered in Lake Balaton, including reference studies, and reported ranges of chl-*a* concentrations and retrieval R^2 therein.

Band combination	**Reported R^2 range**	**Chl-*a* range (mg m^{-3})**
B9/B8[a]	0.84 – 0.91	1.3 - 100
B9/B7[b]	0.87 – 0.97	< 1 – 185
(B9-B12)/(B7-B12)[c]	0.94	1 – 100
(B9-B10)/(B7-B10)[d]	0.90	1.1 – 100
(1/B7-1/B9) * B10[e]	0.78 – 0.95	< 1 – 247.4
FLH (eq. 4.1)[f]	0.57	1.90 – 70.50
MCI (eq.4.1)[g]	0.72 – 0.74	1.90 – 70.50

[a]Flink et al., 2001; Kallio et al., 2001

[b]Matthews et al., 2010; Moses et al., 2009; Koponen et al., 2007; Kallio et al., 2001, 2003; Ammenberg et al., 2002; Gons et al., 2002, 2005.

[c]Koponen et al., 2002

[d]Härmä et al., 2001

[e]Matthews et al., 2010; Gitelson et al., 2009; Moses et al., 2009

[f]Binding et al., 2010

[g]Binding et al., 2010

5.3.3 Validation data

Remote sensing reflectance (R_{rs} (sr^{-1})) was measured *in situ* over the spectral range 350 – 800 nm using a Hyperspectral Ocean Colour Radiometer Surface Acquisition System (HyperOCR-SAS) produced by Satlantic. These data were acquired by colleagues from the University of Stirling School of Biological and Environmental Sciences during a field campaign at Lake Balaton in 2010 and were made available for the current work as part of a GIONET international secondment. R_{rs} measurements on August 22, 2010 coincided with a cloud-free MERIS overpass including Lake Balaton. *In situ* measurements made within three days of this overpass were also considered for validation (Figure 5.1). Measurements were made from a distance of 3.5 metres above the water surface, at a 135° angle from the sun. Downwelling irradiance, water surface radiance and sky radiance measured by three radiometers were used to calculate water-leaving radiance using Satlatntic ProSoft software (v.7.7.10), according to equation 2.4. Water-leaving radiance was converted to R_{rs} and spectrally resampled using the spectral response function of the MERIS bands 1 – 12 (Figures 5.2-5.5). Chl-*a* concentrations concurrent with R_{rs} measurements were also measured and made available.

Archive chl-*a* concentration data from the KdKVI were also used. Monthly (biweekly during the peak phytoplankton biomass period in the summer months) surface (< 50 cm) water samples are collected from the centres of the four main lake basins, spanning the main, longitudinal axis of the lake, as described in Chapters 3 and 4 (Figure 3.2). Chl-*a* concentration of the samples is determined spectrophotometrically in the KdKVI laboratory in accordance with ISO standards, after filtration (1.2 μm), pigment extraction in hot ethanol and centrifugation.

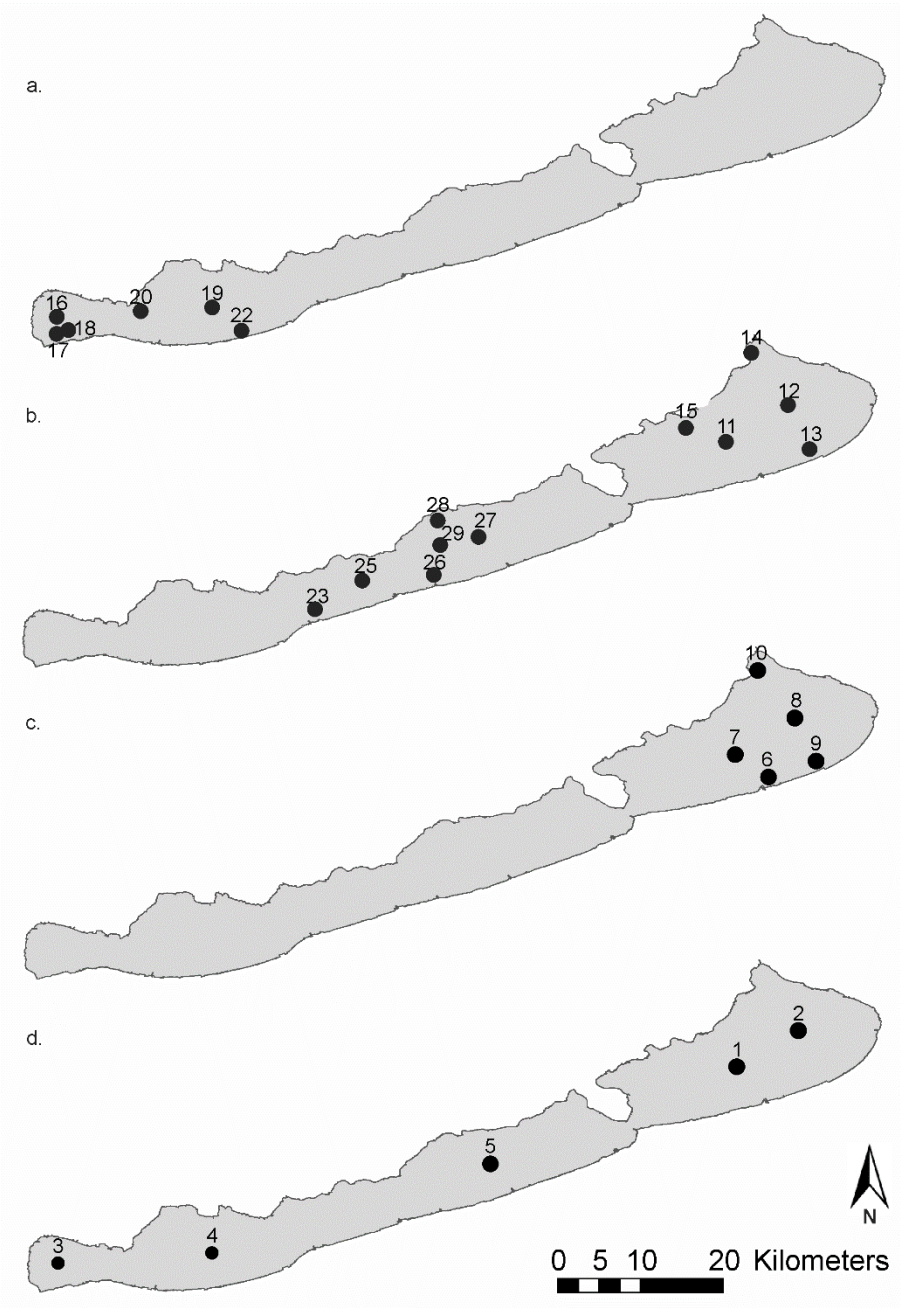

Figure 5.1. Locations of the 2010 field campaign sample sites. Same day (a), ± one day (b), ± two days (c) and ± three days (d) matchups with the August 22 overpass are indicated by the different symbols.

5.3.4 Image processing and validation

Level 1b MERIS data were processed using SCAPE-M_B2, and the atmospheric correction module of the C2R/Lake processor. SCAPE-M_B2 processed images were made available by J.A. Domínguez Gómez of the Universidad Nacional de Educación a Distancia. C2R/Lake processing was carried out using BEAM v.4.10. Mean L1b radiance, SCAPE-M_B2 reflectance and C2R/Lake reflectance, as well as AOT at 550 nm (AOT-550) produced by SCAPE-M_B2 and C2R/Lake, were extracted from a three-by-three pixel kernel centred on the corresponding *in situ* measurement using the pixel extraction tool of the BEAM toolbox.

Reflectance retrieved using SCAPE-M_B2 and C2R/Lake atmospheric correction coinciding with *in situ* R_{rs} measurements (± 0 to 3 days) were converted to R_{rs} via equation 5.1 for validation. The band combination chl-*a* concentration retrieval algorithms listed in Table 5.1 were applied to L1b radiance, SCAPE-M_B2 reflectance and C2R/Lake reflectance matchup image datasets. Correlations with *in situ* chl-*a* concentrations were compared across semi-empirical algorithms, and also compared for a given algorithm using the different input data. K-folds (k = 10) cross-validation was applied to each semi-empirical algorithm, using each input data type in R (using the cv.lm function of the DAAG package), whereby the matchups were split randomly into ten equal groups. One by one, each group was then withheld from the training of the algorithm, and used to validate the model.

$$R_{rs}\ (sr^{-1}) = \text{Reflectance}\ (sr^{-1}) / \pi \qquad \text{Equation 5.1}$$

Retrieval performance of both R_{rs} and chl-*a* concentration in comparison to available *in situ* validation data was assessed in terms of absolute (sr^{-1} and mg m^{-3}, respectively) and relative (%) RMSE, as per equations 4.5 and 4.6 respectively. Absolute and relative RMSE was calculated for each of the ten folds in the k-folds cross-validation applied to the semi-empirical chl-*a* concentration retrievals, and the averages and standard deviations are reported for each algorithm/input data type combination.

5.4 Results

5.4.1 Atmospheric correction

Mean and standard deviations of *in situ* chl-*a*, TSM and R_{rs} measurements from the 2010 field campaign are presented in Table 5.2. Validated SCAPE-M_B2 and C2R/Lake retrieved R_{rs} spectra for individual measurement locations are presented in Figure 5.2 (same day matchups), Figure 5.3 (± 1 day), Figure 5.4 (± 2 days) and Figure 5.5 (± 3 days), and scatterplots combining validation for all measurement locations for SCAPE-M_B2 and for C2R/Lake R_{rs} are presented in Figure 5.6. Matchups are separated into same day, ± 1 day, ± 2 days and ± 3 days. The more pronounced spectral trough near 681 and peak near 708 nm in the *in situ* R_{rs} spectral data in Figure 5.2, from the same day measurements, are associated with greater measured chl-*a* concentrations relative to those measured on the other days. On this date, measurements were made in Basin 1, which is known to have higher phytoplankton productivity than the other basins of Lake Balaton due to the well-known trophic gradient discussed in Chapter 3.

In Figure 5.2 it is clear that the R_{rs} magnitude, as well as the spectral shape produced using the SCAPE-M_B2 atmospheric correction model robustly preserve those measured *in situ* made on the same day. No statistically significant difference between relative RMSEs was found across the different sampling days as determined by the inability of a one-way Analysis of Variance (ANOVA) to reject this null hypothesis ($F(3,40) = 0.308$, $p = 0.82$), indicating that variance in relative RMSE between sampling days is less that than that within sampling days. However, the SCAPE-M_B2 reflectance from all ± 2-3 days matchups (Figures 5.4, 5.5) consistently slightly underestimate *in situ* R_{rs} and spectral shape in ± 1-3 days matchups (Figures 5.3, 5.4, 5.5), especially for spectra from Basins 3 and 4, is less well preserved in the red-NIR range than for same day matchups. The RMSE of SCAPE-M_B2 R_{rs} retrievals is between 0.001 and 0.011 sr^{-1} for all bands and ± 0 to 3 days, typically ranging from approximately 20 to 40 % relative RMSE (Figure 5.7; Table 5.3). Outlying relative RMSE values are associated with same day matchups, for bands one (62.6 %) and eight (48.1 %), rather than with increasing time from the MERIS overpass as would have been expected.

Table 5.2. Descriptive, per day statistics of *in situ* measurements collected during the August 2010 field campaign, within ± 3 days of MERIS image acquisition, including mean ± standard deviation of chl-*a*, TSM and HyperSAS R_{rs} resampled to the MERIS spectral bands.

	Basin	Chl-*a* (mg m^{-3})	TSM (g m^{-3})	B1 (sr^{-1})	B2 (sr^{-1})	B3 (sr^{-1})	B4 (sr^{-1})	B5 (sr^{-1})	B6 (sr^{-1})	B7 (sr^{-1})	B8 (sr^{-1})	B9 (sr^{-1})	B10 (sr^{-1})	B12 (sr^{-1})
Same day	1, 2	27.83 ± 4.81	10.99 ± 1.78	0.006 ± 0.002	0.007 ± 0.002	0.010 ± 0.003	0.013 ± 0.003	0.025 ± 0.006	0.015 ± 0.003	0.012 ± 0.002	0.008 ± 0.001	0.011 ± 0.002	0.004 ± 0.001	0.005 ± 0.001
± 1 day	2, 3, 4	10.15 ± 4.50	8.38 ± 2.15	0.012 ± 0.005	0.014 ± 0.005	0.020 ± 0.006	0.024 ± 0.007	0.035 ± 0.008	0.018 ± 0.005	0.013 ± 0.004	0.009 ± 0.002	0.009 ± 0.003	0.003 ± 0.001	0.004 ± 0.001
± 2 days	4	11.54 ± 1.46	14.62 ± 3.61	0.019 ± 0.003	0.021 ± 0.003	0.028 ± 0.004	0.032 ± 0.005	0.044 ± 0.004	0.026 ± 0.004	0.019 ± 0.003	0.013 ± 0.002	0.014 ± 0.002	0.004 ± 0.000	0.005 ± 0.001
± 3 days	1, 2, 4	18.77 ± 12.84	15.63 ± 4.27	0.015 ± 0.005	0.017 ± 0.006	0.025 ± 0.007	0.029 ± 0.007	0.042 ± 0.006	0.025 ± 0.003	0.020 ± 0.002	0.013 ± 0.001	0.016 ± 0.002	0.004 ± 0.001	0.005 ± 0.002

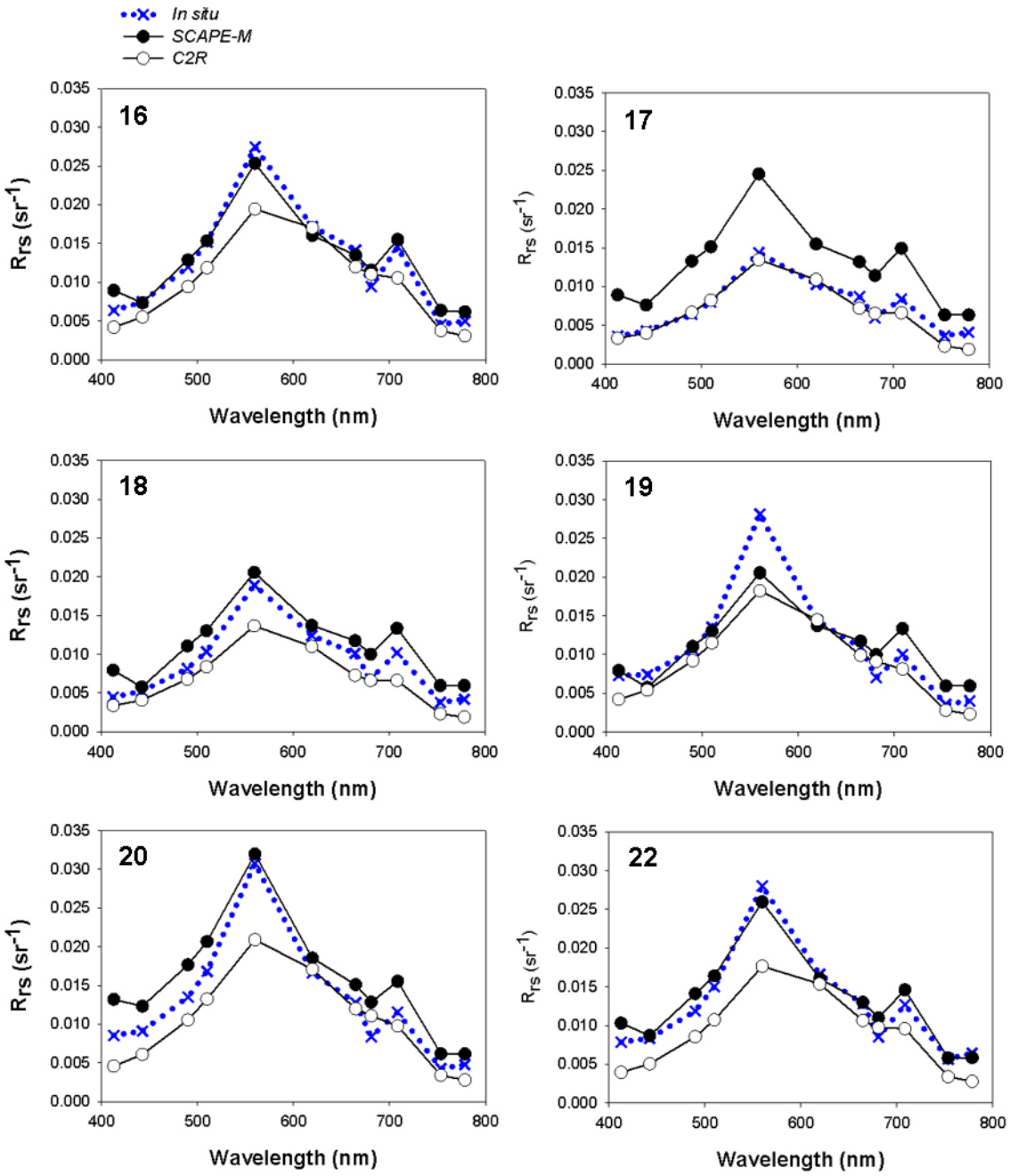

Figure 5.2. Comparison of SCAPE-M_B2 and C2R/Lake retrieved remote sensing reflectance (R_{rs} (sr^{-1})) with *in situ* measured R_{rs} from the same date (August 22 2010) for different sampling locations. Number refers to sample location of Figure 5.1.

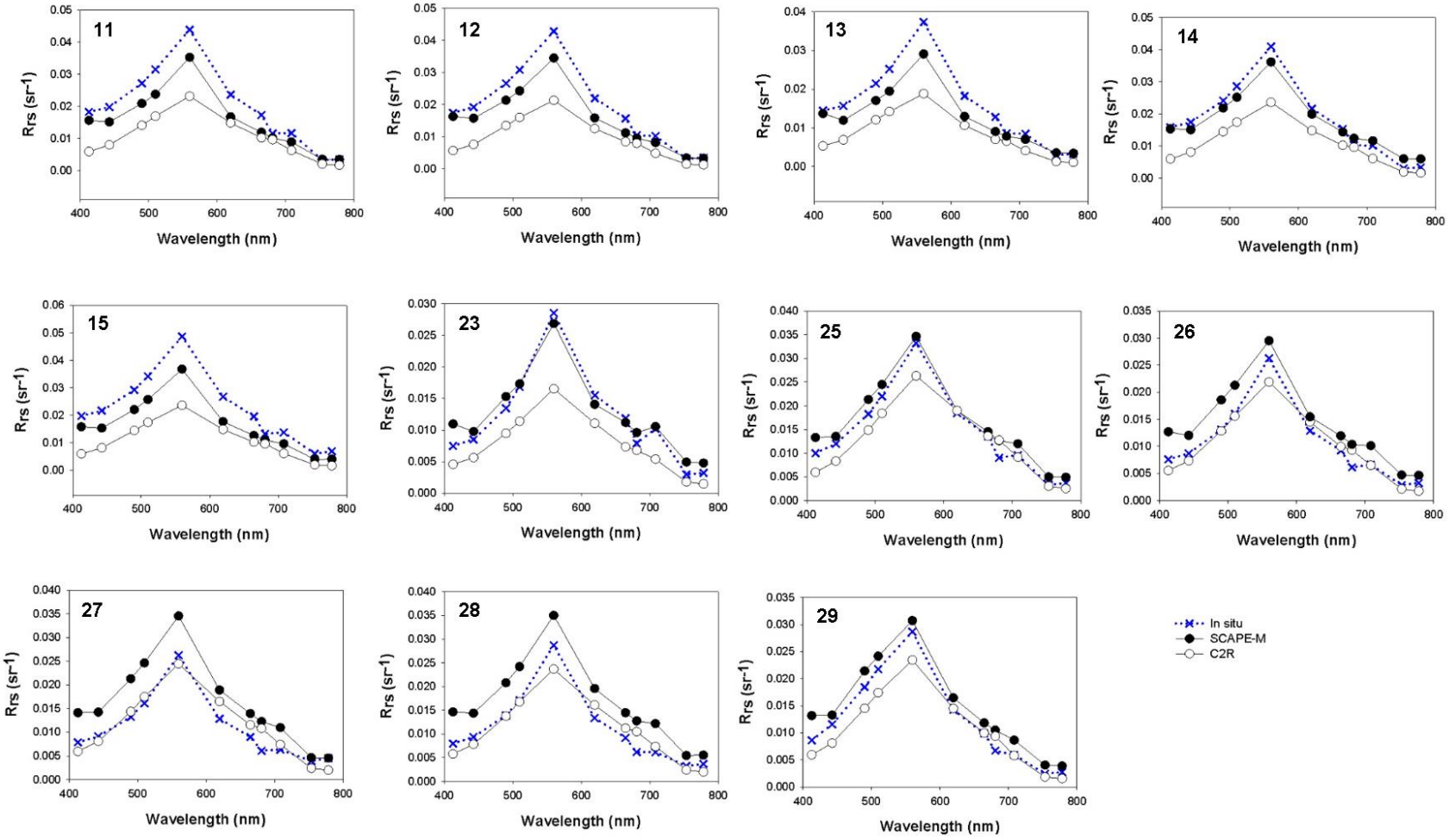

Figure 5.3. Comparison of SCAPE-M_B2 and C2R/Lake retrieved remote sensing reflectance (R_{rs} (sr^{-1})) with *in situ* measured R_{rs} ± 1 day for different sampling locations. Number refers to sample location of Figure 5.1.

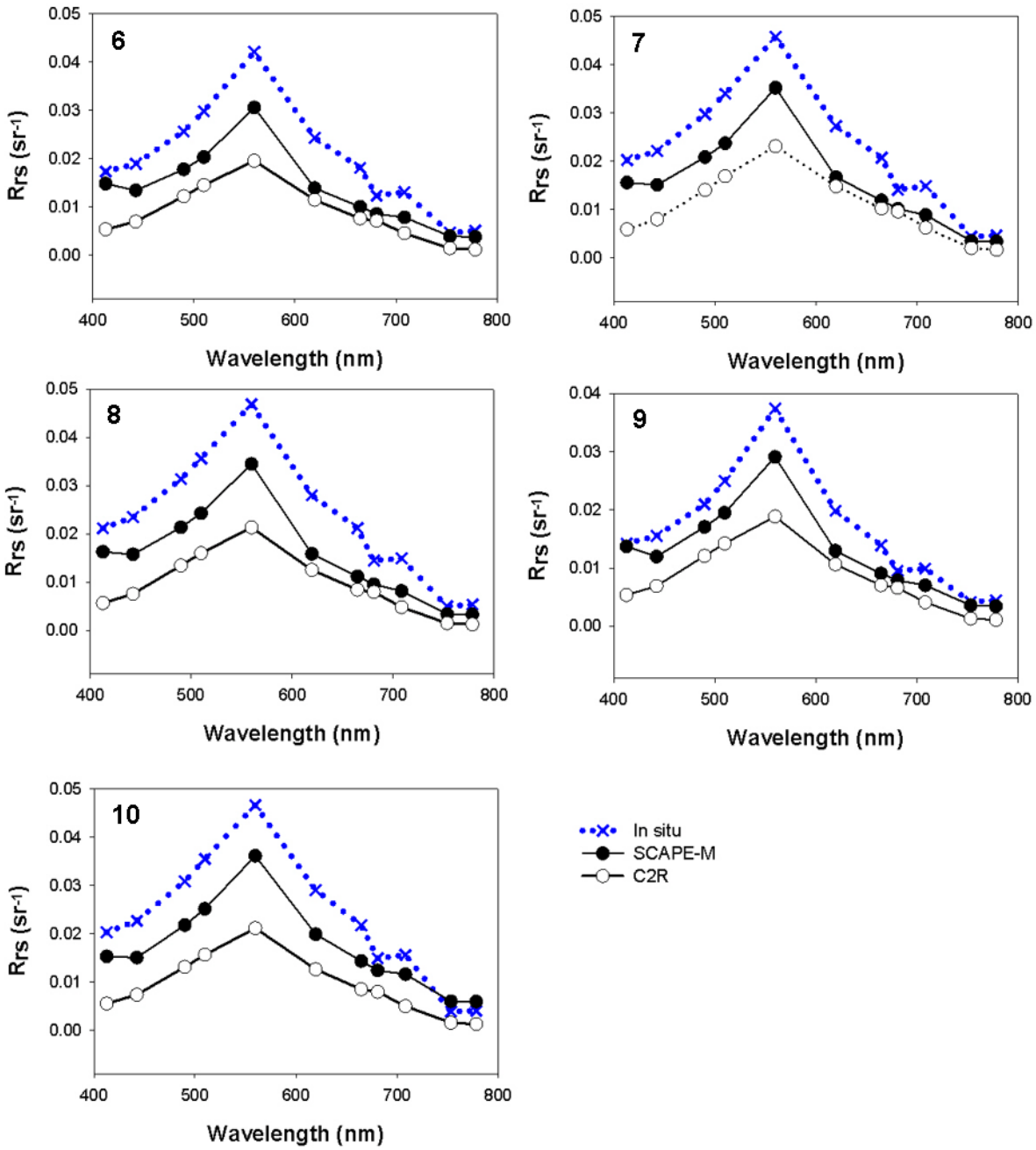

Figure 5.4. Comparison of SCAPE-M_B2 and C2R/Lake retrieved remote sensing reflectance (R_{rs} (sr^{-1})) with *in situ* measured R_{rs} ± 2 days for different sampling locations. Number refers to sample location of Figure 5.1.

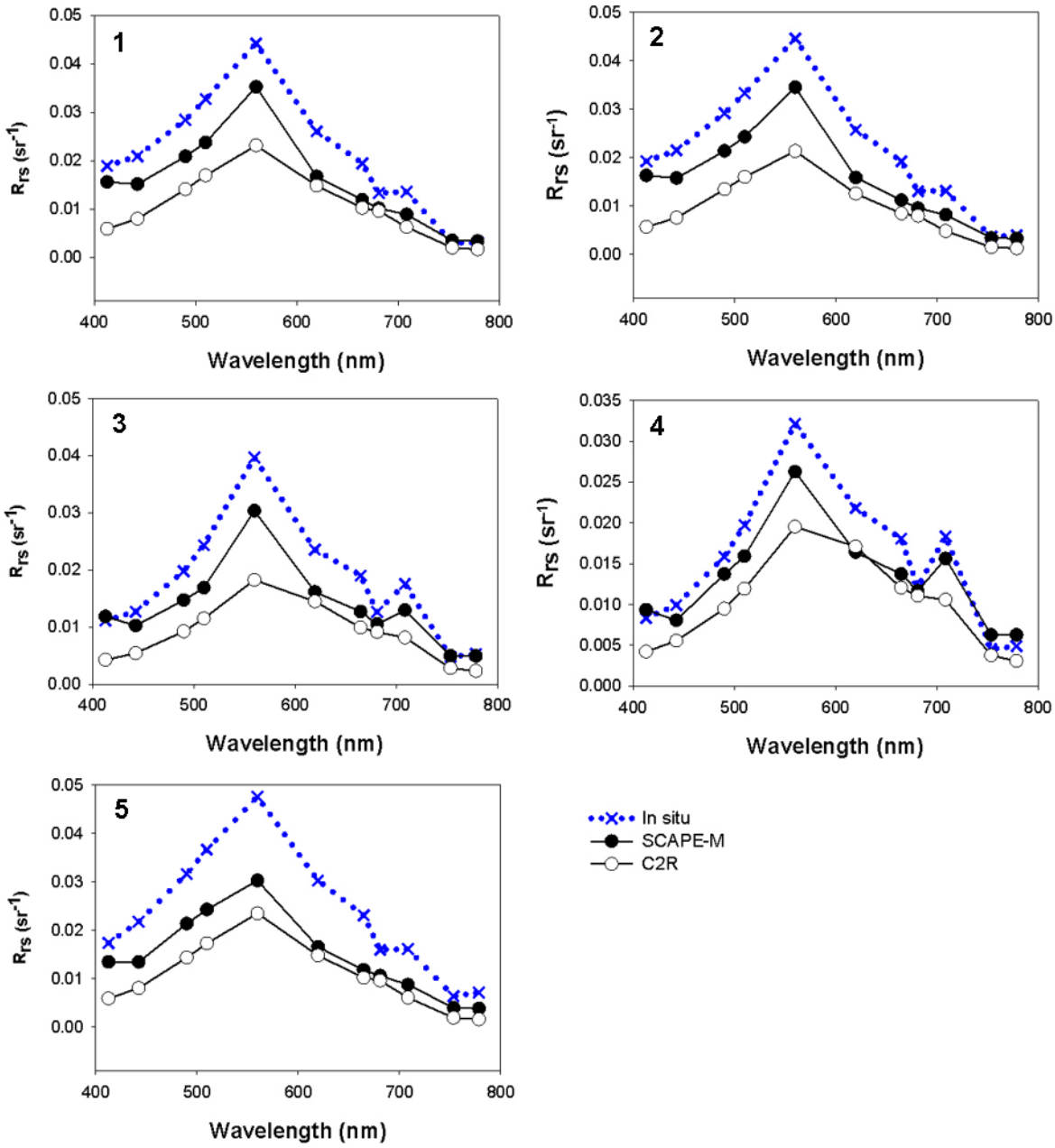

Figure 5.5. Comparison of SCAPE-M_B2 and C2R/Lake retrieved remote sensing reflectance (R_{rs} (sr^{-1})) with *in situ* measured R_{rs} ± 3 days for different sampling locations. Number refers to sample location of Figure 5.1.

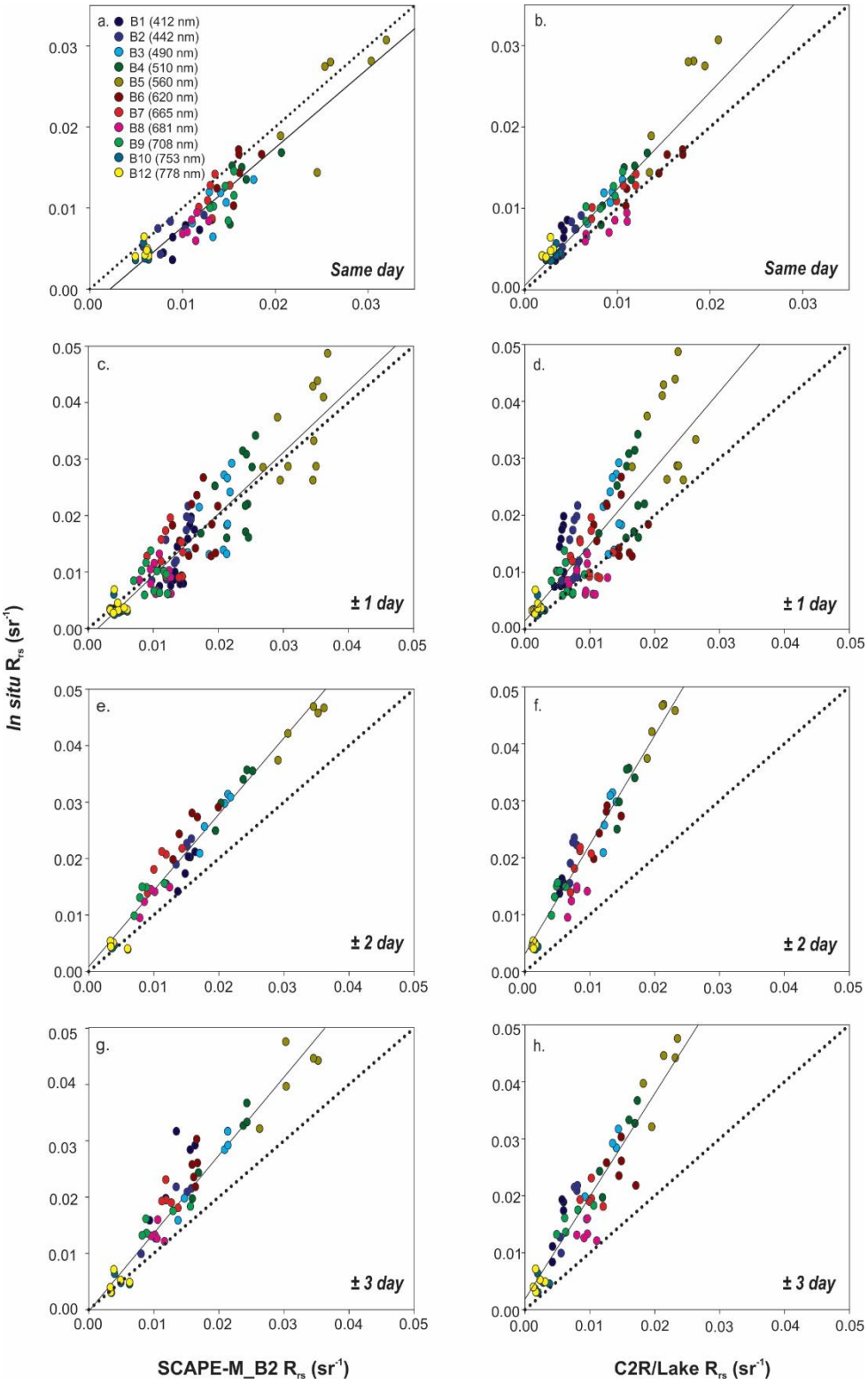

Figure 5.6. Scatter plots comparing SCAPE-M_B2 and C2R/Lake retrieved R_{rs} with *in situ* measured R_{rs} across MERIS bands 1-10, 12 for measurements taken on the same day (within three hours) as the overpass (a, b), ± 1 day (c, d), ± 2 days (e, f) and ± 3 days (g, h).

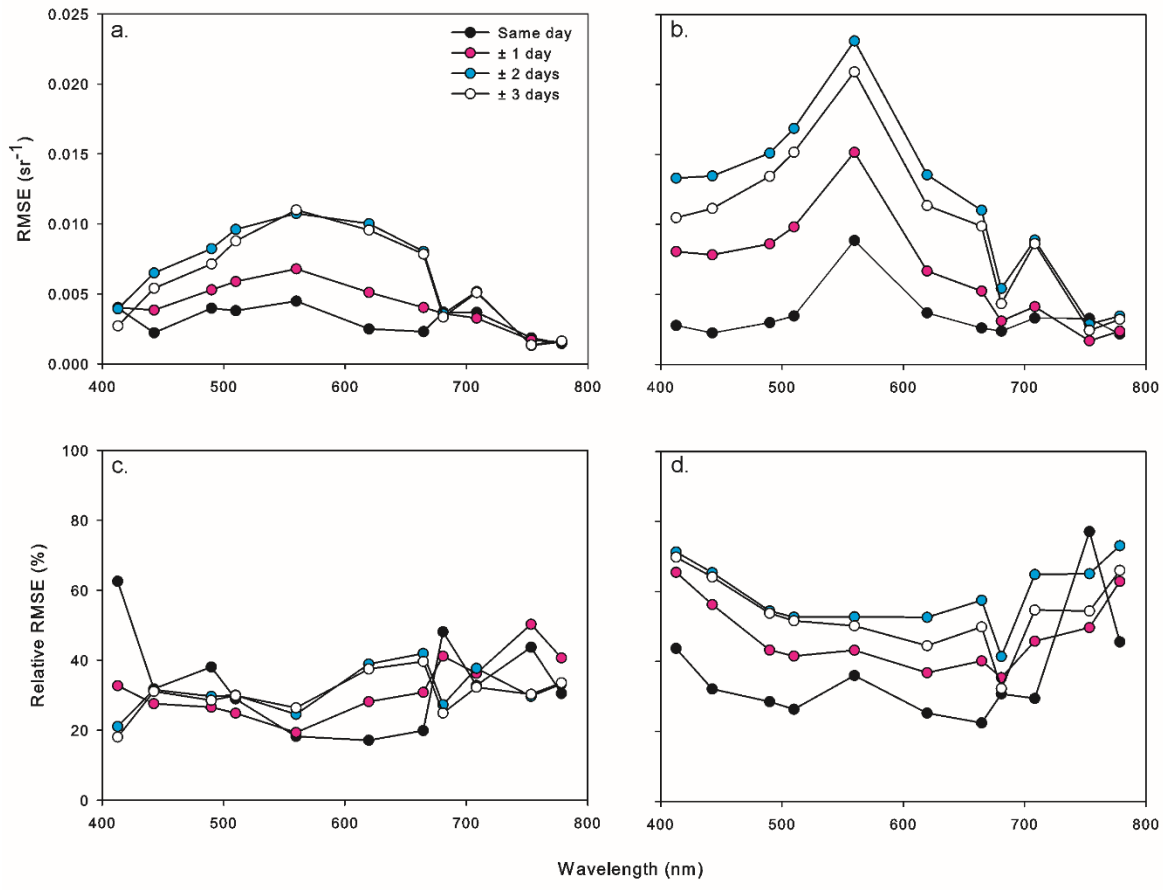

Figure 5.7. Absolute (sr^{-1}) (a, b) and relative (%) (c, d) root mean square error (RMSE) for SCAPE-M_B2 and C2R/Lake retrieved R_{rs} per MERIS band (1-10, 12).

Table 5.3. Remote sensing reflectance retrieval performance (relative and absolute RMSE) of SCAPE-M_B2 and C2R/Lake atmospheric correction for each processed MERIS band.

		SCAPE-M_B2 R_{rs}								**C2R/Lake R_{rs}**							
		RMSE (sr^{-1})				**Relative RMSE (%)**				**RMSE (sr^{-1})**				**Relative RMSE (%)**			
Band #	**Centre wavelength (nm)**	**Same day**	**± 1 day**	**± 2 days**	**± 3 days**	**Same day**	**± 1 day**	**± 2 days**	**± 3 days**	**Same day**	**± 1 day**	**± 2 days**	**± 3 days**	**Same day**	**± 1 day**	**± 2 days**	**± 3 days**
1	412	0.004	0.004	0.004	0.003	62.6	32.7	21.1	18.0	0.003	0.008	0.013	0.010	43.7	65.5	71.3	69.8
2	442	0.002	0.004	0.006	0.005	31.8	27.6	31.6	31.1	0.002	0.008	0.013	0.011	32.1	56.3	65.4	64.2
3	490	0.004	0.005	0.008	0.007	38.1	26.6	29.7	28.6	0.003	0.009	0.015	0.013	28.5	43.2	54.5	53.8
4	510	0.004	0.006	0.010	0.009	29.0	24.9	30.0	29.9	0.003	0.010	0.017	0.015	26.4	41.6	52.7	51.6
5	560	0.005	0.007	0.011	0.011	18.2	19.3	24.5	26.4	0.009	0.015	0.023	0.021	36.0	43.2	52.8	50.2
6	620	0.003	0.005	0.010	0.010	17.1	28.2	38.9	37.5	0.004	0.007	0.014	0.011	25.2	36.8	52.6	44.5
7	665	0.002	0.004	0.008	0.008	19.9	30.8	41.9	39.6	0.003	0.005	0.011	0.010	22.5	40.2	57.5	49.9
8	681	0.004	0.004	0.004	0.003	48.1	41.2	27.3	24.9	0.002	0.003	0.005	0.004	30.7	35.4	41.4	32.3
9	708	0.004	0.003	0.005	0.005	32.8	36.3	37.7	32.3	0.003	0.004	0.009	0.009	29.5	45.8	64.9	54.7
10	753	0.002	0.002	0.001	0.001	43.7	50.3	29.7	30.3	0.003	0.002	0.003	0.002	77.1	49.7	65.1	54.4
12	778	0.002	0.002	0.002	0.002	30.5	40.7	33.2	33.5	0.002	0.002	0.003	0.003	45.6	62.9	73.1	66.0

C2R/Lake R_{rs} retrievals were found to generally underestimate *in situ* R_{rs} across all ± 0-3 days matchups, although robust retrieval of the *in situ* spectral magnitude is found in some cases over part or the entire spectrum. However, a general flattening of the spectral shape was also observed. This is especially the case for the reflectance maximum at 560 nm (MERIS band 5), and also the peaks and troughs of the red-near infrared spectral range, important for chl-*a* retrievals in medium-high productivity waters. The RMSE associated with C2R/Lake retrievals is found to be highly wavelength dependent, closely resembling the spectral shape of the *in situ* measured R_{rs} (Figure 5.7). This is related to the flattening of the retrieved spectral shape by C2R/Lake, as observed in Figures 5.2 to 5.5. RMSE ranges from 0.002 to 0.023 sr^{-1} for all matchups, with relative RMSE typically high, between 20 and 80 % for C2R/Lake R_{rs} retrievals (Figure 5.7; Table 5.3).

Plotting AOT-550 nm retrieved by SCAPE-M_B2 against that retrieved by C2R/Lake during the August 2010 field campaign, much higher AOT-550 nm values estimated by C2R/Lake are clear, as is the effect of the larger SCAPE-M_B2 cell size (30 by 30 km) relative to the per pixel approach of C2R/Lake (Figure 5.8). Constant AOT-550 nm is retrieved across the entire lake surface by SCAPE-M_B2. Whereas more variable results are retrieved by C2R/Lake, the much higher retrievals (two to four times higher than those of SCAPE-M_B2) likely play a large role in the vast underestimation of R_{rs} by the processor.

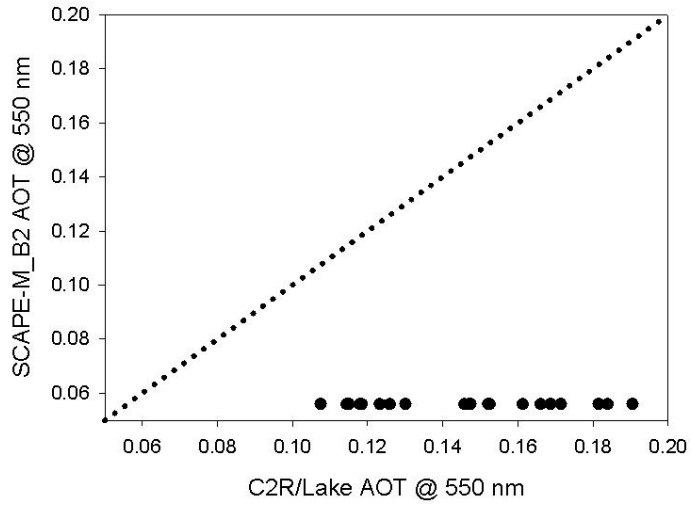

Figure 5.8. AOT at 550 nm estimated by SCAPE-M_B2 atmospheric correction and estimated by C2R/Lake atmospheric correction, coinciding with the August 2010 field campaign.

5.4.2 Chl-*a* concentration retrieval

After removing level 1 flagged pairs, indicating bright, glint risk, suspect coastline, land and invalid pixels, as in Chapter 4, 104 remaining validation matchups from were identified from the dataset used here. An additional four matchups were flagged by the C2R/Lake processor as output of the atmospheric correction exceeding the training range, and in one case the input TOA radiance was also out of the training range. These were removed from analysis using the C2R/Lake reflectance (n = 100). All MERIS-extracted matchup spectra for each atmospheric correction and Level 1b data are found in Figure 5.9, with mean and standard deviation highlighted. The general trend observed in the validation of R_{rs}, whereby C2R/Lake reflectance spectra are much lower in magnitude as well as flatter than the SCAPE-M_B2 spectra is observed for all spectra used in the chl-*a* retrieval. L1b radiance data display a large range of shapes more similar to the SCAPE-M_B2 than to the C2R/Lake spectra, with high radiance in the blue spectral region associated with atmospheric scattering in the uncorrected data. Chl-*a* concentrations associated with the retained matchups range from 1.50 – 57.00 mg m^{-3} (mean: 12.38 mg m^{-3}; standard deviation: 10.58 mg m^{-3}). Results obtained through the application of each of the band math combinations described in Table 5.1 are found in Figure 5.10 and Table 5.4. In general, similar calibration performance was found using L1b radiance and SCAPE-M_B2 reflectance, with R^2 of retrievals ranging between 0.68 and 0.82, and 0.66 and 0.84 respectively (Table 5.4). The best performing of the tested algorithms was again the FLH model. Here, SCAPE-M_B2 reflectance only slightly outperformed L1b radiance (R^2 = 0.84 vs. 0.82). Relatively poor performance was found for all algorithms using C2R/Lake reflectance as input (R^2 = 0.29 – 0.41), as expected based on the poor results of the R_{rs} validation described above.

Results of the k-folds cross-validation similarly indicate a comparably high performance using SCAPE-M_B2 reflectance (RMSE ranging from 3.92 to 5.95 mg m^{-3} (relative RMSE from 31.7 to 48.1 %) for the different chl-*a* algorithms) and L1b radiance (RMSE ranging from 4.35 to 5.94 mg m^{-3} (relative RMSE from 35.1 to 48.1 %)). Standard deviation (SD) of the RMSE retrieved through cross validation is less than 2 mg m^{-3} ($\leq$ 14.2 %) in the case of L1b radiance input data for all algorithms, and less than 3 mg m^{-3} ($\leq$ 21.2 %) in the case of SCAPE-M_B2 reflectance input data for all algorithms, whereas mean and SD

of retrieval RMSE using C2R/Lake reflectance are consistently much higher (Figure 5.11; Table 5.4).

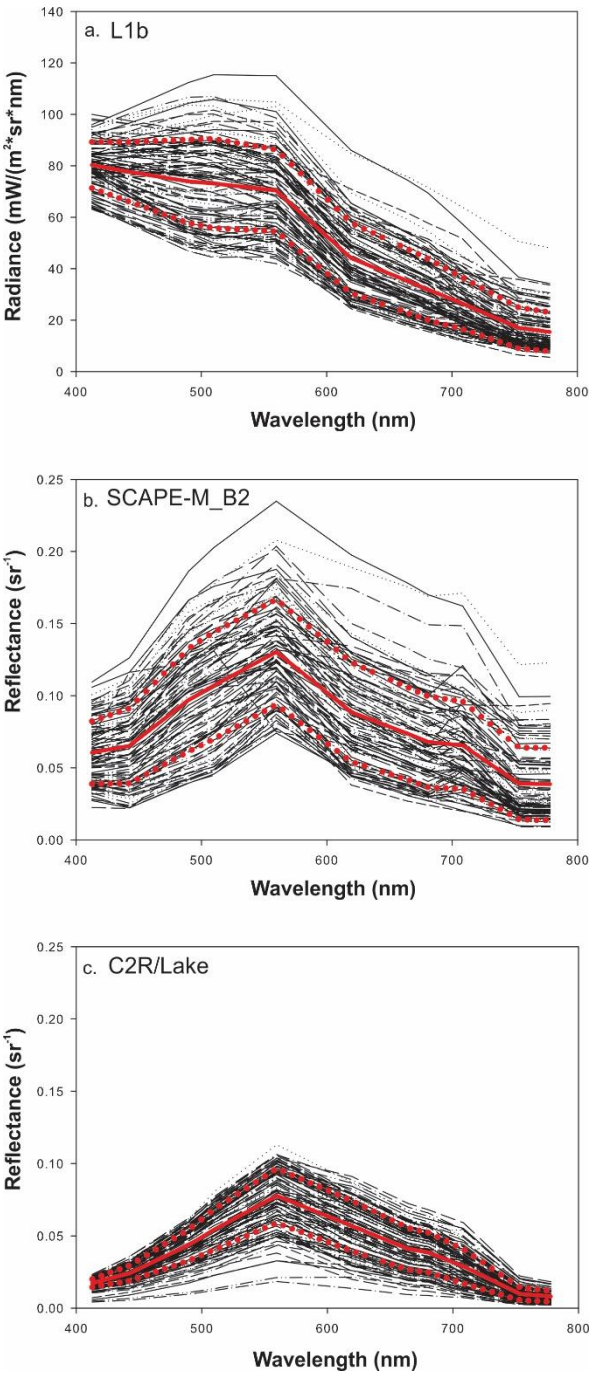

Figure 5.9. Matchup spectra of L1b radiance, SCAPE-M_B2 reflectance and C2R/Lake reflectance used in the band math calibration-validation. The mean (solid line) ± one standard deviation (dotted line) of all spectra are highlighted in red.

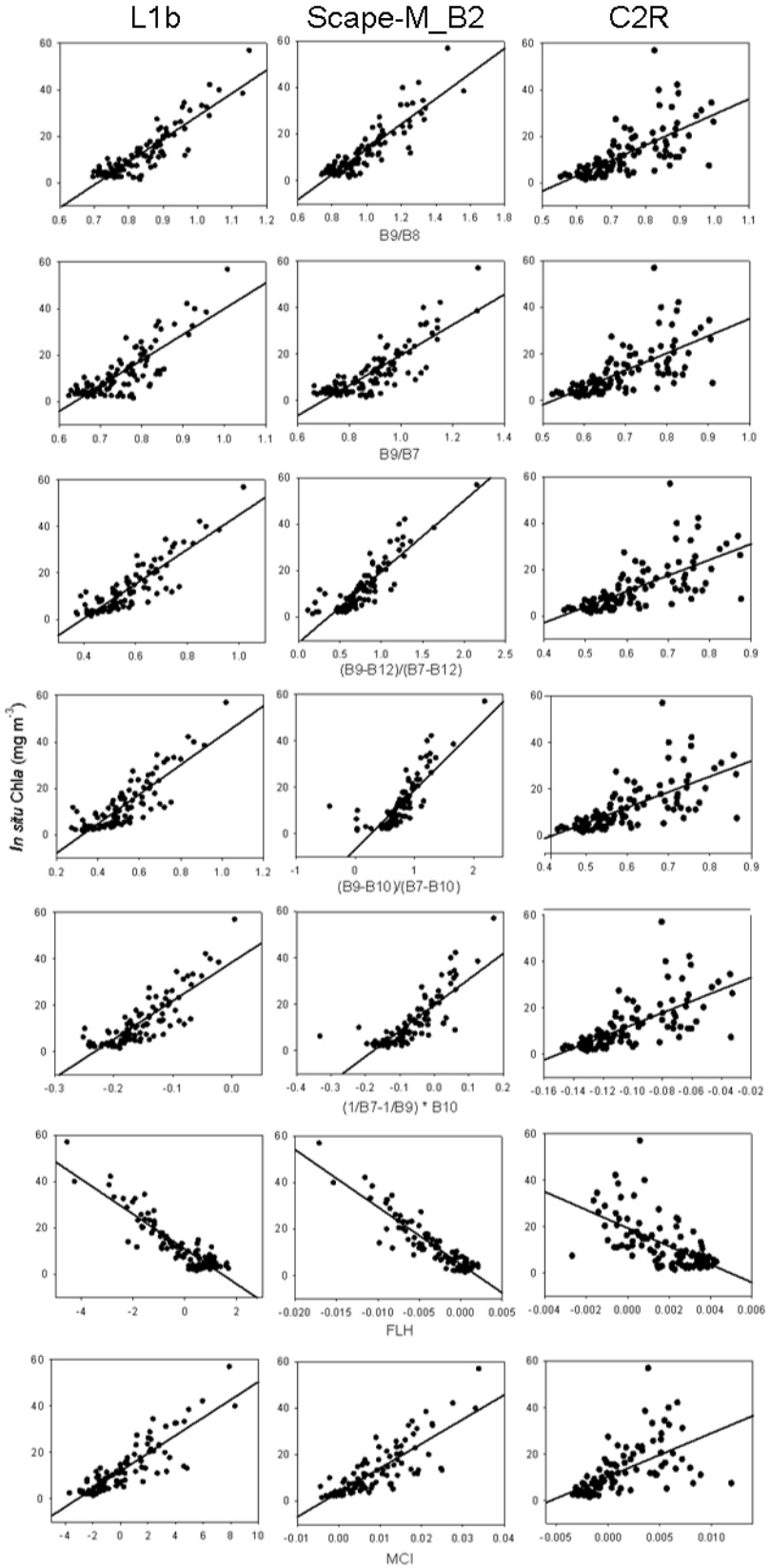

Figure 5.10. Scatterplots of selected semi-empirical chl-*a* concentration retrieval algorithm calibration using L1b radiance, SCAPE-M_B2 reflectance and C2R/Lake reflectance as input.

Table 5.4. Chl-*a* retrieval performance of the selected algorithms and input data, including results of k-folds cross-validation analysis.

	L1b			**SCAPE-M_B2**			**C2R**		
Band combination	**R^2**	***Av. RMSE (mg m^{-3})**	***SD RMSE (mg m^{-3})**	**R^2**	***Av. RMSE (mg m^{-3})**	***SD RMSE (mg m^{-3})**	**R^2**	***Av. RMSE (mg m^{-3})**	***SD RMSE (mg m^{-3})**
B9/B8	0.80	4.52 (36.5 %)	1.49 (12.0 %)	0.78	4.46 (36.0 %)	2.29 (18.5 %)	0.41	7.65 (61.8 %)	3.30 (26.7 %)
B9/B7	0.68	5.94 (48.1 %)	1.48 (12.0 %)	0.71	5.45 (44.0 %)	2.08 (16.8 %)	0.40	7.76 (62.7 %)	3.22 (26.0 %)
(B9-B12)/(B7-B12)	0.78	4.73 (38.2 %)	1.42 (11.5 %)	0.77	4.90 (39.6 %)	1.53 (12.4 %)	0.39	7.68 (62.0 %)	3.54 (28.6 %)
(B9-B10)/(B7-B10)	0.73	5.40 (43.6 %)	1.37 (11.1 %)	0.66	5.88 (47.5 %)	2.62 (21.2 %)	0.39	7.82 (63.2 %)	3.34 (27.0 %)
(1/B7-1/B9) * B10	0.72	5.36 (43.3 %)	1.70 (13.7%)	0.67	5.73 (46.3 %)	2.61 (21.1 %)	0.40	7.73 (62.4 %)	3.36 (27.2 %)
B8 – 1.005*[B7 + (B9 – B7)((λ8 – λ7)/(λ9 – λ7))]	0.82	4.35 (35.1 %)	1.32 (10.7 %)	0.84	3.92 (31.7 %)	1.61 (13.0 %)	0.33	7.84 (64.2 %)	3.11 (25.5 %)
B9 – 1.005* [B8 + (B10 – B8)((λ9 – λ8)/(λ10 – λ8))]	0.77	4.85 (39.2 %)	1.76 (14.2 %)	0.67	5.95 (48.1 %)	1.40 (11.3 %)	0.29	8.07 (66.1 %)	3.04 (24.9 %)

*Average (Av.) and standard deviation (SD) from the k-folds cross-validation (k = 10).

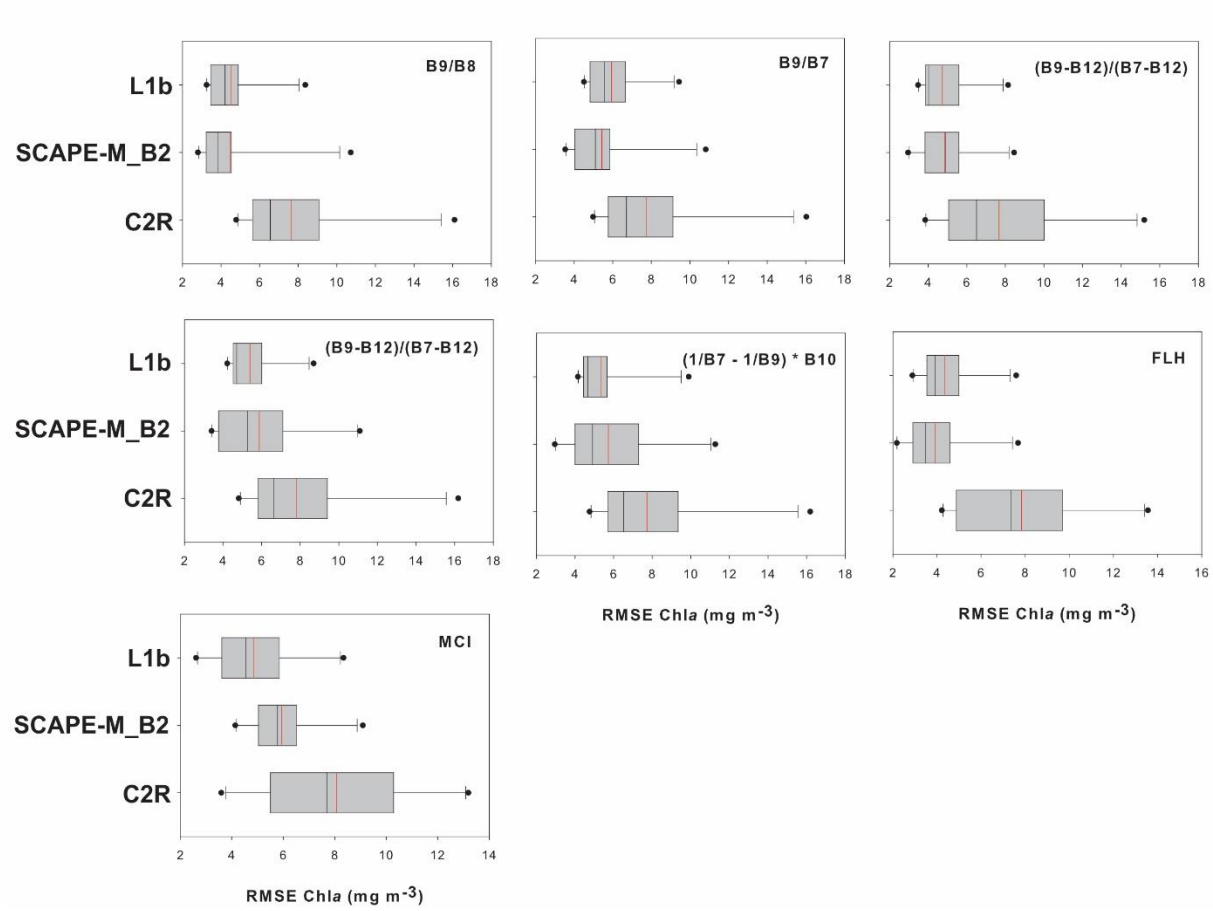

Figure 5.11. Resulting root mean square error (RMSE) of k-folds cross-validation chl-*a* concentration retrievals for each of the selected semi-empirical algorithms, using each of the input data types (L1b radiance, SCAPE-M_B2 corrected reflectance and C2R corrected reflectance). Box plots show mean (centre red line), median (centre black line), 25th and 75th percentiles (grey box), 10th and 90th percentiles (whiskers) and outliers (dots).

5.5 Discussion

The overall robust retrieval of Lake Balaton R_{rs} using the SCAPE-M_B2 atmospheric correction is consistent with results from elsewhere (Domínguez Gómez et al. 2011), and using SCAPE-M (without the adjustment to retrievals in band 2) (Guanter et al. 2010; Jaelani et al. 2013), whereby R_{rs} from highly turbid lakes and reservoirs were accurately retrieved in terms of both spectral shape and magnitude. Conversely, retrievals

from low reflectance lakes, such as Lake Constance and Lake Garda, were found to be poorly retrieved by SCAPE-M and better achieved through atmospheric correction using the C2R/Lake processor (Guanter et al. 2010). In highly turbid and reflective lakes and reservoirs, a similar underestimation and flattening of the spectra using C2R/Lake was observed as for Lake Balaton, although the extent of this effect was highly variable across water bodies (Guanter et al. 2010). In some turbid lakes, the magnitude was generally well retrieved by C2R/Lake, but the spectral shape not. An even greater underestimation and flattening by C2R/Lake atmospheric correction than that reported here was reported for Lake Kasumigaura, Japan in some cases, and a similar retrieval performance relative to those found here in others (Jaelani et al. 2013).

Given the different approaches to atmospheric correction taken by SCAPE-M (and its SCAPE-M_B2 counterpart) and the C2R/Lake processor, it has logically been interpreted that an inversion based approach to modelling atmospheric radiative transfer and AOT, such as that employed by SCAPE-M_B2, will be more broadly applicable, including in extreme cases of hypertrophic or high TSM conditions (Guanter et al. 2010). This is supported by the Lake Balaton results found here. Variable SCAPE-M validation results from elsewhere (Jaelani et al. 2013) are suspected to result from heterogeneity in atmospheric conditions within the 30 by 30km cell, which is not indicated by the current results to be an issue for Lake Balaton. This is likely due to the vastly different atmospheric conditions of the two lakes in question. Whereas Lake Kasumigaura is situated in a coastal setting, and near Tokyo and heavy industrial activity (Jaelani et al. 2013), a dry, continental climate overlays Lake Balaton, which is quite removed from major urban or industrial activity. Concerning temporal heterogeneity, it was expected that error in MERIS R_{rs} retrievals (Figure 5.7) would increase with time from the *in situ* sample due to variability in the bio-optical conditions of the lake. However, this was not found to be significant according to the ANOVA results. However, it is clear in spectral plots that the red-near infrared spectral features are indeed less well preserved in matchups exceeding one day difference compared with same day matchups.

After accounting for solar and viewing angles and surface elevation, aerosol scattering is well known to be the largest source of error in atmospheric correction algorithms (Wang 2007), given the heterogeneous origins and characteristics of aerosols as well as their broad spatial and temporal variability. Aerosol content is often considered in remote sensing via the parameter Aerosol Optical Thickness (AOT) which can be derived at multiple wavelengths, most typically at 550 nm (AOT-550 nm), where AOT is

used in deriving surface reflectance in atmospheric correction. Validation using *in situ* measurements (R^2 = 0.75) over several lakes (Guanter et al. 2010), and over diverse terrestrial settings (R^2 > 0.71, except in one case where R^2 = 0.34) (Guanter et al. 2008), reveals the generally robust nature of AOT-550 nm retrievals by SCAPE-M over a range of conditions. Although no *in situ* AOT-550 nm measurements coinciding with the field measurements presented here were available for validation, the robust performance of SCAPE-M_B2 R_{rs} retrievals is likely a result of strong AOT-550 nm retrieval performance. Although neither chl-*a* nor TSM concentrations during the coinciding field campaign exceed the training range of the C2R/Lake processor, it may be that other water constituents or optical properties, or atmospheric conditions, not measured *in situ* exceed the NN training range and results in the much greater AOT-550 than that estimated by SCAPE-M_B2 (Figure 5.8). In general, the likely inaccurate R_{rs} retrieval of the C2R/Lake atmospheric correction module is expected to contribute in part to the large error in chl-*a* concentration retrieval of the associated C2R, BL and EUL constituent retrieval modules presented in Chapter 4.

Although the use of TOA data in water constituent retrieval has been challenged due the inability to account for spatial and temporal variability in atmospheric conditions resulting in an additional source of error (Binding et al. 2010), this is not supported by the current results for Lake Balaton. Band arithmetic algorithms using the red-NIR spectral region are employed to minimize the atmospheric influence (Matthews et al. 2012). The similar chl-*a* concentration retrieval performance using L1b radiance and SCAPE-M_B2 reflectance and the results of the k-folds cross-validation indicate that the errors unaccounted for by using TOA data are similar in magnitude to the errors related to SCAPE-M_B2 atmospheric correction. Furthermore, if a poor atmospheric correction (i.e., C2R/Lake for Lake Balaton) is applied prior to chl-*a* retrievals, these will in turn be poor.

5.6 Conclusions

SCAPE-M_B2 and C2R/Lake reflectance retrievals are validated for the turbid, optically complex Lake Balaton, and estimated AOT-550 nm of each are compared. SCAPE-M_B2 retrievals are found to be accurate and to produce accurate chl-*a* retrievals when semi-empirical, band math algorithms are applied. C2R/Lake reflectance is found

to more often underestimate and flatten the shape of spectra measured *in situ*, possibly a result of an overestimation of the AOT. The poor performance of the C2R/Lake atmospheric correction expectedly results in poor performance when input into semi-empirical chl-*a* retrieval algorithms, and can reasonably be expected to contribute to the poor chl-*a* concentration retrieval performance of the NN C2R, BL and EUL processors as presented in Chapter 4. FLH is again found to best retrieve chl-*a* concentrations after extending the number of semi-empirical algorithms explored, although reasonable retrievals are also found with other red-NIR semi-empirical algorithms tested. Chl-*a* retrieval algorithm performance using SCAPE-M_B2 reflectance was found to be comparable when TOA L1b radiance data were used. The spatial and temporal range of the data, as well as cross-validation results, suggest the stability of MERIS chl-*a* concentration retrieval algorithm performance using either SCAPE-M_B2 reflectance or L1b radiance for Lake Balaton. The error introduced by unaccounted for temporal variability in atmospheric conditions when using L1b data is not found to greatly exceed the error related to SCAPE-M_B2 atmospheric correction. Therefore, the use of the FLH algorithm using L1b data is proposed for the Lake Balaton full MERIS time series processing.

Chapter 6

Earth observation of freshwater phytoplankton phenology metrics

The work presented in this chapter has been published as:

Palmer, S. C. J., *et al*. (2015b). Satellite remote sensing of phytoplankton phenology in Lake Balaton using 10 years of MERIS observations. *Remote Sensing of Environment*, *158*, 441-452.

6.1 Introduction & rationale

6.1.1 Lake phytoplankton phenology

Phenology refers to the timing of cyclic biological events. It can be understood as the seasonality of recurring events such as leafing, greening-up, flowering and fruiting of vegetation (and the durations thereof), breeding, egg laying, hatching and other reproductive milestones in animals, feeding, pollination, hibernation and migration (Forrest and Miller-Rushing 2010). Phytoplankton phenology is distinct from these examples in that, rather than referring to individual life history events as is commonly the case for other types of organisms, it describes the cyclic nature of demographic, or population-level phenomena (Thackeray 2012; Winder and Cloern 2010). Instead of describing the timing of events such as breeding, flowering, and hibernation in individuals, for example, plankton phenological events include peak biomass of the population and its timing, dictated by the shift in balance between the various processes contributing to population growth and to population loss, in events known as blooms (Thackeray et al. 2008). Furthermore, phytoplankton biomass turns over much more rapidly, daily to weekly (on the order of hundreds of times per year), as a result of fast reproduction, growth and predator consumption (grazing) rates (Calbet and Landry 2004). This rapid turnover results in a high level of background noise overlaid upon the annual phenology of phytoplankton bloom events, particularly in comparison with terrestrial analogs (Winder and Cloern 2010).

Wavelet analysis has been used to extract the dominant periods of variability, and the recurrence strength at those periods for the annual cycles of phytoplankton biomass for 50 lakes, in addition to 70 estuarine and 5 oceanic sites (Winder and Cloern 2010). Between eight and 50 years of monthly sampled data was available for these sites, which spanned latitudes between 22° to 60°. Four patterns were found to emerge: (1) a 12-month

periodicity (one annual bloom event, generally in the spring or summer), (2) a 6-month periodicity (two annual blooms, generally in the spring and late-summer/autumn or in the winter and summer), (3) a 2 – 4 month periodicity, suggesting a highly noisy system lacking a regular annual cycle, and (4) a mixed periodicity (generally a combination of 12- and 6-month periodicity, with a marked shift from one regime to the other at some point in time) (Winder and Cloern 2010). Upon determining a regular periodicity for a given system through such an analysis of the time series, a number of approaches can be taken toward determining phenological features.

Investigation related to freshwater phytoplankton phenology has greatly accelerated over the past decade, by means of laboratory or field mesocosm experiments (Berger et al. 2010a; Diehl et al. 2002; Gaedke et al. 2010; Lewandowska and Sommer 2010; Sommer and Lewandowska 2011; Winder et al. 2012), modelling-based approaches (Elliott 2012; Elliott et al. 2006; Jones et al. 2011) and interpretation of long-term field data (Feuchtmayr et al. 2012; Maberly et al. 1994; Meis et al. 2009; Thackeray et al. 2012; Thackeray et al. 2008; Walters et al. 2013; Winder and Schindler 2004a, b). Studies have variably investigated one or more individual phytoplankton taxa (Feuchtmayr et al. 2012; Thackeray et al. 2008) or have considered phytoplankton biomass generally (Adrian et al. 2006; Gerten and Adrian 2000; Seebens et al. 2009; Thackeray et al. 2012). Some have considered phytoplankton in combination with higher trophic levels (typically zooplankton) (Adrian et al. 2006; Feuchtmayr et al. 2012; Lewandowska and Sommer 2010; Thackeray et al. 2008; Winder and Schindler 2004a, b) with some suggestion of trophic level mismatch whereby higher trophic levels become decoupled from their lower trophic level food source (typically the primary producing phytoplankton in this case) due to differing rates of phenological shifting (Cushing 1990), although limited quantitative evidence to this effect has been documented (Thackeray 2012). A variety of responses to changing environmental conditions, particularly nutrient levels, overwintering phytoplankton populations, predator (zooplankton grazer) population dynamics, light conditions and temperature have been determined, and found in some cases to be species specific (Adrian et al. 2006; Berger et al. 2010b; Feuchtmayr et al. 2012; Thackeray et al. 2012; Thackeray et al. 2008; Winder and Schindler 2004a, b).

Since phytoplankton phenology is sensitive to environmental changes, phenology metrics may be useful to monitor in addition to more conventional phytoplankton biomass monitoring. Several phytoplankton phenology-related features are already included as

part of the European WFD, notably number of blooms per year (bloom frequency) and the magnitude or intensity of blooms (Carvalho et al. 2013; Nõges et al. 2010). Satellite remote sensing may provide a reasonable means to evaluate the phenology of medium to large lakes. This is due to the potential of remote sensing to retrieve chl-*a*, as demonstrated in the preceding thesis chapters, and the repeat image acquisition from sensors such as MERIS, providing the recurrent, high frequency data necessary for such analyses. In addition to the regular revisit/overpass frequency allowing for time series reconstruction, the cohesive spatial coverage would allow for a much more thorough spatial investigation of trends and phenomena than has been possible until now, as well as investigation into lakes lacking conventional monitoring of sufficiently high frequency for the measurement of phenology metrics.

6.1.2 Remote sensing of phenology

Satellite imagery has a long history of use and continues to be important in studies of terrestrial vegetation phenology (Boyd et al. 2011; Dash et al. 2010; Justice et al. 1985; Lüdeke et al. 1996; Malingreau 1986; Zhou et al. 2001), including contributions to identifying phenological shifts at the landscape scale in response to climate change. This is largely due to the long archive of satellite imagery appropriate to the retrieval of vegetation indices (more than 30 years of continued measurement), at the relevant spatial and temporal scales and with synoptic coverage. Imagery from the series of Landsat and NOAA-AVHRR sensors are primary data sources, with continuity provided through more recent sensors. A MODIS standard Level 3 Land Cover Dynamics (MCD12Q2) product has been developed to estimate terrestrial phenology globally (Ganguly et al. 2010). A range of common vegetation indices (VIs) have been used in phenological analysis, including the normalized difference vegetation index (NDVI), leaf area index (LAI), the fraction of absorbed photosynthetically active radiation (*f*APAR), MERIS global vegetation index (MGVI) and MERIS terrestrial chlorophyll index (MTCI) (Boyd et al. 2011). Time series of imagery with a given VI applied are generated, and seasonality functions and features are extracted for a region or pixels of interest. In addition to issues of inter-sensor and geometric, atmospheric and radiometric correction consistency, which plagues the reliability of long satellite image time series, standard methodologies or protocols for the extraction of seasonality functions and features remain to be developed

and adopted, despite the history of satellite imagery use in investigating terrestrial vegetation phenology dating to the 1980s (White et al. 2009).

In recent years, several research groups have begun to advance from satellite validation and mapping of chl-*a* concentrations to the use of satellite chl-*a* mapping in time series and phytoplankton phenological analysis in open ocean contexts (so-called Case 1 waters, as described in Chapter 2). These have largely made use of archive SeaWiFS data (1998 – 2002) (Platt and Sathyendranath 2008; Platt et al. 2010; Platt et al. 2009; Racault et al. 2012; Sasaoka et al. 2011; Siegel et al. 2002; Vargas et al. 2009), with some extending analyses back to also include CZCS (active from 1979 to 1983) (D'ortenzio et al. 2012), or forward to also include MODIS (1999 – present) and/or MERIS (2002-2012) data (Cole et al. 2012; González Taboada and Anadón 2014; Kahru et al. 2011). Satellite data used in such oceanic investigations are typically of quite coarse spatial resolution, with reported grid sizes ranging between 9 km (Siegel et al. 2002) and 300 km (Vargas et al. 2009). They have variably focused on a specific geographic region (e.g., the North Atlantic (González Taboada and Anadón 2014; Platt et al. 2010; Platt et al. 2009; Siegel et al. 2002; Vargas et al. 2009) or the North Pacific (Sasaoka et al. 2011)) or provided a global scope (D'ortenzio et al. 2012; Kahru et al. 2011; Racault et al. 2012). In addition to mapping extracted phenology metrics, spatially explicit investigation was undertaken in a number of cases, either through the selection and comparison of zones of interest from the imagery (e.g., across latitudes (Platt et al. 2010; Platt et al. 2009)) or through cluster analysis using time series functions or phenological features extracted at the pixel level (D'ortenzio et al. 2012; Sasaoka et al. 2011).

In most studies of oceanic phytoplankton phenology using remote sensing, timing of the spring bloom, especially initiation and peak timing, are derived (Kahru et al. 2011; Racault et al. 2012; Siegel et al. 2002). Some additional features are considered in Vargas et al. (2009) ("maturity" and "start of decay" of the bloom, referring to when the chl-*a* concentration is at 90% of either side of the maximum concentration) and D'ortenzio et al. (2012) make use of the full seasonality time series vector (chl-*a* concentration over time) in their cluster analysis. Platt and Sathyendranath (2008) propose a suite of potential phytoplankton phenology-related ecological indicators, including timing-related features (initiation, peak, termination and duration of blooms, etc.) and productivity-related features (amplitude of bloom, bloom and total annual biomass, etc.). These are discussed in relation to sea surface temperature (SST) and photosynthetically active radiation (PAR) time series of the North Atlantic and the outlining of ecological provinces in Platt et al.

(2010), as well as in a spatially cohesive global context by Racault et al. (2012). The same phenology features described by Platt and Sathyendranath (2008) are conceptually applicable to lake settings, depending on the availability of a suitable chl-*a* time series for use as input.

Several specific challenges have rendered the reliable remote sensing of phytoplankton and other optical water quality parameters difficult if not impossible for many inland and coastal waters until quite recently, as discussed in Chapter 2, precluding the use of satellite imagery in such extended time series analysis. As a result, the quantification of phytoplankton phenology metrics using remote sensing has only been carried out to a certain extent for lakes in a few cases to date (e.g., (Binding et al. 2011; Duan et al. 2014; Hu et al. 2010; Matthews 2014; Stumpf et al. 2012). As increasingly robust chl-*a* retrieval algorithms are achieved for a growing number of lakes, such as described in Chapters 4 and 5 for Lake Balaton, an important continued direction in the remote sensing of lakes is foreseen to be the use and interpretation of satellite imagery to derive seasonality functions and extract and map phenology features. The adaptation of tools and approaches from both terrestrial and open ocean phenology remote sensing experience, as well as those from *in situ* phytoplankton phenology and recent lake phytoplankton and cyanobacteria time series analyses, will be invaluable toward the development of such application in lake settings.

6.2 Objectives

The preceding two chapters have validated and compared multiple chl-*a* retrieval algorithms across the range of conditions encountered at Lake Balaton, and have highlighted the suitability of the FLH retrieval algorithm applied to MERIS Level 1b (top-of-atmosphere) radiance imagery for use in the production of time series chl-*a* concentration maps for high biomass bloom events for this site. Although phenology analysis has not yet been extensively carried out for lake systems using satellite imagery, the use of remote sensing for phytoplankton phenology mapping has recently proven to provide invaluable and unprecedented insight in pelagic ocean settings, as described above, in addition to the long history in terrestrial applications, and first results in lakes are promising. The chl-*a* validation results presented in Chapters 4 and 5 (i.e., L1b FLH-

derived chl-*a* time series maps) are therefore used in an Earth Observation-based retrieval and analysis of freshwater phytoplankton phenology to meet the following objectives:

(6) To use validated MERIS chl-*a* maps for time series analysis of Lake Balaton phytoplankton dynamics spanning the full image archive;

(7) To undertake the extraction of satellite image-based phenological analysis through the use of TIMESAT software in a freshwater setting for the first time;

(8) To retrieve and map annual phenology and primary productivity features for Lake Balaton summer blooms; and

(9) To highlight the spatial and interannual variability of, and any correlation between the mapped features.

6.3 Methods

6.3.1 MERIS chl-*a* mapping and time series aggregation

The FLH algorithm applied to TOA Level 1b radiance imagery was identified in Chapters 4 and 5 as highly correlated with chl-*a* concentrations from Lake Balaton time series, and is used as a proxy for phytoplankton biomass mapping. Bulk processing of the full, ten year MERIS archive for Lake Balaton using FLH was undertaken at Brockmann Consult through the ESA Diversity-II and CoastColour projects and using their Calvalus portal, which was designed to facilitate the access to and processing of large volumes of MERIS data (Fomferra et al. 2012). After applying a land mask, screening for cloud contamination and mixed land-water pixels was carried out. The data were then processed to the Level 2 FLH product, and then to the Level 3 through dekad (ten day) mean binning, resulting in 36 images per year. Following the processing of FLH to the Level 3, coefficients found in Chapter 4 to relate the retrieved FLH index to chl-*a* concentrations (Table 4.3) for Lake Balaton via linear regression were employed, producing chl-*a* maps.

Data beginning from January 1, 2003 through December 31, 2011 were used as input, excluding data from the years 2002 and 2012 which were only partially available

(from June onward and until April respectively), because constant numbers of images per year are required by TIMESAT. Data output from Calvalus were then further formatted for input into TIMESAT by converting missing values from "NaN" (not a number) to the integer -9999 and saving as ENVI standard format. As suggested by the TIMESAT developers, dummy years were added to the beginning and end of the time series for smoothing and phenology feature extraction since TIMESAT interpretation of the beginning and end of time series can be problematic and seasons are often missed from these years (Jönsson and Eklundh 2004). Data from these periods were then excluded from subsequent mapping and analysis.

6.3.2 Data smoothing and phenology parameterization

TIMESAT is an open-source software developed by and available from researchers at Malmö University (Dr. Per Jönsson) and Lund University (Dr. Lars Eklundh) for the analysis of satellite image time series data, specifically to explore and extract parameters related to terrestrial vegetation seasonality (Jönsson and Eklundh 2004; http://www.nateko.lu.se/timesat/timesat.asp). It allows users to input image time stacks, select from and apply a variety of time series smoothing techniques, and to output mapped phenology metrics. In TIMESAT, time series of VIs such as NDVI are smoothed following the user's choice of Savitzky-Golay filtering, asymmetrical Gaussian or double logistic functions (Eklundh and Jönsson 2012; Jönsson and Eklundh 2004). Here, MERIS retrieved chl-*a* for Lake Balaton is used as input data.

In both the asymmetric Gaussian and the double logistic smoothing functions, curves are fit to the broad features of the data peaks (Eklundh and Jönsson 2012). The base level and amplitude are determined by linear parameters, c1 and c2, respectively (equation 6.1). The curve is fit to the maxima and minima, in the case of the asymmetric Gaussian function (equation 6.2), and to the inflection points, where shape of the curve shifts from concave to convex and vice versa, and rates of change at these, in the case of the double logistic function (equation 6.3). Two curves per peak are fit for both functions, separately for right and left sides of each peak (which is what the "asymmetric" and "double" prefixes to the two functions refer to, respectively) (Eklundh and Jönsson 2012). In the asymmetric Gaussian function, x1 is equal to the position of the maximum or

minimum with respect to t, the independent time variable. x2 and x4 alter the width of the curve, for right and left sides of the peak respectively, and x3 and x5 alter the flatness of the curve, similarly for respective right and let sides of the peak (equation 6.2a, b) (Eklundh and Jönsson 2012). In the double logistic function, x1 and x3 are inflection points to the left and right of the peak, respectively, and x2 and x4 are the rates of change at these respective inflection points, with respect to time (t) (equation 6.3) (Eklundh and Jönsson 2012).

$$f(t) = c1 + c2g(t; x1, \dots, x5) \qquad \text{Equation 6.1}$$

$$\begin{cases} g(t; x1, \dots, x5) = exp\left[-\left(\frac{t-x1}{x2}\right)^{x3}\right] \ if\ t > x1 & \text{Equation 6.2a} \\ g(t; x1, \dots, x5) = exp\left[-\left(\frac{t-x1}{x4}\right)^{x5}\right] \ if\ t < x1 & \text{Equation 6.2b} \end{cases}$$

$$g(t; x1, \dots, x5) = \frac{1}{1+\exp\left(\frac{x1-t}{x2}\right)} - \frac{1}{1+\exp\left(\frac{x3-t}{x4}\right)} \qquad \text{Equation 6.3}$$

A filtering approach can also be used to smooth time series data, whereby each data value is replaced by a linear combination of nearby values within a window (equation 6.4). Weighting values by a simple moving average typically preserves the area and mean position of the peaks (equation 6.5), but not the width and height of the peaks (Eklundh and Jönsson 2012). This is improved upon through the use of the Savitzky-Golay filter, whereby a quadratic polynomial function (equation 6.6) is instead fit to all 2n + 1 points in a moving window (n), replacing the original data value (y_i) with the calculated value at its associated time step (t_i) (Eklundh and Jönsson 2012). The width of the moving window (n) must be selected by the user to subjectively optimize between the degree of smoothing and the ability to follow rapid changes in the time series. The Savitzky-Golay filter in TIMESAT is adaptive, in that data filtered using a defined n in a first step are subsequently scanned and any abrupt increases or decreases are re-filtered using a smaller n value in a second step (Eklundh and Jönsson 2012).

$$\sum_{j=-n}^{n} cjyi + j \qquad \text{Equation 6.4}$$

$$cj = \frac{1}{(2n+1)} \qquad \text{Equation 6.5}$$

$$f(t) = c1 + c2t + c3t^2 \qquad \text{Equation 6.6}$$

Smoothing is applied for each pixel of an input time series image stack, or using pre-extracted ASCII format (text) data. Least squares fit to an adaptive upper envelope is used to avoid negative bias in the time series, such as that caused by cloud contamination (Eklundh and Jönsson 2012). Parameters such as the definition of the start and end of season and data range must be specified by the user after preliminary exploratory processing on selected pixels prior to application to the full input dataset, in addition to window size when Savitzky-Golay filtering is used (Jönsson and Eklundh 2004). The number of seasons per year (in this case the number of annual phytoplankton blooms) are determined as follows in TIMESAT. Data (t_i, y_i, i = 1, 2, …, N) for each year (with a minimum of three years input) are fit to equation 6.7, where w = 6π / N (N = 36 in this case, as described in section 6.3.1), and a pair of cosine and sine functions are fit for each season of each input year (Eklundh and Jönsson 2012). From equation 6.7, primary maxima are detected if there is at least one season and secondary maxima (two annual blooms) are determined if the ratio between secondary and primary amplitudes are greater than a user defined threshold (Eklundh and Jönsson 2012). If the user has prior knowledge that the system in question is characterized by one season (i.e., annual bloom), this seasonality parameter can be set to 1. Since the ratio between primary and secondary maxima cannot exceed 1 (the primary maxima is always the largest), only one season (associated with the primary maxima) will be considered, regardless of whether a secondary peak in the data is detected or not. Likewise, setting this threshold to 0 (the ratio cannot be less than this) ensures that two seasons will be considered (Eklundh and Jönsson 2012).

$$f(t) = c1 + c2\sin(wt) + c3\cos(wt) + c4\sin(2wt) + c5\cos(2wt) \qquad \text{Equation 6.7}$$

Since Lake Balaton is known to experience two phytoplankton blooms per year (Mózes et al. 2006; Présing et al. 2008), a small one in the spring and a large one in the mid to late summer, the "number of seasons" was set to two in TIMESAT. In the current work, however, only summer blooms were considered, which are more important for Lake Balaton both in terms of magnitude and species composition (commonly

cyanobacteria dominated as opposed to the diatom-dominated, lower biomass spring blooms). This was done by defining peaks to be considered as those occurring between June and October for each year. The data range was set from 0 to 100 mg m^{-3} chl-*a* so as to exclude missing pixel values, set to -9999, and to include all real values. The ability to capture bloom peak, onset and decline of the three available methods was compared. Ten randomly selected points from across the lake were selected for parameterization testing and smoothing method selection, as in Heumann et al. (2007), to qualitatively choose the smoothing function found to best capture bloom peak, increase and decrease relative to the original input data.

Consensus is lacking as to the definition of bloom events in lake ecosystems, which are very generally characterized as "high phytoplankton abundance", in addition to the presence of indicator species (i.e., cyanobacteria) or uneven community composition (Carvalho et al. 2013). A widely used definition of start and end of the season (i.e., bloom) for similar analyses in pelagic ocean settings has been defined as when chl-*a* concentrations rise above and fall below the full time series median for each pixel, plus 5 % (Racault et al. 2012; Siegel et al. 2002). A similar approach to setting the start and end definition has been adapted for use here. Median values across Lake Balaton for the full 2003 to 2011 time series range from approximately 6 to 11 mg m^{-3}. Given the inability to assign an absolute value on a per-pixel basis using TIMESAT, 10 mg m^{-3} was chosen as the threshold value above which concentrations must rise to define the start of the season. Following trial parameterization, this value was found to result in the fewest missed bloom events. The definition of end timing was set to chl-*a* values decreasing below 12 mg m^{-3} following a detected bloom event, as post-bloom values were often found to be 10-11 mg m^{-3}.

The user can then output both the parameterized smoothed function, as well as the input (i.e., FLH chl-*a* dekad binned data in this case) and eleven phenology features (Figure 6.1; Table 6.1). These include the beginning, end and duration of the season, defined by the timing when the measured VI increases above and decreases below the pre-set values (Figure 6.1a and b), and the length of time between the two (Figure 6.1c). Start and end of season can be defined by either a user-defined value (e.g., NDVI = 0.4) or a value relative to the peak (e.g., when NDVI increases to 10% of the associated peak NDVI value). The mid-season timing is defined as the middle position at 80 % of the peak value (Figure 6.1e). Season maximum (Figure 6.1f) and base values, defined as the

average of minimum values to either side of the peak (Figure 6.1d), are also extracted for each season as is amplitude – the difference between the peak and base values (Figure 6.1g). Left and right derivatives are calculated for each season, indicating rate of increase (Figure 6.1h) and decline (Figure 6.1i). Integrals under the curve for each season are also calculated; one above the base value, indicating seasonally active vegetation biomass (Figure 6.1k), and one above the zero value, indicating total vegetation biomass (Figure 6.1j). Maps of each parameter for each bloom event can be generated (Jönsson and Eklundh 2004) since time series have been created, smoothed and analyzed for each pixel, providing rich spatiotemporal data on seasonality.

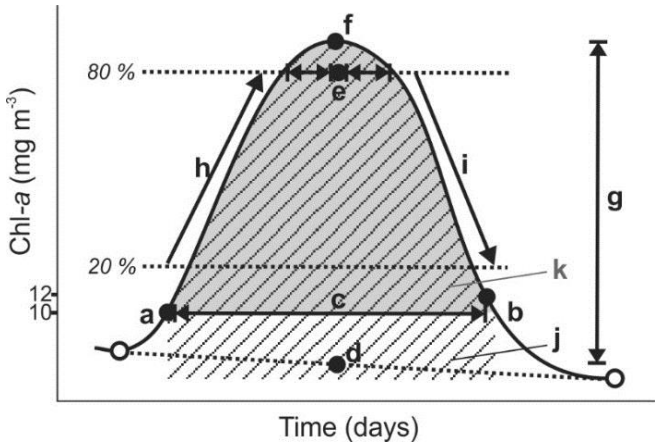

Figure 6.1. Schematic of phenology features extracted from each phytoplankton bloom using TIMESAT, adapted from Jönsson and Eklundh (2004). Letters correspond to feature descriptions in Table 6.1.

Table 6.1. Description of bloom phenology features extracted with TIMESAT, including current parameterization, corresponding with labels in Figure 6.1.

Feature (measurement unit)	**Description**
a. Start timing (day of year)	Date at which chl-*a* concentration rises above 10 mg m^{-3} on the left side of the bloom.
b. End timing (day of year)	Date at which chl-*a* concentration falls below 12 mg m^{-3} on the right side of the bloom.
c. Length (days)	Difference between a. and b.
d. Base concentration (mg m^{-3})	Average of lowest concentrations on the left and right sides of the bloom.
e. Mid-season timing (day of year)	Mid-position between left and right sides at 80 % of the maximum concentration.
f. Maximum concentration (mg m^{-3})	The highest chl-*a* concentration of the fitted function for each pixel during the bloom event.
g. Amplitude (mg m^{-3})	Difference between f. and d.
h. Rate of increase (mg m^{-3} day^{-1})	Amount of concentration increase per unit time on the left side of the bloom, between 20 and 80 % of the maximum concentration.
i. Rate of decrease (mg m^{-3} day^{-1})	Amount of concentration decrease per unit time on the right side of the bloom, between 80 and 20 % of the maximum concentration.
j. Large integral (mg m^{-3} * day)	Integral of the fitted function between start and end timings from 0 mg m^{-3} chl-*a*.
k. Small integral (mg m^{-3} * day)	Integral of the fitted function above the chl-*a* concentrations associated with start and end timing.

6.3.3 Phenology feature mapping and statistical analysis

All *in situ* data spanning the MERIS archive from January 2003 through December 2011 were composited to the same dekad mean bins as the MERIS data (described above in section 6.3.1) for input into TIMESAT. This was done for *in situ* data from each of the four main basins. Where more than one measurement per ten-day bin was available for a basin, the mean of these was used. Three-by-three pixel kernels centred on the *in situ* measurement coordinates were then extracted from the MERIS FLH chl-*a* time series. The TIMESAT parameterization described above was applied to the extracted *in situ* and matchup MERIS time series, and resulting phenology metrics for each year were compared through regression and coefficient of determination (R^2), bias and root mean square errors (RMSE) reported to validate the MERIS phenology metrics.

Maps of features described above and listed in Table 6.1 were output as images for all blooms. Summer blooms, most important for Lake Balaton, were extracted as events starting between June and October of a given year. Spatial and temporal variability of all parameters, for each bloom, were assessed by calculating the mean, and tenth and ninetieth percentiles for the full lake. Percent spatial extent of each bloom was calculated as the surface area over which a bloom event was detected relative to the full lake surface area for each year. Percent surface extent anomalies were calculated by subtracting the mean bloom extent of all nine years considered from the extent of each year. A Pearson correlation analysis was carried out between phenology features extracted for all blooms detected from 30 randomly selected pixels as well as annual spatial extents to confirm and explore relationships between any of these.

6.4 Results

6.4.1 Time series smoothing and phenology parameterization

Asymmetric Gaussian, double logistic and Savitzky-Golay filtering approaches to smoothing were qualitatively compared, as per the example provided in Figure 6.2 which shows the input values and smoothing of an extracted pixel. As shown in this example, Savitzky-Golay filtering (with a moving window size set to four) was found to be best adapted to capture the onset, development and end of the two annual phytoplankton

blooms. Although the asymmetric Gaussian and double logistic smoothing methods often produced very similar results, a number of distinct bloom events were missed by both of these (e.g., spring 2004 and 2007 in Figure 6.2). Likewise, both asymmetric Gaussian and double logistic approaches were found to occasionally introduce artifacts, as is clear in Figure 6.2 (e.g., near the end of 2006 and over the year 2009). An example of Savitzky-Golay filtered data, in comparison with the input chl-*a* concentrations, from across the trophic gradient of Lake Balaton (basins 1 – 4) is found in Figure 6.3. This figure also demonstrates the variability in chl-*a* time series from Lake Balaton, particularly in terms of magnitude, across its longitudinal axis trophic gradient, and the occurrence of two annual blooms. Savitzky-Golay filtering is not found to accurately retrieve minimum chl-*a* concentrations in the spring, however. It can therefore be expected that the dependent features, base and amplitude concentrations, would not be reliably retrieved as a result and were thus excluded from mapping and further analysis.

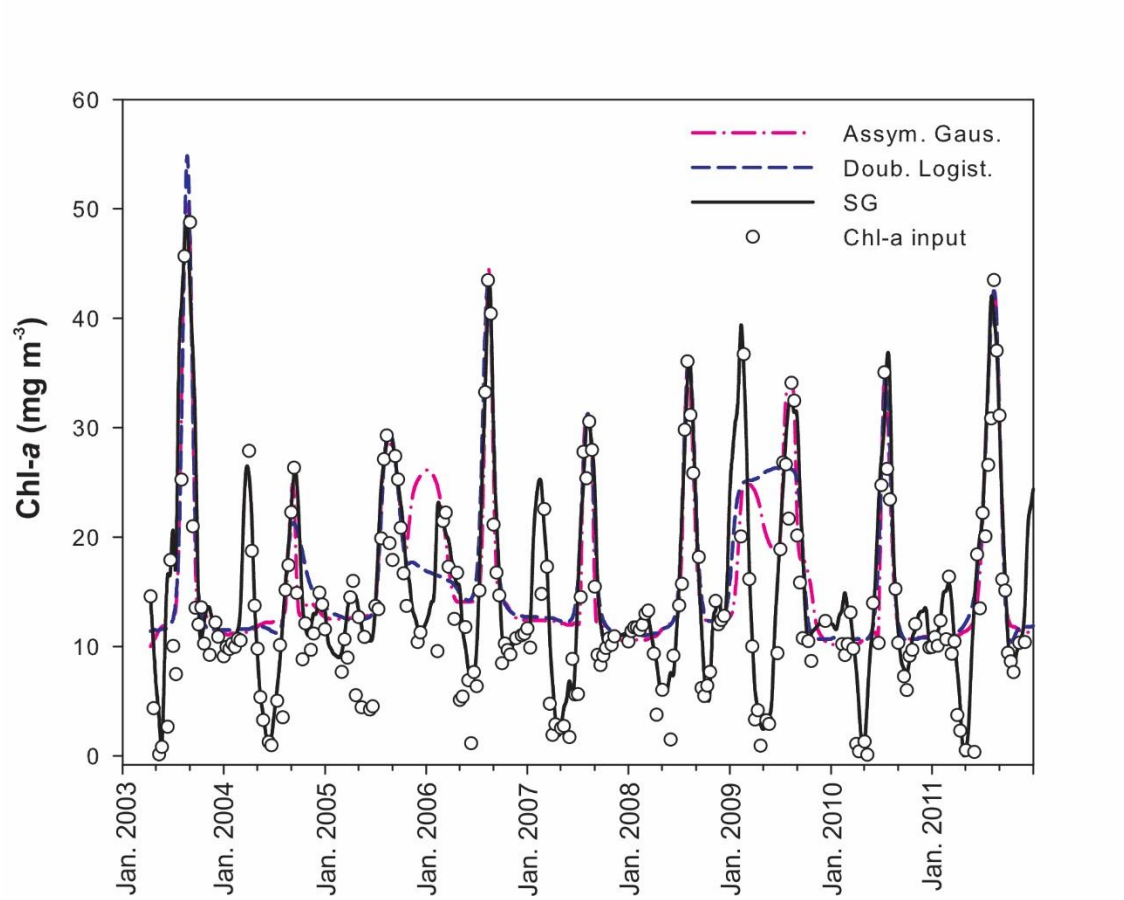

Figure 6.2. An example comparing the three smoothing functions possible in TIMESAT; asymmetrical Gaussian, double logistic and Savitzky-Golay (SG) filtering with input chl-*a* data points extracted for a single pixel. From Palmer et al. (2015b).

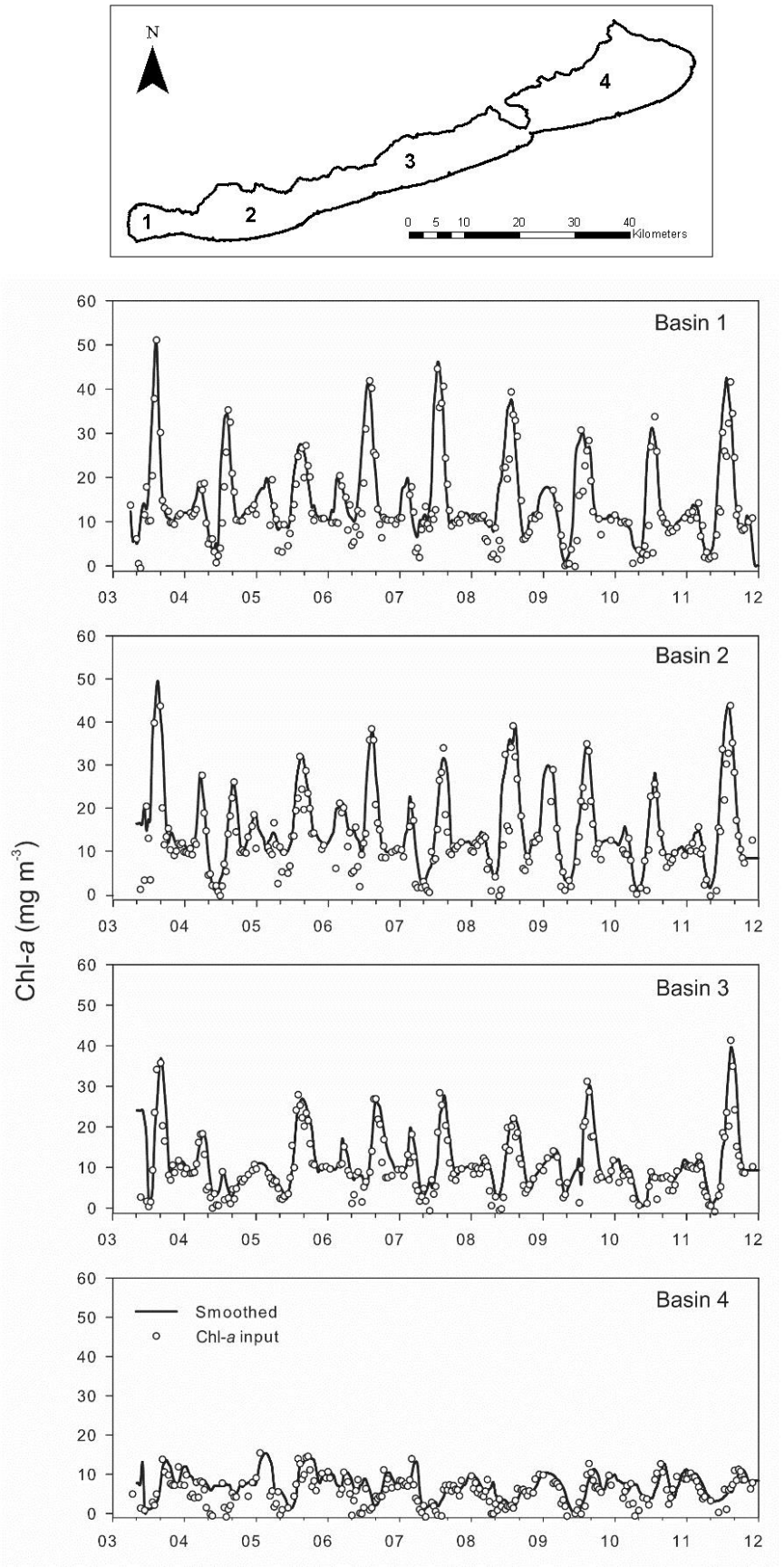

Figure 6.3. Examples of the Savitzky-Golay filtering compared with input data from each of the four main Lake Balaton basins (Figure 3.2).

6.4.2 MERIS phenology validation

Annual summer bloom phenology metrics extracted from MERIS chl-*a* time series using TIMESAT (Savitzky-Golay filtering) are compared with those from coinciding *in situ* chl-*a* time series in Figure 6.4. High correlations are generally found ($0.72 < R^2 < 0.84$), with rates of increase and decline ($R^2 = 0.59$ and 0.58 respectively) performing less well (Figure 6.4). Most metrics (with the exception of start timing; bias = +5.04 days) tend to be slightly underestimated by MERIS with respect to the *in situ* derived metrics. Furthermore, as in the example for start timing for matchups from each of the four basins (Figure 6.5), temporal trends are well recovered.

6.4.3 Phenology feature mapping and variability

The detected spatial extent of the annual summer blooms, mapped in Figure 6.6, was found to range from 24 to 77 % of the total lake surface area, with a mean of 56 %. The yearly anomalies in spatial extent relative to the mean of all nine years (56 %) are presented in Figure 6.7, and reveal extreme conditions from 2003 to 2005 (positive anomalies ≥ +20 % in 2003 and 2005; negative anomaly < -30 % in 2004), with those from 2006 to 2011 remaining between -10 and +10 %. All eight extracted phenology features are mapped for the 2003 summer bloom in Figure 6.8 as an example, highlighting the spatial variability of each. Base and amplitude concentrations, and small integral have been excluded based on the observation of unreliable smoothing of low chl-*a* concentrations. The start timing of summer blooms for all nine years are mapped in Figure 6.9, to demonstrate inter-annual variability superimposed upon the spatial variability of the mapped features. Highlights of spatial and temporal variability for each feature are presented in Figure 6.10, through the annual mean, tenth and ninetieth percentiles of each feature for each year across the full mapped bloom. The full time series maps for all features are also available in Appendix I.

In 2003, summer bloom start timing is found to range from day of year 160 (June 9) to day of year 229 (August 17) (with only outliers (< 0.4 %; n = 23 pixels) mapped as starting later; maximum start date mapped = day of year 323 (November 19) = 0.06 % of pixels (n = 4)). The majority (mean = day of year 209 (July 28) ± one standard deviation) of 2003 pixels' bloom starts are between days of year 175 (June 24) and 235 (August 23)

(Figure 6.10). Start timing is found to occur later from southwest to northeast, not only in 2003, but typically for all nine years mapped (Figure 6.9). Across years, mean start timing ranges from day of year 173 (June 22, in 2008) to 221 (August 9, in 2004), occurring on average on day of year 195 (July 14). In 2008, much less spatial variability was observed in addition to the earlier than average start timing, characterized by a standard deviation of only 10 days in comparison with the average standard deviation across all years of 17 days, and the maximum of the nine years (in 2004), of 24 days. The highest spatial variability, in 2004, coincided with the smallest spatial extent of the bloom as well as later than average start timing. 2003, 2006 and 2009 are also found generally to be later than average bloom starts, whereas 2005, 2010 and 2011, in addition to 2008, are found to be earlier than average bloom starts, with 2007 representing approximately average conditions.

Varying degrees of spatial and temporal variability were also revealed for the other ten extracted and mapped phenology features, which are presented in detail in Figure 6.10 and mapped in Appendix I. Mean end time for the nine years considered ranges from day of year 256 (September 13) to day of year 299 (October 26), mean length from 64 to 109 days, and mean mid-bloom timing from day of year 233 (August 21) to day of year 263 (September 20). Mean maximum concentration across the spatial extent of the bloom ranged from 20.9 to 37.7 mg m^{-3}. Mean rate of increase and decrease ranged from 0.37 to 0.80 mg m^{-3} d^{-1} and 0.19 to 0.63 mg m^{-3} d^{-1} respectively. Mean large integral ranged from 134.7 to 304.0 mg m^{-3} × d.

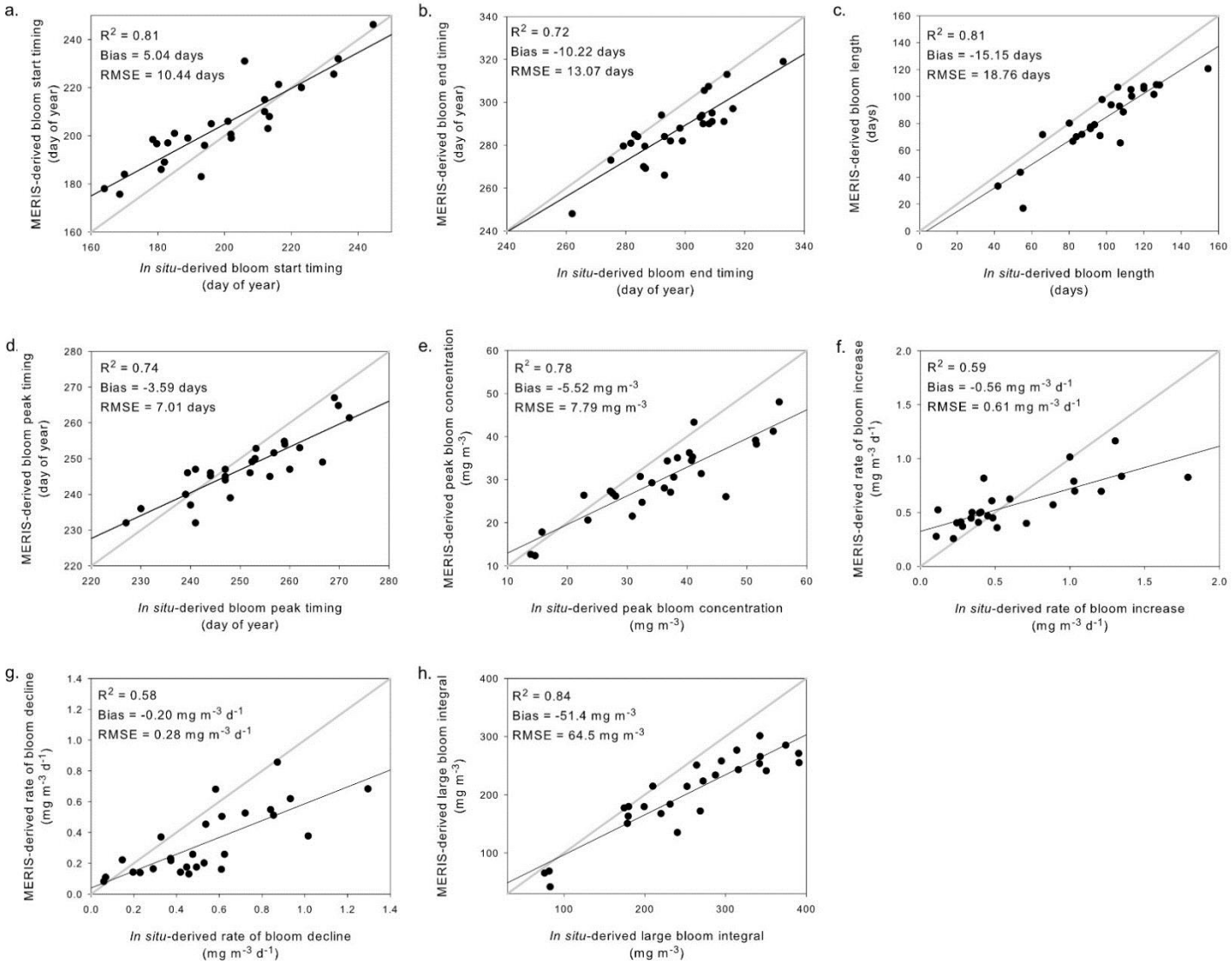

Figure 6.4. Validation of the MERIS derived phenology metrics using phenology of *in situ* chl-*a* measurements. From Palmer et al. (2015b).

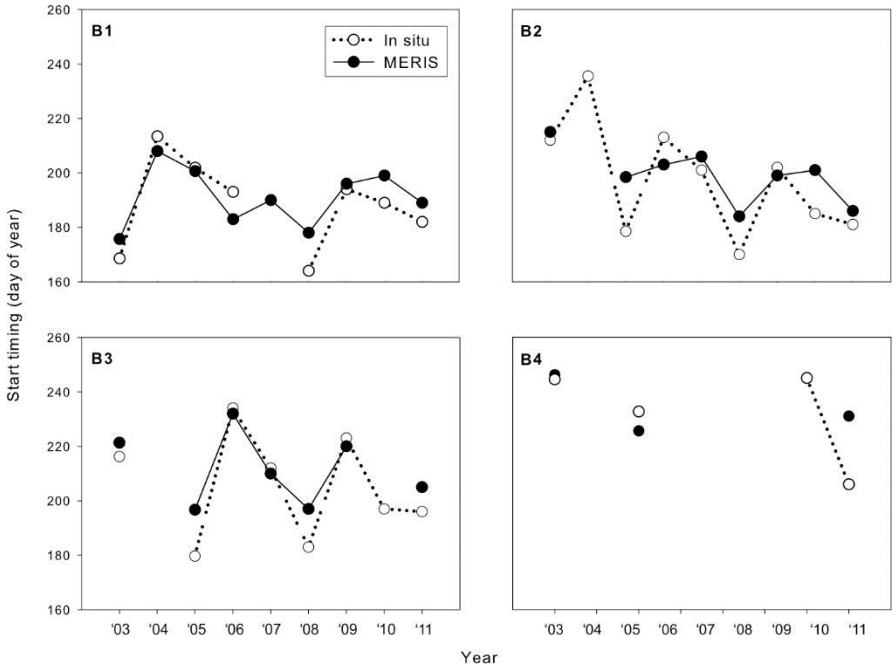

Figure 6.5. Validation of the MERIS FLH chl-*a* derived trend in bloom start timing over the nine-year time series using *in situ* chl-*a* measurement derived start timing, for the four main Lake Balaton basins. From Palmer et al. (2015b).

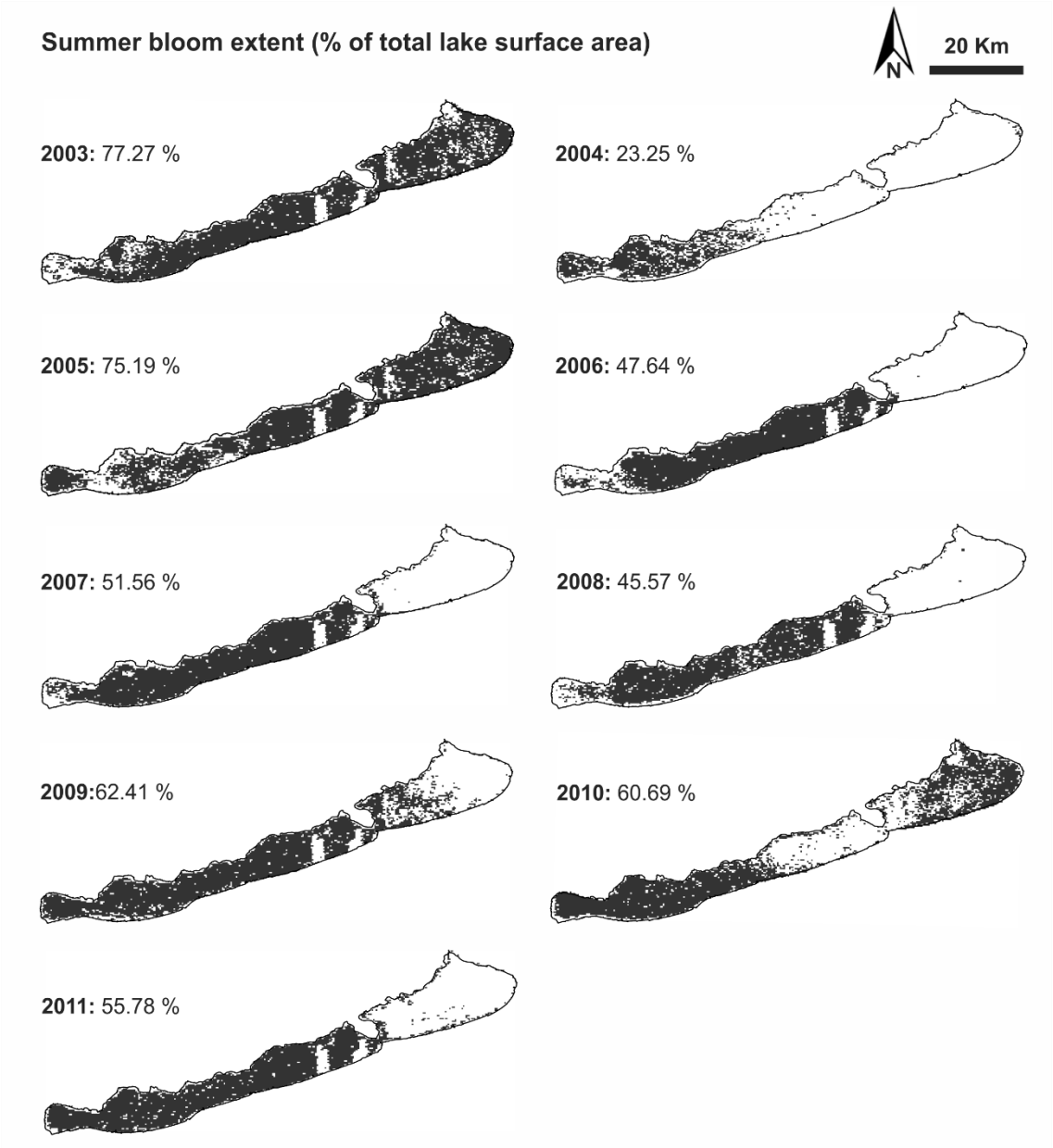

Figure 6.6. The spatial extent over which a summer bloom event was detected for each year, relative to the total lake surface area.

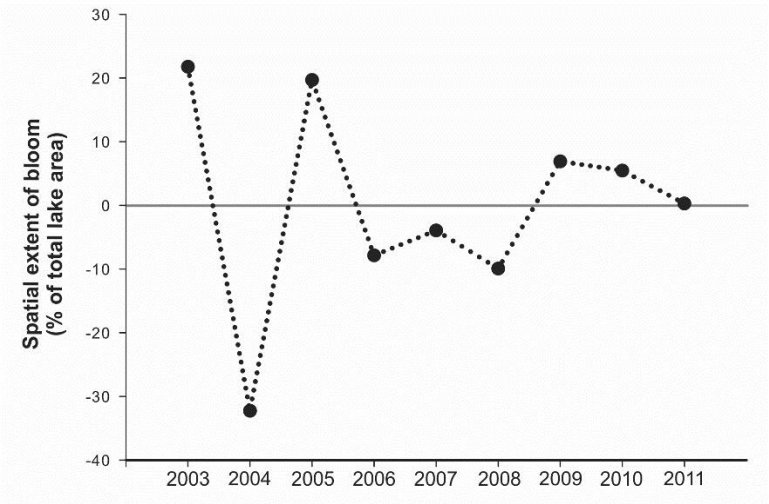

Figure 6.7. Bloom spatial extent anomalies, relative to the mean spatial extent from the nine years considered. From Palmer et al. (2015b).

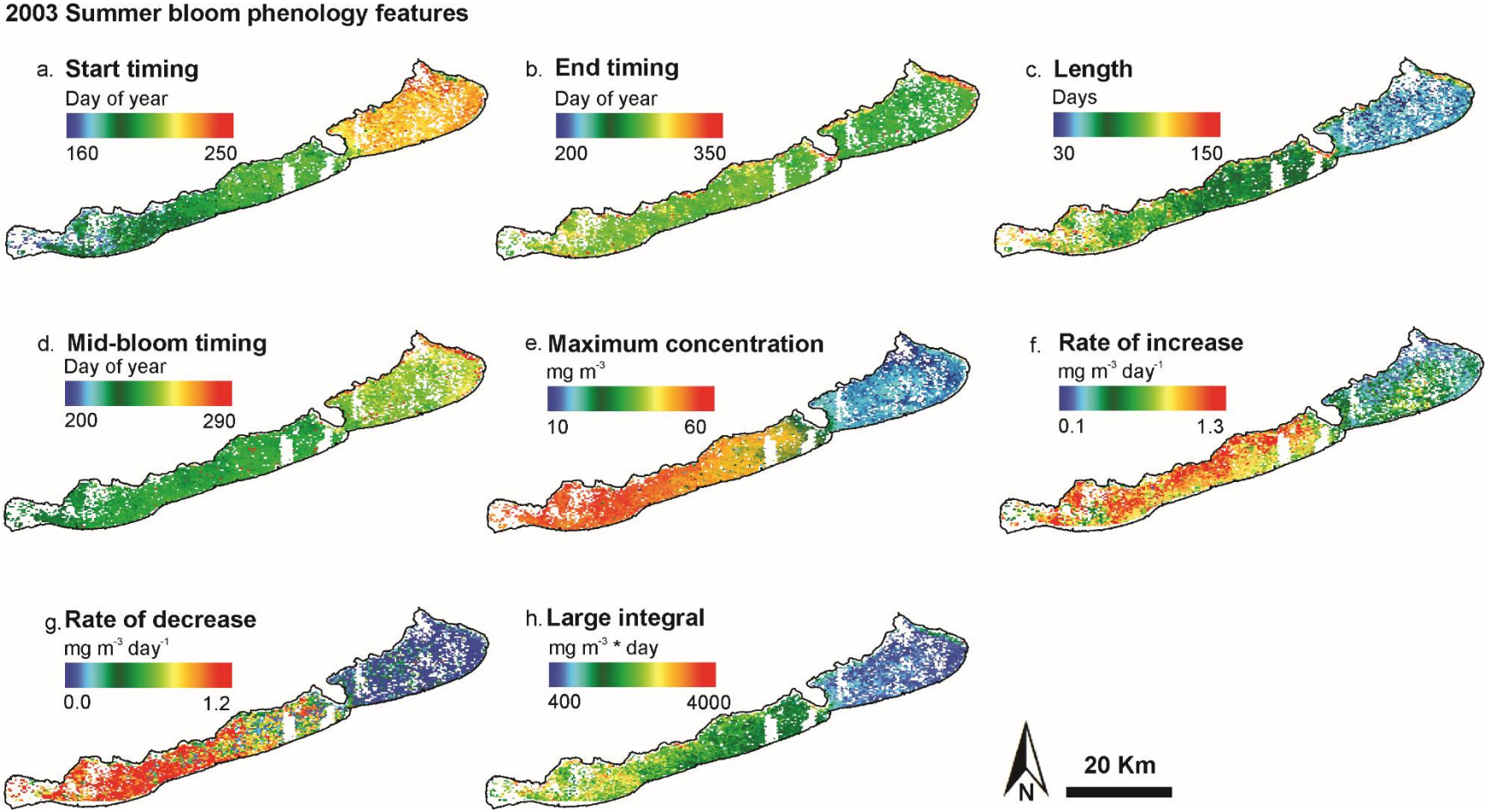

Figure 6.8. An example of each of the eight output TIMESAT phenology features, mapped for the 2003 Lake Balaton summer bloom. From Palmer et al. (2015b).

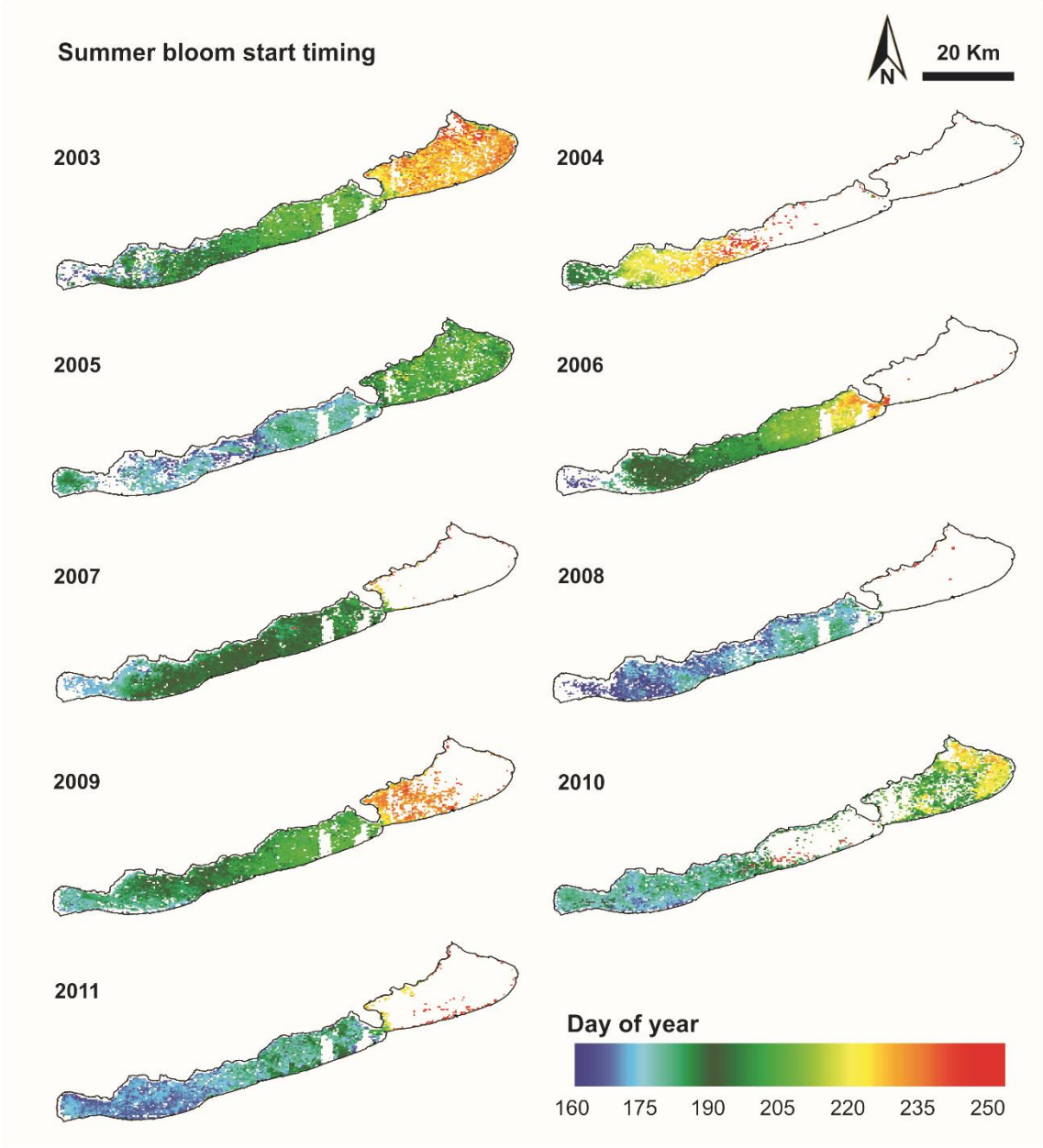

Figure 6.9. Summer bloom start timing, mapped for each of the nine years, as an example of spatial and temporal variability of the phenology features. From Palmer et al. (2015b).

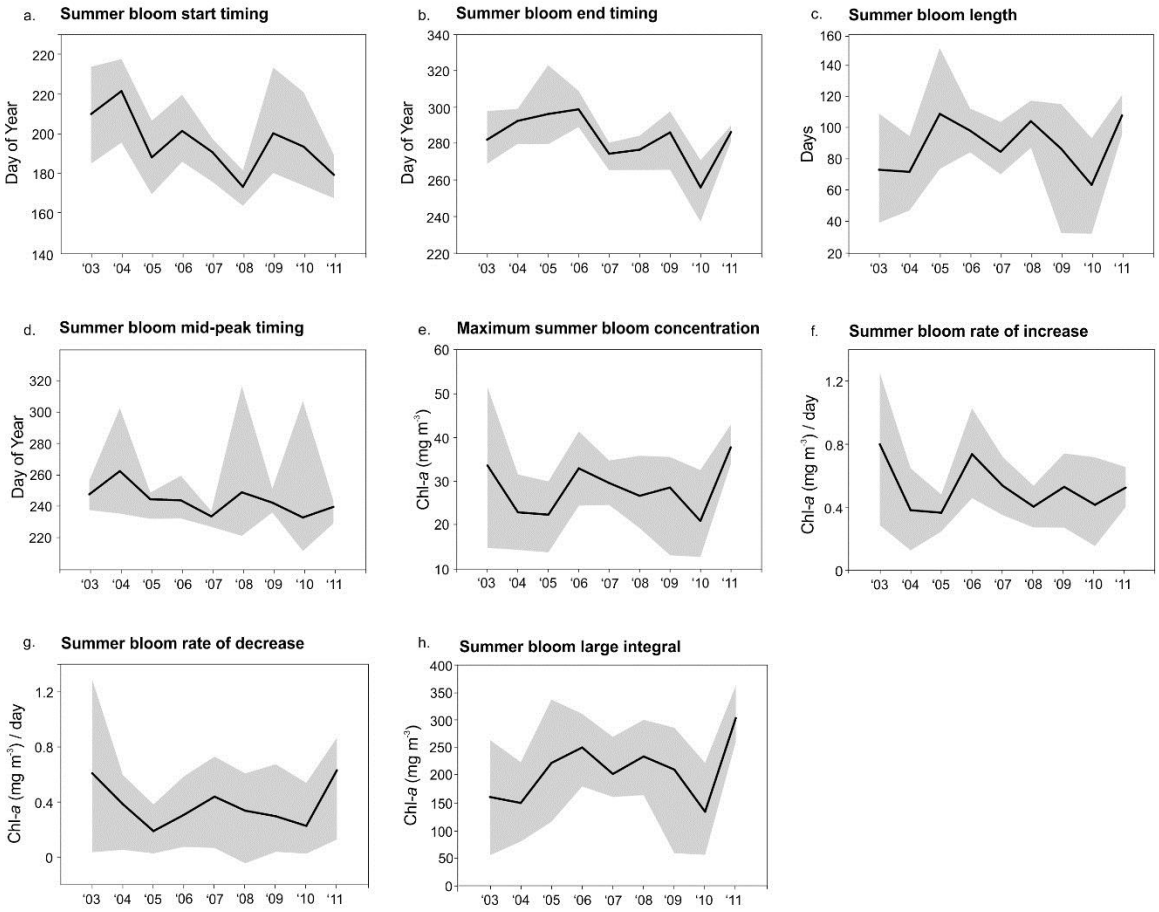

Figure 6.10. Variability of all extracted phenology features over the full lake area and time series. The black line is the mean ± tenth and ninetieth percentiles (shaded grey area). From Palmer et al. (2015b).

6.4.4 Correlation analysis

Results from the Pearson correlation matrix analysis are reported in Table 6.2, with all shaded values significantly different from zero at the alpha = 0.001 level, and colour-coded to represent different positive and negative correlation coefficient (R) values. Although no significant correlation was found between start and end timing, a significant correlation was found between each of these and bloom length (intuitively, earlier start timing and later end timing are correlated with longer bloom events, R = -0.76 and 0.61 respectively). High, positive correlations ($0.64 \leq R \leq 0.77$) were also found between maximum concentration and large integral, rate of increase and rate of decrease. A high degree of correlation was found between length and large integral (R = 0.88), as well as some correlation between start timing (R = -0.63) and large integral as well as end timing and large integral (R = 0.57). No statistically significant correlation was found between any of the extracted phenology features and the spatial extent of the bloom for the given year.

Table 6.2. Pearson correlation coefficient matrix of extracted spring and summer bloom phenology features. Shaded values are different from 0 with a significance level alpha = 0.001. From Palmer et al. (2015b).

	Start timing	End timing	Length	Mid-bloom timing	Maximum concentration	Rate of increase	Rate of decrease	Large integral	Spatial extent
Start timing	**1**								
End timing	-0.02	**1**							
Length	**-0.76**	**0.61**	**1**						
Mid-bloom timing	**0.40**	**0.32**	-0.11	**1**					
Maximum concentration	**-0.27**	**0.29**	**0.44**	-0.20	**1**				
Rate of increase	0.17	0.09	-0.03	-0.16	**0.66**	**1**			
Rate of decrease	-0.13	0.10	0.19	-0.09	**0.64**	**0.42**	**1**		
Large integral	**-0.63**	**0.57**	**0.88**	-0.16	**0.77**	**0.32**	**0.44**	**1**	
Spatial extent	0.17	0.02	-0.06	0.09	0.08	0.15	0.05	0.05	**1**

0.75 to 1
0.50 to 0.75
0.25 to 0.50
-0.25 to 0.25
-0.50 to -0.25
-0.75 to -0.50
-1 to -0.75

6.5 Discussion

No quantitative, universal definition exists for phytoplankton bloom events in lakes, which are considered rather generally to be periods of high biomass, or to be dominated by certain indicator species such as cyanobacteria (Carvalho et al. 2013). Here, a threshold-based definition was used for quantification, considering approximately median concentrations of the full time series, plus 5 %, as has been the approach in similar oceanographic works. In exploratory pre-processing steps, the chosen threshold values were found to most adequately capture bloom events, and are held constant over the full spatial and temporal ranges considered here. An important consideration for future work, however, is that these thresholds will not be transferable to other lakes where the dynamics are different from those of Lake Balaton. This is especially crucial to consider when progressing to inter-lake comparisons of phenology metrics. Consistency among phenology metric definitions has been explored in works using archive *in situ* plankton data and highlighted as important in assessing trends, drivers of phenology shifts and comparisons of phenology metrics among studies (Rolinski et al. 2007; Thackeray et al. 2012). The use of consistent metrics will likewise be a priority for future remote sensing works, and should be adapted to correspond as much as possible with those used in *in situ*, modeling and mesocosm studies so as to promote the complementarity and comparability of results.

Blank, white areas in the phenology or spatial extent maps indicate that no summer bloom was detected for the associated pixels in that year, according to both the bloom start and the bloom end criteria used here being met. In addition to no bloom event having occurred in reality, two scenarios have been revealed that lead to a bloom event having occurred, but not being detected by the present approach. As such, the spatial extents presented in Figure 6.6 and used to calculate yearly anomalies should be considered to be rough, minimum estimates. One of these non-detection of a real bloom event scenarios is that for a given pixel there were too many missing values in the input time series. In such cases, no smoothed time series will be generated and no phenology metrics will be calculated for any year of the time series for that pixel. A clear example of this is the cluster of unmapped pixels to the southwest of the Tihany Peninsula in Basin 2 (Figure 6.6), which is constant for all nine years of the time series. Some individual, scattered unmapped pixels where a bloom is otherwise mapped may also be a result of

this. Where missing values in the time series of a given pixel exceed a certain threshold, these pixels are excluded, however there is also error introduced when there are missing values in a pixel's time series but this pixel is not excluded (i.e., there are less missing values than the threshold for exclusion). Error related to missing SeaWiFS image data on global ocean spring bloom initiation and peak timing was found by Cole et al. (2012) to be ± 2 to 3 days for 10% missing data, and as much as ± 15 to 30 days for 80% missing data, common in sub-polar regions. A similar analysis to quantify this source of error for Balaton and other lakes in future work is recommended.

The second scenario is that, for the given pixel and the given bloom event, chl-*a* concentrations did not rise from below to above the defined bloom start threshold (i.e., 10 mg m^{-3}) or did not fall from above to below the defined bloom end threshold (i.e., 12 mg m^{-3}). For example, if chl-*a* concentrations were greater than 10 mg m^{-3} prior to the detected peak or remained above 12 mg m^{-3} following it, a bloom will not be mapped even when a peak is apparent in the smoothed function. The concentration thresholds for the lake were selected after exploratory analysis and were found to minimize, but not to completely preclude this phenomenon, which is another explanation for the scattered unmapped pixels where a bloom is otherwise mapped. An alternative approach to capturing all cyclic phytoplankton biomass peaks, regardless of background biomass magnitude would be to assess the median + 5 % for each pixel, which is unfortunately not possible using TIMESAT.

Superimposed upon the unmapped pixels resulting from the two scenarios described above, blooms as defined here (chl-*a* concentrations rising above 10 mg m^{-3} and falling below 12 mg m^{-3}) are found not to occur in several years in Basin 4 and occasionally in Basin 3 as well (Figure 6.6). This is thought to be related to the typically much lower chl-*a* concentrations measured in Basin 4, and increasing toward Basin 1 (Figure 6.3). In addition to the mapped phenology features, the inter-annual variability in spatial extents is also valuable information in itself. No correlation with any of the phenology features was found here (Table 6.2), but the variable environmental drivers such as temperature and nutrient loading may underlie year-to-year discrepancies in extent, and are to be examined in depth in future work.

Considerable and novel insight into the phenology of Lake Balaton was revealed through the MERIS chl-*a* map time series analysis of this chapter, particularly regarding

the spatial and interannual variability of the mapped features. The reliability of MERIS retrieved and mapped phenology metrics, including the spatial and temporal variability thereof, are further supported by robust validation using phenology metrics retrieved from *in situ* data (Figures 6.4 and 6.5). Going beyond the use of point *in situ* data (typically one point per lake) to examine phytoplankton phenology allows us to assess the compounded spatial and temporal variability (i.e., not only the variability for a given point in space from year to year, but also the variability in space for a given year and most interestingly the variability in spatial variability from year to year). Blooms varied widely in terms of timing and magnitude from year to year and basin to basin, and were absent in some years over varying extents of the lake. Most of the metrics are characterized by at least as much variability spatially, within a given year, as temporally, for a given pixel throughout the full time series. This may suggest that the lake would have a certain buffering capacity, or adaptability, in terms of the impacts of potential shifts in phenological metrics related to environmental change throughout the aquatic food web. Although overall or mean conditions (or those recorded by a single *in situ* measurement) might vary substantially from year to year, or shift over time, the diversity or range of conditions present over the spatial extent of the lake may still encompass key conditions necessary for ecological functioning (e.g., mean start timing in 2005 is only Day of Year (DoY) 190, compared with DoY 215 in 2003, but the tenth and ninetieth percentile ranges overlap, from 170 to 210 in 2005 and 185 to 235 in 2003). In this way, variability in the extremes (e.g., earliest and latest start dates) and the temporal variability in the spatial variability itself are expected to be important to consider. Likewise, the changes in the spatial gradients and ranges may themselves be an important response to changes in environmental conditions.

Apparent in Figure 6.8, as well as the maps in Appendix II, is the strong positive or negative gradient of several mapped phenology features coinciding with the general trophic gradient of the lake. This would be expected to be displayed by metrics such as maximum concentration or large integral, consistent with the already well-documented trophic gradient of the lake, but is also clear for rates of increase and decrease for example. Start timing also displays the strong southwest to northeast gradient, suggesting that nutrient loading from the Zala River and subsequent lake water circulation in this direction is the main underlying factor. End and mid-bloom timing, however, show a much weaker gradient, suggesting that different drivers or mechanisms underlie these

metrics. These may be more strongly driven by, for example, temperature dynamics (perhaps via temperature-mediated zooplankton grazing) which are typically more spatially consistent across the lake. As such, differences in the shifts or trends in different phenological metrics would be expected in response to changing environmental conditions, depending on the specifics of the latter (e.g., warming vs. nutrient loading).

Some significant, positive or negative correlations are highlighted in the results of the Pearson correlation matrix (Table 6.2). Correlation between some of the retrieved phenology metrics would be expected as a result of similarities or inverse patterns in their mapped gradients as well as their related conceptual definitions in some cases (Table 6.1). Although some are quite obvious, such as the strong, positive relationships between maximum bloom concentrations and large integral (R = 0.77) and length and large integral (R = 0.88), some nuanced insight is provided. For example, although both start and end timing correlate highly with length (R = -0.76 and 0.61 respectively), start and end timing do not correlate with each other either positively or negatively, indicating rather that blooms do not shift completely but remain more or less fixed in length, and that longer blooms have either earlier starts or later ends, but not both. Start and end timing are also found to be weakly associated with larger magnitude blooms, through correlation with maximum concentration (R = -0.27 and 0.29) and with large integral (R = -0.63 and 0.57).

Although the retrieval of phenology metrics was demonstrated for only the annual summer blooms here, which are more important for Lake Balaton in terms of peak and total biomass, the metrics of annual spring bloom phenology can be similarly mapped. However, given that FLH has been found to be insensitive to lower phytoplankton biomass concentrations, as revealed in chapter 4, an algorithm better suited to such conditions would need to be used to generate the input chl-*a* time series. This would also require a reparameterization of the TIMESAT settings used here, as lower biomass Balaton spring blooms would often not be detected using the start and end thresholds of the current study. Remote sensing has been found to robustly identify cyanobacteria blooms (Matthews et al. 2012; Wynne et al. 2008) and to retrieve phycocyanin (PC) concentrations, a proxy for cyanobacteria presence and biomass in phytoplankton blooms (Hunter et al. 2010; Li et al. 2012; Li et al. 2015; Matthews et al. 2012; Mishra et al. 2013; Simis et al. 2005; Wynne et al. 2008). Given this, and that cyanobacteria are of particular interest from an ecotoxicology perspective and are associated with eutrophic conditions

(Smith 2003), the extraction of cyanobacteria phenology using remotely sensed phycocyanin concentrations and a similar approach as demonstrated here is of high interest for future work. It should be noted, however, that to achieve reliable phenology metric retrievals and mapping for lake phytoplankton, whether for phytoplankton biomass more generally or for cyanobacteria more specifically, the use of validated, robust retrieval algorithms for input chl-*a* or PC mapping is essential.

A number of previous works have taken different approaches to considering phytoplankton phenology in lakes using remote sensing, and particularly that of cyanobacteria. Several have looked at temporal changes in cyanobacteria surface scum areal extent using the floating algae index (FAI) applied to MODIS (Hu et al. 2010) and to both MODIS and Landsat (Duan et al. 2014) data for Lake Taihu, China. A threshold is applied to the retrieved FAI maps to indicate the presence or absence of surface scum, and bloom start timing and duration are determined from the time series, for each pixel. Matthews (2014) investigated time series of lake-wide median chl-*a*, as well as cyanobacteria bloom and surface scum (chl-*a* > 350 mg m^{-3}) areal extent for 50 lakes throughout South Africa using the MPH algorithm (Matthews et al. 2012) applied to MERIS data from 2002 to 2012. Monthly averages of each were input into time series analysis. Timing (month) of maximum chl-*a* concentration and maximum cyanobacteria and surface scum surface area (referred to as phase) were retrieved, as was yearly amplitude of chl-*a* concentrations (the concentration difference between months with maximum and with minimum concentrations in a given year). Monthly anomalies and monthly and yearly trends were also calculated between 2005 and 2011. Binding et al. (2011) investigated yearly cyanobacteria blooms in the US/Canadian Lake of the Woods, similarly took lake-wide median chl-*a* concentrations (retrieved from MERIS Maximum Chlorophyll Index (MCI) algorithm (Gower et al. 2005)) as input into the generation of their time series (using all available imagery), and subsequently investigated the timing of maximum chl-*a* concentrations (referred to as phase in Matthews (2014) and peak timing here) as well as the maximum concentrations themselves, and the surface area of different trophic levels of the yearly blooms. Stumpf et al. (2012) estimated cyanobacteria concentrations in Lake Erie using the Cyanobacteria Index (CI) algorithm (Wynne et al. 2008) applied to MERIS imagery from 2002 to 2011. CI images were dekad-binned (to maximum CI values) and "bloom intensity" of each dekad-binned image was calculated as the sum of CI, for all lake pixels where CI is greater than 0.001 (indicative of the

presence of a significant cyanobacteria (Microcyctis) bloom), as a proxy for total biomass of the associated period. Bloom area was calculated as the total area with CI greater than 0.001 and annual "bloom severity" was calculated as the mean of the three highest "bloom intensities" for a given year.

The TIMESAT approach used here is distinct from most previous works in that time series (of chl-*a* as in the current work, but maps of PC or other parameters with a regular seasonality could also be input) are generated and phenology metrics retrieved at the individual pixel level, which can then be examined and analysed through mapping. Current results highlight the high degree of spatial variability that can comprise phytoplankton phenology, even within a single lake, which is not captured through approaches that use lake-wide median or cumulative concentrations to examine the temporal evolution of bloom events. Although the FAI threshold approach to mapping the presence/absence of surface scums and the temporal evolution thereof enables the determination and mapping of start timing and duration of scum-forming blooms for each water pixel (Duan et al. 2014; Hu et al. 2010), this type of approach is limited to application for lakes wherein blooms typically form surface scums, does not account for non-scum forming blooms, and was also found to be limited due to the inability of the FAI algorithm to distinguish surface scums from macrophytes (Hu et al. 2010). Furthermore, since bloom concentration magnitude is not accounted for (rather seasonality metrics are based on a binary presence or absence of scum), several of the metrics demonstrated here (i.e., maximum concentration, rates of increase and decline, large integral) would be unable to be calculated. Each approach taken and set of parameters generated in the previous and current works provide a unique and potentially complementary perspective on bloom dynamics, and each is associated with its respective advantages and limitations. The tailoring of some phenology metrics to the specific contexts of the lake system or systems studied may be necessary or desirable in some instances. However, the cross-evaluation and standardization of features where possible would greatly facilitate the comparison of different lakes' behaviours over time and the understanding of underlying environmental drivers, which is of clear importance within the context of global climate change for example.

Phenology events generally respond to cues from biotic or abiotic environmental signals or changes. Typical responses of phenology metrics to changing environmental conditions reported from laboratory, mesocosm, modelling and field studies include shifts

in the timing of phytoplankton blooms, in terms of onset, peak and end (Berger et al. 2010a; Lewandowska and Sommer 2010; Meis et al. 2009; Sommer and Lewandowska 2011; Winder et al. 2012; Winder and Schindler 2004a, b; Winder and Sommer 2012), variable growth rates (Maberly et al. 1994), changes in overall phytoplankton biomass (or bloom magnitude) (Elliott et al. 2006; Lewandowska and Sommer 2010; Sommer and Lewandowska 2011), as well as decreased overall biodiversity and increased dominance of cyanobacteria (Elliott 2012; Elliott et al. 2006). The main underlying controls on freshwater phytoplankton phenology have been found to be temperature (Gaedke et al. 2010; Thackeray et al. 2008; Winder et al. 2012; Winder and Schindler 2004a) and related stratification timing (Winder and Schindler 2004b), ice break up (Adrian et al. 2006), light conditions (Gaedke et al. 2010; Winder et al. 2012), grazing pressure (Gaedke et al. 2010), overwintering population levels (Gaedke et al. 2010) and nutrient levels (Feuchtmayr et al. 2012; Thackeray et al. 2008). Winder and Schindler (2004b) linked phytoplankton phenology shifts in Lake Washington, USA with the extended stratified period related to Pacific Decadal Oscillation (PDO) (akin to the North Atlantic Oscillation (NAO) effects observed in European lakes (Straile et al. 2003)) and El Niño Southern Oscillation (ENSO) events. A meta-analysis carried out by Blenckner et al. (2007) demonstrated coherent direct and indirect responses to climate forcing of the North Atlantic Oscillation (NAO) by various biophysical and biochemical factors on long-term data from European lakes spanning diverse settings (northern, central and western regions). These include increased summer cyanobacteria biomass during positive NAO years, for example.

Links between environmental drivers and shifts in phytoplankton phenology features have also been revealed in the remote sensing studies of the pelagic ocean mentioned in the introduction. Generally, differences in phenology metrics have been reported by latitude, especially in the timing and duration of spring bloom events, related to predominance of light or nutrient limitation which varies with latitude (Siegel et al. 2002). Sea surface temperature (SST) and photosynthetically active radiation (PAR) have also been considered and found to have a strong influence on phenology, in addition to the influence of latitude by González Taboada and Anadón (2014) and Racault et al. (2012). El Niño/La Niña events and other climate indices such as the Southern Oscillation Index (SOI) and the Pacific Decadal Oscillation (PDO) have been correlated with phenological indices (González Taboada and Anadón 2014; Racault et al. 2012; Sasaoka

et al. 2011). Earlier end of ice cover was reported to be an important driver of earlier spring phytoplankton blooms in the Artic, with the timing of the maximum annual chl-*a* concentration advancing by up to 50 days over the 13 years of the study (Kahru et al. 2011). Although the *in situ*, mesocosm and modelling studies discussed here, as well as remote sensing analyses of pelagic ocean phytoplankton phenology, typically focus on the spring bloom, summer/fall blooms in many temperate lakes are of particular concern due to their high biomass concentrations and cyanobacteria dominance, as in the case of Balaton. This is particularly the case under predicted climate change scenarios, with intensified cyanobacteria blooms associated with warming and eutrophication (Paerl and Huisman 2009).

Some of the remote sensing investigations into phytoplankton and cyanobacteria phenology in lakes have also extended their results to comparison with potential underlying environmental drivers of variability. Stumpf et al. (2012) found a significant correlation between spring discharge and total phosphorous (TP) load of the Maumee River to Lake Erie and summer cyanobacteria blooms in the latter, and used this to construct a bloom forecasting model. Binding et al. (2011) found April through July cumulative rainfall to be significantly correlated with chl-*a* concentration peak timing and January through August cumulative temperature to be significantly correlated with peak concentrations. Nutrient ratios (total nitrogen (TN):TP) and preceding winter temperatures were found by Duan et al. (2014) to underlie the start timing of surface scum-forming blooms in Lake Taihu. Such previous works as well as the current results encourage the application of the methodology described here to other lakes, as well as the exploration of the effect of variable environmental conditions on mapped phenology features.

Satellite remote sensing as used here provides general approximations of phytoplankton biomass via chl-*a* and will therefore be unable to address species specific phenology, including shifts in individual species' phenology in response to various environmental drivers and across trophic levels as has been able to be documented through several *in situ*, mesocosm and modelling works described above. However, it is hoped that remote sensing products such as those explored here can nevertheless complement ongoing *in situ*, mesocosm and modelling phenological analyses. This is supported by the use of more general phytoplankton biomass indicators in a number of *in situ* studies (Adrian et al. 2006; Gerten and Adrian 2000; Seebens et al. 2009; Thackeray

et al. 2012). Another limitation of remote sensing in this capacity is the relatively limited temporal coverage. The MERIS time series used here is only available between mid-2002 and early 2012 for example, compared with *in situ* datasets that have been used extending back multiple decades, in some cases to 1946 (Maberly et al. 1994). However, results from Meis et al. (2009) demonstrate that a significant trend in the advancement of bloom initiation could be obtained using a time series of only 15 years, a temporal coverage soon to be obtained by MODIS. Similarly, the use of satellite imagery is currently restricted to medium and large lakes, given the spatial resolutions of suitable sensors. Potential improvement is foreseen with the Sentinel-2 MultiSpectral Instrument (MSI), characterized by spatial resolution of less than 60 m and improved spectral resolution in comparison with Landsat.

Ongoing and future work aims to bring together diverse datasets (nutrient loading, temperature, ice cover, irradiance, etc.) to thoroughly examine potential environmental drivers that might underlie such variability. Although MERIS data are no longer acquired on an ongoing basis, the future Sentinel-3 OLCI and Sentinel-2 MSI sensors will provide ongoing and improved sources of data for mapping Lake Balaton chl-*a* (ESA 2013b, c). In addition to chl-*a*, the validation and mapping of PC, an indicator pigment of cyanobacteria, is currently being tested for retrieval from MERIS and Sentinel data for Lake Balaton. As mentioned in Chapter 2, cyanobacteria detection and mapping is of particular interest due to the high biomass, eutrophic conditions which they tend to be associated with as well as their potential toxicity (Paerl and Huisman 2009; Smith 2003). The mapping of Lake Balaton chl-*a* phenology presented here, and increasingly robust measurements of phycocyanin using satellite imagery suggests the potential to similarly map cyanobacteria phenology. In addition to the application and adaptation of phytoplankton phenology mapping to other lake ecosystems, and their comparison with the current results, as well as the dedicated investigation into the influence of environmental drivers on phytoplankton phenology, cyanobacteria phenology metric mapping is of high interest for future work. As is the case for chl-*a* phenology mapping however, it is important to note that the robust performance of the retrieval algorithms used to produce the input phycocyanin maps is crucial.

6.6 Conclusions

Phenology features of Lake Balaton phytoplankton have been retrieved and mapped here for the first time using MERIS satellite imagery, making use of a validated chl-*a* time series product and TIMESAT software. Lake Balaton summer bloom phenology features and bloom spatial extent were shown to display a high degree of both spatial and temporal variability, revealed through mapping as well as through statistical analysis. Correlation between some extracted bloom features revealed further nuance in bloom dynamics. The satellite-based mapping of phytoplankton phenology in inland waters shows great promise for furthering the understanding of phytoplankton dynamics, but is dependent on the accuracy of the chl-*a* product input. Chl-*a* retrieval validation therefore remains a crucial step, and will also influence the potential for inter-lake comparison, as will selected smoothing techniques and parameterization. Future research directions include quantitatively assessing the roles of potential environmental drivers of phenology feature variability, such as temperature and nutrient conditions. Also of interest would be the retrieval and comparison of phenology features from other lakes and notably from across diverse environmental, climatological, latitudinal and watershed settings, and the mapping of cyanobacteria biomass phenology specifically, making use of phycocyanin retrieval algorithms that are currently in development and testing stages. The fine-tuning of methodology adapted to freshwater phytoplankton phenology retrievals and mapping, considering some of the encountered issues discussed above, is another priority.

Chapter 7

Ultraviolet Fluorescence Light Detection and Ranging measurements of water quality parameters under turbid lake conditions

The work presented in this chapter has been published as:

Palmer, S. C. J. *et al.* (2013). Ultraviolet Fluorescence LiDAR (UFL) as a Measurement Tool for Water Quality Parameters in Turbid Lake Conditions. *Remote Sensing*, 5, 4405-4422.

7.1 Introduction & rationale

In addition to the passive optical remote sensing techniques used to retrieve chl-*a* and other physiochemical water quality parameters, described in the preceding chapters of this thesis, active fluorescence Light Detection and Ranging (LiDAR) approaches have also been used for many years in oceanographic settings (Farmer et al. 1979; Hoge and Swift 1981). Sensors aboard airborne, ship-mounted and stationary platforms have made measurements in diverse coastal, estuarine and pelagic ocean contexts. Sensor instrument types vary from hyperspectral to fluorosensor to imaging LiDAR and make use of different types of lasers, different optical geometries and are optimized to measure certain parameters (Babichenko 2008; Barth et al. 2000). In addition to measuring phytoplankton biomass through the fluorescence peak of chl-*a* near 685 nm, CDOM is measured through its broad-peak fluorescence centred near 440 nm (Rogers et al. 2012; Vodacek et al. 1995), TSM has been estimated from the sea surface using its backscattering (Aibulatov et al. 2008), and pollutants such as oil spills have been detected (Abramov et al. 1977; Babichenko 2008; Barbini et al. 1999; Chubarov and Fadeev 2004; Pelevin et al. 1995). Synergy between fluorescence LiDAR and passive, satellite remote sensing has been achieved through the use of fluorescence LiDAR measurements in pelagic ocean settings as abundant *in situ* validation data (Fiorani et al. 2004; Hoge et al. 2003).

Airborne fluorescence LiDAR was used in inland waters settings in some early testing and application (Bristow et al. 1985), however more recent examples of its use in the research and monitoring of freshwater systems are very few (Babichenko et al. 2006; Babichenko et al. 2004). Fluorescence spectroscopy itself has provided enormous insight in both freshwater and marine settings through the characterization of CDOM, pollutants and phytoplankton (Anttila et al. 2008; Beutler et al. 2002; Proctor and Roesler 2010; Stedmon et al. 2003; V.-Balogh et al. 2003; Vodacek 1989). Combining the remote sensing capabilities of LiDAR with the ecological insight provided by fluorescence

spectroscopy would allow the characterization of lake water quality features *in situ* over large spatial areas and non-intrusively. The spatial scale of measurements able to be achieved by ship-mounted measurements, typically between one and five meters apart, would increase our understanding of small to medium scale ecological processes in lakes and provide a large number of measurements at the sub-pixel level for satellite sensor algorithm validation.

The Ultraviolet Fluorescence LiDAR (UFL), version 9, of the Shirshov Institute of Oceanology was used to undertake the current work during a research visit by and field campaign with its operating scientists. It is designed to measure the backscattering and/or fluorescence associated with the measurement of chl-*a* concentration, CDOM absorbance and TSM concentration, with distinct, non-overlapping channels for each and a strong signal due to its active, laser-induced nature (compared with the weaker signals induced by solar energy in passive remote sensing). It is thus ideally suited to measure all three groups of optically significant substances important in lakes. Given the novelty of fluorescence LiDAR measurements in lake waters, possible limitations that may be related to the high turbidity and optical complexity remain to be examined, particularly saturation at high concentrations. At high concentrations, the absorbance or backscattering features across the visible and near-infrared spectral range may mask the fluorescence signal, or the emitted fluorescence may itself be absorbed or scattered. The variety of different species and groups of phytoplankton found in natural communities may present additional challenges or opportunities through their varying chl-*a* fluorescence yield and distinct accessory pigments.

7.2 Objectives

This chapter details laboratory and field fluorescence LiDAR measurements carried out in a lake setting for the first time at Lake Balaton. The objectives are thus exploratory in nature and can be summarized as follows:

(1) To determine the reliability of UFL chl-*a*, CDOM and TSM measurements under the turbid and optically-complex conditions encountered in Lake Balaton during field measurements;

(2) To extend the range and variability of concentrations through a series of tank measurements carried out in the laboratory;

(3) To identify the influence on UFL chl-*a* measurements when multiple phytoplankton species are present and to explore the possibility of distinguishing species via their UFL emission signals;

(4) To point to possible extensions of the current work for ongoing investigation.

7.3 Methods

7.3.1 Ultraviolet Fluorescence Light Detection and Ranging (UFL)

The series of Ultraviolet Fluorescence Light Detection and Ranging (LiDAR), UFL instruments 1 – 9, was developed by the Shirshov Institute of Oceanology of the Russian Academy of Sciences, Moscow (Aibulatov et al. 2008; Pelevin et al. 2001). Specific features of the Shirshov UFL-9, used during 2012 laboratory experiments and Lake Balaton field campaigns, are described here. Instrument details can also be found in Table 7.1.

Dual neodymium-doped yttrium aluminum garnet (Nd:YAG) excitation laser pulses of the UFL-9 are emitted at a frequency of 2 Hz for a duration of 6 ns. The resulting distance between point measurements depends on the travel velocity of the transporting vehicle; these generally range from between one and five metres. Low pass filtering over a three point moving average window is then used to reduce noise. Measurements can be taken from a distance of between 1.5 and 25 m above the target (the water surface) by adjusting the telescope length accordingly, and with an incidence angle of between 10° and 60° degrees relative to the surface. During the 2012 field campaign, the UFL-9 was mounted on the front of the research boat of the BLI, as demonstrated in Figure 7.1. The dual excitation wavelengths of the emitted laser beams are 355 (1.5 mJ energy) and 532 nm (3 mJ energy), however in the current work only the 355 nm beam was used. The 532 nm pulse is employed under conditions of low insolation to strengthen the measured signal, and was not found to be necessary during either field or laboratory measurements.

The eleven bands of the UFL-9 spectral receiver are centred at 354, 385, 404, 424, 440, 460, 499, 532, 620, 651, and 685 nm, so as to specifically target the identification and measurement of chl-*a*, TSM and CDOM, as well as water Raman backscattering. Figure 7.2 demonstrates a typical spectrum across the spectral receivers. Similar to elsewhere in the literature (Barbini et al. 2003; Barbini et al. 2001; Wright et al. 2001), CDOM is estimated through the fluorescence of each measurement point at 440 nm normalized to water Raman backscattering of the same point at 404 nm upon excitation by the 355 nm wavelength laser and fluorescence at 685 nm is normalized to water Raman backscattering to estimate chl-*a* concentrations at each measurement location. Specific to the UFL series, TSM is measured by backscattering of the 355 nm laser pulse at this same wavelength, normalized to Raman scattering. To our knowledge, the UFL series is the first to incorporate a spectral receiver band at 355 nm for the measurement of TSM backscattering, thus integrating a crucial parameter in the study of optically complex waters. Empirical coefficients derived between the normalized fluorescence signal of a subset of UFL measurements and coinciding *in situ* measured concentrations are then applied to the full suite of UFL measurements for chl-*a*, CDOM and TSM mapping.

Figure 7.1. UFL-9 aboard the BLI research boat for the 2012 field campaign.

Table 7.1. Key features of the Ultraviolet Fluorescence LiDAR (UFL-9). From Palmer et al. (2013).

Excitation laser wavelengths	355, 532 nm
Receiver spectral channels	355, 385, 404, 424, 440, 460, 499, 532, 620, 651, 685 nm
Sounding frequency	2 Hz
Pulse duration	6 ns
Pulse energy	1.5 mJ (355 nm pulse), 3 mJ (532 nm pulse)
Telescope	Kepler; adjustable length to target range 1.5–25 m
Power supply	220 V, 50 Hz, 120 W
Dimensions; weight	1.0 × 0.7 × 0.3 m; 35 kg
Receivers	Photomultipliers
Channel filters	Four-channel beam splitter; interference filters; high-frequency Analogue-to-Digital Conversion (ADC)
Telescope clear aperture	140 mm
Analog-to-Digital Converter frequency	50 MHz
Analog-to-Digital Converter resolution	10 bit

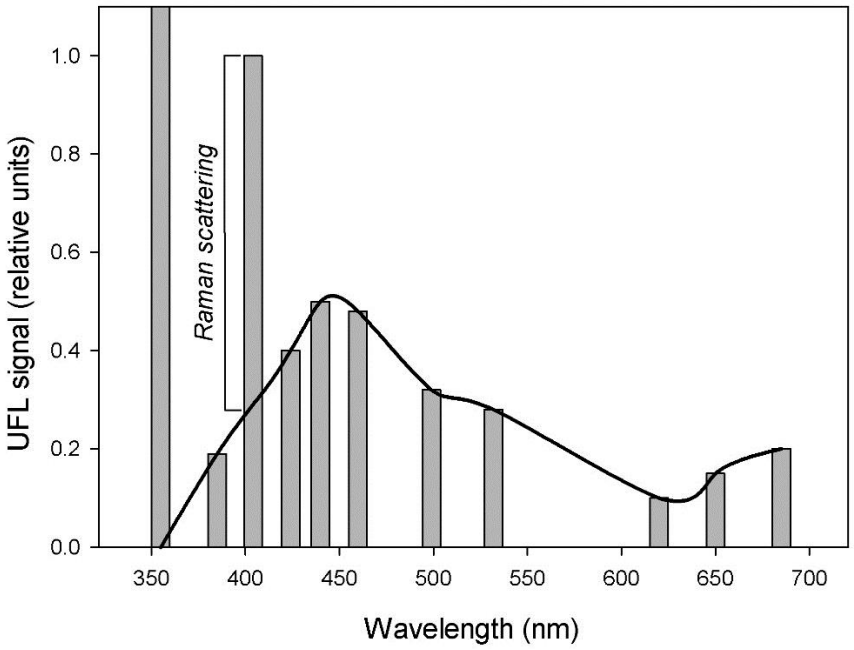

Figure 7.2. Example fluorescence and backscattering signals measured by UFL (355 nm excitation laser pulse) across its 11 bands, including the removal of the colored dissolved organic matter (CDOM) baseline at 404 nm to establish Raman scattering for normalization. From Palmer et al. (2013).

The field campaigns on Lake Balaton represent the first attempt to our knowledge to use ship-mounted fluorescence LiDAR techniques in investigations in a lake setting. It should be noted, however, that a particularly interesting feature of the application of fluorescence LiDAR systems to assess water components is the possibility to derive concentration measurements with depth for each measurement point, allowing for 3D profiles. As excitation laser depth penetration decreases under increasingly turbid conditions (i.e., is a function of turbidity as well as laser wavelength and strength (Babichenko 2008)), this is unfortunately not possible in the case of Lake Balaton (characterized by high turbidity; Secchi depth ranging from 20 cm to just under one metre). Rather, measurements of the CDOM absorption coefficient, and chl-*a* and TSM concentrations are only available for the water surface layer. Elsewhere, under less turbid conditions, the UFL series has measured chl-*a* fluorescence over depths of 2 to 3 m, CDOM fluorescence and TSM backscattering over depths of approximately 10 m (Kopova et al. 2010), ranges typical of fluorescence LiDAR systems (Babichenko 2008).

The UFL-9 weighs a total of 35 kg and measure 100 x 70 x 30 cm, including water resistant housing, enabling its installation aboard medium to small research vessels as well as small motor boats, typical in limnological studies, in addition to larger vessels, more typical of oceanographic research (e.g., the RV Akademik Ioffe of the Shirshov Institute of Oceanology, which is 117 m in length, 6600 gross tons). Power can be supplied from an on-board network or generator (220 V, 50 Hz, 120 W), further enhancing the flexibility and portability of the instrument in diverse environments. Through the combination of instrument and hardware design, and the addition of a receiver band targeting the measurement of TSM (in addition to more common fluorescence-based measurements of chl-*a* and CDOM), UFL instruments present new opportunities for fluorescence LiDAR measurement of water components in limnology.

7.3.2 Tank measurements

In June 2012, a sequence of tank measurements were designed to be carried out in the laboratories of the BLI, with the overarching purpose of extending the range of water constituent concentrations and combinations expected to be encountered in the field measurements from the same period, and thus examine the limits of UFL measurements in highly turbid and optically complex conditions as well as potential application to other lakes. Phytoplankton biomass was measured between chl-*a* concentrations of 0.01 and 400 mg m^{-3}, using phytoplankton cultivated in the months leading up to the tank measurements at the BLI. Two algal species were used, to allow insight into the sensitivity of UFL measurements to the distinct chl-*a* fluorescence yields and the fluorescing accessory pigments characterizing each. One was the cyanobacteria *Cylindrospermopsis raciborskii* (ACT 9502) and the other the chlorophyta *Scenedesmus armatus* (ACT 9710). Both species are commonly found in Lake Balaton. Cyanobacteria blooms occur regularly in the summer months, and are of particular concern due to their high productivity and potential toxicity. Measurements were made of individual species' cultures, diluted with filtered Lake Balaton water, as well as varying concentrations of the two cultures combined in a 2:1 (*Cylindrospermopsis raciborskii* : *Scenedesmus armatus*) ratio. Sediment for use in the experimental measurements was collected from Lake Balaton and oven-dried. TSM concentrations were expected to range between less than 0.1 and 120 g m^{-3}. Relatively CDOM-rich water from the Zala River was collected

for use as the high-CDOM end-member in the tank measurement, diluted at varying intervals by filtered Lake Balaton water. CDOM absorbance was expected to range between 0 and 0.15 absorption m^{-1} at 440 nm (aCDOM(440)), limited by the maximum absorbance of the Zala River water.

The tank used consisted of a 1.2 m high cylindrical, matte black polyvinyl tube, sealed at one end. Water level (1.0 m) and volume (32 L) were constant across all 32 measurements. The UFL was stabilized at a height of 2.0 m above the water surface, at an angle of approximately 5°, so as to avoid surface glint identified in trial measurements. The UFL excitation laser beam was directed to the centre of the tank, and the collection of 2 L of tank water sample immediately followed the UFL measurement for conventional laboratory measurements of TSM, CDOM and chl-*a* (described in Sections 4.3.3 and 7.3.4).

7.3.3 Field measurements

In situ UFL measurements were made of Lake Balaton between June 4th and 7th 2012. The UFL was attached to the research boat of the BLI approximately two metres above the water surface and at a 45° angle. In addition to UFL measurements made while the boat was in motion for mapping, 34 UFL measurements coinciding with water samples were taken for validation by conventional laboratory measurement. Measurements were made across the full, longitudinal trophic gradient characterizing Lake Balaton in an attempt to maximize the range of chl-*a* concentrations encountered. Likewise, measurements were made into the mouth of the Zala River to maximize the range of CDOM encountered.

7.3.4 Validation data

All water samples collected during both tank and field measurements were analyzed as per the protocol of the Nutrient Cycling Laboratory of the BLI described in Section 4.3.3. However, samples coinciding with field measurements were taken from the surface layer (< 50 cm depth) rather than integrated over the water-column, as is standard practice, to coincide more closely with the UFL measurements. Coloured

dissolved organic matter (CDOM) was also determined following conventional methodology (Cuthbert and del Giorgio 1992), through its absorbance at 440 nm (m^{-1}), measured using a using a Shimadzu spectrophotometer, model UV 160A.

7.3.5 Data processing and statistical analysis

Fluorescence emission and backscattering measured during tank and field campaigns was normalized to Raman scattering at 404 nm through the establishment and subtraction of a baseline between emission at 385 and 424 nm to remove the effect of CDOM at this wavelength. Above this baseline, any signal at 404 nm is considered to be from Raman Scattering alone (Figure 7.2). Empirical relationships were determined between the normalized fluorescence emission at 440 nm and CDOM absorbance, the normalized fluorescence emission at 685 nm and chl-*a* concentration and normalized backscattering at 355 nm and TSM concentration. The field measurement dataset was randomly split 70:30 for training and testing, respectively, in cross-validation. Regressions were performed within SigmaPlot statistical and graphing software, v. 12.3 (© 2014 Systat Software Inc.).

7.4 Results

7.4.1 Tank measurements

Results of the 32 conventional BLI sample analyses coinciding with UFL tank measurements are summarized in Table 7.2. Unfortunately, only 34 % (n = 11) of the tank measurements corresponded with a valid CDOM absorbance measurement, due to the remaining 66 % (n = 21) falling below the detection limit. The ranges of CDOM measured was 0.003 to 0.122 aCDOM(440), that of phytoplankton biomass was 0.01 to 377.9 mg m^{-3} chl-*a* and that of TSM was <0.10 to 128.4 g m^{-3}.

Linear models were found to best relate normalized fluorescence and backscattering signals at 440, 685 and 355 nm to CDOM absorbance, chl-*a* concentration and TSM concentration respectively (Table 7. 3). UFL measurements performed highly across the full measured ranges of TSM concentrations (Figure 7.3a; R^2 = 0.91, p <

0.001), of CDOM absorbance (Figure 7.3b; $R^2 = 0.95$, $p < 0.001$) and of chl-*a* concentrations (Figure 7.3c; $R^2 = 0.85$, $p < 0.001$).

Table 7.2. Descriptive statistics of TSM, chl-*a* and CDOM measurements used to validate laboratory tank UFL measurements. From Palmer et al. (2013).

	n	**Minimum**	**Maximum**	**Average**	**Median**	**Standard Deviation**
TSM (g m^{-3})	32	<0.10	128.4	24.21	2.62	39.39
CDOM ($a_{CDOM}(440)$)	11	0.003	0.122	0.023	0.007	0.037
Chl*a* (mg m^{-3})	32	0.01	377.9	44.86	3.31	96.47

Table 7.3. Validation of UFL tank measurements, including equation and coefficients, coefficient of determination (R^2) and significance (p-value). From Palmer et al. (2013).

	Equation	**R^2**	***p***
TSM (g m^{-3})	$0.13 \times UFL_{355} - 5.14$	0.91	< 0.001
CDOM ($a_{CDOM}(440)$)	$0.002 \times UFL_{440} + 0.004$	0.95	< 0.001
Chl*a* (mg m−3)	$288.85 \times UFL_{685} - 4.84$	0.85	< 0.001

It was further found that the relationships between chl-*a* concentration and normalized fluorescence at 685 nm were robust and distinct for *C. raciborskii* and for *S. armatus* species. Whereas normalized fluorescence at 685 nm and chl-*a* concentration correlated linearly across the full concentration range for *S. armatus* (1.04–82.79 mg m^{-3}, $R^2 = 0.99$, $p < 0.004$, $n = 4$), normalized fluorescence at 685 nm increased exponentially with increasing chl-*a* concentrations in the case of *C. raciborskii* (0.19–377.88 mg m^{-3}, $R^2 = 0.96$, $p < 0.005$, $n = 5$). Furthermore, measurements containing the 2:1 mixture of the two cultures fell between the relationships described for the individual species (Figure 7.4; 2.30–292.09 mg m^{-3}, $R^2 = 0.99$, $p < 0.001$, $n = 4$).

C. raciborskii cultures were found to display a distinct fluorescence emission peak at 650 nm which is not apparent for *S. armatus* cultures (Figure 7.5), and the ratio of fluorescence emission at 650 nm to that at 685 nm was found to distinguish species cultures across chl-*a* concentrations (Figure 7.6). A Generalized Linear Model (GLM) performed in RExcel revealed that species is the only significant source of variance ($F = 18.68$, $p < 0.002$) when chl-*a* concentration ($F = 0.11$, $p = 0.75$), species and the combined effect of the two ($F = 0.07$, $p = 0.93$) are considered (chl-*a* concentration, species and the combined effect of the two are considered = independent variables; the ratio of normalized fluorescence emission at 650 nm to that at 685 nm = dependent variable). Measurements of the two species combined again fell between the two species considered separately (Figure 7.6).

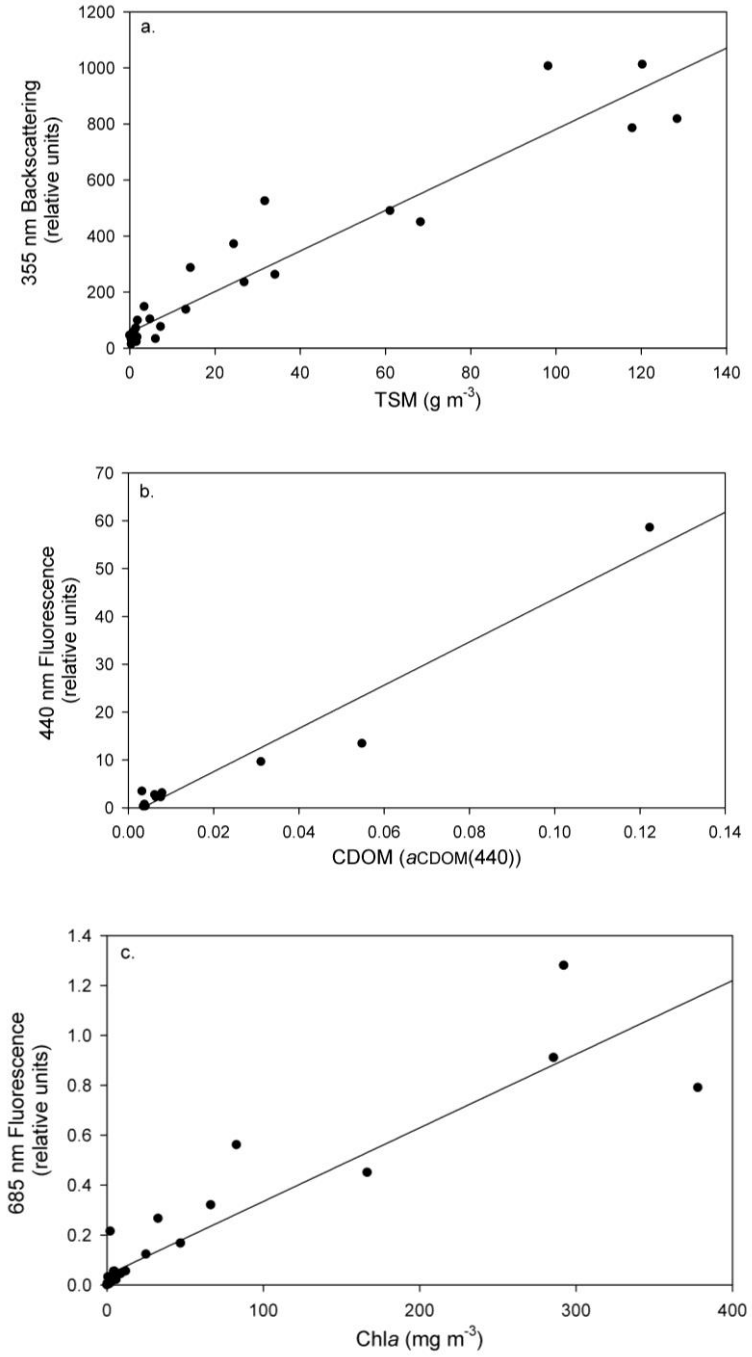

Figure 7.3. Relationships of coinciding UFL (excitation wavelength = 355 nm) and validation measurements of (a) TSM (TSM (g m^{-3}) = 0.13 × UFL_{355} (backscattering) – 5.14; R^2 = 0.91; p < 0.001; *n* = 32); (b) CDOM absorbance ($a_{CDOM(440)}$) (CDOM = 0.002 × UFL_{440} (fluorescence emission) + 0.004; R^2 = 0.95; p < 0.001; *n* = 11); and (c) chl-*a* concentration (mg m^{-3}) (chl-*a* = 288.85 × UFL_{685} (fluorescence emission) - 4.84; R^2 = 0.85; p < 0.001; *n* = 32). From Palmer et al. (2013).

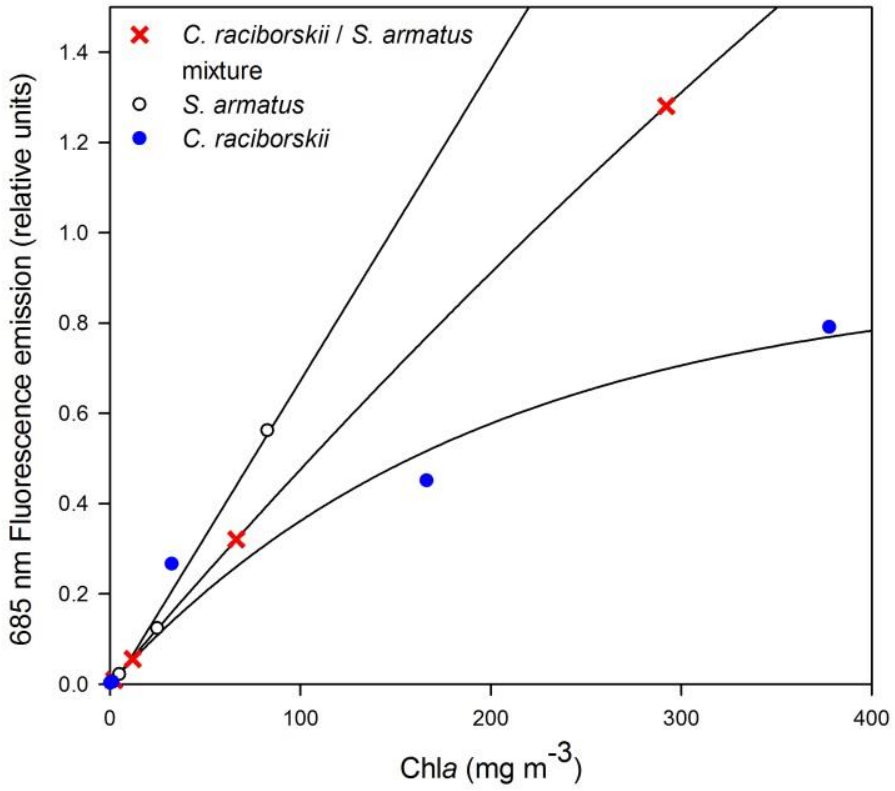

Figure 7.4. Distinct relationships between chl-*a* concentration and fluorescence emission at 685 nm (excitation laser pulse wavelength = 355 nm) for *Cylindrospermopsis raciborskii* (chl-*a* = 332.77 × UFL685 $^{1.13}$; R^2 = 0.96; p < 0.005; *n* = 5), *Scenedesmus armatus* (chl-*a* = 143.98 × UFL_{685} + 2.80; R^2 = 0.99; p < 0.004; *n* = 4), and a mixture of the two (chl-*a* = 212.98 × UFL685 $^{0.97}$; R^2 = 0.99; p < 0.001; *n* = 4). From Palmer et al. (2013).

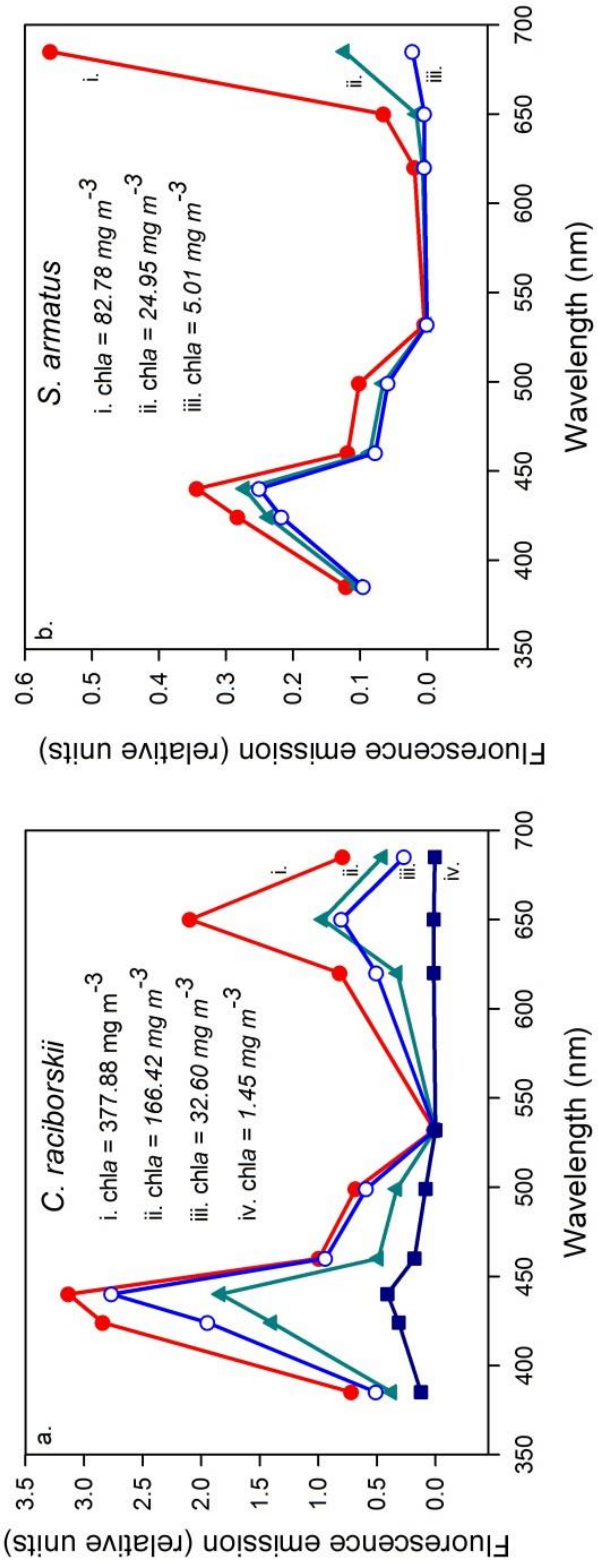

Figure 7.5. UFL fluorescence emission spectra (excitation laser pulse wavelength = 355 nm) for (a) *Cylindrospermopsis raciborskii* and (b) *Scenedesmus armatus* cultures of varying biomass concentrations. From Palmer et al. (2013).

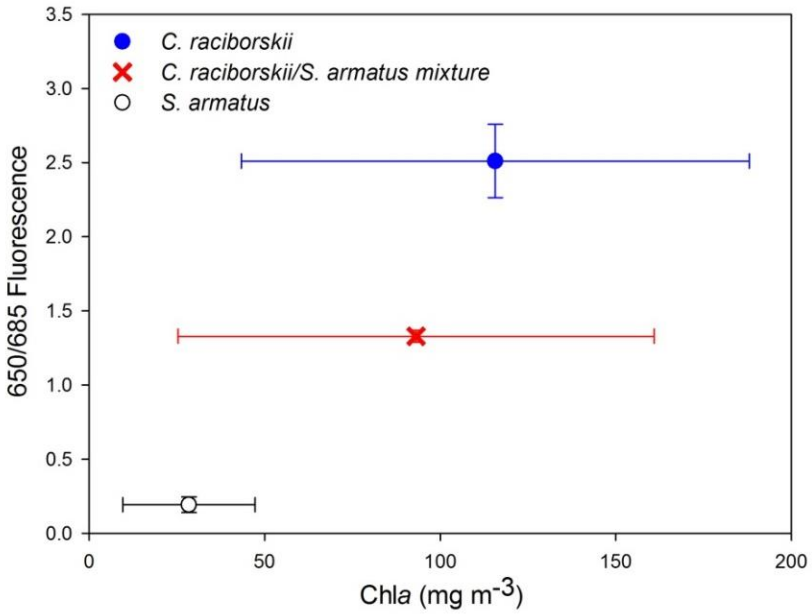

Figure 7.6. Discrimination of phytoplankton cultures, *Cylindrospermopsis raciborskii* and *Scenedesmus armatus*, through the ratio of fluorescence emission at 650 nm to that at 685 nm (excitation laser pulse wavelength = 355 nm; $F = 18.68$; $p < 0.002$). Averages are shown by symbols, bars report ± standard error. From Palmer et al., (2013).

7.4.2 Field measurements

Results of the 34 conventional BLI sample analyses coinciding with UFL field measurements are summarized in Table 7.4. TSM varied highly (over the range of 2.93 to 30.50 mg m^{-3}) over the study period, responding rapidly to changing wind conditions. Field measurements were unfortunately only possible between the spring and summer blooms, thus limiting the range of phytoplankton biomass encountered (measured between 2.66 to 7.33 mg m^{-3}). CDOM absorbance coinciding with UFL measurements in the field ranged from 0.03 to 0.12 aCDOM(440).

Relationships between TSM, chl-*a* and CDOM and their associated normalized UFL-measured backscattering and fluorescence signals were found to differ greatly between tank and field measurements, and a separate calibration was deemed necessary. Cross-validation based on only field UFL measurements and coinciding measurements of CDOM absorbance, chl-*a* and TSM concentrations resulted in highly robust retrievals in all cases. Strong linear relationships were found for both TSM (Figure 7.7) and chl-*a*

(Figure 7.8), whereas the relationship between CDOM and normalized fluorescence at 440 nm was exponential (Figure 7.9).

Table 7.4. Descriptive statistics of TSM, CDOM and chl-*a* measurements used in Lake Balaton UFL field measurement calibration and validation. From Palmer et al. (2013).

	n	**Minimum**	**Maximum**	**Average**	**Median**	**Standard Deviation**
TSM ($mg \cdot m^{-3}$)	34	2.93	30.50	15.86	15.01	5.79
CDOM ($a_{CDOM}(440)$)	34	0.006	0.120	0.014	0.008	0.019
Chl*a* ($mg \cdot m^{-3}$)	34	2.66	7.33	4.35	3.95	1.20

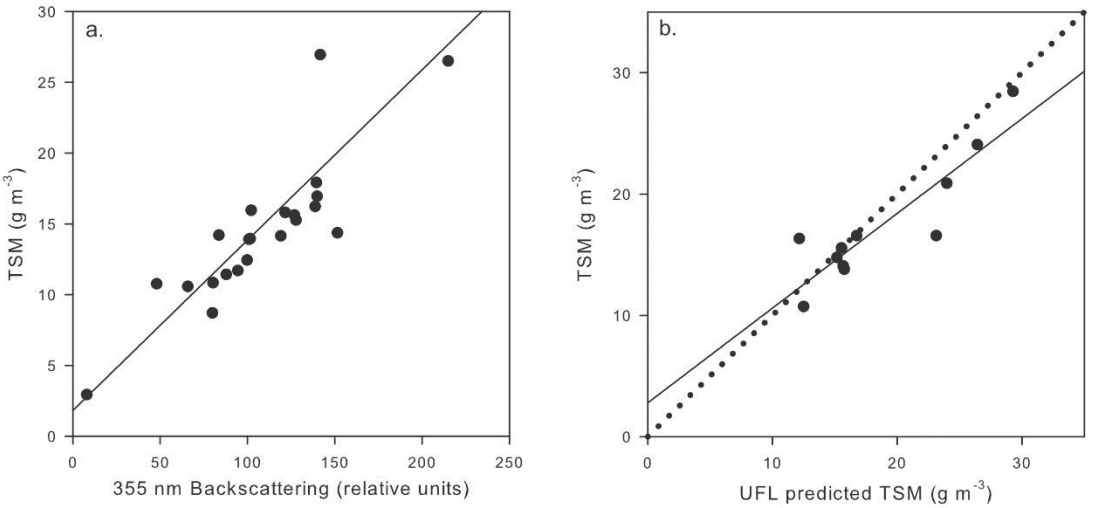

Figure 7.7. Field campaign specific (a) calibration (TSM = 0.12 × UFL_{355} + 1.81; R^2 = 0.72; $p < 0.001$) and (b) validation of UFL TSM measurements (*in situ* TSM = 0.78 × UFL TSM + 2.79; R^2 = 0.81; $p < 0.001$; RMSE = 2.80 g m^{-3}). Solid line is regression trend line; dotted line is 1:1. From Palmer et al. (2013).

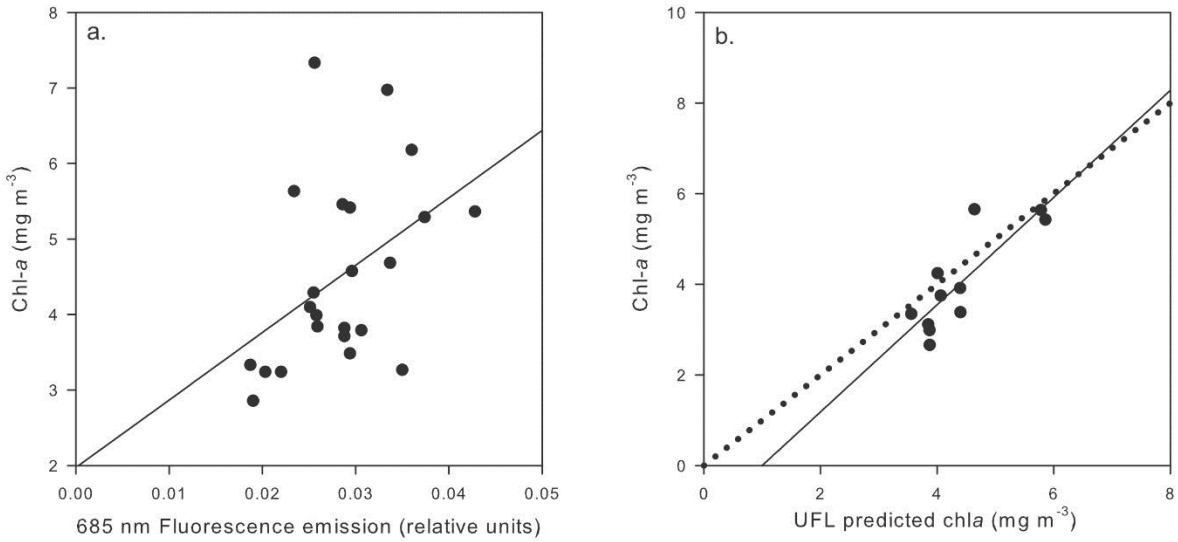

Figure 7.8. Field campaign specific (a) calibration (chl-*a* = 89.2 × UFL_{685} + 1.98; R^2 = 0.19; p = 0.04) and (b) validation of UFL chl-*a* measurements (*in situ* chl-*a* = 1.18 × ULF chl-*a* – 1.18; R^2 = 0.69; p = 0.04; RMSE = 0.71 mg m^{-3}). Solid line is regression trend line; dotted line is 1:1. From Palmer et al. (2013).

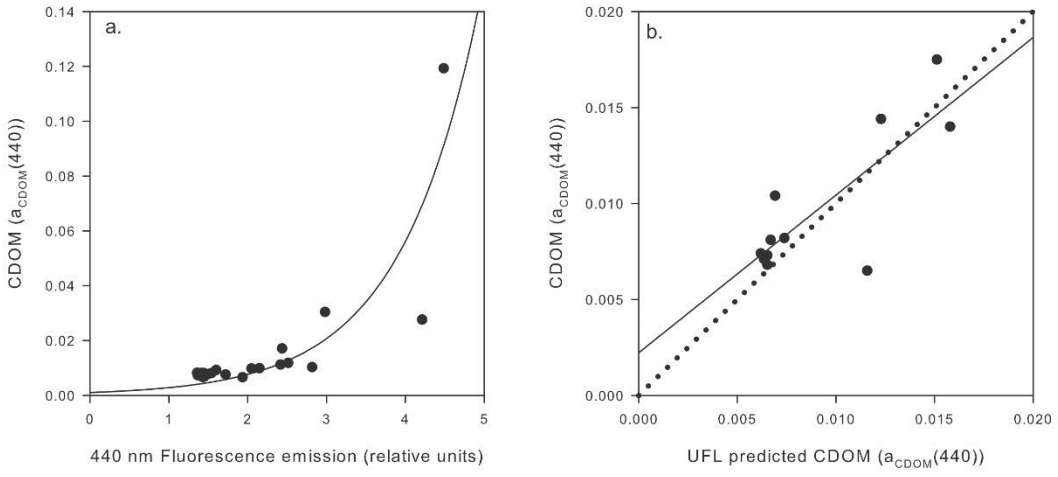

Figure 7.9. Field campaign specific (a) calibration (CDOM = 0.003 × exp (0.69 × UFL_{440}); R^2 = 0.82; p < 0.001) and (b) validation of UFL CDOM measurements (*in situ* CDOM = 0.82 × UFL CDOM + 0.002; R^2 = 0.66; p < 0.003; RMSE = 0.0022 a440 nm m^{-1}). Solid line is regression trend line; dotted line is 1:1. From Palmer et al. (2013).

7.5 Discussion

The retrieval of TSM concentration, chl-*a* concentration and CDOM absorbance using UFL measurements of related backscattering and fluorescence emission features has been shown to be possible under turbid, optically complex lake conditions, as well as largely robust. Tank measurements made in the laboratory generally extended the range of the parameters measured in the field, particularly in the case of phytoplankton biomass, which was found to be limited *in situ* at the time of the field campaign relative to conditions during bloom events in the lake, whereby chl-*a* concentrations typically exceed 30 mg m^{-3}. The TSM concentration range was also extended, from concentrations between 2.93 and 35 g m^{-3} measured in the field, to concentrations less than 0.1 g m^{-3} and greater than 120 g m^{-3} measured in the tank experiment. Concentrations as high as 115 g m^{-3} have been measured through regular BLI monitoring following high wind events, thus the concentration range is considered representative for Lake Balaton, as well as encompassing of a large concentration range that is likely to be encountered at other sites. Over this entire range, the relationship between gravimetrically measured TSM and normalized backscattering of the 355 nm UFL excitation laser pulse was robust.

The range of CDOM measured in the field was not greatly extended by the tank measurements (from 0.006 to 0.120 in the field to 0.003 to 0.122 in the laboratory), as the high-CDOM end member used in the tank measurements was collected from the Zala River, where field measurements were also made. However, a twofold lowering of the minimum CDOM absorbance measured was achieved. Many of the CDOM absorbance measurements coinciding with UFL tank measurements (66%) were below the detection limit. This is thought to result from the relatively short optical path of the spectrometer (cuvette length = 5 cm), and a longer cuvette would allow for more sensitive CDOM absorbance measurements in the low range to better understand the UFL measurement performance there. Furthermore, low UFL measurements at 440 nm associated with these below detection limit samples qualitatively supports the calibration undertaken here. The exponential, rather than linear relationship found between CDOM absorbance and normalized UFL fluorescence emission at 440 nm during field measurements likely results from slight error in removing the CDOM baseline to establish Raman scattering. This leads to an over-estimation of Raman scattering, and under-estimation of CDOM which is proportionately greater at higher concentrations. Although it was not possible to

remove this effect, the exponential correlation observed in Figure 7.9 is highly significant, and can be used for reliable CDOM retrievals from the field measurements.

The experimental tank measurements carried out also revealed significant differences in the fluorescence signatures of the two phytoplankton species, *C. raciborskii* and *S. armatus*. This was in terms of the distinct relationship of the chl-*a* concentration of each with the normalized fluorescence signal at 685 nm, typically associated with chl-*a* fluorescence. These are expected to result from differences in the chl-*a* fluorescence yield (or efficiency) of each, essentially the amount of fluorescence that results from the amount of light energy absorbed (Johnsen and Sakshaug 2007). Differences in fluorescence yield result from structural and pigmentation differences in the photosystems of the species, which are responsible for absorbing light and carrying out photosynthesis and energy and electron transferral (Johnsen and Sakshaug 2007). It has been found elsewhere that up to 90 % of the chl-*a* concentration in cyanobacterial species may be located in the non-fluorescing photosystem I (PSI) (Beutler et al. 2003; Bryant 1986; Johnsen and Sakshaug 1996; Seppälä et al. 2007), which could result in the underestimation of cyanobacteria chl-*a* concentrations using the fluorescence maximum at 685 nm if a cyanobacteria-specific relationship is not first calibrated. Chl-*a* has been found to reside predominantly in the fluorescing photosystem II (PSII) of chlorophyta species (Beutler et al. 2002), which would explain the linear relationship established between *S. armatus* culture chl-*a* concentration and normalized fluorescence at 685 nm.

Environmental factors, such as ambient light conditions, and nutrient concentrations and availability, can also affect the fluorescence efficiency of pigments. As the phytoplankton cultivation and the measurements of individually cultured species and manipulated combinations, were carried out under constant conditions in the laboratory, however, this is not expected to be a significant factor. Such factors should be considered if attempting similar comparisons and interpretations in field measurements where these could be expected to have an effect and are more variable and difficult to account for given their complexity. Another difference in fluorescence spectra between *C. raciborskii* and *S. armatus* was found in association with the normalized fluorescence emission at 650 nm. This took the form of a clear peak in the cyanobacteria species which was absent in the chlorophyta, and is thought to be related to the fluorescence maxima of the phycobilisome pigment, phycocyanin found in its PSII. The ratio of UFL measured

normalized fluorescence at 650 nm to that at 685 nm resulted in a strong separation of the two species, confirmed via GLM (Figure 7.6).

The phytoplankton species cultivated and used in the tank measurements are commonly found in Lake Balaton. Their distinction via ULF measurements here points to the investigation of UFL measurements of other species with varying accessory pigments as an interesting future direction, potentially toward the creation of a fluorescence spectral library for different species with further investigation into identifying end member and mixed spectra, as has been carried out using passive spectrometry (Hunter et al. 2008a) and laboratory and *in vivo* fluorescence spectroscopy (Beutler et al. 2002; Gregor and Maršálek 2005; Johnsen and Sakshaug 1996; Seppälä et al. 2007) elsewhere. The conventional analysis of other pigment concentrations, not possible in the current work, would be necessary. This would be valuable in extending the use of UFL to other sites where different phytoplankton species may be present or dominant, and possibly to identifying the presence of species or taxa of interest, such as cyanobacteria which are known to be potentially toxic (Codd et al. 2005) and have been shown here to have a distinct UFL signature from that of the investigated chlorophyta species. The advantage of making such distinctions using LiDAR remote sensing approaches include the much greater spatial coverage and resolution possible, in comparison with conventional *in situ* measurements. Furthermore, the signatures of different water constituents and potentially phytoplankton taxa can be more clearly separated in comparison with passive optical remote sensing. However, in contrast to passive optical sensors found aboard satellite platforms, regular revisits are not possible where regular access to both site and instrumentation does not occur. As the UFL and its operation are highly specialized, this technology is currently not broadly accessible and therefore not likely to prove a regular feature in limnological monitoring at present.

Until now, ship-mounted fluorescence LiDAR has only been applied in marine settings, where constituent concentrations and optics are vastly different from those in Lake Balaton and other inland waters. Here, TSM, CDOM and chl-*a* have been shown to be accurately retrieved via UFL over a wide range of conditions. No negative effects related to the masking of one constituent's signal by another or to the saturation or dampening of the retrieved signal at high concentrations were apparent. This stands UFL in contrast to passive optical remote sensing techniques used to retrieve the same constituents, where overlapping signals and variable constituent concentrations pose a

significant challenge (IOCCG 2000). However, the normalization of the UFL signal for the retrieval of CDOM concentrations in the field was found to be a challenge. UFL is considered applicable to the range of conditions encountered at Lake Balaton, and would be interesting to test in other lake types. Boreal lakes in particular would be of interest given the much larger CDOM range in comparison to that encountered at Lake Balaton (with absorbance as high as 11 m^{-1} $a_{CDOM}(420)$ (Kutser et al. 2005)). Highly eutrophic lakes would further test the limits of the UFL in the field. Tank measurements successfully retrieved chl-*a* concentrations up to 377 mg m^{-3}, but *in situ* concentrations were very limited in the current work.

7.6 Conclusions

Fluorescence LiDAR has been demonstrated to be a useful tool to measure ecologically important physiochemical and biological water quality parameters for the first time in a lake setting, through a series of UFL field and laboratory tank measurements. The high and variable concentrations investigated here are in contrast to those typically encountered in marine settings where ship-mounted fluorescence LiDAR has been employed for such measurements to date. In a mapping context, greater spatial coverage and resolution would be possible than is through conventional point measurements, to capture nuanced variation related to ecological processes on the small to medium spatial scales. The ability to distinguish different groups of algae via their UFL signal has also been proven, and the inclusion of further phytoplankton species and divisions is recommended for future work, as is the application to other lake ecosystems.

Chapter 8

Conclusions, research contributions and outlook

This thesis has examined both passive, satellite-based and active, ship-mounted LiDAR remote sensing of biogeochemical water quality parameters, particularly phytoplankton biomass via the proxy chl-*a*, and has demonstrated the feasibility and potential novel contributions to be made by such remote sensing tools and approaches within a limnological context. Not only has the work undertaken added to knowledge of Lake Balaton with regards to remote sensing potential and water constituent dynamics, but methodologies previously unreported in application to freshwater settings are explored with Lake Balaton as a case study, that could be applied to other inland water bodies in the future.

8.1 Original research contributions

For the first time, a suite of chl-*a* algorithms compatible with MERIS image data have been extensively evaluated for Lake Balaton, which presents unique and complex optical conditions. This is crucial so as to benefit from the reliable use of the ten year MERIS archive for phytoplankton mapping from space, and comprised a validation study of neural network and band arithmetic algorithms using *in situ* data from across the lake and all seasons over five years (n = 289 matchups) (Palmer et al. 2015a). Likewise, the broad range of conditions presented by Lake Balaton may offer insight into conditions expected to be encountered at other lakes and the current work may inform the algorithm selection for these. However, as pointed out in Chapter 4, dedicated calibration and validation of algorithms should be carried out using data from any other targeted site prior to choosing and applying a retrieval algorithm, as conditions are highly variable from lake to lake. Similarly, the validation of two atmospheric correction techniques was undertaken for the first time at Lake Balaton, and the influence thereof on chl-*a* retrievals was considered.

The resulting algorithm selection and application to the full MERIS archive allowed for the exploration and evaluation of spatiotemporal dynamics of Lake Balaton phytoplankton, namely phenology metrics (Palmer et al. 2015b). This was the first time that TIMESAT has been used to extract and map phenology metrics in a freshwater setting. Not only does such an approach add an explicit and cohesive spatial component to investigations of phenology, which have traditionally been approached using point

data, but the regular revisit time of MERIS allows the possibility of phenological analysis where the high frequency *in situ* data that would otherwise be necessary are lacking. Such a progression from chl-*a* concentration algorithm validation and mapping to the use of time series chl-*a* maps in such a way is foreseen to be an important and continuing direction in the remote sensing of lakes. Furthermore, the phenology of Lake Balaton phytoplankton has been shown to be highly variable both spatially and temporally.

The use of ship-mounted UFL to measure and map a suite of biogeochemical parameters important in lake water quality has also been evaluated in a freshwater setting for the first time as part of this thesis (Palmer et al. 2013). Measurements of chl-*a*, TSM and CDOM were found to be accurate in both field and laboratory tank measurements, across broad concentration ranges and in various combinations, and a distinct signal was found for the different phytoplankton taxa examined (chlorophyta and cyanobacteria).

8.2 Thesis conclusions

In **Chapter 4**, the results of an extensive calibration-validation exercise of chl-*a* retrieval algorithms are reported. Several general as well as more nuanced conclusions were drawn in response to, and extending beyond, the defined research objectives of this chapter:

- The FLH algorithm robustly retrieves Lake Balaton chl-*a*, especially under meso- and eutrophic conditions (chl-*a* > 10 mg m^{-3}), but does not perform well under oligotrophic conditions (chl-*a* < 10 mg m^{-3}).
- Local tuning of SIOP coefficients relating neural network-retrieved pigment absorption to chl-*a* concentration is confirmed to greatly reduce the error of associated retrievals, although neural network retrievals remain inaccurate overall.
- Under oligotrophic conditions, the FUB/WeW neural network-based algorithm, locally-tuned through adjusting the SIOPs relating pigment absorption to chl-*a* concentration, outperformed FLH. Although a step-wise, ensemble approach combining FLH and FUB/WeW algorithms led to a slight improvement in low concentration retrievals, the use of FLH alone was found to be sufficient to monitor and map the onset and development of bloom events and was recommended for use in Chapter 6 analyses.

- FLH is found to have a physical basis related to phytoplankton absorption and backscattering rather than fluorescence for Lake Balaton, as is clear from the negative relationship between the two, which is likely indicative of cyanobacteria dominance in the phytoplankton community composition.
- Classification using FLH-derived chl-*a* was found to add important spatial information for WFD reporting. Remote sensing is thus confirmed to have the potential to complement and inform WFD reporting for Lake Balaton.
- The importance of such validation exercises is highlighted, with either poor or good performance of the tested algorithms apparent through regression-based calibration and validation, and mapping alike. Poor or uninformed algorithm selection could result in missed bloom events, false alarms or generally inaccurate mapping.

In **Chapter 5**, the atmospheric correction of MERIS images coinciding with *in situ* water-leaving spectral and chl-*a* measurements was undertaken using two models, the atmospheric correction component of the C2R/Lake processor and the SCAPE-M_B2 model, to validate each and understand the influence of atmospheric correction on subsequent chl-*a* retrievals. The following conclusions were drawn:

- Of the tested atmospheric corrections, the SCAPE-M_B2 model was found to generally retrieve measured *in situ* R_{rs} values accurately, whereas *in situ* measurements were typically underestimated, and spectra flattened, by the atmospheric correction of the C2R/Lake processors.
- This discrepancy in performance is discussed with regards to the underlying assumptions and approaches of the two models. Although SCAPE-M_B2 assumes spatial homogeneity over larger areas than the C2R/Lakes processor, more accurate retrievals overall suggest that this is not a hindrance to algorithm performance in this case.
- The comparison of AOT(550) retrieved by the two atmospheric corrections suggests that an overestimation by the C2R/Lake processor may underlie, at an intermediate step, the poor R_{rs} retrievals, although *in situ* data to confirm and quantify this were unfortunately not available for the thesis work.
- Uncorrected, TOA data were found to retrieve chl-*a* concentrations to a similar level of accuracy as SCAPE-M_B2 corrected data, when semi-empirical retrieval algorithms were applied, and were thus deemed appropriate to use in MERIS chl-

a mapping and time series analysis in combination with the FLH algorithm. This suggests that the error associated with temporal variability in atmospheric conditions not accounted for when using uncorrected data is similar to the error associated with the atmospheric correction itself in this case.

- Although FLH was again found to best retrieve chl-*a*, several other band math algorithms using red-NIR spectral bands were also found to be robust.

Chapter 6 presents a novel approach, combining MERIS satellite imagery and TIMESAT software to extract and map lake phytoplankton phenology metrics. Conclusions related to the methodology and to the variability of phenology metrics and underlying causes thereof include:

- Phytoplankton phenology metrics of lakes can be measured and mapped using MERIS and TIMESAT software.
- The Savitzky-Golay filtering approach to data smoothing was found to be superior to both the Double Logistic and Asymmetrical Gaussian approaches, likely as a result of its more local nature which is better adapted to phytoplankton dynamics. Rather than fitting the curve based on broad maxima, minima or inflection features, as in the Gaussian and Logistic approaches, the Savitzky-Golay filter is based on a moving window approach using temporally adjacent values, and therefore more sensitive to rapidly changing dynamics.
- Such an EO approach added a cohesive spatial component to phenology analyses, revealing significant spatial variability of Lake Balaton phenology metrics. A high degree of temporal (inter-annual) variability of all phenology metrics and of bloom spatial extent was also revealed.
- Spatial gradients in phenology metrics paralleling the main, longitudinal axis of Lake Balaton are expected to be associated with nutrient inflow in the southwest basin from the Zala River and a general northeastern water circulation.
- Missing pixels in resulting phenology metric maps are attributed to three causes (1) no bloom occurrence in reality; (2) too many missing values in the input time series, which results in a blank pixel for each year of the time series; and (3) defined bloom conditions not met (rising from below to above the defined threshold and vice versa), resulting in a blank pixel for just that given bloom event.

Experimental UFL measurements conducted in both field and laboratory settings are described in **Chapter 7**, and result in the following conclusions:

- UFL accurately and simultaneously retrieved chl-*a* concentrations, TSM concentrations and CDOM absorbance measured through coinciding conventional laboratory analysis of water samples. This included field measurements in Lake Balaton, and extended concentration ranges through an experimental setup of tank measurements.
- Distinct multispectral fluorescence emission signatures were detected from cultures of chlorophyta species and cultures of cyanobacteria species used in the tank measurements, with mixtures of the two falling between. This was mainly related to the fluorescence peak at 650 nm of the cyanobacteria, related to the fluorescence of its accessory pigment, phycocyanin, as well as to the lower fluorescence at 685 nm per conventionally measured (extraction/spectroscopy) chl-*a* concentration as compared with the chlorophyta species culture. The cultures were therefore found to be clearly distinguished using a 650/685 nm fluorescence ratio.
- The separation of Raman scattering and CDOM-fluorescence at 440 nm from field measurements proved difficult, resulting in a significant, but non-linear relationship with validation *in situ* data.

8.3 Outlook and future research directions

With MERIS no longer actively transmitting data as of April 2012, the launch of the upcoming ESA Sentinel-3A mission with the Ocean and Land Colour Imager (OLCI) sensor aboard is highly anticipated by the lake remote sensing community. OLCI will be characterized by similar spatial and temporal resolutions as MERIS, as well as similar spectral band placement, but with several additional bands in the blue and red/NIR ranges (ESA 2013a, c). This will allow for the continuity and improvement of activities begun using MERIS, including the mapping and monitoring of Lake Balaton phytoplankton. The same FLH algorithm for chl-*a* retrieval will be transferable to OLCI data for Lake Balaton (Figure 8.1), although coefficient tuning and subsequent validation will again be necessary. Also aboard Sentinel-3 will be the Sea and Land Surface Temperature

Radiometer (SLSTR), providing continuity to the ENVISAT (A)ATSR instrument, as well as the SAR altimeter (SRAL), the Doppler Orbitography and Radiopositioning Integrated by Satellite (DORIS) and the Microwave radiometer (MWR), which will provide topographic measurements of ocean and lake water (ESA 2013c). The MultiSpectral Imager (MSI) aboard the anticipated Sentinel-2 mission will also provide opportunities for lake remote sensing. Although its spectral resolution is less well-suited to inland waters as compared with OLCI (Figure 8.1), MSI will be characterized with a finer spatial resolution (from 10 to 60 m) favourable to the inclusion of a greater number of smaller lakes (Figure 8.2). Preparation for the forthcoming Sentinel data is already formally underway by members of the lake remote sensing community who comprise part of the Sentinel-3 Validation Team, including the European Union 7th Framework Programme project, Global Lakes Sentinel Services (GLaSS), which is working on algorithm development, automated processing, and integration of the upcoming data for use in inland waters.

Upon the validation and re-establishment of phytoplankton and other water quality parameter mapping using the Sentinel missions, an important next direction will be the translation of detailed maps, such as those presented in the current thesis, to the language of WFD reporting. Following the first results in this direction, presented in Chapter 4, a more thorough analysis comparing WFD-oriented classification using satellite-based measurements and those from the point, *in situ* data of the KdKVI (currently used in WFD reporting) is recommended, as is an investigation of the spatial variability revealed through satellite remote sensing, over the full MERIS archive time series and in application to Sentinel-3 OLCI data once available. Likewise, the integration of satellite remote sensing into the monitoring programs of the BLI and the KdKVI is foreseen. Several larger, international projects currently underway (GloboLakes - http://www.globolakes.ac.uk/; ESA Diversity-2 - http://www.diversity2.info/; ChoroGIN - http://www.chlorogin.org/) will provide additional satellite products for many lakes throughout the world, including Balaton, and as such are expected to promote a greater use and value of remote sensing by local stakeholders.

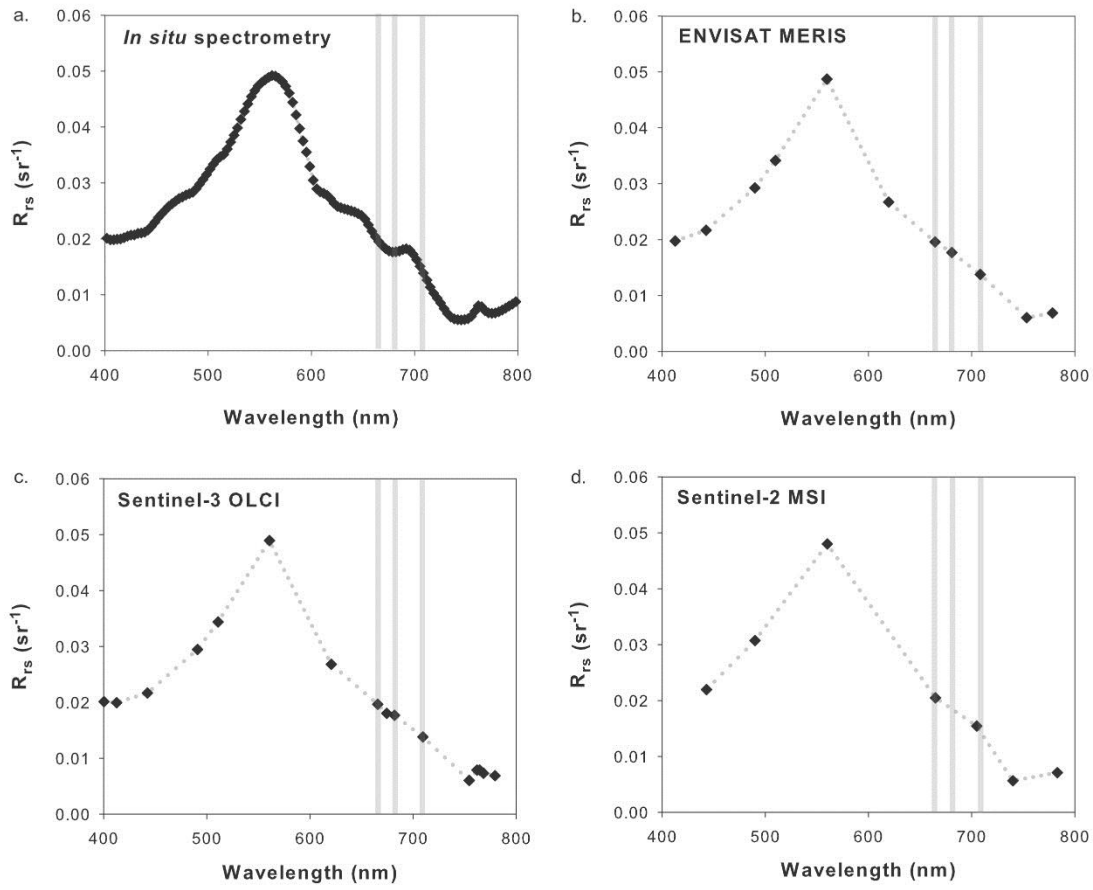

Figure 8.1. Hyperspectral Remote Sensing reflectance spectra (5 nm spectral resolution) measured in Lake Balaton (a), resampled to the spectral bands of ENVISAT MERIS (b), Sentinel-3 Ocean and Land Colour Imager bands (c) and Sentinel-2 MultiSpectral Imager (d). MERIS bands 7, 8 and 9, used for FLH chl-*a* concentration retrieval, are highlighted to compare band placement of OLCI and MSI.

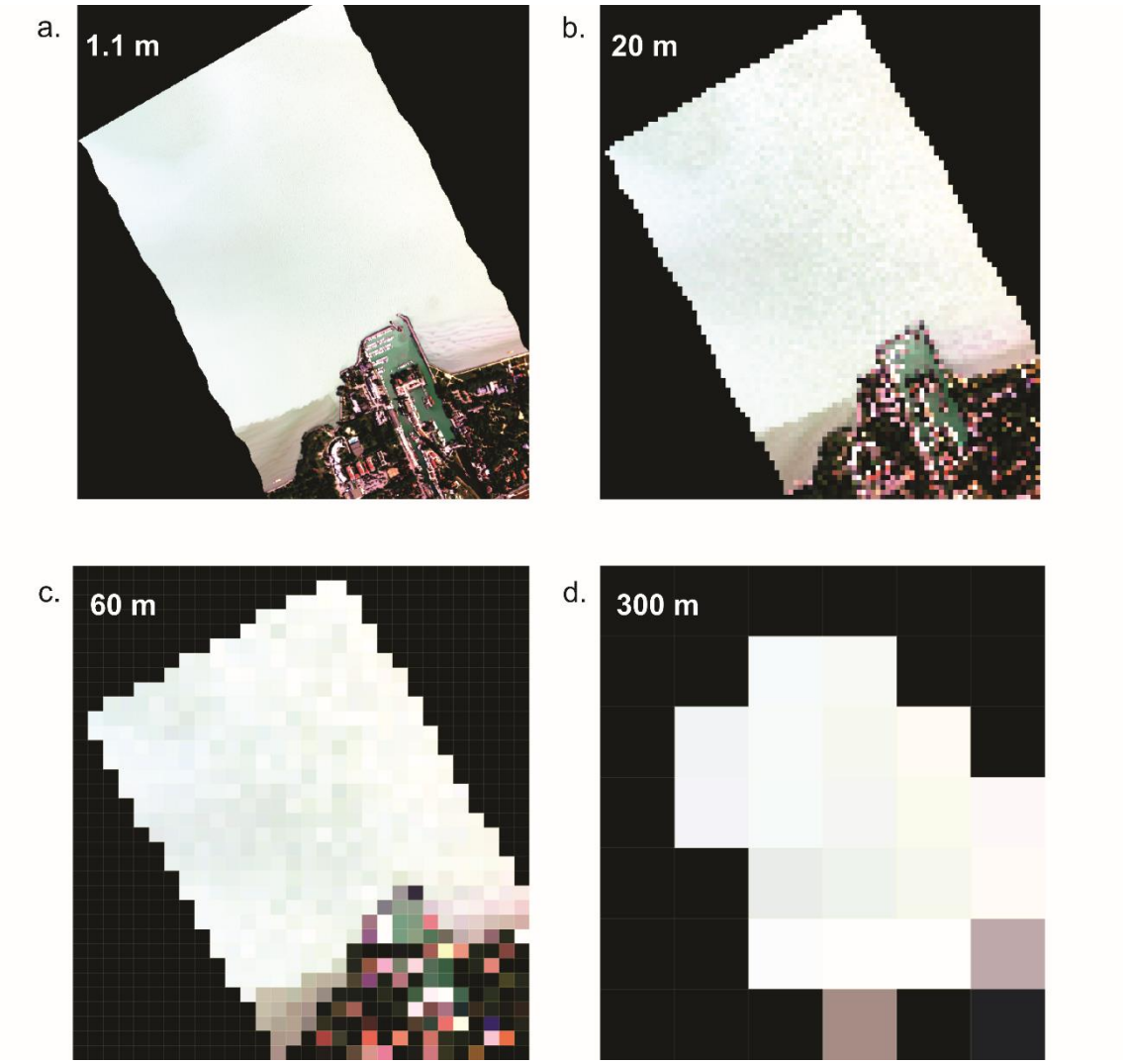

Figure 8.2. AISA airborne hyperspectral imagery (1.1 m spatial resolution) over the southern shoreline of northeastern Lake Balaton (Siofok basin) (a), resampled to the spatial resolutions of Sentinel-2 MultiSpectral Imager (b, c) and MERIS and Sentinel-3 Ocean and Land Colour Imager bands (d).

Several future and priority research directions have been revealed through the phenology analysis and mapping carried out in Chapter 6. In relation to future satellite missions, the extension of phenology mapping using the Sentinel mission sensors should be carried out upon validation of chl-*a* retrieval algorithms and maps to be used as input. Furthermore, current ongoing work by a fellow PhD student (C. Riddick of the University of Stirling) aims to optimize the retrieval of phycocyanin concentrations, indicative of cyanobacteria biomass, for Lake Balaton using MERIS imagery. As cyanobacteria are typically associated with the higher biomass conditions in Lake Balaton and elsewhere, and because of concerns regarding their potential toxicity, the use of phycocyanin maps as input into time series phenology mapping would be of high interest to the research and lake/reservoir water management communities. This should be considered with future Sentinel data as well as with archive MERIS data. Application of the methodology presented here to additional lakes, as well as inter-lake comparisons of both general phytoplankton biomass (via mapped chl-*a* concentrations) and cyanobacteria biomass (via phycocyanin concentration) would be of great interest. However, a careful examination of the definition of bloom events and the fine-tuning of other methodological aspects will be crucial, especially when moving beyond site-specific analysis, and should be the subject of ongoing work. For example, the thresholds used to define bloom events in the current work are likely not be appropriate for other lakes where background and/or bloom concentration levels may be much higher or lower than the concentrations characteristic of Lake Balaton. The results presented in Chapter 6 pointed to the main location of nutrient influx in the southwestern basin and the general water circulation pattern as underlying the spatial patterns apparent in the phenology metric mapping. Phenology metrics have been found elsewhere to also be sensitive to climate forcing and to meteorological conditions, especially temperature and light availability. Ongoing work intends to closely examine both climate and nutrient drivers of mapped phenology variability at Balaton and other sites.

In terms of potential new directions making use of UFL in inland water bodies, four main directions are clear from the current work. One is to undertake measurements at additional lake sites, particularly those characterized by vastly different conditions from those encountered at Balaton. This includes waters characterized by both extremely high and extremely low TSM. The latter would assess the interference by bottom signal in very clear ("optically shallow") waters, however it should be noted that in the

laboratory tank measurements with TSM < 1 g m^{-3}, no such signal was detected at a depth of only 1 m. The CDOM-rich, boreal-type lakes of Sweden, Finland and Estonia would also be ideal candidates, as CDOM concentrations are typically low and with relatively little variability in Balaton and they would therefore provide a great contrast. Highly eutrophic waters, such as documented in several Spanish reservoirs (Domínguez Gómez et al. 2011; Ruiz-Verdú et al. 2008a; Ruiz-Verdú et al. 2008b) and the Canadian/American Lake of the Woods (Binding et al. 2010) would be of similar interest so as to extend the *in situ* chl-*a* conditions encountered at Balaton. Lakes presenting the potential for cyanobacteria bloom mapping would be of particular interest, so as to further test the differentiation between cyanobacteria and non-cyanobacteria species, found possible here through laboratory UFL measurements. Both future laboratory and field measurements should explicitly consider the detection and quantification of cyanobacteria and other taxa by complementing UFL measurements with validation measurements of various accessory pigments, especially phycocyanin in the case of cyanobacteria. The use of calibrated and validated UFL measurements as abundant *in situ* validation for Sentinel and other satellite sensors could also be considered. However, for the resulting algorithm to be robust over time as well as space, and thus to allow its reliable application to other images from those coinciding with ULF measurements, UFL data would need to be available from multiple dates coinciding with satellite overpass, including across seasons and spanning bloom and non-bloom events in particular. This is foreseen to be hindered by the highly specialized nature of the UFL and its operation, however, precluding regular measurement campaigns at Balaton throughout the year.

Bibliography

Abramov, O., Eremin, V., Karlsen, G., Lobov, L., & Polovinko, V. (1977). Application of laser ranging to determine the pollution of sea surface by oil products. *Atmospheric and Oceanic Physics, 13*, 331-334

Adrian, R., O'Reilly, C.M., Zagarese, H., Baines, S.B., Hessen, D.O., Keller, W., Livingstone, D.M., Summaruga, R., Straile, D., Van Donk, E., Weyhenmeyer, G.A., & Winder, M. (2009). Lakes as sentinels of climate change. *Limnology and Oceanography, 54*, 2283-2297

Adrian, R., Wilhelm, S., & Gerten, D. (2006). Life-history traits of lake plankton species may govern their phenological response to climate warming. *Global Change Biology, 12*, 652-661

Aguirre-Gómez, R., Boxall, S.R., & Weeks, A.R. (2001a). Detecting photosynthetic algal pigments in natural populations using a high-spectral-resolution radiometer. *International Journal of Remote Sensing, 22*, 2867-2884

Aguirre-Gómez, R., Weeks, A.R., & Boxall, S.R. (2001b). The identification of phytoplankton pigments from absorption spectra. *International Journal of Remote Sensing, 22*, 315-338

Aibulatov, N., Zavialov, P., & Pelevin, V. (2008). Features of hydrophysical purification Russian Black Sea coastal area near the mouths of rivers. *Geoecology, 4*, 301-310

Albert, A., & Mobley, C.D. (2003). An analytical model for subsurface irradiance andremote sensing reflectance in deep and shallowcase-2 waters. *Optics Express, 11*, 283-2890

Alikas, K., & Reinart, A. (2008). Validation of the MERIS products on the large European lakes: Peipsi, Vänern and Vättern. *Hydrobiologia, 599*, 161−168

Anttila, S., Kairesalo, T., & Pellikka, P. (2008). A feasible method to assess inaccuracy caused by patchiness in water quality monitoring. *Environmental Monitoring & Assessment, 142*, 11-22

Babichenko, S. (2008). Laser remote sensing of the European marine environment: LIF technology and applications. V Barale, M Gade (eds.). *Remote sensing of the European Seas*

Babichenko, S., Dudelzak, A., Lapimaa, J., Lisin, A., Poryvkina, L., & Vorobiev, A. (2006). Locating water pollution and shore dischares in coastal zone and inland waters with FLS lidar. In

Babichenko, S., Dudelzak, A., & Poryvkina, L. (2004). Laser remote sensing of coastal and terrestrial pollution by FLS-LIDAR. In (pp. 1-7): EARSeL eProdeedings

Barbini, R., Colao, F., Fantoni, R., Ferrari, G.M., Lai, A., & Palucci, A. (2003). Application of a lidarfluorosensor system to the continuous monitoring of the Southern Ocean and Antarctic Ross Sea: Results collected during the XIII and XV Italian oceanographic campaigns. *International Journal of Remote Sensing, 24*, 3191-3204

Barbini, R., Colao, F., Fantoni, R., Fiorani, L., & Palucci, A. (2001). Remote sensing of the southern ocean: techniques and results. *Journal of Optoelectronics and Advanced Materials, 3*, 817-830

Barbini, R., Colao, F., Fantoni, R., Micheli, A., Palucci, A., & Ribezzo, S. (1998). Design and application of a lidar fluorosensor system for remote monitoring of phytoplankton. *ICES Journal of Marine Science, 55*, 793-802

Barbini, R., Colao, F., Fantoni, R., Palucci, A., & Ribezzo, S. (1999). Shipborne laser remote sensing of the Venice lagoon. *International Journal of Remote Sensing, 20*, 2405-2421

Barth, H., Reuter, R., & Schröder, M. (2000). Measurement and simulation of substance specific contributions of phytoplankton, gelbstoff, and mineral particles to the underwater light field in coastal waters. *EARSeL eProceedings, 1*, 165-174

Bastviken, D., Tranvik, L.J., Downing, J.A., Crill, P.M., & Enrich-Prast, A. (2011). Freshwater methane emissions offset the continental carbon sink. *Science, 331*, 50-50

Bates, B., Kundzewicz, Z.W., Wu, S., & Palutikof, J. (2008). . Intergovernmental Panel on Climate Change *Climate change and water*

Beeton, A.M. (2002). Large freshwater lakes: present state, trends, and future. *Environmental Conservation, 29*, 21-38

Berger, S.A., Diehl, S., Stibor, H., Trommer, G., & Ruhenstroth, M. (2010a). Water temperature and stratification depth independently shift cardinal events during plankton spring succession. *Global Change Biology, 16*, 1954-1695

Berger, S.A., Diehl, S., Stibor, H., Trommer, G., & Ruhenstroth, M. (2010b). Water temperature and stratification depth independently shift cardinal events during plankton spring succession. *Global Change Biology, 16*, 1954-1965

Beutler, M., Wiltshire, K., Meyer, B., Moldaenke, C., Lüring, C., Meyerhöfer, M., Hansen, U., & Dau, H. (2002). A fluorometric method for the differentiation of algal populations in vivo and in situ. *Photosynthetic Research, 72*, 39-53

Beutler, M., Wiltshire, K.H., Arp, M., Kruse, J., Reineke, C., Moldaenke, C., & Hansen, U.-P. (2003). A reduced model of the fluorescence from the cyanobacterial photosynthetic apparatus designed for the in situ detection of cyanobacteria. *Biochimica et Biophysica Acta (BBA)-Bioenergetics, 1604*, 33-46

Bicheron, P., Amberg, V., Bourg, L., Petit, D., Huc, M., Miras, B., Brockmann, C., Delwart, S., Ranéra, F., Hagolle, O., Leroy, M., & Arino, O. (2008). Geolocation assessment of 300 m resolution MERIS Globcover ortho- rectified products. In, *2nd MERIS / (A)ATSR User Workshop*. Frascati, Italy: ESA

Binding, C., Greenberg, T., & Bukata, R. (2013). The MERIS maximum chlorophyll index; its merits and limitations for inland water algal bloom monitoring. *Journal of Great Lakes Research, 39*, 100-107

Binding, C., Greenberg, T., Jerome, J., Bukata, R., & Letourneau, G. (2010). An assessment of MERIS algal products during an intense bloom in Lake of the Woods. *Journal of Plankton Research*, fbq133

Binding, C.E., Greenberg, T.A., & Bukata, R.P. (2011). Time series analysis of algal blooms in Lake of the Woods using the MERIS maximum chlorophyll index. *Journal of Plankton Research, 33*, 1847-1852

Binding, C.E., Greenberg, T.A., Bukata, R.P., Smith, D.E., & Twiss, M.R. (2012). The MERIS MCI and its potential for satellite detection of winter diatom blooms on partially ice-covered Lake Erie. *Journal of Plankton Research*, fbs021

Binding, C.E., Jerome, J.H., Bukata, R.P., & Booty, W.G. (2007). Trends in water clarity of the lower Great Lakes from remotely sensed aquatic color. *Journal of Great Lakes Research, 33*, 828-841

Blenckner, T., Adrian, R., Livingstone, D.M., Jennings, E., Weyhenmeyer, G.A., George, D., Jankowski, T., Järvinen, M., Aonghusa, C.N., & Noges, T. (2007). Large-scale climatic signatures in lakes across Europe: a meta-analysis. *Global Change Biology, 13*, 1314-1326

Bourg, L., D'Alba, L., & Colagrande, P. (2008). MERIS SMILE effect characterisation and correction. *ESA Technical Note, 4921*, 25

Boyd, D.S., Almond, S., Dash, J., Curran, P.J., & Hill, R.A. (2011). Phenology of vegetation in Southern England from Envisat MERIS terrestrial chlorophyll index (MTCI) data. *International Journal of Remote Sensing, 32*, 8421-8447

Brando, V. (2008). c-WOMBAT-c user manual v0. Environmental Remote Sensing Group

Brando, V.E., & Dekker, A.G. (2003). Satellite hyperspectral remote sensing for estimating estuarine and coastal water quality. *IEEE Transactions on Geoscience and Remote Sensing 41*, 1378-1387

Braun, C.L., & Smirnov, S.N. (1993). Why is water blue? *Journal of chemical education, 70*, 612-614

Bresciani, M., Bolpagni, R., Laini, A., Matta, E., Bartoli, M., & Giardino, C. (2013). Multitemporal analysis of algal blooms with MERIS images in a deep meromictic lake. *European Journal of Remote Sensing, 46*, 445-458

Bresciani, M., & Giardini, C. (2011). EuLakes: Water quality of the CE lakes by remote Sensing technique. In, *Project EULAKES*

Bresciani, M., Stroppiana, D., Odermatt, D., Morabito, G., & Giardino, C. (2011). Assessing remotely sensed chlorophyll-a for the implementation of the Water Framework Directive in European perialpine lakes. *Science of the Total Environment, 409*, 3083-3091

Brezonik, P., Menken, K.D., & Bauer, M. (2005). Landsat-based remote sensing of lake water quality characteristics, including chlorophyll and colored dissolved organic matter (CDOM). *Lake and Reservoir Management, 21,* 487-502

Bricaud, A., Morel, A., Babin, M., Allali, K., & Claustre, J. (1998). Variations of light absorption by suspended particles with chlorophyll a concentration in oceanic (case 1) waters: Analysis and implications for bio-optical models. *Journal of Geophysical Research, 103,* 31,033-031,044

Bristow, M., Bundy, D., Edmonds, C., Ponto, P., Frey, B., & Small, L. (1985). Airborne laser fluorosensor survey of the Columbia and Snake rivers: simultaneous measurements of chlorophyll, dissolved organics and optical attenuation. *International Journal of Remote Sensing, 6,* 1707-1734

Brivio, P.A., Giardino, C., & Zilioli, E. (2001). Calibration and validation of satellite data for quality assurance in lakes monitoring applications. *The Science of the Total Environment 268,* 3-18

Brönmark, C., & Hansson, L.-A. (2002). Environmental issues in lakes and ponds: current state and perspectives. *Environmental Conservation, 29,* 209-306

Bryant, D. (1986). The cyanobacterial photosynthetic apparatus: comparison to those of higher plants and photosynthetic bacteria. *Can. Bull. Fish. Aquat. Sci, 214,* 423-500

Calbet, A., & Landry, M.R. (2004). Phytoplankton growth, microzooplankton grazing, and carbon cycling in marine systems. *Limnology and Oceanography, 49,* 51-57

Campbell, G., Phinn, S.R., Dekker, A.G., & Brando, V.E. (2011). Remote sensing of water quality in an Australian tropical freshwater impoundment using matrix inversion and MERIS images. *Remote Sensing of Environment, 115,* 2402-2414

Candiani, G., Floricioiu, D., Giardino, C., & Rott, H. (2005). Monitoring water quality of the perialpine Italian Lake Garda through multi-temporal MERIS data. In, *MERIS (A)ASTR Workshop* (p. 1). Frascati, Italy

Carvalho, L., Poikane, S., Solheim, A.L., Phillips, G., Borics, G., Catalan, J., De Hoyos, C., Drakare, S., Dudley, B., & Järvinen, M. (2013). Strength and uncertainty of phytoplankton metrics for assessing eutrophication impacts in lakes. *Hydrobiologia, 704,* 127-140

Chavula, G., Brezonik, P., Thenkabail, P., Johnson, T., & Bauer, M. (2009). Estimating chlorophyll concentration in Lake Malawi from MODIS satellite imagery. *Physics and Chemistry of the Earth 34,* 75-760

Chawira, M., Dube, T., & Gumindoga, W. (2013). Remote sensing based water quality monitoring in Chivero and Manyame lakes of Zimbabwe. *Physics and Chemistry of the Earth, Parts A/B/C, 66,* 38-44

Chen, Q., Zhang, Y., A., E., & Hallikainen, M. (2007). The role of remote sensing technology in the EU water framework directive (WFD). *Environmental & Science Policy, 7,* 267-276

Chubarov, V., & Fadeev, V. (2004). Ecological monitoring in the Caspian Sea (mouth zone of the River Volga) with a shipboard laser spectrometer. In (pp. 316-322): EARSeL eProceedings

Codd, G.A., Morrison, L.F., & Metcalf, J.S. (2005). Cyanobacterial toxins: risk management for health protection. *Toxicology and applied pharmacology, 203*, 264-272

Cole, H., Henson, S., Martin, A., & Yool, A. (2012). Mind the gap: The impact of missing data on the calculation of phytoplankton phenology metrics. *Journal of Geophysical Research: Oceans (1978–2012), 117*

Cushing, D. (1990). Plankton production and year-class strength in fish populations: an update of the match/mismatch hypothesis. *Advances in marine biology, 26*, 249-293

Cuthbert, I.D., & del Giorgio, P. (1992). Toward a standard method of measuring color in freshwater. *Limnology and Oceanography, 37*, 1319-1326

D'ortenzio, F., Antoine, D., Martinez, E., & Ribera d'Alcalà, M. (2012). Phenological changes of oceanic phytoplankton in the 1980s and 2000s as revealed by remotely sensed ocean-color observations. *Global Biogeochemical Cycles, 26*

Dall'Olmo, G., Gitelson, A.A., Rundquist, D.C., Leavitt, B., Barrow, T., & Holz, J.C. (2005). Assessing the potential of SeaWiFS and MODIS for estimating chlorophyll concentration in turbid productive waters using red and near-infrared bands. *Remote Sensing of Environment, 96*, 176-187

Dash, J., Jeganathan, C., & Atkinson, P. (2010). The use of MERIS Terrestrial Chlorophyll Index to study spatio-temporal variation in vegetation phenology over India. *Remote Sensing of Environment, 114*, 1388-1402

Dash, J., Jones, M., & Nightingale, J. (2013). Validating Satellite-Derived Vegetation Phenology Products. *Eos, Transactions American Geophysical Union, 94*, 127-127

Dekker, A., & Peters, S. (1993). The use of the Thematic Mapper for the analysis of eutrophic lakes: a case study in the Netherlands. *International Journal of Remote Sensing, 14*, 799-821

Dekker, A.G., Vos, R., & Peters, S. (2002). Analytical algorithms for lake water TSM estimation for retrospective analyses of TM and SPOT sensor data. *International Journal of Remote Sensing, 23*, 15-35

Diehl, S., Berger, S., Ptacnik, R., & Wild, A. (2002). Phytoplankton, light, and nutrients in a gradient of mixing depths: field experiments. *Ecology, 83*, 399-411

Doerffer, R., & Schiller, H. (2007). The MERIS Case 2 water algorithm. *International Journal of Remote Sensing, 28*, 517-535

Doerffer, R., & Schiller, H. (2008). MERIS lake water algorithm for BEAM ATBD. *GKSS Research Center, Geesthacht, Germany*

Domínguez Gómez, J.A., Alonso Alonso, C., & Alonso Garcia, A. (2011). Remote sensing as a tool for monitoring water quality for Mediterranean Lakes of European

Union water framework directive (WFD) and as a system of surveillance of cyanobacterial harmful algae blooms (SCyanoHABs). *Environmental Monitoring and Assessment, 181*, 317-334

Dömötörfy, Z., Reeder, D., & Pomogyi, P. (2003). Changes in the macro-vegetation of the Kis-Balaton Wetlands over the last two centuries: a GIS perspective. *Hydrobiologia*

Doxaran, D., Froidefond, J.M., Castaing, P., & Babin, M. (2009). Dynamics of the turbidity maximum zone in a macrotidal estuary (the Gironde, France): observations from field and MODIS satellite data. *Estuarine, Coastal and Shelf Science, 81*, 321-332

Duan, H., Ma, R., Zhang, Y., & Loiselle, S.A. (2014). Are algal blooms occurring later in Lake Taihu? Climate local effects outcompete mitigation prevention. *Journal of Plankton Research, 36*, 866-871

Dudgeon, D., Arthington, A.H., Gessner, M.O., Kawabata, Z.I., Knowler, D.J., Lévêque, C., Naiman, R.J., Prieur-Richard, A.H., Soto, D., Stiassny, M.L.J., & Sullivan, C.A. (2006). Freshwater biodiversity: importance, threats, status and conservation challenges. *Biological Reviews 81*, 163-182

Duker, L., & Borre, L. (2001). Biodiversity conservation of the world's lakes: A preliminary framework for identifying priorities. In, *LakeNet Report Series*: Annapolis, Maryland USA

Dworak, T., Gonzalez, C., Laaser, C., & Interwies, E. (2005a). The need for new monitoring tools to implement the WFD. *Environmental & Science Policy 8*, 301-306

Dworak, T., Laaser, C., Kuntz, S., & Seifert, F.M. (2005b). Possible contributions of ESA Global Monitoring for Environment and Security initiative for the WFD implementation. *Environmental & Science Policy, 8*, 321-326

Eklundh, L., & Jönsson, P. (2012). TIMESAT 3.1 software manual. *Lund University, Sweden*

Eleveld, M.A. (2012). Wind-induced resuspension in a shallow lake from Medium Resolution Imaging Spectrometer (MERIS) full-resolution reflectances. *Water Resources Research, 48*

Elliott, J.A. (2012). Predicting the impact of changing nutrient load and temperature on the phytoplankton of England's largest lake, Windermere. *Freshwater Biology, 57*, 400-413

Elliott, J.A., Jones, I.D., & Thackeray, S.J. (2006). Testing the sensitivity of phytoplankton communities to changes in water temperature and nutrient load, in a temperate lake. *Hydrobiologia, 559*, 401-411

Erlandsson, M., Folster, J., Laudon, H., Weyhenmeyer, G.A., & Bishop, K. (2008). Natural variability in lake pH on seasonal, interannual and decadal time scales: Implications for assessment of human impact. *Environmental Science & Technology 42*, 5594-5599

ESA (2013a). MERIS design. In. https://earth.esa.int/web/guest/missions/esa-operational-eo-missions/envisat/instruments/meris/design: ESA Earthnet Online

ESA (2013b). Sentinel 2. In. https://earth.esa.int/web/guest/missions/esa-future-missions/sentinel-2: ESA Earthnet Online

ESA (2013c). Sentinel 3. In. https://earth.esa.int/web/guest/missions/esa-future-missions/sentinel-3: ESA Earthnet Online

Farmer, F., Brown, C.J., Jarrett, O., Campbell, J., & Staton, W. (1979). Remote Sensing of Phytoplankton Density and Diversity in Narragansett Bay Using an Airborne Fluorosensor. In, *13th International Symposium for Remote Sensing of Environment*. Ann Arbor, MI, USA

Feuchtmayr, H., Thackeray, S.J., Jones, I.D., de Ville, M., Fletcher, J., James, B., & Kelly, J. (2012). Spring phytoplankton phenology – are patterns and drivers of change consistent among lakes in the same climatological region. *Freshwater Biology, 57*, 331-344

Fiorani, L., Barbini, R., Colao, F., De Dominicis, L., Fantoni, R., Palucci, A., & Artamonov, E. (2004). Combination of lidar, MODIS and SeaWiFS sensors for simultaneous chlorophyll monitoring. In (pp. 8-17): EARSeL eProceedings

Fomferra, N., Bottcher, M., Zuhlke, M., Brockmann, C., & Kwiatkowska, E. (2012). Calvalus: Full-mission EO cal/val, processing and exploitation services. In, *Geoscience and Remote Sensing Symposium (IGARSS), 2012 IEEE International* (pp. 5278-5281): IEEE

Fomferra, N., & Brockmann, C. (2005). Beam-the ENVISAT MERIS and AATSR toolbox. In, *MERIS (A) ATSR Workshop 2005* (p. 13)

Forrest, J., & Miller-Rushing, A.J. (2010). Toward a synthetic understanding of the role of phenology in ecology and evolution. *Philosophical Transactions of the Royal Society B: Biological Sciences, 365*, 3101-3112

Gaedke, U., Ruhenstroth-Bauer, M., Wiegand, I., Tirok, K., Aberle, N., Breithaupt, P., Lengfellner, K., Wohlers, J., & Sommer, U. (2010). Biotic interactions may overrule direct climate effects on spring phytoplankton dynamics. Global Change Biology. *Global Change Biology, 16*, 1122-1136

Ganguly, S., Friedl, M.A., Tan, B., Zhang, X., & Verma, M. (2010). Land surface phenology from MODIS: Characterization of the Collection 5 global land cover dynamics product. *Remote Sensing of Environment, 114*, 1805-1816

Gerten, D., & Adrian, R. (2000). Climate-driven changes in spring plankton dynamics and the sensitivity of shallow polymictic lakes to the North Atlantic Oscillation. *Limnology and Oceanography, 45*, 1058-1066

Giardino, C., Bresciani, M., Villa, P., & Martinelli, A. (2010). Application of remote sensing in water resource management: the case study of Lake Trasimeno, Italy. *Water resources management, 24*, 3885-3899

Giardino, C., Candiani, G., Bresciani, M., Lee, Z., Gagliano, S., & Pepe, M. (2011). A tool for estimating water quality and bottom properties from remote sensing images. *Computers & Geosciences*

Giardino, C., Candiani, G., & Zilioli, E. (2005). Detecting chlorophyll-a in Lake Garda using TOA Meris radiances. *Photogrammetric Engineering and Remote Sensing, 71*, 1045-1051

Gitelson, A., Garbuzov, G., Szilagyi, F., Mittenzwey, K., Karnieli, A., & Kaiser, A. (1993). Quantitative remote sensing methods for real-time monitoring of inland waters quality. *International Journal of Remote Sensing, 14*, 1269-1295

Glasgow, H.B., Burkholder, G.M., Reed, R.E., Lewitus, A.J., & Kleinman, J.E. (2004). Real-time remote monitoring of water quality: a review of current applications,and advancements in sensor, telemetry, and computing technologies. *Journal of Experimental Marine Biology and Ecology, 300*, 409-448

Gons, H.J., Auer, M.T., & Effler, S.W. (2008). MERIS satellite chlorophyll mapping of oligotrophic and eutrophic waters in the Laurentian Great Lakes. *Remote Sensing of Environment, 24*, 4098-4106

González Taboada, F., & Anadón, R. (2014). Seasonality of North Atlantic phytoplankton from space: impact of environmental forcing on a changing phenology (1998–2012). *Global Change Biology, 20*, 698-712

Gordon, H.R. (1997). Atmospheric correction of ocean color imagery in the Earth Observing System era. *Journal of Geophysical Research: Atmospheres (1984–2012), 102*, 17081-17106

Gordon, H.R. (2010). *Some reflections on Thirty-five yearsof Ocean Color Remote Sensing*.

Gordon, H.R., Brown, O.B., & Jacobs, M.M. (1975). Computed relationships between the inherent and apparent optical properties of a flat homogeneous ocean. *Applied Optics, 14*, 417-427

Gordon, H.R., & Clark, D.K. (1981). Clear water radiances for atmospheric correction of coastal zone color scanner imagery. *Applied Optics, 20*, 4175-4180

Gordon, H.R., & Morel, A.Y. (1983). Remote Assessment of Ocean Color for Interpretation of Satellite Visible Imagery: A review. *American Geophysical Union, 4*, 1-114

Gordon, H.R., & Wang, M. (1994). Retrieval of water-leaving radiance and aerosol optical thickness over the oceans with SeaWiFS: a preliminary algorithm. *Applied Optics, 33*, 443-452

Gower, J.F.R., Brown, L., & Borstad, G.A. (2004). Observation of chlorophyll fluorescence in west coast waters of Canada using the MODIS satellite sensor. *Canadian Journal of Remote Sensing, 30*, 17-25

Gower, J.F.R., Doerffer, R.B., & Borstad, G.A. (1999). Interpretation of the 685 nm peak in water-leaving radiance spectra in terms of fluorescence, absorption and

scattering, and its observation by MERIS. *International Journal of Remote Sensing, 20*, 1771-1786

Gower, J.F.R., King, S., Borstad, G.A., & Brown, L. (2005). Detection of intense plankton blooms using the 709 nm band of the MERIS imaging spectrometer. *International Journal of Remote Sensing, 26*, 2005-20012

Gregor, J., & Maršálek, B. (2005). A simple in vivo fluorescence method for the selective detection and quantification of freshwater cyanobacteria and eukaryotic algae. *Acta hydrochimica et hydrobiologica, 33*, 142-148

Guanter, L., Del Carmen González-Sanpedro, M., & Moreno, J. (2007). A method for the atmospheric correction of ENVISAT/MERIS data over land targets. *International Journal of Remote Sensing, 28*, 709-728

Guanter, L., Gómez-Chova, L., & Moreno, J. (2008). Coupled retrieval of aerosol optical thickness, columnar water vapor and surface reflectance maps from ENVISAT/MERIS data over land. *Remote Sensing of Environment, 112*, 2898-2913

Guanter, L., Ruiz-Verdú, A., Odermatt, D., Giardino, C., Simis, S., Estellés, V., Heege, T., Domínguez-Gómez, J.A., & Moreno, J. (2010). Atmospheric correction of ENVISAT/MERIS data over inland waters: Validation for European lakes. *Remote Sensing of Environment, 114*, 467-480

Hajnal, E., & Padisák, J. (2008). Analysis of long-term ecological status of Lake Balaton based on the ALMOBAL phytoplankton database. *Hydrobiologia, 599*, 227-237

Hatvani, I.G., Kovács, J., Székely Kovács, I., Jakusch, P., & Korponai, J. (2011). Analysis of long-term water quality changes in the Kis-Balaton Water Protection System with time series-, cluster analysis and Wilks' lambda distribution. *Ecological Engineering 37*, 629-635

Havens, K.E., Beaver, J.R., Casamatta, D.A., East, T.L., James, R.T., McCormick, P., Philips, E.J., & Rodusky, A.J. (2011). Hurricane effects on the planktonic food web of a large subtropical lake. *Journal of Plankton Research, 33*, 1081-1094

Hays, G.C., Richardson, A.J., & Robinson, C. (2005). Climate change and marine plankton. *Trends in Ecology and Evolution 20*, 337-344

Heim, B., Oberhaensli, H., Fietz, S., & Kaufmann, H. (2005). Variation in Lake Baikal's phytoplankton distribution and fluvial input assessed by SeaWiFS satellite data. *Global and Planetary Change, 46*, 9-27

Hering, D., Borja, A., Carvalho, L., & Feld, C.K. (2013). Assessment and recovery of European water bodies: key messages from the WISER project. *Hydrobiologia, 704*, 1-9

Herodek, S., Lackó, L., & Virág, Á. (1988). Lake Balaton research and management

Heumann, B.W., Seaquist, J., Eklundh, L., & Jönsson, P. (2007). AVHRR derived phenological change in the Sahel and Soudan, Africa, 1982–2005. *Remote Sensing of Environment, 108*, 385-392

Hoge, F.E., Lyon, P.E., Swift, R.N., Yungel, J.K., Abbott, M.R., Letelier, R.M., & Esais, W.E. (2003). Validation of Terra-MODIS phytoplankton chlorophyll fluorescence line height. I. Initial airborne lidar results. *Applied Optics, 42*, 2767-2771

Hoge, F.E., & Swift, R.N. (1981). Airborne simultaneous spectroscopic detection of laser-induced water Raman backscatter and fluorescence from chlorophyll a and other naturally occurring pigments. *Applied Optics, 20*, 3197-3205

Horváth, H., Mátyás, K., Süle, G., & Présing, M. (2013). Contribution of nitrogen fixation to the external nitrogen load in of a water quality control reservoir (Kis-Balaton Water Protection System, Hungary). In

Hu, C., Carder, K.L., & Muller-Karger, F.E. (2000). Atmospheric correction of SeaWiFS imagery over turbid coastal waters: a practical method. *Remote Sensing of Environment, 74*, 195-206

Hu, C., Chen, Z., Clayton, T.D., Swarzenski, P., Brock, J.C., & Muller-Karger, F.E. (2004). Assessment of estuarine water-quality indicators using MODIS medium-resolution bands: Initial results from Tampa Bay, FL. *Remote Sensing of Environment, 93*, 423-441

Hu, C., Lee, Z., Ma, R., Yu, K., Li, D., & Shang, S. (2010). Moderate resolution imaging spectroradiometer (MODIS) observations of cyanobacteria blooms in Taihu Lake, China. *Journal of Geophysical Research: Oceans (1978–2012), 115*

Hunter, P.D., Tyler, A.N., Carvalho, L., Codd, G.A., & Maberly, S.C. (2010). Hyperspectral remote sensing of cyanobacterial pigments as indicators for cell populations and toxins in eutrophic lakes. *Remote Sensing of Environment, 114*, 2705-2718

Hunter, P.D., Tyler, A.N., Présing, M., Kovács, M.W., & Preston, T. (2008a). Spectral discrimination of phytoplankton colour groups: The effect of suspended particulate matter and sensorspectral resolution. *Remote Sensing of Environment, 112*, 1527-1544

Hunter, P.D., Tyler, A.N., Willby, N.J., & Gilvear, D.J. (2008b). The spatial dynamics of vertical migration by Microcystisaeruginosain a eutrophic shallow lake: A case study using high spatial resolution time-series airborne remote sensing. *Limnology and Oceanography, 53*, 2391-2406

IOCCG (2000). Remote Sensing of Ocean Colour in Coastal, and Other Optically-Complex, Waters. In S. Sathyendranath (Ed.), *Reports of the International Ocean-Colour Coordinating Group*. Dartmouth, Canada: IOCCG

IOCCG (2006). Remote sensing of inherent optical properties: Fundamentals, tests of algorithms, and applications. In Z. Lee (Ed.), *Reports of the International Ocean-Colour Coordinating Group*. Dartmouth, Canada: IOCCG

Istvánovics, V. (2010). Eutrophication of Lakes and Reservoirs. *Plankton of Inland Waters*

Istvánovics, V., Clement, A., Somlyódy, L., Specziár, A., Tóth, L.G., & Padisák, J. (2007). Updating water quality targets for shallow Lake Balaton, Hungary, recovering from eutrophication. *Hydrobiologia, 581*, 301-318

Istvánovics, V., Somlyódy, L., & Clement, A. (2002). Cyanobacteria-mediated internal eutrophication in shallow Lake Balaton after load reduction. *water research, 36*, 3314-3322

Iwamura, T., Nagai, H., & Ishimura, S. (1970). Improved methods for determining the contents of chlorophyll, protein, ribonucleic and deoxyribonucleic acid in planktonic populations. *Internationale Revue der gesamten Hyrdobiologie, 55*, 131-147

Jaelani, L.M., Matsushita, B., Yang, W., & Fukushima, T. (2013). Evaluation of four MERIS atmospheric correction algorithms in Lake Kasumigaura, Japan. *International Journal of Remote Sensing, 34*, 8967-8985

James, R.T., Havens, K., Zhu, G., & Qin, B. (2009). Comparative analysis of nutrients, chlorophyll and transparency in two large shallow lakes (Lake Taihu, P.R. China and Lake Okeechobee, USA). *Hydrobiologia, 627*, 211-231

Johnsen, G., & Sakshaug, E. (1996). Light harvesting in bloom-forming marine phytoplankton: species-specificity and photoacclimation. *Scientia Marina, 60*, 47-56

Johnsen, G., & Sakshaug, E. (2007). Biooptical characteristics of PSII and PSI in 33 species (13 pigment groups) of marine phytoplankton, and the relevance for pulse-amplitude-modulated and fast-repetition-rate fluorometry1. *Journal of Phycology, 43*, 1236-1251

Johnson, N., Revenga, C., & Echeverria, J. (2001). Managing water for people and nature. *Science, 292*, 1071-1072

Jones, I.D., Page, T., Elliott, J.A., Thackeray, S.J., & Heathwaite, A.L. (2011). Increases in lake phytoplankton biomass caused by future climate-driven changes to seasonal river flow. *Global Change Biology, 17*, 1809-1820

Jönsson, P., & Eklundh, L. (2004). TIMESAT—a program for analyzing time-series of satellite sensor data. *Computers & Geosciences, 30*, 833-845

Justice, C.O., Townshend, J., Holben, B., & Tucker, e.C. (1985). Analysis of the phenology of global vegetation using meteorological satellite data. *International Journal of Remote Sensing, 6*, 1271-1318

Kahru, M., Brotas, V., Manzano-Sarabia, M., & Mitchell, B. (2011). Are phytoplankton blooms occurring earlier in the Arctic? *Global Change Biology, 17*, 1733-1739

Kallio, K., Kutser, T., Hannonen, T., Koponen, S., Pulliainen, J., Vepsalainen, J., & Pyhalahti, T. (2001). Retrieval of water quality from airborne imaging spectrometry of various lake types in different seasons. *The Science of the Total Environment, 268*, 59-77

Kaufman, Y.J., & Joseph, J.H. (1982). Determination of surface albedos and aerosol extinction characteristics from satellite imagery. *Journal of Geophysical Research, 87*, 1287-1299

Kay, J.E., Kampf, S.K., Handcock, R.N., Cherkauer, K.A., Gillespie, A.R., & Burges, S.J. (2005). Accuracy of lake and stream temperatures determined from

atmospherically corrected thermal-infrared imagery. *Journal of the American Water Resource Association 41*, 1161-1175

Khan, F.A., & Ansari, A.A. (2005). Eutrophication: An ecological vision. *The Botanical Review 71*, 449-482

Kirk, J.T. (1994). Estimation of the absorption and the scattering coefficients of natural waters by use of underwater irradiance measurements. *Applied Optics, 33*, 3276-3278

Knaeps, E., Dogliotti, A., Raymaekers, D., Ruddick, K., & Sterckx, S. (2012). < i> In situ</i> evidence of non-zero reflectance in the OLCI 1020nm band for a turbid estuary. *Remote Sensing of Environment, 120*, 133-144

Koponen, S., Ruiz Verdu, A., Heege, T., Heblinski, J., Sorensen, K., Kallio, K., Pyhälahti, T., Doerffer, R., C., B., & Peters, M. (2008). Development of MERIS lake water algorithms: Validation report. In. Helsinki, Finland: Helsinki University of Technology

Kopova, L.I., Konovalov, B.V., Pelevin, V.V., & Khlebnikov, D.V. (2010). Variations in a set of optical and hydrologic parameters of the Atlantic surface waters. *Izvestiya, Atmospheric and Oceanic Physics, 46*, 192-207

Korponai, J., Braun, M., Buczkó, K., Gyulai, I., Forró, L., Nédli, J., & Papp, I. (2010). Transition from shallow lake to a wetland: a multi-proxy case study in Zalavári Pond, Lake Balaton, Hungary. *Hydrobiologia, 641*, 225-244

Kutser, T., Pierson, D.C., Kallio, K.Y., Reinart, A., & Sobek, S. (2005). Mapping lake CDOM by satellite remote sensing. *Remote Sensing of Environment, 94*, 535-540

Kutser, T., Verpoorter, C., Paavel, B., & Tranvik, L.J. (2014). Estimating lake carbon fractions from remote sensing data. *Remote Sensing of Environment*

Landres, P.B., Morgan, P., & Swanson, F.J. (1999). Overview of the use of natural variability concepts in managing ecological systems. *Ecological applications, 9*, 1179-1188

Lankester, T., Dash, J., Baret, F., & Hubbard, S. (2010). Introduction of the PHenologyAnd Vegetation Earth Observation Service (PHAVEOS). In, *Remote Sensing and the Carbon Cycle*. Burlington House, London

LBDCA, L.B.D.C.A. (2005). Lake Balaton Region. In, *10th International Living Lakes*

Lee, Z., Carder, K.L., & Arnone, R.A. (2002). Deriving inherent optical properties from water color: a multiband quasi-analytical algorithm for optically deep waters. *Applied Optics, 41*, 5755-5772

Lee, Z., Carder, K.L., Hawkes, S.K., Steward, R.G., T.G., P., & Davis, C.O. (1994). Model for interpretation of hyperspectral remote-sensing reflectance. *Applied Optics, 33*, 5721-5732

Lee, Z., Carder, K.L., Mobley, C.D., Steward, R.G., & Patch, J.S. (1999). Hyperspectral remote sensing for shallow waters: 2. Deriving bottom depths and water properties by optimization. *Applied Optics, 38*, 3831-3843

Lewandowska, A., & Sommer, U. (2010). Climate change and the spring bloom: a mesocosm study on the influence of light and temperature on phytoplankton and mesoplankton. *Marine Ecology Progress Series 405*, 101-111

Li, L., Li, L., Shi, K., Li, Z., & Song, K. (2012). A semi-analytical algorithm for remote estimation of phycocyanin in inland waters. *Science of the Total Environment, 435*, 141-150

Li, L., Li, L., & Song, K. (2015). Remote sensing of freshwater cyanobacteria: An extended IOP Inversion Model of Inland Waters (IIMIW) for partitioning absorption coefficient and estimating phycocyanin. *Remote Sensing of Environment, 157*, 9-23

Lodhi, M.A., & Rundquist, D.C. (2001). A spectral analysis of bottom-induced variation in the colour of Sand Hills lakes, Nebraska, USA. *International Journal of Remote Sensing, 229*, 1665-1682

Lovett, G.M., Burns, D.A., Driscoll, C.T., Jenkins, J.C., Mitchell, M.J., Rustad, L., Shanley, J.B., Likens, G.E., & Haeuber, R. (2007). Who needs environmental monitoring? *Frontiers in Ecolology and the Environment 5*, 253-260

Lüdeke, M.K., Ramage, P.H., & Kohlmaier, G. (1996). The use of satellite NDVI data for the validation of global vegetation phenology models: application to the Frankfurt Biosphere Model. *Ecological Modelling, 91*, 255-270

Lunetta, R.S., Schaeffer, B.A., Stumpf, R.P., Keith, D., Jacobs, S.A., & Murphy, M.S. (2015). Evaluation of cyanobacteria cell count detection derived from MERIS imagery across the eastern USA. *Remote Sensing of Environment, 157*, 24-34

Ma, R., Duan, H., Liu, Q., & Loiselle, S.A. (2011). Approximate bottom contribution to remote sensing reflectance in Taihu Lake, China. *Journal of Great Lakes Research, 37*, 18-25

Maberly, S.C., Hurley, M.A., Butterwick, C., Corry, J.E., Heaney, S.I., Irish, A.E., Jaworski, G.H.M., Lund, J.W.G., Reynolds, C.S., & Roscoe, J.V. (1994). The rise and fall or Asterionella formosa in the South Basin of Windermere: analysis of a 45-year series of data. *Freshwater Biology, 31*, 19-34

MacCallum, S.N., & Merchant, C.J. (2012). Surface water temperature observations of large lakes by optimal estimation. *Canadian Journal of Remote Sensing, 38*, 25-45

Malingreau, J.-P. (1986). Global vegetation dynamics: satellite observations over Asia. *International Journal of Remote Sensing, 7*, 1121-1146

Maritorena, S., Siegel, D.A., & Peterson, A.R. (2002). Optimization of a semianalytical ocean color model for global-scale applications. *Applied Optics, 41*, 2705-2714

Martin, J.M., & Windom, H.L. (1990). Present and future roles of ocean margins in regulating marine biogeochemical cycles of trace elements. In, *Ocean margin processes in global change* (pp. 45-67). Berlin: Dahlem workshop

Martinez, G., Bizikova, L., Blobel, D., & Swart, R. (2011). Emerging climate coastal adaptation strategies and case studies around the world. *Global Change and Baltic Coastal Zones 1*, 249-273

Matthews, M.W. (2011). A current review of empirical procedures of remote sensing in inland and near-coastal transitional waters. *International Journal of Remote Sensing, 32*, 6855-6899

Matthews, M.W. (2014). Eutrophication and cyanobacterial blooms in South African inland waters: 10 years of MERIS observations. *Remote Sensing of Environment, 155*, 161-177

Matthews, M.W., Bernar, S., & Winter, K. (2010). Remote sensing of cyanobacteria-dominant algal blooms and water quality parameters in Zeeloevlei, a small hypertrophic lake, using MERIS. *Remote Sensing of Environment, 114*, 2070-2087

Matthews, M.W., Bernard, S., & Robertson, L. (2012). An algorithm for detecting trophic status (chlorophyll-a), cyanobacterial-dominance, surface scums and floating vegetation in inland and coastal waters. *Remote Sensing of Environment, 124*, 637-652

Matthews, M.W., & Odermatt, D. (2015). Improved algorithm for routine monitoring of cyanobacteria and eutrophication in inland and near-coastal waters. *Remote Sensing of Environment, 156*, 374-382

Maul, G.A. (1985). *Introduction to satellite oceanography*. Dordrecht: Martinus Nijhoff

Mayer, L.M., Keil, R.G., Macko, S.A., Joye, S.B., Ruttenberg, K.C., & Aller, R.C. (1998). The importance of suspended particulates in riverine delivery of bioavailable nitrogen to coastal zones. *Global Biogeochemical Cycles, 12*, 573-579

Meis, S., Thackeray, S.J., & Jones, I.D. (2009). Effects of recent climate change on phytoplankton phenology in a temperate lake. *Freshwater Biology, 54*, 1888-1898

Miller, R.L., & McKee, B.A. (2004). Using MODIS Terra 250 m imagery to map concentrations of total suspended matter in coastal waters. *Remote Sensing of Environment, 93*, 259-266

Mimuro, M., & Fujita, Y. (1977). Excitation energy transfer between pigment system II units in blue-green algae. *Biochimica et Biophysica Acta – Bioenergetics, 504*, 406-412

Mischke, U., Thackeray, S., Dunbar, M., McDonald, C., Carvalho, L., de Hoyos, C., Jarvinen, M., Laplace-Treyture, C., Morabito, G., & Skjelbred, B. (2012). WISER deliverable D3. 1-4: guidance document on sampling, analysis and counting standards for phytoplankton in lakes

Mishra, S., Mishra, D.R., Lee, Z., & Tucker, C.S. (2013). Quantifying cyanobacterial phycocyanin concentration in turbid productive waters: A quasi-analytical approach. *Remote Sensing of Environment, 133*, 141-151

Mobley, C.D. (1994). *Light and water: radiative transfer in natural waters*. New York: Academic

Mobley, C.D., Stramski, D., Bissett, W.P., & Boss, E. (2004). Optical Modeling of Ocean Waters: Is the Case 1 - Case 2 Classification Still Useful? *Oceanography, 17*, 61-67

Moore, G.F., Aiken, J., & Lavender, S.J. (1999). The atmospheric correction of water colour and the quantitative retrieval of suspended particulate matter in Case II waters: application to MERIS. *International Journal of Remote Sensing, 20*, 1713-1733

Morel, A. (1988). Optical modeling of the upper ocean in relation to its biogeneous matter content (Case 1 waters). *Journal of Geophysical Research 93*, 10749-10768

Morel, A., & Antoine, D. (2000). Pigment index retrieval in Case 1 waters. *MERIS ATBD, 2*

Morel, A., & Prieur, L. (1977). Analysis of variations in ocean color. *Limnology and Oceanography, 22*, 709-722

Moses, W.J., Gitelson, A.A., Berdnikov, S., & Povazhnyy, V. (2009a). Estimation of chlorophyll-a concentration in case II waters using MODIS and MERIS data – successes and challenges. *Environmental Research Letters 4*

Moses, W.J., Gitelson, A.A., Berdnikov, S., & Povazhnyy, V. (2009b). Satellite estimation of chlorophyll-a concentration using the red and NIR bands of MERIS – the Azov Sea case study. *IEEE Geoscience and Remote Sensing Letters 6*, 845849

Moss, B. (2012). Cogs in the endless machine: Lakes, climate change and nutrient cycles: A review. *Science of the Total Environment, 434*, 130-142

Mózes, A., Présing, M., & Vörös, L. (2006). Seasonal Dynamics of Picocyanobacteria and Picoeukaryotes in a Large Shallow Lake (Lake Balaton, Hungary). *International Review of Hydrobiology, 91*, 35-50

Mueller, J.L., & Austin, R.W. (1995). *Ocean Optics Protocols for SeaWiFS Validation, Revision 1, SeaWiFS Technical Report Series*.

Nõges, P., Adrian, R., Anneville, O., Arvola, L., Blenckner, T., George, G., Jankowski, T., Järvinen, M., Maberly, S., Padisák, J., Straile, D., Teubner, K., & Weyhenmeyer, G. (2010). *The Impact of Climate Change on European Lakes*.

Odermatt, D., Giardino, C., & Heege, T. (2010). Chlorophyll retrieval with MERIS Case-2-Regional in perialpine lakes. *Remote Sensing of Environment, 114*, 607-617

Odermatt, D., Gitelson, A., Brando, V.E., & Schaepman, M. (2012). Review of constituent retrieval in optically deep and complex waters from satellite imagery. *Remote Sensing of Environment, 118*, 116-126

Odermatt, D., Heege, T., Nieke, J., Kneubühler, M., & Itten, K. (2008). Water quality monitoring for Lake Constance with a physically based algorithm for MERIS data. *Sensors, 8*, 4582-4599

OECD (1982). *Eutrophication of water, monitoring, assessment and control*. Paris: Organization for Economic Cooperation and Development

Omernik, J.M. (2004). Perspectives on the nature and definition of ecological regions. *Environmental Management, 34*, S27-S38

Padisak, J., Molnar, G., Soroczki-Pinter, E., Hajnal, E., & George, D.G. (2006). Four consecutive dry years in Lake Balaton (Hungary): consequences for phytoplankton biomass and composition. *Proceedings-International Association of Theoretical and Applied Limnology, 29,* 1153

Padisák, J., & Reynolds, C.S. (1998). Selection of phytoplankton associations in Lake Balaton, Hungary, in response to eutrophication and restoration measures, with special reference to the cyanoprokaryotes. *Hydrobiologia, 384,* 41-53

Paerl, H.W., & Huisman, J. (2008). Blooms like it hot. *Science, 320,* 57

Paerl, H.W., & Huisman, J. (2009). Climate change: a catalyst for global expansion of harmful cyanobacterial blooms. *Environmental Microbiology Reports, 1,* 27-37

Palmer, S.C., Hunter, P.D., Lankester, T., Hubbard, S., Spyrakos, E., Tyler, A., Présing, M., Horváth, H., Lamb, A., Balzter, H., & Tóth, V.R. (2015a). Validation of Envisat MERIS algorithms for chlorophyll retrieval in a large, turbid and optically-complex shallow lake. *Remote Sensing of Environment, 157,* 158-169

Palmer, S.C., Odermatt, D., Hunter, P.D., Brockmann, C., & Balzter, H. (2015b). Satellite remote sensing of phytoplankton phenology in Lake Balaton using 10 years of MERIS observations. *Remote Sensing of Environment, 158,* 441-452

Palmer, S.C., Pelevin, V.V., Goncharenko, I., Kovács, A.W., Zlinszky, A., Présing, M., Horváth, H., Nicolás-Perea, V., Balzter, H., & Tóth, V.R. (2013). Ultraviolet fluorescence LiDAR (UFL) as a measurement tool for water quality parameters in turbid lake conditions. *Remote Sensing, 5,* 4405-4422

Pelevin, V., Abramov, O., & Karlsen, G. (1995). Subsatellite experiment in the Mediterranean Sea: a comparative study of water pollution of the seas surrounding Europe, using laser sensing from moving ship. *Engineering Ecology, 6,* 31-41

Pelevin, V., Abramov, O., Karlsen, G., Pelevin, V., Stogov, A., & Khlebnikov, D. (2001). Laser sensing of surface waters of the Atlantic and the seas surrounding Europe. *Atmospheric And Oceanic Optics, 14,* 704-709

Petus, C., Chust, G., Gohin, F., Doxaran, D., Froidefond, J.M., & Sagarminaga, Y. (2010). Estimating turbidity and total suspended matter in the Adour River plume (South Bay of Biscay) using MODIS 250-m imagery. *Continental Shelf Research 30,* 379-392

Platt, T., & Sathyendranath, S. (2008). Ecological indicators for the pelagic zone of the ocean from remote sensing. *Remote Sensing of Environment, 112,* 3426-3436

Platt, T., Sathyendranath, S., White III, G.N., Fuentes-Yaco, C., Zhai, L., Devred, E., & Tang, C. (2010). Diagnostic properties of phytoplankton time series from remote sensing. *Estuaries and Coasts, 33,* 428-439

Platt, T., White III, G.N., Zhai, L., Sathyendranath, S., & Roy, S. (2009). The phenology of phytoplankton blooms: Ecosystem indicators from remote sensing. *Ecological Modelling, 220,* 3057-3069

Pomogyi, P. (1993). Nutrient retention by the Kis-Balaton Water Protection System. *Hydrobiologia, 251,* 309-320

Postel, S.L. (2000). Entering an era of water scarcity: the challenges ahead. *Ecological applications, 10*, 941-948

Pozdnyakov, D., Shuchman, R., Korosov, A., & Hatt, C. (2005). Operational algorithm for the retrieval of water quality in the Great Lakes. *Remote Sensing of Environment, 97*, 352-370

Pozdnyakov, D.V., Korosov, A.A., Petrova, N.A., & Grassl, H. (2013). Multi-year satellite observations of Lake Ladoga's biogeochemical dynamics in relation to the lake's trophic status. *Journal of Great Lakes Research, 39*, 34-45

Preisendorfer, R.W. (1961). Application of radiative transfer theory to light measurements in the sea

Présing, M., Preston, T., Takátsy, A., Speőber, P., Kovács, A.W., Vörös, L., Kenesi, G., & Kóbor, I. (2008). Phytoplankton nitrogen demand and the significance of internal and external nitrogen sources in a large shallow lake (Lake Balaton, Hungary). *Hydrobiologia, 599*, 87-95

Proctor, C., & Roesler, C. (2010). New insights on obtaining phytoplankton concentration and composition from in situ multispectral Chlorophyll fluorescence. *Limnology & Oceanography Methods, 8*, 695-708

Puczkó, L., & Rátz, T. (2000). Tourist and resident perceptions of the physical impacts of tourism at Lake Balaton, Hungary: Issues for sustainable tourism management. *Journal of Sustainable Tourism 8*, 458-478

Racault, M.-F., Le Quéré, C., Buitenhuis, E., Sathyendranath, S., & Platt, T. (2012). Phytoplankton phenology in the global ocean. *Ecological Indicators, 14*, 152-163

Reinersman, P.N., & Carder, K.L. (1995). Monte Carlo simulation of the atmospheric point-spread function with an application to correction for the adjacency effect. *Applied Optics, 34*, 4453-4471

Reynolds, C.S. (2006). Ecology of Phytoplankton. In, *Cambridge University Press*

Ricciardi, A., & Rasmussen, J.B. (1999). Extinction rates of North American freshwater fauna. *Conservation Biology 13*, 1220-1222

Richardson, A.J. (2008). In hot water: zooplankton and climate change. *ICES Journal of Marine Sciences, 65*, 279-295

Rogers, S., Webster, T., Livingstone, W., & O'Driscoll, N.J. (2012). Airborne Laser-Induced Fluorescence (LIF) Light Detection and Ranging (LiDAR) for the Quantification of Dissolved Organic Matter Concentration in Natural Waters. *Estuaries and Coasts, 35*, 959-975

Rolinski, S., Horn, H., Petzoldt, T., & Paul, L. (2007). Identifying cardinal dates in phytoplankton time series to enable the analysis of long-term trends. *Oecologia, 153*, 997-1008

Ruddick, K.G., Ovidio, F., & Rijkeboer, M. (2000). Atmospheric correction of SeaWiFS imagery for turbid coastal and inland waters. *Applied Optics, 39*, 897-912

Ruiz-Verdú, A., Koponen, S., Heege, T., Doerffer, R., Brockmann, C., Kallio, K., Pyhälahti, T., Peña, R., Polvorinos, A., Heblinski, J., Ylöstalo, P., Conde, L., Odermatt, D., V., E., & Pulliainen, J. (2008a). Development of MERIS lake water algorithms: validation results from Europe. In, *2nd MERIS / (A)ATSR User Workshop*. Frascati, Italy: ESA

Ruiz-Verdú, A., Simis, S.G., de Hoyos, C., Gons, H.J., & Peña-Martínez, R. (2008b). An evaluation of algorithms for the remote sensing of cyanobacterial biomass. *Remote Sensing of Environment, 112*, 3996-4008

Sala , O.E., Chapin, F.S., Armesto, J.J., Berlow, E., Bloomfield, J., Dirzo, R., Huber-Sanwald, E., Huenneke, L.F., Jackson, R.B., Kinzig, A., Leemans, R., Lodge, D.M., Mooney, H.A., Oesterheld, M., Poff, N.L., Sykes, M.T., Walker, B.H., Walker, M., & Wall, D.H. (2000). Global biodiversity scenarios for the year 2010. *Science, 287*, 1770-1774

Santer, R., & Zagolski, F. (2008). Improve Contrast between Ocean and Land (ICOL): Algorithm Theoretical Basis Document (ATBD): The MERIS Level-1C. *Université du Littoral Côte d'Opale, ADRINORD*

Sasaoka, K., Chiba, S., & Saino, T. (2011). Climatic forcing and phytoplankton phenology over the subarctic North Pacific from 1998 to 2006, as observed from ocean color data. *Geophysical Research Letters, 38*

Schroeder, T. (2005). Variations Remote sensing of coastal waters with MERIS on basis of explicit and implicit atmospheric correction algorithms. In, *Department of Earth Sciences*: Free University of Berlin

Schroeder, T., Behnert, I., Schaale, M., Fischer, J., & Doerffer, R. (2007a). Atmospheric correction algorithm for MERIS above case-2 waters. *International Journal of Remote Sensing, 28*, 1459-1486

Schroeder, T., Schaale, M., & Fischer, J. (2007b). Retrieval of atmospheric and oceanic properties from MERIS measurements: A new Case-2 water processor for BEAM. *International Journal of Remote Sensing, 28*, 5627-5632

Seebens, H., Einsle, U., & Straile, D. (2009). Copepod life cycle adaptations and success in response to phytoplankton spring bloom phenology. *Global Change Biology, 15*, 1394-1404

Sentlinger, G.I., Hook, S.J., & Laval, B. (2008). Sub-pixel water temperature estimation from thermal-infrared imagery using vectorized lake features. *Remote Sensing of Environment, 112*, 1678-1688

Seppälä, J., Ylöstalo, P., Kaitala, S., Hällfors, S., Raateoja, M., & Maunula, P. (2007). Ship-of-opportunity based phycocyanin fluorescence monitoring of the filamentous cyanobacteria bloom dynamics in the Baltic Sea. *Estuarine, Coastal and Shelf Science, 73*, 489-500

Shi, W., & Wang, M. (2009). An assessment of the black ocean pixel assumption for MODIS SWIR bands. *Remote Sensing of Environment, 113*, 1587-1597

Shuchman, R., Korosov, A., Hatt, C., Pozdnyakov, D., Means, J., & Meadows, G. (2006). Verification and application of a bio-optical algorithm for Lake Michigan using

SeaWiFS: a 7-year inter-annual analysis. *Journal of Great Lakes Research, 32*, 258-279

Siegel, D., Doney, S., & Yoder, J. (2002). The North Atlantic spring phytoplankton bloom and Sverdrup's critical depth hypothesis. *Science, 296*, 730-733

Siegel, D.A., Wang, M., Maritorena, S., & Robinson, W. (2000). Atmospheric correction of satellite ocean color imagery: The black pixel assumption. *Applied Optics, 39*, 3582-3591

Simis, S.G., Peters, S.W., & Gons, H.J. (2005). Remote sensing of the cyanobacterial pigment phycocyanin in turbid inland water. *Limnology and Oceanography, 50*, 237-245

Smith, V.H. (2003). Eutrophication of freshwater and coastal marine ecosystems a global problem. *Environmental Science and Pollution Research, 10*, 126-139

Sommer, U., & Lewandowska, A. (2011). Climate change and the phytoplankton spring bloom: warming and overwintering zooplankton have similar effects on phytoplankton. *Global Change Biology, 17*, 154-162

Sriwongsitanon, N., Surakit, K., & Thianpopirug, S. (2011). Influence of atmospheric correction and number of sampling points on the accuracy of water clarity assessment using remote sensing application. *Journal of Hydrology 401*, 203-220

Stedmon, C., Markager, S., & Bro, R. (2003). Tracing dissolved organic matter in aquatic environments using a new approach to fluorescence spectroscopy. *Marine Chemistry, 82*, 239-254

Sterckx, S., Knaeps, E., & Ruddick, K. (2011). Detection and correction of adjacency effects in hyperspectral airborne data of coastal and inland waters: the use of the near infrared similarity spectrum. *International Journal of Remote Sensing, 32*, 21

Sterckx, S., Knaeps, E., Santer, R., Danne, O., & Brockmann, C. (2012). Environment correction for inland and coastal water scences: a comparison of methods. In, *Sentinel-2 Preparatory Symposium*. Frascati, Italy

Straile, D., Livingstone, D.M., Weyhenmeyer, G.A., & George, G.D. (2003). *The response of freshwater ecosystems to climate variability associated with the North Atlantic oscillation*. Washington, DC: American Geophysical Union

Stratoulias, D., Balzter, H., Zlinszky, A., & Tóth, V.R. (2015). Assessment of ecophysiology of lake shore reed vegetation based on chlorophyll fluorescence, field spectroscopy and hyperspectral airborne imagery. *Remote Sensing of Environment, 157*, 72-84

Stumpf, R.P., Wynne, T.T., Baker, D.B., & Fahnenstiel, G.L. (2012). Interannual variability of cyanobacterial blooms in Lake Erie. *PloS one, 7*, e42444

Suski, C.D., & Cooke, S.J. (2007). Conservation of aquatic resources through the use of freshwater protected areas: Opportunities and challenges. *Biodiversity and Conservation 16*, 2015-2029

Sváb, E., Tyler, A.N., Preston, T., Présing, M., & Balogh, K.V. (2005). Characterizing the spectral reflectance of algae in lake waters with high suspended sediment concentrations. *International Journal of Remote Sensing, 26*, 919-928

Szabó, G., Khayer, B., Rusznyák, A., Tátrai, I., Dévai, G., Márialigeti, K., & Borsodi, A.K. (2011). Seasonal and spatial variability of sediment bacterial communities inhabiting the large shallow Lake Balaton. *Hydrobiologia, 663*, 217-232

Tarrant, P., Amacher, J., & Neuer, S. (2010). Assessing the potential of Medium-Resolution Imaging Spectrometer (MERIS) and Moderate-Resolution Imaging Spectroradiometer (MODIS) data for monitoring total suspended matter in small and intermediate sized lakes and reservoirs. *Water Resources Research, 46*

Tátrai, I., György, Á.I., Mátyás, K., Korponai, J., Pomogyi, P., Vári, Á., Józsa, V., & Boros, G. (2011). Intrinsic processes causing periodic changes in stability in a shallow biomanipulated lake. *Marine and Freshwater Research, 62*, 197-204

Tátrai, I., Istvánovics, V., Tóth, L.G., & Kóbor, I. (2008). Management measures and long-term water quality changes in Lake Balaton (Hungary). *Fundamental and Applied Limnology, 172*, 1-11

Tátrai, I., Mátyás, K., Korponai, J., Paulovits, G., & Pomogyi, P. (2000). The role of the Kis-Balaton Water Protection System in the control of water quality of Lake Balaton. *Ecological Engineering, 16*, 73-78

Taylor, A.H., Allen, J.I., & Clark, P.A. (2002). Extraction of a weak climatic signal by an ecosystem. *Nature, 416*

Tebbs, E., Remedios, J., & Harper, D. (2013). Remote sensing of chlorophyll-< i> a</i> as a measure of cyanobacterial biomass in Lake Bogoria, a hypertrophic, saline–alkaline, flamingo lake, using Landsat ETM+. *Remote Sensing of Environment, 135*, 92-106

Thackeray, S., Henrys, P., Jones, I., & Feuchtmayr, H. (2012). Eight decades of phenological change for a freshwater cladoceran: what are the consequences of our definition of seasonal timing? *Freshwater Biology, 57*, 345-359

Thackeray, S.J. (2012). Mismatch revisited: what is trophic mismatching from the perspective of the plankton? . *Journal of Plankton Research, 34*, 1001-1010

Thackeray, S.J., Jones, I.D., & Maberly, S.C. (2008). Long-term changes in the phenology of spring phytoplankton: species-specific responses to nutrient enrichment and climate change. *Journal of Ecology, 96*, 523-535

Thackeray, S.J., Nõges, P., Dunbar, M.J., Dudley, B.J., Skjelbred, B., Morabito, G., Carvalho, L., Phillips, G., Mischke, U., & Catalan, J. (2013). Quantifying uncertainties in biologically-based water quality assessment: A pan-European analysis of lake phytoplankton community metrics. *Ecological Indicators, 29*, 34-47

Torbick, N., Hession, S., Hagen, S., Wiangwang, N., Becker, B., & Qi, J. (2013). Mapping inland lake water quality across the Lower Peninsula of Michigan using Landsat TM imagery. *International Journal of Remote Sensing, 34*, 7607-7624

Trescott, A., & Park, M.-H. (2013). Remote sensing models using Landsat satellite data to monitor algal blooms in Lake Champlain. *Water Science & Technology, 67*, 1113-1120

Tyler, A.N., Svab, E., Preston, T., & Kovacs, W.A. (2006). Remote sensing of the water quality of shallow lakes: A mixture modelling approach to quantifying phytoplankton in water characterized by high-suspended sediment. *International Journal of Remote Sensing, 27*, 1521-1537

V.-Balogh, K., Vörös, L., Tóth, N., & Bokros, M. (2003). Changes of Organic Matter Quality along the Longitudinal Axis of a large shallow lake (Lake Balaton). *Hydrobiologia, 506-509*, 67-74

Vaillancourt, R.D., Brown, C.W., Guillard, R.R.L., & Balch, W.M. (2004). Light backscattering properties of marine phytoplankton: Relationships to cell size, chemical composition and taxonomy. *Journal of Plankton Research, 26*, 191-212

Van Mol, B., & Ruddick, K. (2004). The Compact High Resolution Imaging Spectrometer (CHRIS): the future of hyperspectral satellite sensors. Imagery of Oostende coastal and inland waters. In, *Airborne Imaging Spectroscopy workshop* Bruges, Belgium

Vargas, M., Brown, C., & Sapiano, M. (2009). Phenology of marine phytoplankton from satellite ocean color measurements. *Geophysical Research Letters, 36*

Vermote, E.F., Kotchenova, S.Y., & Ray, J.P. (2011). *ODIS Surface Reflectance User's Guide, version 1.3*.

Vermote, E.F., Tanre, D., Deuze, J.L., Herman, M., & Morcette, J.J. (1997). Second simulation of the satellite signal in the solar spectrum, 6S: an overview. *IEEE Transactions on Geoscience and Remote Sensing, 35*, 675-686

Vidot, J., & Santer, R. (2005). Atmospheric correction for inland waters—Application to SeaWiFS. *International Journal of Remote Sensing, 26*, 3663-3682

Vodacek, A. (1989). Synchronous fluorescence spectroscopy of dissolved organic matter in surface waters: Application to airborne remote sensing. *Remote Sensing of Environment, 30*, 239-247

Vodacek, A., Hoge, F., Swift, R., Yungel, J., Peltzer, E., & Bough, N. (1995). The use of in situ and airborne fluorescence measurements to determine UV absorption coefficients and DOC concentrations in surface waters. *Limnology & Oceanography, 40*, 411-415

Voss, R.J., Hakvoort, J.H.M., Jordans, R.W.J., & Ibelings, B.W. (2003). Multiplatform optical monitoring of eutrophication in temporally and spatially variable lakes. *The Science of the Total Environment, 312*, 221-243

Walters, A.W., Gonzalez Sagrario, M.A., & Schindler, D.E. (2013). Species and community level responses combine to drive phenology of lake phytoplankton. In, *Ecology*

Wang, M. (2007). Remote sensing of the ocean contributions from ultraviolet to near-infrared using the shortwave infrared bands: simulations. *Applied Optics, 46*, 1535-1547

Wang, M., & Shi, W. (2007). Remote sensing of the ocean contributions from ultraviolet to near-infrared using the shortwave infrared bands: simulations. *Applied Optics, 46*, 1535-1547

White, M.A., Beurs, D., Kirsten, M., Didian, K., Inouye, D.W., Richardson, A.D., Jensen, O.P., O'Keefe, J., Zhang, G., & Nemani, R.R. (2009). Intercomparison, interpretation, and assessment of spring phenology in North America estimated from remote sensing for 1982–2006. *Global Change Biology, 15*, 2335-2359

Williamson, C.E., Saros, J.E., Vincent, W.F., & Smol, J.P. (2009). Lakes and reservoirs as sentinels, integrators, and regulators of climate change. *Limnology and Oceanography, 54*, 2273

Winder, M., Berger, S.A., Lewandowska, A., Aberle, N., Lengfellner, K., Sommer, U., & Diehl, S. (2012). Spring phenological responses of marine and freshwater plankton to changing temperature and light conditions. *Marine Biology 159*, 2491-2501

Winder, M., & Cloern, J.E. (2010). The annual cycles of phytoplankton biomass. *Philosophical Transactions of the Royal Society B: Biological Sciences, 365*, 3215-3226

Winder, M., & Schindler, D.E. (2004a). Climate change uncouples trophic interactions in an aquatic ecosystem. *Ecology, 85*, 2100-2106

Winder, M., & Schindler, D.E. (2004b). Climate effects on the phenology of lake processes. *Global Change Biology, 10*, 1844-1856

Winder, M., & Sommer, U. (2012). Phytoplankton response to a changing climate. *Hydrobiologia, 598*, 5-16

Wright, C.W., Hoge, F.E., Swift, R.N., Yungel, J.K., & Schirtzinger, C.R. (2001). Next-generation NASA airborne oceanographic lidar system. *Applied Optics, 40*, 336-342

Wu, G.G., De Leeuw, J., Skidmore, A.K., Prins, H.H.T., & Liu, Y. (2008). Comparison of MODIS and Landsat TM5 images for mapping tempo-spatial dynamics of Secchi disk depths in Poyang Lake national nature reserve, China. *International Journal of Remote Sensing, 29*

Wu, M., Zhang, W., Wang, X., & Luo, D. (2009). Application of MODIS satellite data in monitoring water quality parameters of Chaohu Lake in China. *Environmental Monitoring and Assessment, 148*, 255-264

Wynne, T., Stumpf, R., & Briggs, T. (2013a). Comparing MODIS and MERIS spectral shapes for cyanobacterial bloom detection. *International Journal of Remote Sensing, 34*, 6668-6678

Wynne, T., Stumpf, R., Tomlinson, M., Warner, R., Tester, P., Dyble, J., & Fahnenstiel, G. (2008). Relating spectral shape to cyanobacterial blooms in the Laurentian Great Lakes. *International Journal of Remote Sensing, 29*, 3665-3672

Wynne, T.T., Stumpf, R.P., Tomlinson, M.C., Fahnenstiel, G.L., Dyble, J., Schwab, D.J., & Joshi, S.J. (2013b). Evolution of a cyanobacterial bloom forecast system in western Lake Erie: Development and initial evaluation. *Journal of Great Lakes Research, 39*, 90-99

Zhou, L., Tucker, C.J., Kaufmann, R.K., Slayback, D., Shabanov, N.V., & Myneni, R.B. (2001). Variations in northern vegetation activity inferred from satellite data of vegetation index during 1981 to 1999. *Journal of Geophysical Research: Atmospheres (1984–2012), 106*, 20069-20083

Zlinszky, A., & Molnár, G. (2008). The first bathymetric maps of Lake Balaton (Hungary). *European Geosciences Union General Assembly*

Zlinszky, A., Mücke, W., Lehner, H., Briese, C., & Pfeifer, N. (2012a). Categorizing wetland vegetation by airborne laser scanning on Lake Balaton and Kis-Balaton, Hungary. *Remote Sensing, 4*, 1617-1650

Zlinszky, A., Mücke, W., Lehner, H., Briese, C., & Pfeifer, N. (2012b). Vegetation mapping from medium density discrete echo Airborne Laser Scanning data: a case study of the Lake Balaton wetlands. In, *Geophysical Research Abstracts*

Zlinszky, A., & Timár, G. (2013). Historic maps as a data source for socio-hydrology: a case study of the Lake Balaton wetland system, Hungary. *Hydrology and Earth System Sciences, 17*, 4589-4606

Appendix I. Contributions of co-authors

This thesis comprises four methodology and results chapters which have been published or are in preparation for publication, and represent the collaborative efforts of several co-authors. The co-authors, including the PhD candidate, and their respective contributions are detailed below. Permission with regards to the use of this published material in the thesis have been obtained from the publishers as necessary.

Ch. 4: "MEdium Resolution Imaging Spectrometer (MERIS) chlorophyll retrieval, mapping and time series validation"

Parts of the work presented in this chapter have published as:

Palmer, S. C. J., Hunter, P. D., Lankester, T., Hubbard, S., Spyrakos, E., Tyler, A. N., Présing, M., Horváth, H., Lamb, A., Balzter, H., Tóth, V.R. (2015). Validation of Envisat MERIS algorithms for chlorophyll retrieval in a large, turbid and optically-complex shallow lake. *Remote Sensing of Environment*, *157*, 158-169.

Respective co-author contributions:

Palmer, S. C. J. (University of Leicester/Balaton Limnological Institute): Carried out project planning with advice of co-authors, performed data analysis (comparison of *in situ* datasets; algorithm application in BEAM to supplement that of PHAVEOS; all pixel value extraction and matchup compilation; calibration and validation) created all Tables and Figures, chapter and publication writing and revisions.

Hunter, P.D., Spyrakos, E., Tyler, A. N. (University of Stirling); Lamb, A. (Airbus, UK); Balzter, H. (University of Leicester); Tóth, V. R. (Balaton Limnological Institute): Provided supervision and/or feedback throughout the planning and completion of the work, as part of the current PhD (H. Balzter) and GIONET work package 4.3 (V. R. Tóth), as well as during GIONET international (P. D. Hunter, A. N. Tyler, E. Spyrakos) and industrial (A. Lamb) secondments during which the bulk of the work was done.

Lankester, T., Hubbard, S. (Airbus, UK): Undertook bulk MERIS image processing using their PHAVEOS processing chain after adapting selected BEAM algorithms to PHAVEOS.

Présing, M., Horváth, H. (Balaton Limnological Institute): Provision of archive chl-*a* data, collected and analyzed in the laboratory of the BLI.

Ch. 5: "MERIS atmospheric correction validation and influence on chlorophyll-a retrieval"

Parts of the work presented in this chapter are in preparation for publication.

Respective co-author contributions:

Palmer, S. C. J. (University of Leicester/Balaton Limnological Institute): Extracted and compiled matchup image - *in situ* dataset and carried out calibration-validation analyses, as well as supplementary image processing using BEAM, Figure/Table creation and writing.

Dominguez Gomez, J. A. (National Distance Education University, Spain): Processed selected MERIS images using SCAPE-M_B2 and provided feedback throughout the planning and completion of the work.

Riddick, C. A., Hunter, P. D., Spyrakos, E., Tyler, A. N. (University of Stirling): Provided *in situ* spectroradiometer measurements collected as part of their 2010 field campaign, as well as supervision and feedback during the planning and completion of the work.

Balzter, H. (University of Leicester): Provided supervision and feedback during the planning and completion of the work.

Ch. 6: "Earth observation of freshwater phytoplankton phenology metrics"

Parts of the work presented in this chapter have published as:

Palmer, S. C. J., Odermatt, D., Hunter, P. D., Brockmann, C., Présing, M., Balzter, H., Tóth, V. R. (2015). Satellite remote sensing of phytoplankton phenology in Lake Balaton using 10 years of MERIS observations. *Remote Sensing of Environment, 158*, 441-452.

Respective co-author contributions:

Palmer, S. C. J. (University of Leicester/Balaton Limnological Institute): Performed all research design, phenological analyses, chapter and article writing, and Figure and Table creation with feedback from co-authors.

Odermatt, D. (Odermatt & Brockmann GmbH): Provided MERIS chl-*a* products used as input into the phenological analyses, processed using CALVALUS.

Hunter, P. D. (University of Stirling); Brockmann, C. (Brockmann Consults); Balzter, H. (University of Leicester); Tóth, V. R. (Balaton Limnological Institute): Provided supervision and/or feedback during the planning and completion of the work.

Présing, M. (Balaton Limnological Institute): Provision of archive chl-*a* data, collected and analyzed in the laboratory of the BLI.

Ch. 7: "Ultraviolet Fluorescence Light Detection and Ranging measurements of water quality parameters under turbid lake conditions"

Parts of the work presented in this chapter have published as:

Palmer, S. C. J., Pelevin, V. V., Goncharenko, I., Kovács, A. W., Zlinszky, A., Présing, M., Horváth, H., Nicolás-Perea, V., Balzter, H., Tóth, V. R. (2013). Ultraviolet Fluorescence LiDAR (UFL) as a measurement tool for water quality parameters in turbid lake conditions. *Remote Sensing, 5*, 4405-4422.

Respective co-author contributions:

Palmer, S. C. J. (University of Leicester/Balaton Limnological Institute): Carried out experimental design, coordinated and carried out fieldwork and laboratory tank measurements, participated in (conventional) laboratory analyses of collected water samples for calibration-validation under the supervision of Dr. Présing and his team. Performed data analyses and interpretation of results, chapter and article writing, and Figure and Table creation with feedback from co-authors.

Pelevin, V. V., Goncharenko, I. (Shirshov Institute of Oceanology): Provided and operated the fluorescence LiDAR during field and laboratory tank measurements, and provided resulting measurements for analysis presented in the chapter.

Kovács, A. W. (Balaton Limnological Institute): Provided advice during research planning and algae cultures for use in the laboratory tank experiments.

Présing, M., Horváth, H. (Balaton Limnological Institute): Analyzed water samples collected during fieldwork and laboratory tank measurements for chl-*a*, TSM and CDOM in the laboratory of the BLI.

Zlinszky, A. (Balaton Limnological Institute); Nicolás-Perea, V., Balzter, H. (University of Leicester): Provided supervision and/or feedback during the planning and completion of the work.

Tóth, V. R. (Balaton Limnological Institute): Provided supervision and feedback during the planning and completion of the work; provided logistical support for and participated in the fieldwork and laboratory measurements.

Appendix II. Annual maps of summer bloom phenology features, 2003 to 2011

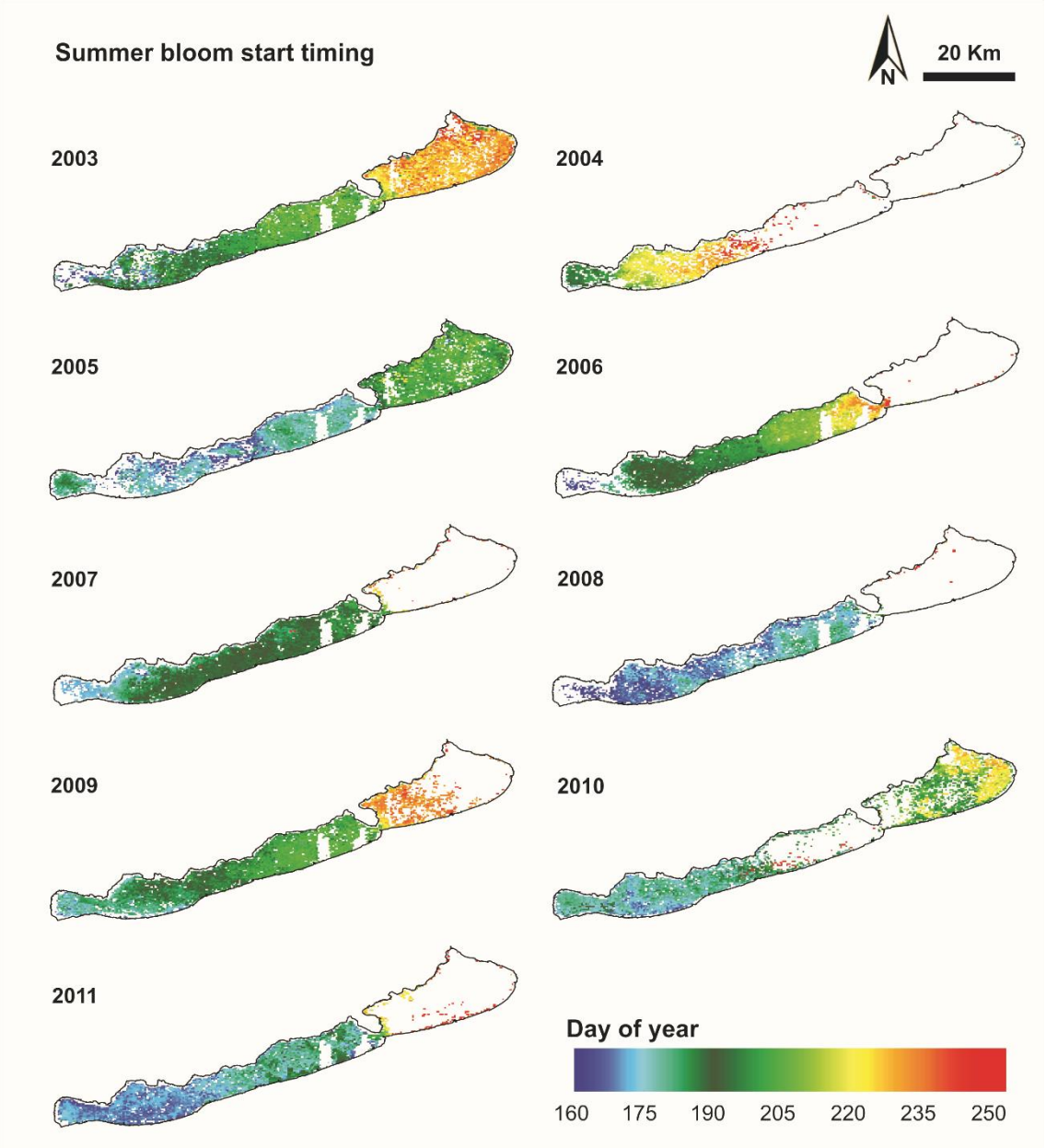

Figure AII.1. Summer bloom start timing, mapped for each of the nine years 2003-2011.

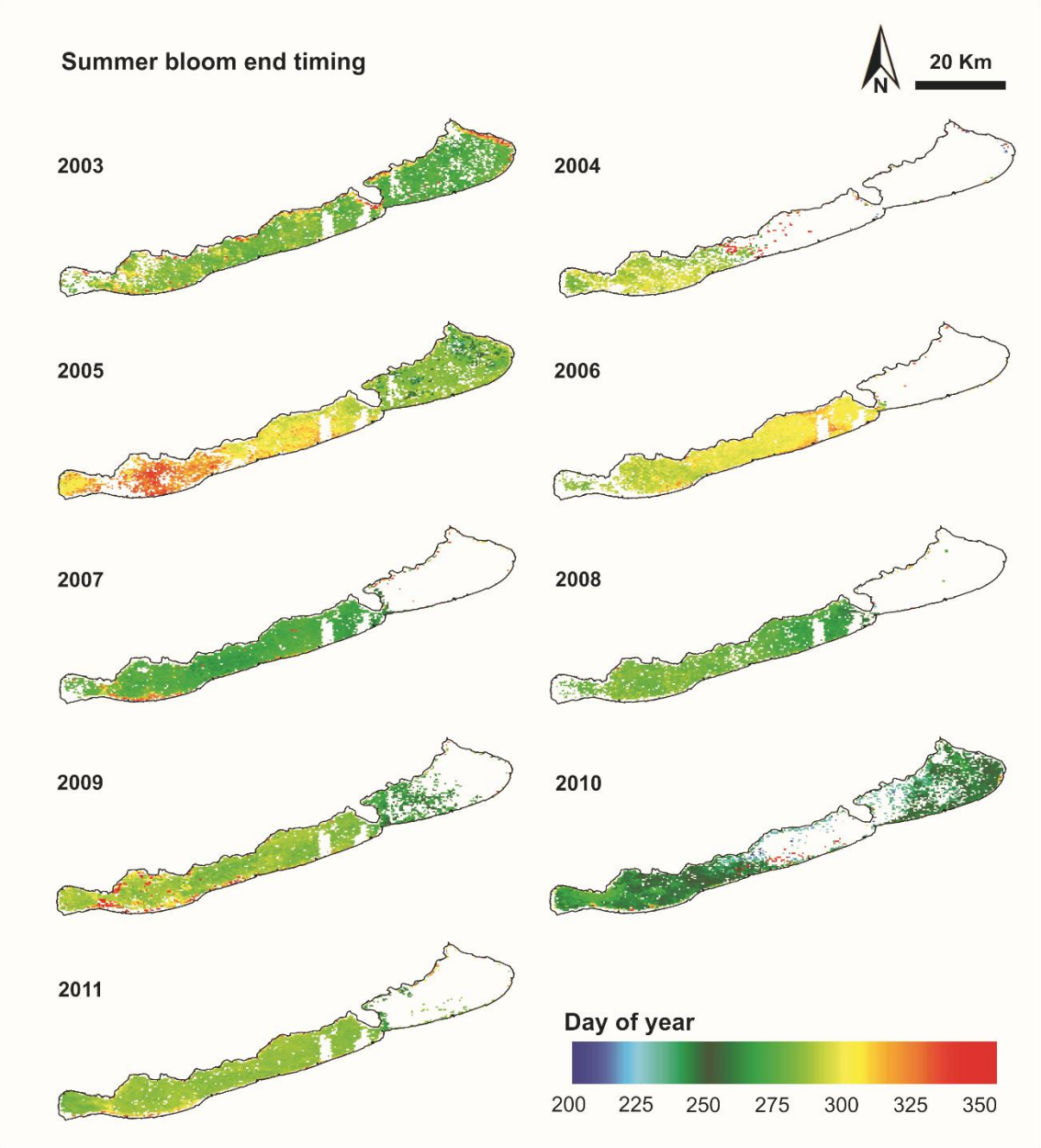

Figure AII.2. Summer bloom end timing, mapped for each of the nine years 2003-2011.

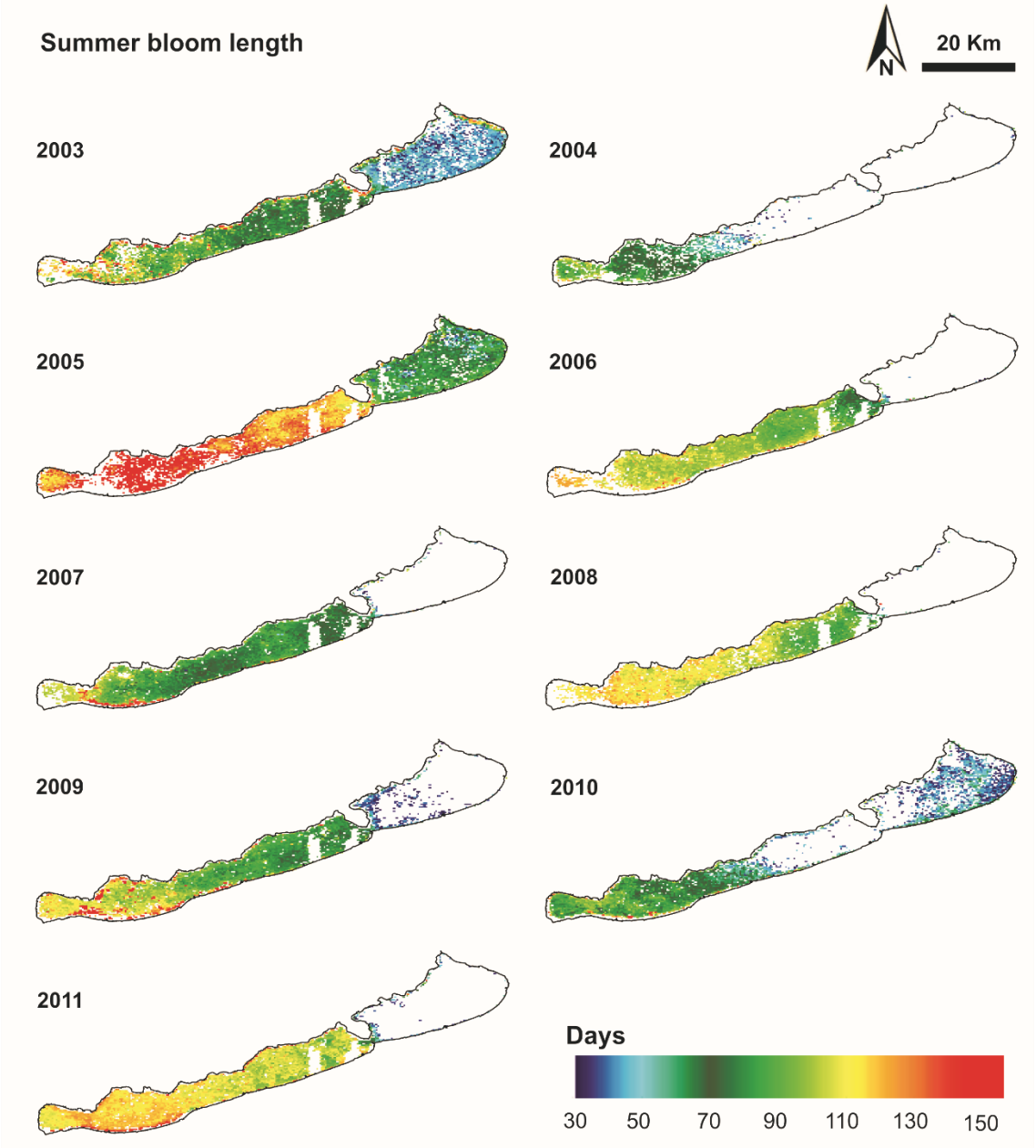

Figure AII.3. Summer bloom length, mapped for each of the nine years 2003-2011.

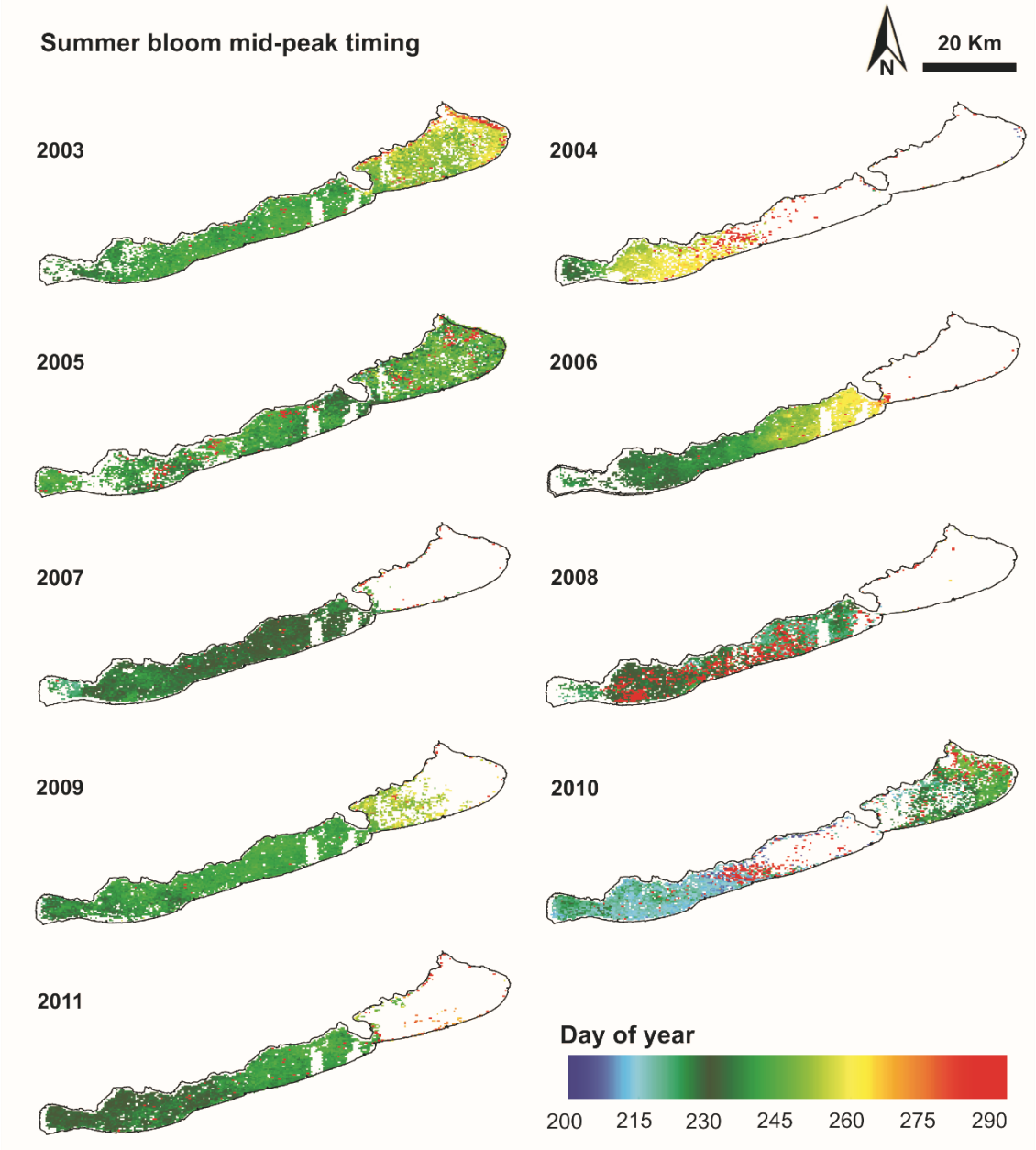

Figure AII.4. Summer bloom mid-bloom timing, mapped for each of the nine years 2003-2011.

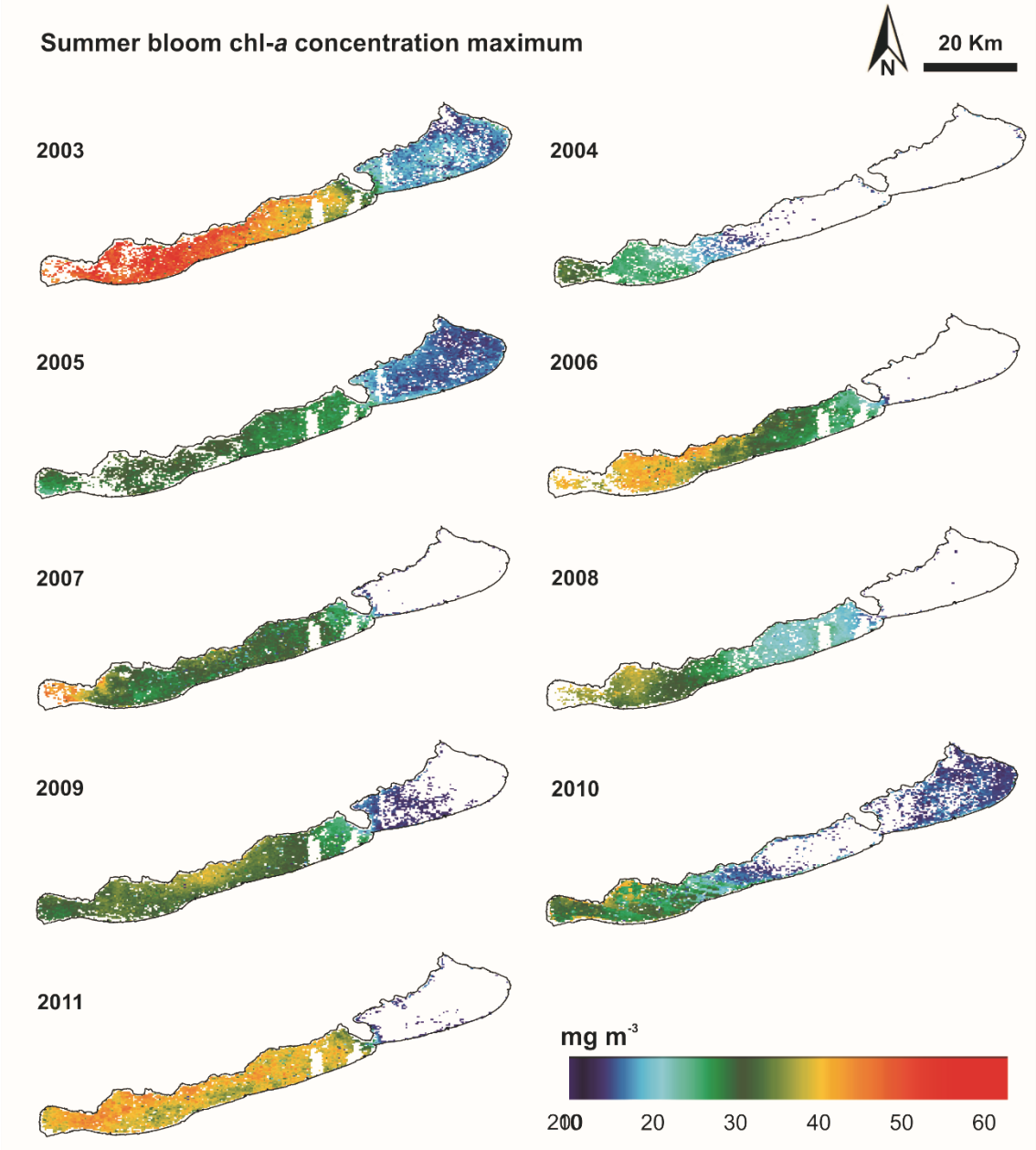

Figure AII.5. Summer bloom maximum chl-*a* concentration, mapped for each of the nine years 2003-2011.

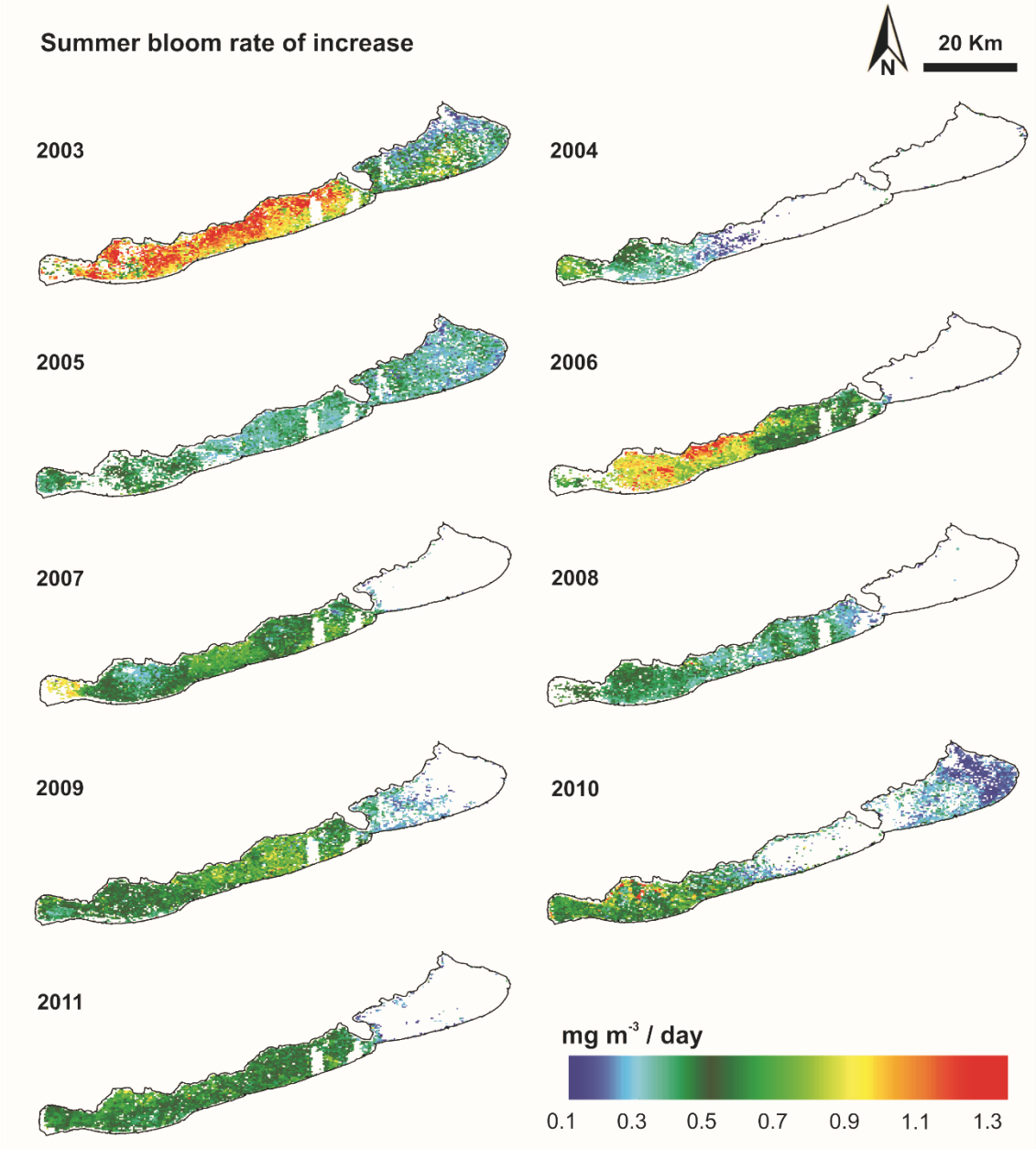

Figure AII.6. Summer bloom rate of chl-*a* concentration increase, mapped for each of the nine years 2003-2011.

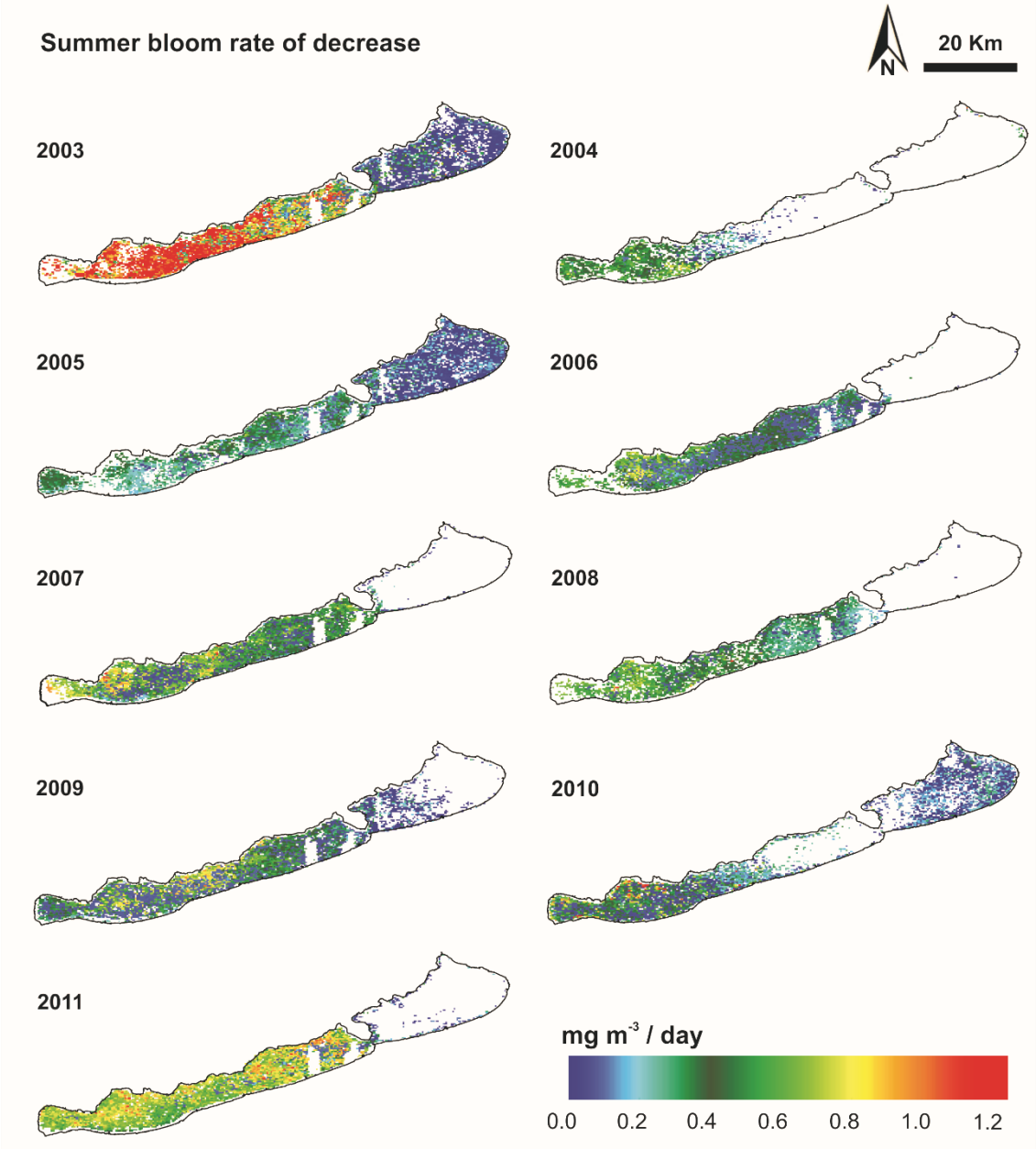

Figure AII.7. Summer bloom rate of chl-*a* concentration decrease, mapped for each of the nine years 2003-2011.

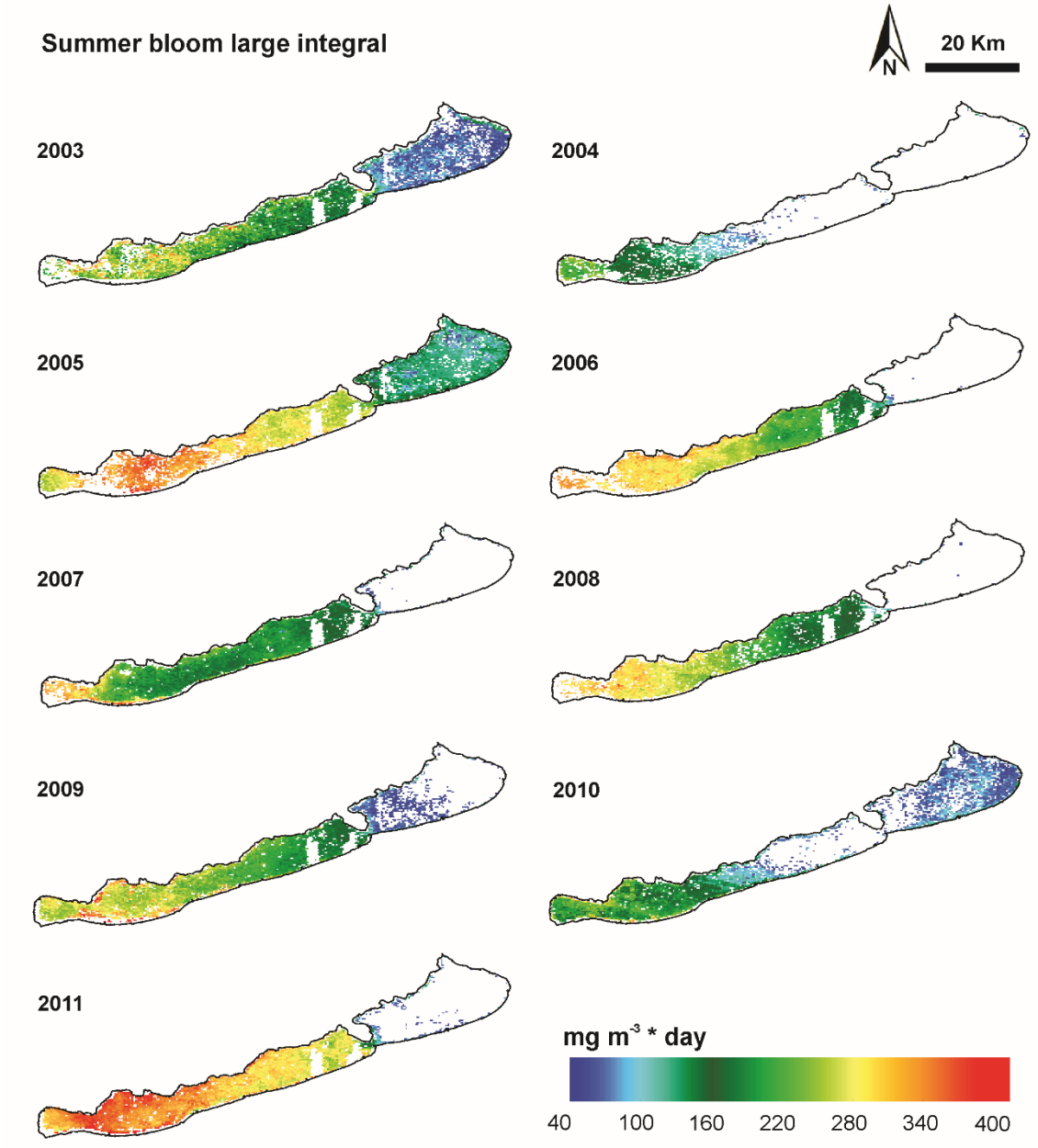

Figure AII.8. Summer bloom large integral, mapped for each of the nine years 2003-2011.